



**HAL**  
open science

# New enantioselective transformations induced by cyclodextrins: applications in the preparation of molecular building blocks of biological interest

Ali Taher Mansour

► **To cite this version:**

Ali Taher Mansour. New enantioselective transformations induced by cyclodextrins: applications in the preparation of molecular building blocks of biological interest. Organic chemistry. Université Paris Saclay (COMUE); Université Libanaise, 2018. English. NNT : 2018SACLS186 . tel-02343180

**HAL Id: tel-02343180**

**<https://theses.hal.science/tel-02343180>**

Submitted on 2 Nov 2019

**HAL** is a multi-disciplinary open access archive for the deposit and dissemination of scientific research documents, whether they are published or not. The documents may come from teaching and research institutions in France or abroad, or from public or private research centers.

L'archive ouverte pluridisciplinaire **HAL**, est destinée au dépôt et à la diffusion de documents scientifiques de niveau recherche, publiés ou non, émanant des établissements d'enseignement et de recherche français ou étrangers, des laboratoires publics ou privés.

# New Enantioselective Transformations Induced by Cyclodextrins: Applications in the Preparation of Molecular Building Blocks of Biological Interest

Thèse de doctorat de l'Université Libanaise et de l'Université Paris-Saclay, préparée à l'Université Paris Sud

École doctorale n°571 sciences chimiques : molécules, matériaux,  
instrumentation et biosystèmes (2MIB)

Ecole doctorale des sciences et technologie de l'Université  
Libanaise (EDST)

Spécialité de doctorat: Chimie

Thèse présentée et soutenue à Beyrouth, le 5 Juillet 2018, par

**M. Ali Taher Mansour**

Composition du Jury :

M. Kamal Bouhadir Professeur, American University of Beirut	Président
M. Olivier Piva Professeur, Université Claude Bernard (– SURCOOF)	Rapporteur
M. Mahmoud Faraj Professeur, Lebanese International University	Rapporteur
M. David J. Aitken Professeur, Université Paris Sud (– CP3A)	Directeur de thèse
M. Daoud Naoufal Professeur, Université libanaise (– LCIO)	Directeur de thèse
Mme Sylvie Robin Maître de conférences, Université Paris Descartes (– CP3A)	Co-encadrante
Mme Ogaritte Yazbeck Assistante Professeur, Université libanaise (– LCIO)	Co-encadrante



## Acknowledgments

First, I would like to express my gratitude to Pr. Mahmoud Faraj, the person who triggered my interest in organic chemistry, and Pr. Olivier Piva, for being reporters for my PhD thesis; and to Pr. Kamal Bouhadir for being the examiner. I am honored to have all of you as jury members.

I would also like to express my gratitude to my research supervisors; Dr. Ogaritte Yazbeck who always believed in my potentials, and tough me how to have the spirit of a researcher; Dr. Sylvie Robin who patiently followed my work on daily basis; Pr. David J. Aitken who provided top class scientific supervision, and Pr. Daoud Naoufal who was especially helpful in setting up a wok place for organic chemistry in his lab, here in Lebanon. You were all encouraging, supportive, and vital for the success of this research.

A special thanks goes to all the personnel at the Chimie Peptidomimétique Photochimie, Procédés Alternatifs (CP3A) group, from permanents to students, for their hospitality and scientific guidance, especially Ms. Florence Charnay-Pouget for her help with the HPLC, Mr. Jean-Pierre Baltaze for his help with the NMR experiments, Dr. Thomas Boddaert for his help with the photoreactor setup, Dr. Julien Buendia for his technical advices and Elodie Tran whose masters 1 work was integrated within this thesis. It has been a great pleasure, I learned enormously from each one of you.

I would also like to show my appreciation to Dr, Ali Hachem and all his research group (LCMPN), especially my colleagues, Layal Haris, Tourin Bziea, Ranin Kawtharani, and Ali Solaiman.

I am also grateful to the CIOES for their financial support, and to my family, and friends, who stood by me throughout this doctoral research.

# Contents

<b>Chapter 1: Introduction</b> .....	1
<b>1.1 Photochirogenesis</b> .....	1
1.1.1 Non-supramolecular photochirogenesis .....	2
1.1.1.1 Photochirogenesis via a chiral photosensitizer.....	2
1.1.1.2 Photochirogenesis via a chiral auxiliary.....	4
1.1.2 Supramolecular Photochirogenesis .....	6
1.1.2.1 Chiral templates.....	6
1.1.2.2 Supramolecular photochirogenesis with cyclodextrins .....	9
<b>1.2 Study of CD complexes</b> .....	16
1.2.1 Complex stoichiometry .....	16
1.2.1.1 Determination of a CD complex stoichiometry.....	17
1.2.2 1D NMR studies of CD complexes .....	18
1.2.3 Determination of the binding constant $K_b$ .....	19
1.2.3 2D NMR in the characterization of CD host/guest complexes .....	20
<b>1.3 <math>\gamma</math>-Amino acids</b> .....	23
1.3.1 GABA and constrained analogs .....	23
1.3.1.1 Constrained $\gamma$ -amino acids.....	24
1.3.1.2 GABA analogs in the field of foldamers.....	25
1.3.2 Literature synthesis of <i>cis</i> - and <i>trans</i> - <sup>2,3</sup> CB-GABA.....	26
1.3.3 Literature synthesis of <i>cis</i> - and <i>trans</i> - <sup>3,4</sup> CB-GABA.....	28
<b>1.4 Aims of this project</b> .....	31

<b>Chapter 2: The Photochemical Reactivity of <i>N</i>-Allyl-<i>N</i>-(4-methoxyphenyl)acrylamide</b>	33
<b>2.1 Introduction</b>	33
<b>2.2 Results and discussion</b>	35
2.2.1 Synthesis of <i>N</i> -allyl- <i>N</i> -(4-methoxyphenyl)acrylamide 1	35
2.2.2 The $\beta$ -CD/ <i>N</i> -allyl- <i>N</i> -(4-methoxyphenyl)acrylamide 1 complex	37
2.2.2.1 Formation of the $\beta$ -CD/1 complex	37
2.2.2.2 Evidence of complexation by powder X-ray diffraction	37
2.2.2.3 Determination of the complex stoichiometry	38
2.2.2.4 1D NMR studies of the $\beta$ -CD/1 complex	39
2.2.2.5 Determination of the binding constant $K_b$	42
2.2.3 The photochemical reactivity of compound 1	42
2.2.3.1 Photoreactivity of compound 1 in solution, without $\beta$ -CD	42
<b>2.3 Conclusion</b>	46
<b>Chapter 3: The Photochemical Reactivity of 1,3-dihydro-2<i>H</i>-azepin-2-one</b>	47
<b>3.1 Introduction</b>	47
<b>3.2 Results and discussion</b>	49
3.2.1 Synthesis of azepinone 8	49
3.2.2 Photoelectrocyclization of azepinone 8 in the absence of $\beta$ -CD	50
3.2.2.1 Photoelectrocyclization of azepinone 8 in solution	50
3.2.2.1.1 Photoelectrocyclization of azepinone 8 in ether	50
3.2.2.1.2 Photoelectrocyclization of azepinone 8 in water	50
3.2.2.2 Photoelectrocyclization of azepinone 8 in solid state	51

3.2.3 Analysis of the enantiomeric excess in photoadduct 9.....	51
3.2.4 The $\beta$ -CD/azepinone 8 complex .....	52
3.2.4.1 Formation of the $\beta$ -CD/azepinone 8 complex:.....	52
3.2.4.2 Evidence of complexation by powder X-Ray diffraction .....	53
3.2.4.3 Determination of the complex stoichiometry.....	54
3.2.4.3.1 <i>The azepinone 8 to <math>\beta</math>-CD ratio in the precipitate</i> .....	54
3.2.4.3.2 <i>The Job's method of continuous variation:</i> .....	55
3.2.4.4 1D NMR studies of the $\beta$ -CD/azepinone 8 complex .....	56
3.2.4.5 Determination of the binding constant $K_b$ .....	59
3.2.4.6 2D ROESY NMR studies of the complex.....	60
3.2.5 Photoelectrocyclization of azepinone 8 in the presence of $\beta$ -CD .....	63
3.2.5.1 Recovery of the photoadduct 9 .....	63
3.2.5.2 Reduction of photoadduct 9 .....	64
3.2.5.3 Analysis of the enantiomeric excess compound ( $\pm$ )-10 .....	65
3.2.6 Photoelectrocyclization/Reduction of azepinone 8 in presence of $\beta$ -CD.....	66
3.2.6.1 Irradiation of $\beta$ -CD/azepinone 8 complex in fluid state.....	66
3.2.6.1.1 <i>Experiment A: "1:1 Hot solution"</i> .....	66
3.2.6.1.2 <i>Irradiation of 1 <math>\beta</math>-CD/azepinone 8 in Suspension</i> .....	68
3.2.6.1.2.1 <i>Experiment B: "1:1 <math>\beta</math>-CD/azepinone 8, Cold suspension"</i> .....	68
3.2.6.1.2.2 <i>Experiment C: "3:1 <math>\beta</math>-CD/azepinone 8 Cold suspension"</i> .....	69
3.2.6.2 Irradiation of $\beta$ -CD/azepinone 8 complex in solid state .....	70
3.2.6.2.1 <i>Irradiation of <math>\beta</math>-CD/azepinone 8 complex in solid state powder form</i> .....	70
3.2.6.2.1.1 <i>Experiment D: Mechanically ground mixture of <math>\beta</math>-CD and azepinone 8</i> .....	70
3.2.6.2.1.2 <i>Experiment E: "<math>\beta</math>-CD/8 complex, filtered then irradiated in powder form"</i> .....	71
3.2.6.2.2 <i>Irradiation in thin film form</i> .....	73

3.2.6.2.2.1 Experiment F: "1:1 film from 15 mM suspension" .....	73
3.2.6.2.2.2 Experiment G: "2:1 film from 15 mM suspension" .....	75
3.2.6.2.2.3 Experiment H: "1:1 film from 5 mM clear solution" .....	75
3.2.7 The $\beta$ -CD/8 complex film texture .....	76
3.2.7.1 Scanning electron microscopy (SEM) of $\beta$ -CD/azepinone 8 complex films .....	78
3.2.8 The absolute configuration of compound 10.....	78
<b>3.3 Chiral resolution of (<math>\pm</math>)-cis-<sup>3,4</sup>CB-GABA by HPLC .....</b>	<b>81</b>
3.3.1 Preparation of the Boc protected amino acid ( $\pm$ )-12 .....	81
3.3.1.2 Photoelectrocyclization of azepinone 8 in ether .....	81
3.3.1.3 Catalytic hydrogenation of photoadduct ( $\pm$ )-9.....	82
3.3.1.4 Activation of the 2-azabicyclo[3.2.0]heptan-3-one ( $\pm$ )-10 .....	82
3.3.1.5 Basic hydrolysis of ( $\pm$ )-11 .....	83
3.3.2 Chiral HPLC resolution of <i>N</i> -Boc amino acid ( $\pm$ )-12.....	83
3.3.3 Switching to the <i>N</i> -Boc benzylic ester ( $\pm$ )-13.....	85
3.3.3.1 Preparation of <i>N</i> -Boc benzyl ester ( $\pm$ )-13 .....	85
3.3.3.2 Chiral HPLC resolution of <i>N</i> -Boc benzylic ester ( $\pm$ )-13.....	86
<b>3.4 Conclusion .....</b>	<b>89</b>
<b>Chapter 4: Synthesis and Folding Pattern of <math>\gamma/\alpha</math>-Hybrid Peptides .....</b>	<b>90</b>
<b>4.1 Introduction .....</b>	<b>90</b>
4.1.1 The Three dimensional conformation of polypeptides.....	91
4.1.1.1 The conformation of the peptide link.....	91
4.1.1.2 The conformation around the peptide bond .....	92
4.1.2 The folding pattern in natural peptides .....	93
4.1.2.1 The Ramachandran diagram .....	93

4.1.2.2 Conformation of natural peptides .....	94
4.1.2.2.1 The $\alpha$ -helix “natural helix” .....	95
4.1.3 The folding pattern in unnatural peptides .....	96
4.1.3.1 Folding pattern in homo-peptides .....	97
4.1.3.1.1 $\beta$ -Peptides .....	97
4.1.3.1.1.1 Example and application of the $\beta$ -Peptides .....	98
4.1.3.1.2 $\gamma$ -peptides .....	99
4.1.3.1.2.1 Examples and application of the $\gamma$ -peptides .....	100
4.1.3.2 Folding pattern in hybrid peptides .....	101
4.1.3.2.1 Mixed $\alpha/\beta$ -peptides .....	102
4.1.3.2.1.1 Examples of $\alpha/\beta$ -peptides and applications .....	102
4.1.3.2.2 Mixed $\beta/\gamma$ -peptides .....	103
4.1.3.2.2.1 Examples of $\beta/\gamma$ and applications .....	103
4.1.3.2.3 Mixed $\alpha/\gamma$ -peptides .....	104
4.1.3.2.3.1 Examples and applications .....	105
4.1.3.3 Stereochemistry effect on the peptide secondary structure .....	109
4.1.4 Objectives of this work .....	111
<b>4.2. Results and discussion</b> .....	<b>113</b>
4.2.1 The starting amino acids: Enantiomerically pure protected $\gamma$ - and $\alpha$ -amino acids .....	113
4.2.1.1 The enantiomerically pure Boc- <i>cis</i> - <sup>3,4</sup> CB-GABA-OBn .....	113
4.2.1.2 The Enantiomerically pure D-Alanine .....	114
4.2.2 The general Synthetic method .....	115
4.2.2.1 The activation/ coupling strategy .....	115
4.2.2.2 Choice of the coupling agent .....	116
4.2.2.3 Convergent peptide synthesis .....	118

4.2.3 Synthesis of Boc-( <i>S,S</i> )- <i>cis</i> - <sup>3,4</sup> CB-GABA/( <i>R</i> )-Ala-OBn peptides .....	119
4.2.3.1 Synthesis of the Boc-[( <i>S,S</i> )- <i>cis</i> - <sup>3,4</sup> CB-GABA/( <i>R</i> )-Ala]-OBn peptide p1 .....	120
4.2.3.2 Synthesis of the Boc-[( <i>S,S</i> )- <i>cis</i> - <sup>3,4</sup> CB-GABA/( <i>R</i> )-Ala] <sub>2</sub> -OBn peptide p2.....	120
4.2.4 Synthesis of Boc-( <i>R,R</i> )- <i>cis</i> - <sup>3,4</sup> CB-GABA/( <i>R</i> )-Ala-OBn peptides .....	121
4.2.4.1 Synthesis of the Boc-( <i>R,R</i> )- <i>cis</i> - <sup>3,4</sup> CB-GABA-( <i>R</i> )-Ala-OBn peptide p3.....	122
4.2.4.2 Synthesis of the Boc-[( <i>R,R</i> )- <i>cis</i> - <sup>3,4</sup> CB-GABA-( <i>R</i> )-Ala] <sub>2</sub> -OBn peptide p4.....	123
4.2.5 Structural and Conformational analysis in solution .....	123
4.2.5.1 General methods for structural and conformational analysis .....	123
4.2.5.1.1 <i>Structural analysis</i> .....	123
4.2.5.1.2 <i>DMSO-d<sub>6</sub> NMR titration experiments</i> .....	124
4.2.5.1.3 <i>Conformational analysis</i> .....	124
4.2.5.1.4 <i>Molecular modeling</i> .....	124
4.2.5.2 Determining the linear structure of the peptides p2 and p4 .....	125
4.2.5.2.1 <i>DMSO-d<sub>6</sub> titration experiment</i> .....	125
4.2.5.3 Conformational analysis of the peptides p2 and p4 .....	126
4.2.5.3.1 <i>2D ROESY NMR experiment</i> .....	126
4.2.5.3.2 <i>Molecular modeling</i> .....	127
4.2.6 Boc-( <i>S,S</i> )- <i>cis</i> - <sup>3,4</sup> CB-GABA/( <i>R</i> )-Ala-NHBn peptides .....	130
4.2.6.1 <i>Synthesis of the Boc-(<i>S,S</i>)-<i>cis</i>-<sup>3,4</sup>CB-GABA-(<i>R</i>)-Ala-NHBn peptide p5</i> .....	131
<b>4.3 Conclusion</b> .....	133
<b>Perspective and Overall Conclusion</b> .....	134
<b>Experimental Part</b> .....	137
<b>Index</b> .....	184
<b>Thesis Summary in French (Résumé français)</b> .....	188

**Bibliography**..... 216

**Abstract** ..... 224



# Chapter 1: Introduction

## 1.1 Photochirogenesis

The majority of natural and biologically relevant chiral molecules on Earth have a defined configuration which is linked to their molecular function. It is marvelous how living organisms have the ability to preferentially choose or selectively biosynthesize only a single enantiomer of a given molecule.<sup>1</sup> Chemists are envious of this and seek to imitate biological systems; thus, the *asymmetric synthesis* of organic compounds has become a popular playground for research.<sup>2</sup> Selective preparation of molecules in single enantiomer form also has industrial importance, due to the requirement of stereochemically pure molecules in the field of medicine and material science.

Over the last few decades, the asymmetric synthesis of organic compounds has been conventionally achieved by either *catalytic*<sup>3</sup> or *enzymatic*<sup>4</sup> transformations, and a wide range of methods have been developed in order to gain stereochemical control over a variety of chemical transformations. Photochemistry has proven itself to be a versatile tool in organic synthesis,<sup>5, 6</sup> and it is receiving even more attention today since it qualifies as a method for the preparation of new materials in an “environmentally friendly” context, referred to as *green chemistry*.<sup>7</sup> Nonetheless, asymmetric photochemical transformations are not widely studied. The term “*photochirogenesis*” is rather new. It was coined in 1996, and is conceptually synonymous to more traditional “asymmetric photochemistry” or “chiral photochemistry” with the emphasis on the creation of molecular chirality through the use of a photon.<sup>8</sup>

Asymmetric induction from the excited electronic state is hard to achieve due to fundamental factors that make conventional approaches difficult to apply in photochemical reactions.<sup>9</sup> For instance, a chiral catalyst in thermal reactions often functions by decreasing the reaction activation barrier and channels the reaction profile towards an enantioselective pathway; whereas in a photochemical reaction, the irradiated molecules gain sufficient energy to undergo fast subsequent reactions, which do not require further catalysis. So, the biggest challenge in photochirogenesis relates to the inherent high-energy nature of the electronical excited state. Indeed, the much smaller activation parameters for excited-state

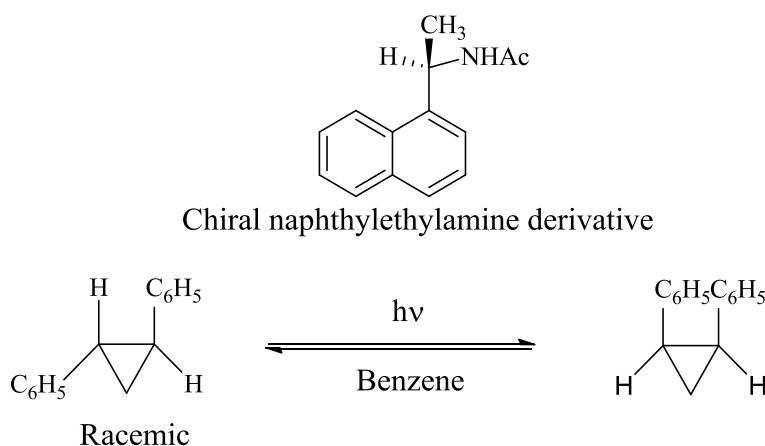
(as opposed to ground-state) reactions leave little space for energetically differentiating the diastereomeric transition states leading to a pair of enantiomers. So how can chirality be controlled in the highly reactive, short lived excited state?

Photochirogenesis research has made great progress both quantitatively and qualitatively due to new methodologies developed for controlling the processes involved. Essentially, in order to achieve stereochemical control over a photochemical reaction, one must make sure that the substrate molecule already resides in a chiral environment during the excitation step.<sup>10</sup> In this regard, photochirogenesis can be conveniently split into two major categories. The first includes reactions in which chirality is transferred to a reacting molecule due to the presence of a chiral substituent, covalently or ionically connected to the reactant. Chirality, with such an approach, can be induced through the intramolecular interaction between the chiral center, acting as a “*chiral auxiliary*”, and the reacting moiety. The second category, *supramolecular photochirogenesis*, can be described as a host-guest interaction between the reactant, as the guest, and a host molecule that provides a chiral environment for the photochemical reaction to proceed in an asymmetric manner. Here, chirality is transferred from one molecule to another through intermolecular interactions between the substrate and a neighboring molecule bearing some chiral properties.

## **1.1.1 Non-supramolecular photochirogenesis**

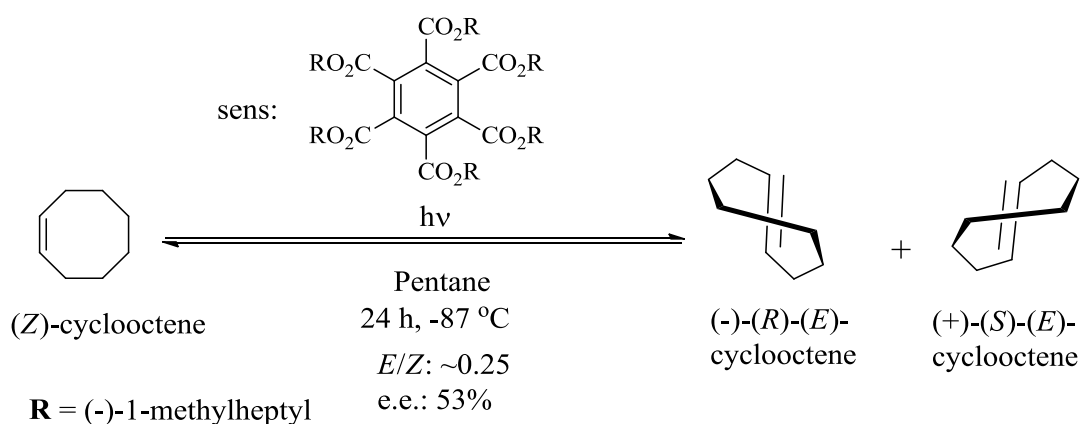
### **1.1.1.1 Photochirogenesis via a chiral photosensitizer**

Hammond and Cole,<sup>11</sup> were the first to exploit chiral photosensitizers for asymmetric induction in photochemistry. They studied the geometrical photoisomerization of racemic 1,2-diphenylcyclopropane sensitized by a chiral (*R*)-*N*-acetylnaphthylethylamine (see Scheme 1). By monitoring the development of the optical activity during the course of the photoisomerization, they established a photostationary state at a *cis/trans* ratio of 1.03 with an enantiomeric excess of 7% of the chiral *trans*-isomer, thus showing the potential of using a chiral photosensitizer to induce chirality in a photoreaction.



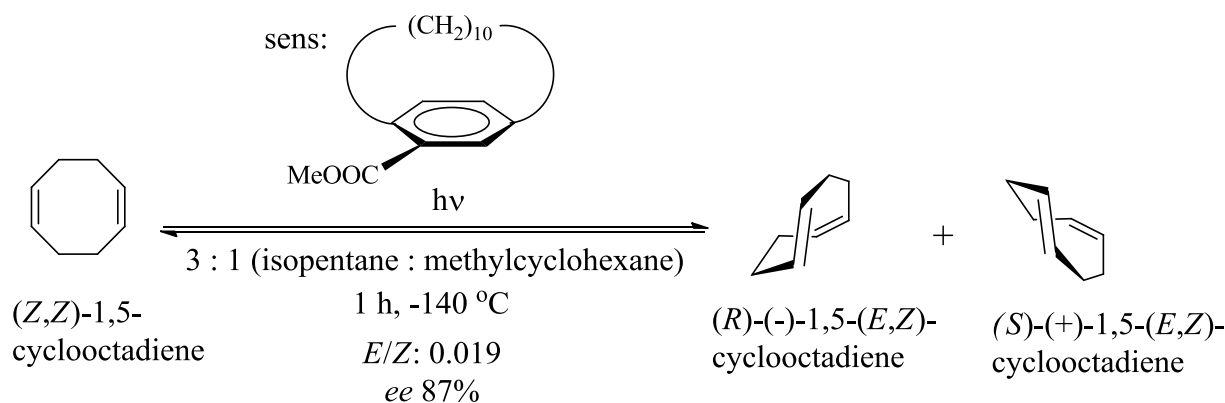
*Scheme 1: The asymmetric photoisomerization of 1,2-diphenylcyclopropane sensitized by a chiral naphthylethylamine derivative.*

However, after 20 year of rather slow progress; the unprecedentedly high 53% *ee* achieved by the Inoue group,<sup>12</sup> in a systematic study of the enantiodifferentiating isomerization of cyclooctenes sensitized by chiral polyalkyl benzene(poly)carboxylates (see Scheme 2), triggered a boost of interest in photochirogenesis.



*Scheme 2: The asymmetric photoisomerization of cyclooctene sensitized by chiral polyalkyl benzene(poly)carboxylates.*

Most recently the Inoue group<sup>13</sup> exploited chiral methyl (*R*)-[10]paracyclophane-12-carboxylate as a sensitizer, to achieve an enantiomeric excess of 87% in the photoisomerization of (*Z,Z*)-1,5-cyclooctadiene (see Scheme 3). In this system the decamethylene bridge provided a shield on one of the enantiotopic faces of the chiral cyclophanes sensitizer. This shielding was attributed by the authors to both enthalpically and entropically factors, which makes the approach, and subsequently the isomerization of the substrate more enantioselective.

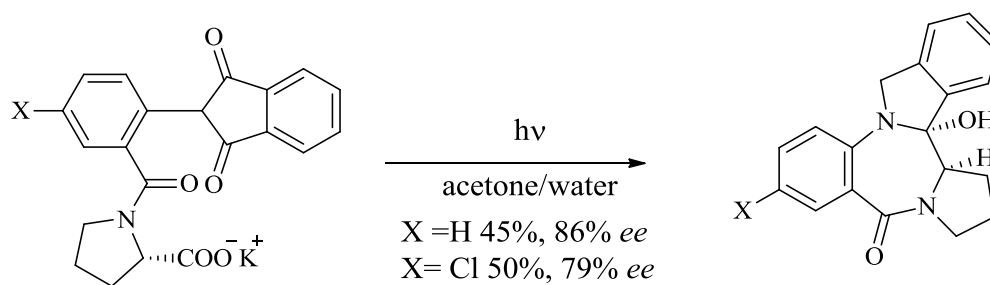


*Scheme 3: The asymmetric photoisomerization of cyclooctadiene sensitized by (R)-[10]paracyclophane-12-carboxylate derivative.*

Aside from this quite unique example of enantioselective photosensitized isomerization of cyclooctadiene, it had pretty much been established that conventional photochirogenesis induced via chiral sensitizers alone are generally considered not very efficient. The exciplex between an excited chiral sensitizer and a ground-state substrate, despite being at lower energy than the excited state alone, still has large conformational freedom which minimizes the prospects for chiral induction.<sup>14</sup>

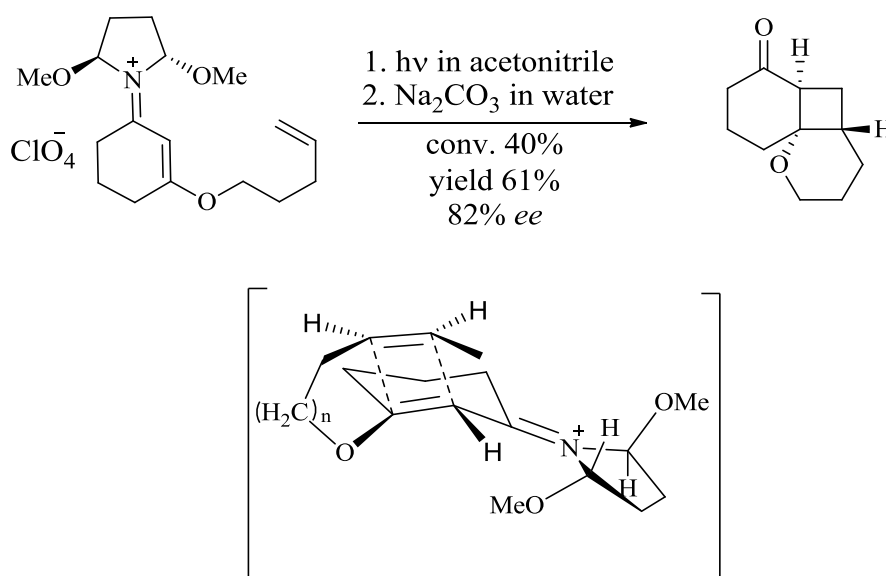
#### 1.1.1.2 Photochirogenesis via a chiral auxiliary

After the mid-1990's, with more understanding of chirality transfer, much greater stereoselectivity was reported in photochemical reactions. Griesbeck and coworkers studied the photodecarboxylation of *N*-phthaloylanthranilic acid derivatives (see Scheme 4).<sup>15</sup> Photodecarboxylation of the corresponding chiral potassium salt allowed access to the pentacyclic pyrrolo[1,4]benzodiazepine photo-adduct with a diastereoselectivity greater than 98% and an enantiomeric excess up to 86%.



*Scheme 4: The asymmetric photodecarboxylation of N-phthaloylanthranilic acid derivatives.*

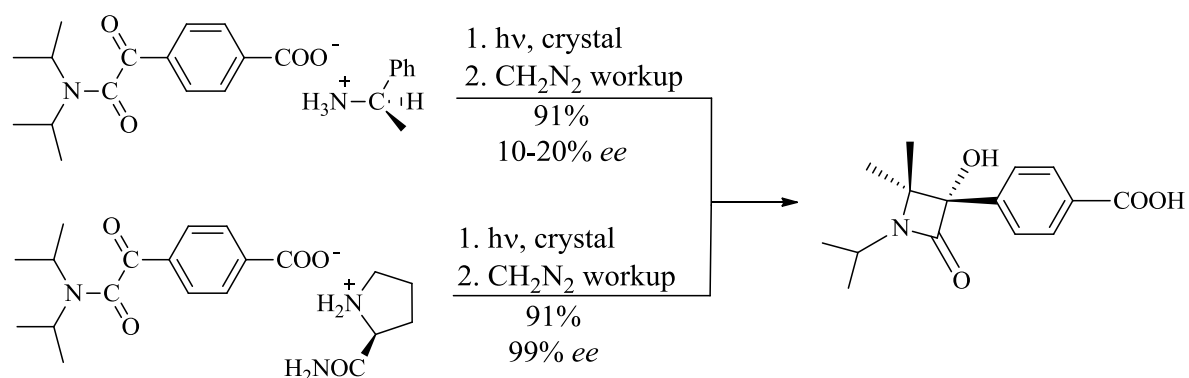
At around the same period, the Mariano group studied the [2+2] photocycloaddition of chiral pyrrolidino-cyclohexeniminium perchlorates (see Scheme 5).<sup>16</sup> The presence of the chiral pyrrolidine makes the photocycloaddition facially selective favoring the *anti* transition state that gives rise to an enantiomeric excess of up to 82%.



*Scheme 5: The asymmetric photocycloaddition of chiral pyrrolidino-cyclohexeniminium perchlorate.*

Later, much higher enantiomeric excess was found through photochirogenesis using chiral auxiliaries. Scheffer and Wang studied the photochemical synthesis of  $\beta$ -lactams via the asymmetric Norrish Type II photochemical reaction of salt crystals formed from ionic chiral auxiliaries and 4-(2-(diisopropylamino)-2-oxoacetyl)benzoate (see Scheme 6).<sup>17</sup> Irradiation of the chiral crystals in the solid state yielded the target photoadduct in *ee* up to 99%. The

high enantioselectivity was attributed by the authors to the ability of the chiral salt substrate to crystallize into a single conformational enantiomer.



*Scheme 6: The asymmetric Norrish Type II photochemical reaction of chiral salts of 4-(2-(diisopropylamino)-2-oxoacetyl)benzoate, forming a  $\beta$ -lactam derivative.*

## 1.1.2 Supramolecular Photochirogenesis

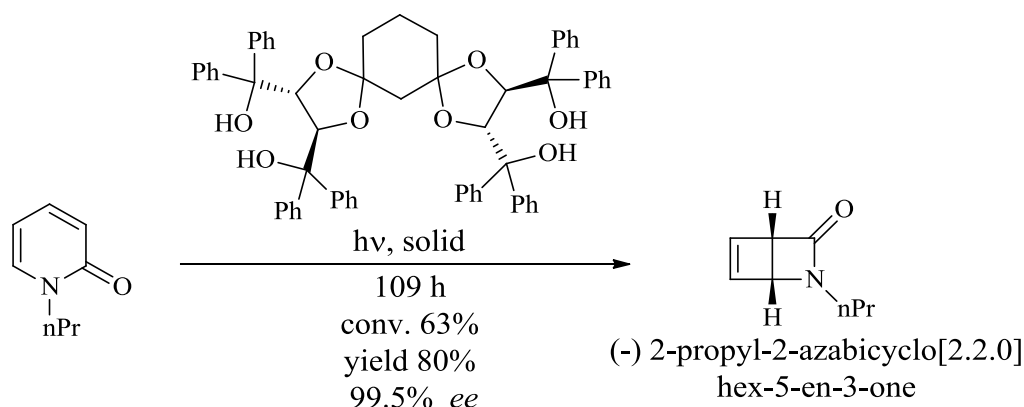
Supramolecular photochirogenesis<sup>18</sup> is an evolving field of research implicating photochemistry, asymmetric synthesis, and supramolecular chemistry. Stereochemical control in supramolecular photoreactions is mostly attributed to the non-covalent interactions between the host and the substrate; by confining a prochiral substrate in a chiral supramolecular environment prior to photo-excitation, there is more likelihood of effective chirality transfer in the excited state. The substrate is likely to have a preferred conformation within the host cavity; this is conveyed to the product chirality upon irradiation. Also, confinement extenuates the difference in free energy of activation between two diastereomeric transition states, thus facilitating their discrimination, and boosting enantioselectivity. Several macromolecules have been used as hosts in asymmetric photosynthesis, including zeolite, urea clathrates, cucurbiturils, octaacids, metal nanocages, chiral organic templates, and cyclodextrins (CDs). There are a number of excellent recent reviews on supramolecular photochirogenesis;<sup>19</sup> here we shall illustrate some of the more recent studies or examples with fairly high enantioselectivity.

### 1.1.2.1 Chiral templates

Chiral templates are among the best supramolecular hosts utilized in the field of asymmetric photochemistry. Several chiral templates have been used to induce high enantioselectivity. Chiral templates possess a well-defined three-dimensional space to confine a guest

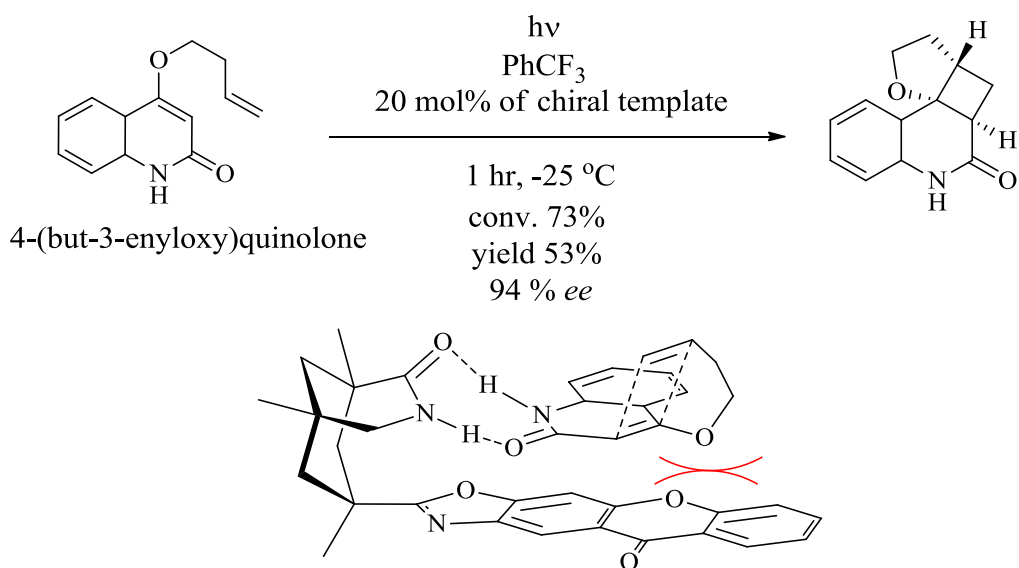
substrate; they do not have a cavity, but achieve chirality transfer by directly interacting with substrates through strong and directional non-covalent interactions, such as hydrogen-bonding and/or electrostatic interactions. In their interactions they are considered supramolecular hosts, even though they are more “molecular” due to their size and architectural simplicity. Several chiral templates have been used to induce high enantioselectivity.

The Lipkowska group utilized chiral diols as templates to perform enantioselective photocyclizations of 1-alkyl-2-pyridones in inclusion crystals, to give  $\beta$ -lactams in good yield with *ee* up to 99% (see Scheme 7).<sup>20</sup> The high enantioselectivity was attributed to the spatial situation of the pyridone derivative substrate relative to the template molecule in the solid crystal form, which sterically allows the formation of one enantiomer.



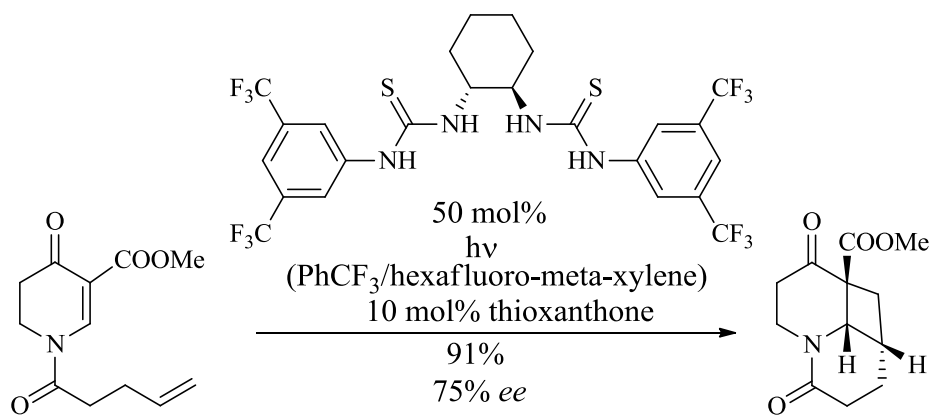
*Scheme 7: The asymmetric photocyclizations of an 1-alkyl-2-pyridone into a  $\beta$ -lactam derivative.*

A similar approach was later studied by the Bach group who developed a lactam/xanthone based template for the intramolecular [2+2]-photocycloaddition of prochiral 4-(but-3-enyloxy)quinolone (see Scheme 8 ).<sup>21</sup> The template allowed high directionality in the binding of its lactam segment to a photoreactive substrate, making only one enantiotopic face available for the [2+2]-cycloaddition reaction to proceed. This was validated by the high enantioselectivity of the reaction, with *ee* values up to 94%.



*Scheme 8: The asymmetric photocyclization of 4-(but-3-enyloxy)quinolone.*

The same research group also utilized thiourea based molecules as templates to host, by the same logic, another enantioselective intramolecular [2+2] photocycloaddition reaction with *ee* up to 91% (see Scheme 9).<sup>22</sup>



*Scheme 9: The asymmetric photocycloaddition of a 2,3-dihydropyridone-5-carboxylate derivative.*

### 1.1.2.2 Supramolecular photochirogenesis with cyclodextrins

Cyclodextrins (CDs) are macrocyclic nano-buckets that are capable of forming stable inclusion complexes with many molecules. Due to this property, CDs have many applications in supramolecular chemistry,<sup>23, 24</sup> in the catalysis of organic reactions,<sup>25</sup> and in encapsulation of pharmaceuticals in order to serve as drug delivery agents.<sup>26, 27</sup> CDs also play a prominent role in the field of supramolecular photochirogenesis, as we shall illustrate below.

Before discussing asymmetric photochemistry induced by cyclodextrins, one must appreciate the structural features of these molecules. Natural CDs are cyclic oligomers comprised of 6, 7, or 8 D-glucopyranose units (corresponding to  $\alpha$ -,  $\beta$ -, and  $\gamma$ -CD respectively), that are linked through  $\alpha$ -(1,4) glycosidic bonds. Due to the chair conformation of the glucopyranose units the CD is shaped like a truncated cone rather than a perfect cylinder (see Figure 1).<sup>28</sup> The internal cavity of the truncated cone is lined by the H<sub>3</sub> and H<sub>5</sub> protons and the lone pair of the glycosidic oxygen atoms, thus rendering the interior of the structure lipophilic; this allows CDs to form host-guest complexes with a variety of organic and inorganic molecules. On the other hand, the hydroxyls on C-2, C-3, and C-6 are directed towards the exterior, thus rendering the outer face hydrophilic. As a combined effect of this arrangement of atoms, CDs are soluble in polar (*e.g.* physiological) media and at the same time can carry lipophilic molecule in their cavity.<sup>29</sup>

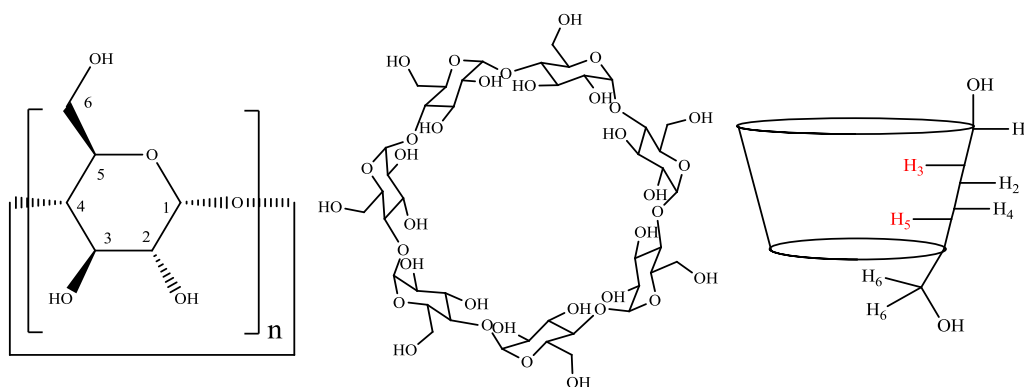
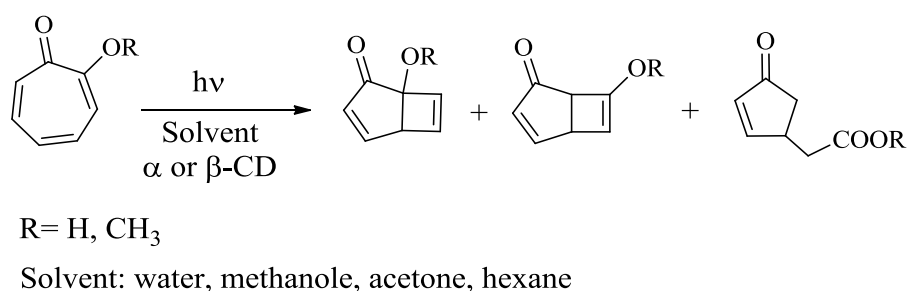


*Figure 1: Glucopyranose unit (left), the  $\beta$ -CD torus (middle), and the orientation of the CD protons relative to its cavity (right).*

CDs are transparent in the UV-vis region of electromagnetic radiation and are inherently chiral and compatible with many electronically excited species, making them among the

most frequently employed supramolecular hosts for mediating photochirogenic reactions.<sup>30</sup> In the past 30 years, the CD cavity has provided a chiral environment for a wide range of photochemical reactions, including photolysis reactions,<sup>31, 32</sup> unimolecular photoelectrocyclizations, intermolecular<sup>33</sup> and intramolecular photocycloadditions,<sup>34, 35</sup> as well as photocyclodimerization reactions.<sup>36, 37, 38</sup> Since CDs can be chemically modified,<sup>39</sup> sensitizer-grafted CDs can be envisaged as supramolecular photosensitizing systems for better enantiodifferentiation.

In 1980, Takeshita and coworkers studied the intramolecular photochemical electrocyclicization of tropolone and its methyl ether derivative in the presence of  $\alpha$ - or  $\beta$ -CDs, in water, methanol, acetone, or hexane (see Scheme 10).<sup>40</sup> The authors did not report *ee* values for the photoproducts; rather, they validated the occurrence of enantioselective transformations through optical rotation measurements. They also noted that the amplitude of the optical rotation was largest in photoadducts obtained from irradiation in aprotic solvents in the presence of  $\beta$ -CD compared to those obtained in the presence of  $\alpha$ -CD.

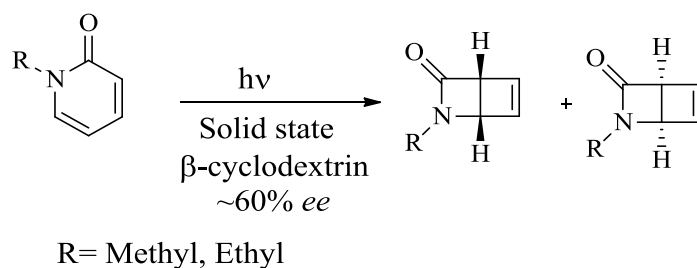


*Scheme 10: The intramolecular photochemical electrocyclicization of tropolone and its methyl ether derivative in the presence of CDs.*

Twenty years later, the Ramamurthy group conducted new studies on the photochemical electrocyclicizations of tropolone alkyl ethers bearing different alkyl substituents, in the presence of  $\alpha$ ,  $\beta$  and  $\gamma$ -CDs, both in solution and in the solid state.<sup>41</sup> observed a near zero *ee* in solution and a moderate *ee* (20-30%) in solid state, suggesting that the rigidity of the medium is an important parameter for the chiral induction during this photoreaction. Moreover, they suggested that a tight-binding complexation between the reactant and the CD host is a requirement for a good enantioselectivity.

Subsequently, the same group studied the photochemical electrocyclicization of *N*-alkyl pyridines in the presence of  $\beta$ -CD (see Scheme 11).<sup>42</sup> Enantiomeric excesses 60% was

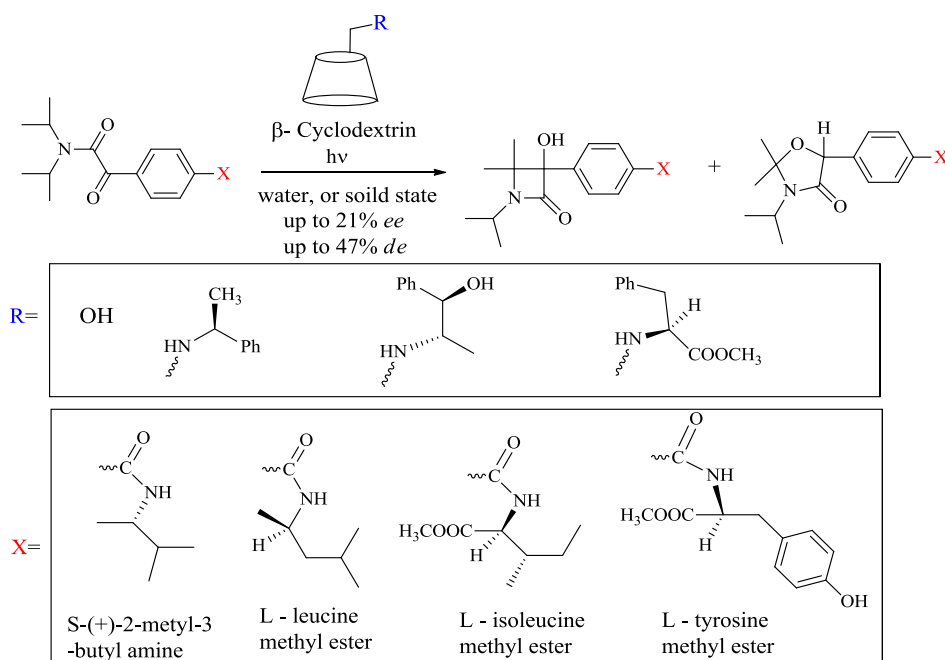
obtained by irradiating a mechanically ground mixture of the  $\beta$ -CD host and the pyridone guest in solid state.



*Scheme 11: The photochemical electrocyclization of N-alkyl pyridones in the presence of  $\beta$ -CD.*

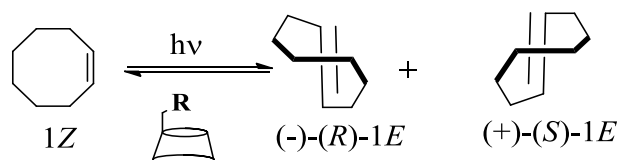
Despite the higher *ee*, the authors were unable to exceed a conversion of 15% even when controlling the wavelength of the irradiation, an observation which was attributed to the photoreversibility of the reaction.

Chirally modified CDs were utilized as hosts for Norrish Type II / Yang cyclization reactions of chiral derivatives of *N,N*-diisopropyl-2-oxo-2-arylacetamides, in aqueous solutions as well as in solid state (see Scheme 12).<sup>43</sup> Although an increase of the enantiomeric (up to 21% *ee* and 47% *de*) was noted when either the host or the guest were chirally modified; neither a reliable model that would help to predict the outcome of the chiral induction in a photochemical reaction, nor an understanding of the effect of the chiral center in the substrate emerged from this investigation.



*Scheme 12: Asymmetric Norrish Type II / Yang cyclization reaction of chiral N,N-diisopropyl-2-oxo-2-arylacetamide derivatives in the presence of  $\beta$ -CD and chirally modified  $\beta$ -CD.*

Inoue and coworkers investigated the photoisomerization of *Z*-cyclooctene in the presence of native  $\beta$ -CD<sup>44</sup> and functionalized  $\alpha$ ,  $\beta$ , and  $\gamma$ -CDs bearing a photosensitizer on the primary face.<sup>45, 37</sup> They observed an improvement in the *ee* from near 0% with native  $\beta$ -CD to 24% with a sensitizer functionalized  $\beta$ -CD (see Scheme 13). The authors pointed out the importance of the “fit” between the CD cavity and the guest for the enantioselectivity. The same photoisomerization reaction was further investigated in aqueous methanol by Li and coworkers.<sup>46</sup> This group showed that, in the presence of a sensitizer functionalized  $\beta$ -CD, the *ee* and the photostationary *E/Z* ratio are dependent on the solvent composition. They reported *ee* values up to 47% through optimization of the methanol/H<sub>2</sub>O ratio and the temperature of the reaction mixture (See Scheme 13).

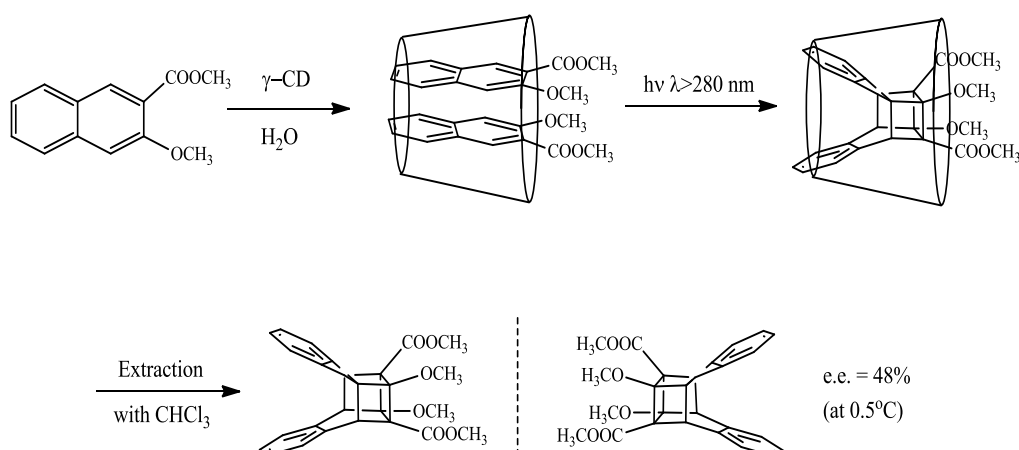


R	% MeOH	Temp (°C)	E/Z	% ee
OH	0	not specified	0.47	0.24*
	50	-40	0.22	24
	10	-5	22.8	47

\*Reported optical yield

*Scheme 13: The photoisomerization of Z-cyclooctene in the presence of native or functionalized  $\beta$ -CDs.*

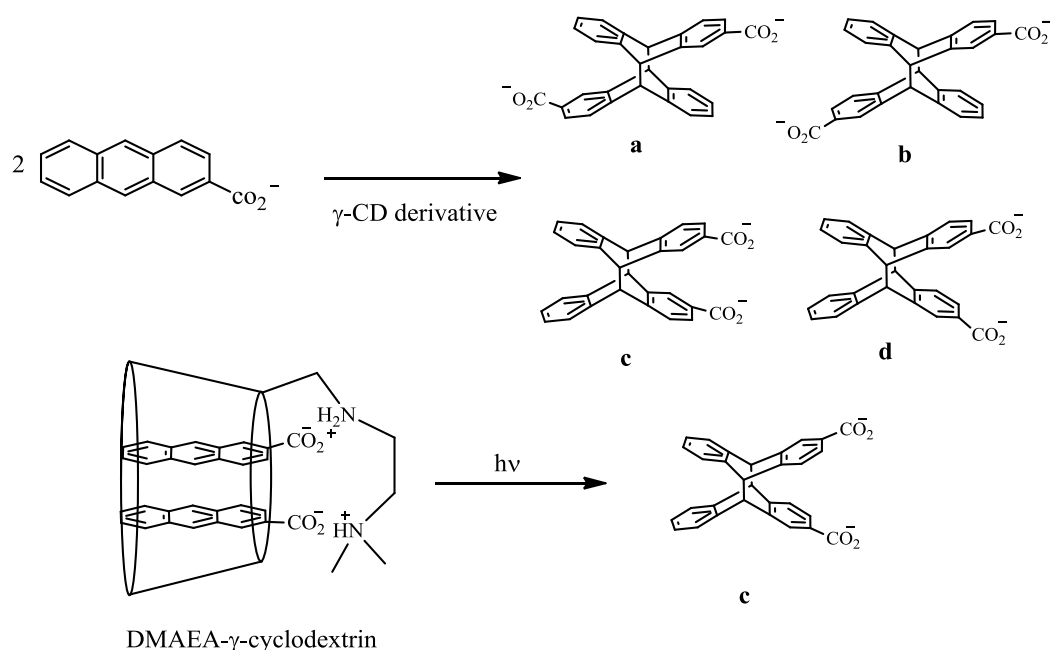
CDs have also been employed as hosts for bimolecular photoreactions. For instance, Luo and coworkers studied the photocyclodimerization of methyl 3-methoxynaphthalene-2-carboxylate inside a  $\gamma$ -CD host (see Scheme 14).<sup>47</sup> The authors reported an *ee* of 48% in aqueous solution, at 0.5 °C, which was the highest value achieved for the asymmetric photodimerization in solution at that time.



*Scheme 14: The photocyclodimerization of methyl 3-methoxynaphthalene-2-carboxylate in the presence of  $\gamma$ -CD.*

Inoue's research group has extensively studied the chiral photocyclodimerization of 2-anthracenecarboxylates (ACs) in the presence of native  $\gamma$ -CD and 6<sup>A</sup>-2(2-

(dimethylamino)ethylamino)-6<sup>A</sup>-deoxy- $\gamma$ -CD (DMAEA- $\gamma$ -CD)<sup>3</sup> (see Scheme 15).<sup>36, 48</sup> In the case of native  $\gamma$ -CD, the head to tail enantiomer **b** was the major compound, obtained with an *ee* of 32% at 25 °C. This was improved to an *ee* of 41% when the reaction temperature was lowered to 0 °C. On the other hand, when DMAEA- $\gamma$ -CD was used as the chiral host, ionic interactions between the carboxylate part of the ACs and the ammonium part the DMAEA- $\gamma$ -CD led to substrate reorientation inside the CD cavity such that the head to head enantiomer **c** became the major compound, still with 41% *ee*.

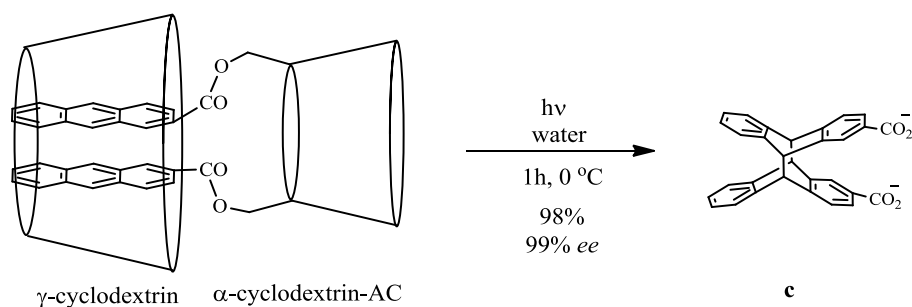


Host	Solvent	Temp °C	Relative yield % <sup>a</sup>				% <i>ee</i> <sup>b</sup>	
			1	2	3	4	2	3
none	water	25	41.8	37.0	12.6	8.6	0.2	0.5
$\gamma$ -CD	water/ EG <sup>c</sup>	0	42.6	<b>46.3</b>	<b>6.1</b>	4.7	<b>41.2</b>	<b>1.2</b>
DMAEA- $\gamma$ -CD	water/ EG <sup>c</sup>	-59	20.1	<b>5.5</b>	<b>41.7</b>	32.7	<b>3.2</b>	<b>41.2</b>

<sup>a,b</sup> relative yield and the *ee* were determined using an analytical HPLC, <sup>c</sup> EG = ethylene glycol

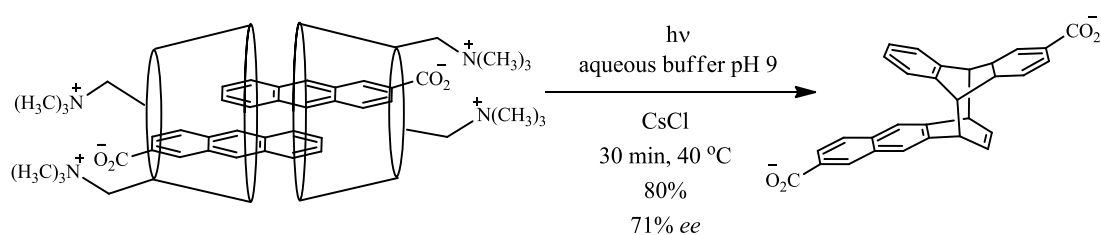
*Scheme 15: The chiral photo-cyclodimerization of 2-anthracenecarboxylate inside  $\gamma$ -CDs.*

Later, the same group devised a novel, “dual chiral, dual-supramolecular” system in which they anchored two AC acid molecules to the primary face of an  $\alpha$ -CD in order to pre-orient the two photosubstrates before adding the  $\gamma$ -CD as the chiral confining host. This dual system allowed selective access to the major cyclodimer **c** in 98% yield and unprecedented 99% *ee* (see Scheme 16).<sup>49</sup>



*Scheme 16: The dual-supramolecular system for a chiral photocyclodimerization of 2-anthracenecarboxylate.*

Continuing their research, Inoue's group recently published the cyclodimerization of ACs encapsulated by two  $6^A,6^C$ -dideoxy- $6^A,6^C$ -triethylammonium derivatives of  $\beta$ -CD (see Scheme 17).<sup>50</sup> In this 2:2 AC/ $\beta$ -CD complex, two ACs moieties are partially stacked to each other exclusively in a head-to-tail fashion which allowed access to the non-conventional slipped cyclodimer with an *ee* of 71% under optimized conditions.



*Scheme 17: Formation of the non-conventional slipped cyclodimer as a product of the photocyclodimerization of the 2:2 AC/ $\beta$ -CD complex.*

## 1.2 Study of CD complexes

### 1.2.1 Complex stoichiometry

When studying a molecular inclusion complex, a key matter is to determine its stoichiometry (see Figure 2). For CD complexes several host:guest ratios have been reported, among which the most commonly observed is the 1:1 complex, wherein one CD molecule includes only one guest inside its cavity.<sup>51</sup> Nevertheless, other ratios are known, e.g. 1:2, where two guest molecules are (totally or partially) included inside the same CD cavity;<sup>52</sup> 2:1, where two CD molecules encapsulate a single guest;<sup>53</sup> or a 2:2 complex made of 2 CD molecules and 2 Guest molecules.<sup>54</sup>

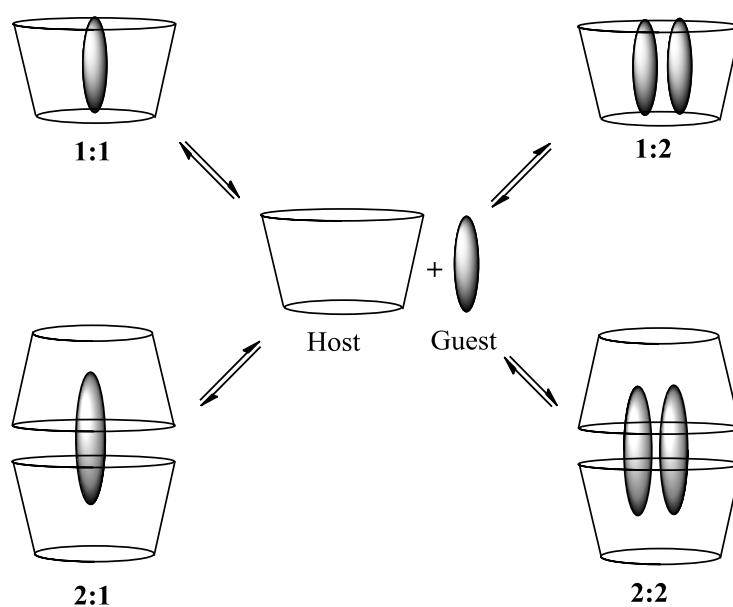


*Figure 2: The most common binding stoichiometries between CDs and guest molecules.<sup>55</sup>*

Three-component CD complexes are also known. These ternary complexes are usually composed of the CD, a guest, and an alcohol that serves to optimize the fit of the guest in the CD cavity.<sup>51</sup>

Interestingly, the stoichiometry in a CD complex can be temperature dependent. For instance, the 1:1 stoichiometry of a  $\beta$ -CD/1-adamantanecarboxylic acid complex at 25 °C changes to a 1:2 stoichiometry when the temperature is lowered to 0 °C.<sup>56</sup>

### 1.2.1.1 Determination of a CD complex stoichiometry

One of the frequently applied procedures to determine the stoichiometry of a molecular complex is the Job's method of continuous variation.<sup>29</sup> In a typical experiment, a physical property that is sensitive to complex formation is recorded while the relative proportions of the host and the guest are varied in a solution in which the total solute concentration is kept constant.<sup>57</sup>

The most common variable used for a Job's plot is UV-vis absorbance, but any property that correlates linearly with the concentration of complex formation, including kinetics, conductivity, NMR spectroscopy etc., can be used.<sup>58</sup> The collected data are usually plotted in the form of the molar fraction ( $\chi$ ) of one species (host or guest) multiplied by the induced change in the observed property ( $\Delta P$ ), against that molar fraction ( $\chi$ ), where  $\chi = \frac{[\text{species a}]}{[\text{species a}] + [\text{species b}]}$  (see Figure 3).

The position of the maximum in a Job's plot identifies the stoichiometric ratio of the formed complex. Although the data obtained is not convenient for estimating the binding constant,<sup>57</sup> the shape of the Job's plot curve provides qualitative insight into the magnitude of the binding constant. Strong binding ( $K_b \gg 1$ ) affords a more angular plot, whereas a lower bonding constant affords a gentle curvature.<sup>58</sup>

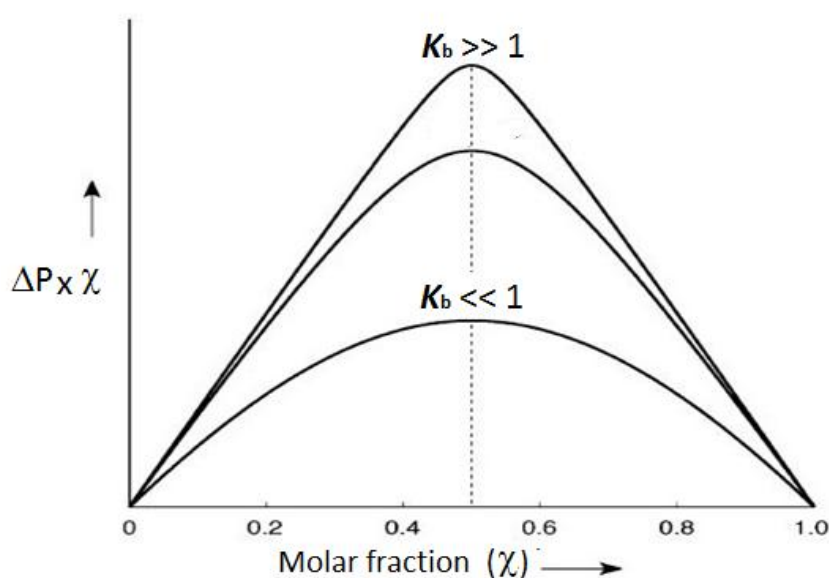
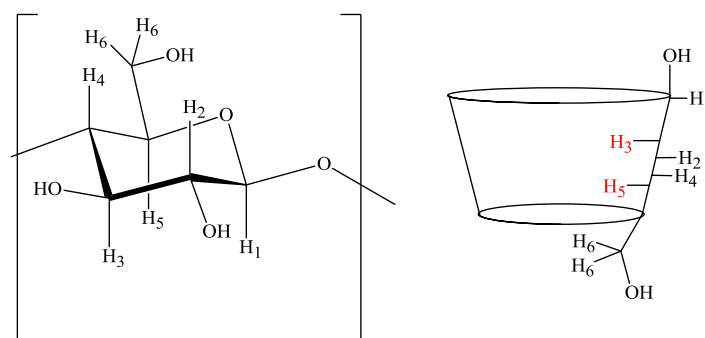


Figure 3: A general form of a Job's plot for a 1:1 complex showing the difference in curvature shape when  $K_b \ll 1$  and,  $K_b \gg 1$ .

## 1.2.2 1D NMR studies of CD complexes

The simplest NMR experiment for studying an inclusion complex is to monitor the changes in the proton chemical shifts between the free host and guest species and the putative complex. Thakkar and Demarco described an NMR method for examining the mode of interaction of CDs with a variety of aromatic substrates.<sup>59, 60</sup> Their method is based upon the rationale that when an aromatic guest is incorporated inside the cavity of the CD molecule, protons located within the cavity (H<sub>3</sub>, H<sub>5</sub> and, possibly, H<sub>6</sub>), (see Figure 4), undergo a noticeable shift in their <sup>1</sup>H NMR signals due to the anisotropy of the aromatic moiety. On the other hand, protons which are oriented toward the outside of the CD cavity (H<sub>1</sub>, H<sub>2</sub>, and H<sub>4</sub>), are relatively unaffected. These induced variations in the chemical shifts could provide evidence for the formation of an inclusion complex in solution.<sup>61, 62</sup>



*Figure 4: Orientation of CD protons with respect to the cavity.*

Apart from qualitative information, NMR titration experiments can lead to valuable information not just for how the host and guest(s) interact, but can also be used to quantitate how strong this interaction is. Indeed, values exceeding  $10^5$  for the equilibrium binding constant  $K_b$  can be estimated using modern NMR instruments from the observed induced chemical shifts ( $\Delta\delta$ ).<sup>63</sup> The induced chemical shift is defined as the difference in the chemical shift of a proton belonging to one molecule, in the presence and absence of another molecule.<sup>64</sup> In our case, the induced shifts were calculated by the following equation:  $\Delta\delta = \delta_{(\text{free})} - \delta_{(\text{complexed})}$ . In this convention, a positive sign of  $\Delta\delta$  designates an upfield shift in the presence of another molecule.

### 1.2.3 Determination of the binding constant $K_b$

The equilibrium constant ( $K$ ) for a complex formed between a host (H) and a guest (G) can be formulated from the general equilibrium reaction:



When the stoichiometry of a  $\beta$ -CD/guest complex is 1:1, the desired equilibrium (in this case binding) constant  $K_b$  is given by:

$$K_b = \frac{[HG]}{[H][G]} \quad (1)$$

Where  $[G]$  is the concentration of free guest,  $[H]$  is the concentration of free host, *i.e.*  $\beta$ -CD, and  $[HG]$  the concentration of the formed host/guest complex.

Because the complexation phenomenon is a dynamic equilibrium, the individual concentration of each species is not readily measurable. Instead of measuring separate concentrations, a well-known approach to determine the binding constant is to generate the binding curve then to deduce  $K_b$  via a regression analysis based on the Benesi-Hildebrand equation.<sup>65, 66</sup> A plot of  $1/\Delta\delta$  vs  $[G]$  establishes a straight line whose slope is directly related to the value of  $K_b$ , for a 1:1 - Guest:Host complex (see Figure 5). (For more details see index -A)

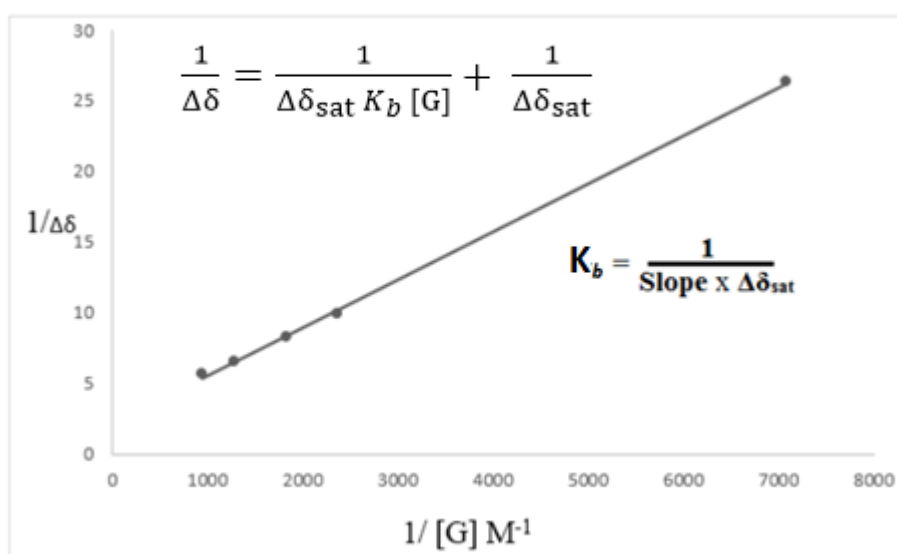
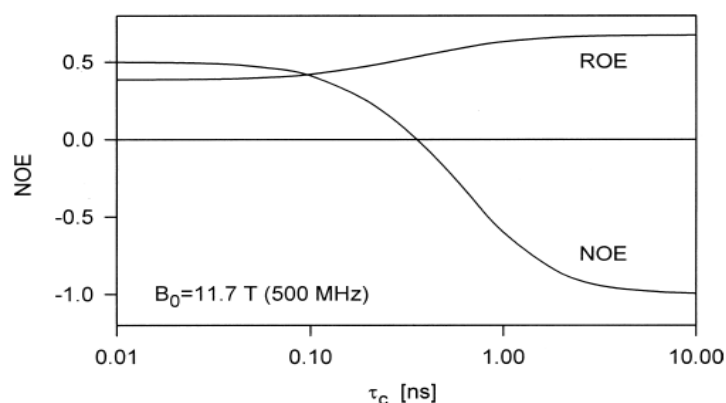


Figure 5: A plot of  $1/\Delta\delta$  vs  $1/[G]$ , based on the Benesi-Hildebrand equation.

### 1.2.3 2D NMR in the characterization of CD host/guest complexes

In order to investigate the geometry of a complex and to propose a mode of complexation between CD and a guest, 2D ROESY NMR experiments are very useful. At the level of NMR spectroscopy, nuclear spins can interact via both through-bond phenomena (spin-spin coupling) and through-space phenomena (dipolar coupling). The through-bond interaction is commonly observed as a split in the NMR signal and characterized by the coupling constant  $J$ . On the other hand, the through-space dipolar interactions do not split the NMR signal since the effect is completely averaged by the normal tumbling of molecules in isotropic solutions. Nevertheless, these dipolar interactions manifest themselves indirectly, generating the Nuclear Overhauser Effect (NOE).<sup>29</sup>

NOE magnitudes depend, among others, on the effective correlation times  $\tau_{\text{eff}}$  characterizing overall molecular tumbling and intramolecular motions. CD complexes with molecular masses around 1-2 kDa display  $\tau_{\text{eff}}$  of a fraction of a nanosecond and are placed near the transition between positive and negative NOEs. Fortunately NOE in the rotating frame (ROE) is always positive, (see Figure 6), thus becoming a method of choice in the studies of medium-sized molecules and complexes.<sup>67</sup> Consequently the (ROESY) pulse sequence is typically the NOE-based experiment of choice for CD complexes.<sup>68</sup>



*Figure 6: The variation of the  $^1\text{H}/^1\text{H}$  nuclear Overhauser effect (NOE) and rotating-frame Overhauser effect (ROE) with respect to correlation time  $\tau_c$ .*

In Rotating-frame Overhauser Effect Spectroscopy (ROESY) experiment, the spatial proximity between atoms of the host and guest molecules is obtained by observing the intermolecular dipolar cross-correlations. The intensities of the cross peaks are proportional

to  $1/r^6$ , where  $r$  is the mean distance between the protons in dipolar interaction.<sup>69</sup> A NOE cross-peak between a proton of a guest molecule and a proton of the CD moiety will be observed in a ROESY spectrum if these two protons are closer than 4 Å through space. Therefore, if the guest molecule is included in the CD cavity, NOE correlations between the protons of the guest and the protons (H<sub>3</sub>, H<sub>5</sub>, or H<sub>6</sub>) that appear in the CD inner cavity will be observed.<sup>62</sup>

Although 1D NMR titration experiments could provide evidence on the formation of an inclusion complex between two molecules, 2D NOESY or ROESY experiments are essential to understand the dynamics and the overall geometry of the inclusion complex.<sup>64</sup> Several research groups have relied on interpretation of 2D as well as the 1D (selective) ROESY spectra to extract valuable information on the mode of complexation of various organic guest molecules inside CD cavities.

For instance, Forgo and D'Souza used 1D ROE experiments to study the host-guest interactions of β-CD with *p*-nitrophenol (see Figure 7).<sup>70</sup> The selective excitation of H<sub>3'</sub> and H<sub>5'</sub> of *p*-nitrophenol shows a ROE correlation with H<sub>3</sub> and H<sub>5</sub> of the β-CD indicating that former set of protons are in close proximity to both H<sub>3</sub> and H<sub>5</sub>, placing this part of the *p*-nitrophenol molecule deep inside the β-CD cavity (see Figure 7 spectrum B). On the other hand, selective excitation of H<sub>2'</sub> and H<sub>6'</sub> of the *p*-nitrophenol shows a correlation only with H<sub>3</sub> indicating that this part of the *p*-nitrophenol molecule is located in a more shallow manner, towards the secondary face of the β-CD. (see Figure 8 spectrum C).

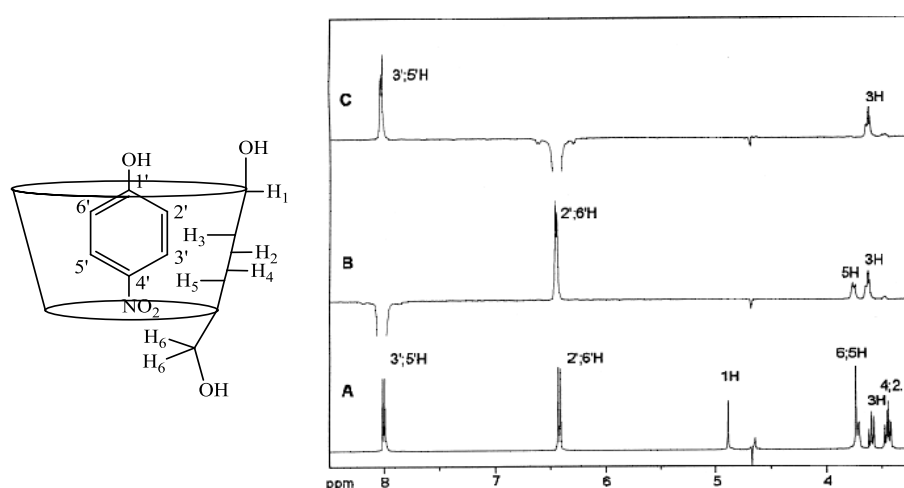
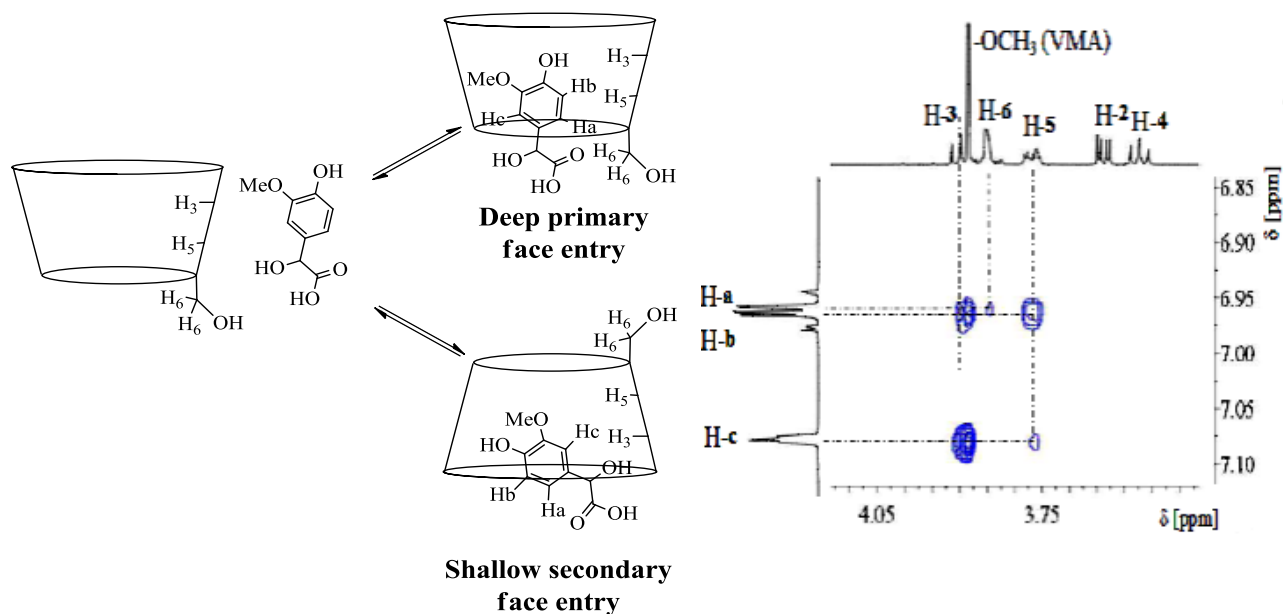


Figure 7: The proposed β-CD/*p*-nitrophenol complex (left), 1D selective ROE spectra (right).

Similarly, Korytkowska-Walach and coworkers,<sup>71</sup> studied the inclusion complexes formed between  $\beta$ -CD and vanillylmandelic acid (VMA), homovanillic acid (HVA) and vanillin (VA). The ROE correlations extracted from a 2D ROESY experiment allowed the authors to distinguish between partial and deep inclusion loci of the guest inside the CD, as well as on the face from which the guest enters the cavity (see Figure 8).



*Figure 8: The proposed inclusion complexes formed between  $\beta$ -CD and vanillylmandelic acid VMA (left), and the 2D ROESY spectrum leading to this proposal (right)*

## 1.3 $\gamma$ -Amino acids

Amino acids are elementary building blocks of the biological system. From a structural point of view, amino acids can be classified as  $\alpha$ ,  $\beta$ ,  $\gamma$ , *etc.*, depending on the relative position of the amino group ( $\text{-NH}_2$ ) with respect to the carboxylic acid ( $\text{-COOH}$ ) on the common carbon chain (see Figure 9).

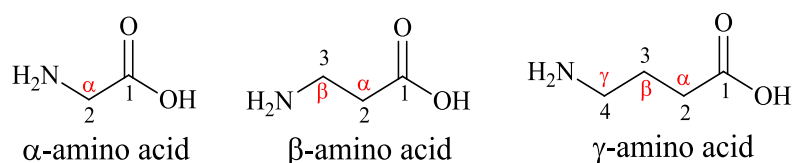


Figure 9: The  $\alpha$ -,  $\beta$ - and  $\gamma$ -amino acid backbones.

While  $\beta$ - and  $\gamma$ -amino acids are non-proteinogenic, they have a great importance in the field of biology and in medicinal chemistry.<sup>72, 73</sup>

### 1.3.1 GABA and constrained analogs

Structurally,  $\gamma$ -amino acids are sub-classified according to the position of the substituents they bear. For example, a  $\gamma$ -amino acid which is monosubstituted at the C-2 position is labelled a  $\gamma^2$ -amino acid, while a  $\gamma$ -amino acid which is disubstituted at its C-2 and C-3 positions is considered a  $\gamma^{2,3}$ -amino acid (see Figure 10).

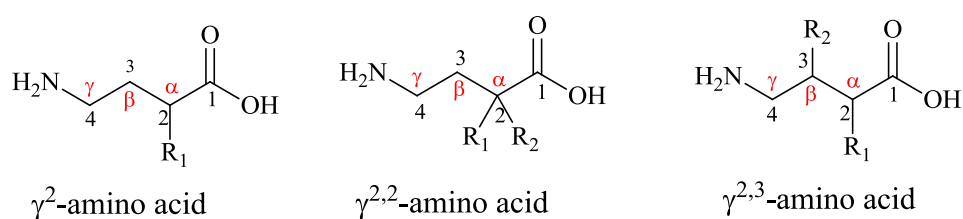


Figure 10: Three different structural sub-classes of  $\gamma$ -amino acids.

In the human body,  $\gamma$ -amino acids operate mainly as neurotransmitters. In particular, the parent compound  $\gamma$ -aminobutyric acid (GABA) serves as the principle inhibitory neurotransmitter of the central nervous system.<sup>74</sup> GABA also has an influence on different biological events during the nervous system development.<sup>75</sup> Abnormal levels of GABA in

the human brain have been correlated with serious neurological disorders such as epilepsy, anxiety,<sup>76</sup> schizophrenia,<sup>77</sup> and Alzheimer's disease.<sup>78</sup> Due to their potential significance in human biology and their potential applications in pharmacology,<sup>79</sup> GABA analogs have gained considerable attention over the past decades and a large number of strategies have been developed for their stereoselective synthesis.<sup>80</sup>

### 1.3.1.1 Constrained $\gamma$ -amino acids

$\gamma$ -Amino acids can be considered as doubly-homologated  $\alpha$ -amino acids, and as such the two extra carbons between the amine and carboxylic acid functions provide the backbone with more flexibility when compared to  $\alpha$ - and  $\beta$ -amino acids. Consequently, GABA can adopt many low-energy conformations, each one having its own specific biological relevance.

In order to acquire analogs that mimic a particular bioactive conformation of GABA, the synthesis of conformationally restricted GABA analogs has been of recent interest.<sup>81</sup> Various types of GABA analogs, both acyclic,<sup>82</sup> and cyclic,<sup>81</sup> have been reported in the literature. Figure 11 shows some of these analogs that act as agonists for specific GABA receptors. For example, *trans*-4-aminocrotonic acid (TACA) was more potent than GABA as a ligand for the ionotropic receptors GABA<sub>A</sub> and GABA<sub>C</sub>, but less potent for the metabotropic receptor GABA<sub>B</sub>.<sup>83, 84</sup> The *cis*-isomer (CACA) showed preferred binding to the GABA<sub>C</sub> receptor over GABA<sub>A</sub>, whereas 4-aminotetrolic acid (ATA) had the opposite selectivity profile.<sup>82</sup> *cis*-2-(Aminomethyl)cyclopropanecarboxylic acid ((+)-CAMP) was found to be a selective agonist of GABA<sub>C</sub>.<sup>85</sup> Gabapentin (GBP, Neurontin®) is a GABAergic agonist that has important anticonvulsant,<sup>86</sup> and analgesic<sup>87</sup> properties; on the other hand, Gabapentin lactam (GBP-L) is neuroprotective in retinal ischemia.<sup>88</sup>

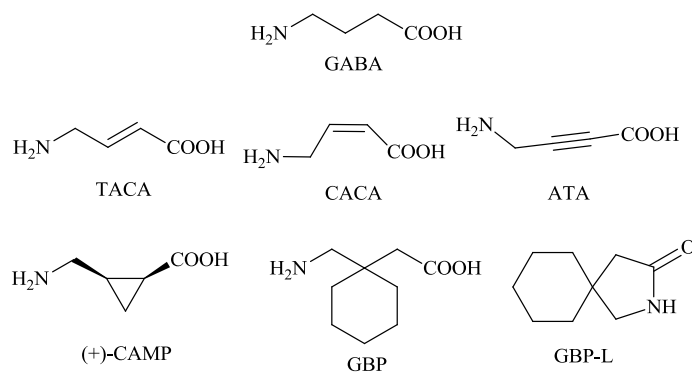


Figure 11: The parent  $\gamma$ -amino acid GABA and some of its bioactive constrained analogs.

### 1.3.1.2 GABA analogs in the field of foldamers

Aside from their biological importance as discrete molecules,  $\gamma$ -amino acids are also becoming increasingly popular as building blocks for peptidomimetics, in the form of  $\gamma$ -oligopeptides or of mixed  $\alpha,\gamma$ - or  $\beta,\gamma$ - hybrid peptides, because of the distinct, well-defined 3D folding patterns that these compounds can adopt (as will be discussed in more detail in Chapter 4).<sup>89, 90</sup>

Here again,  $\gamma$ -amino acids with cyclic constraints are of particular interest since their rigid backbones provide the severe conformational restrictions needed to impose well-defined low-energy conformations in  $\alpha,\gamma$ - and  $\beta,\gamma$ -hybrid peptides.<sup>91, 92</sup> Figure 12 shows examples of three,<sup>93</sup> four,<sup>94</sup> five,<sup>95</sup> and six<sup>96</sup> membered ring cyclic constrained  $\gamma$ -amino acids which have been employed as building blocks for oligo-peptides that adopt well-defined 3D structures.<sup>90</sup>

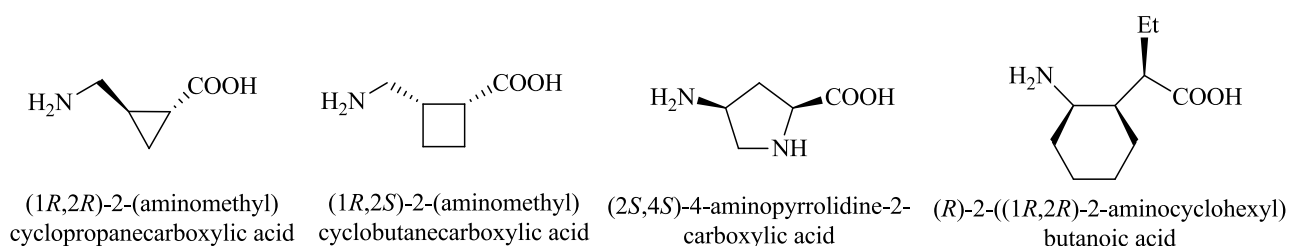


Figure 12: Example of different sized cyclic-constrained  $\gamma$ -amino acids used as building blocks for peptide foldamers.

### 1.3.2 Literature synthesis of *cis*- and *trans*-<sup>2,3</sup>CB-GABA

In this section we will focus our attention on two cyclobutane constrained  $\gamma$ -amino acids: 2-(aminomethyl)cyclobutanecarboxylic acid (<sup>2,3</sup>CB-GABA) and 2-(2-aminocyclobutyl)acetic acid (<sup>3,4</sup>CB-GABA) (see Figure 13).

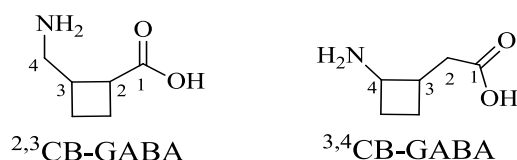
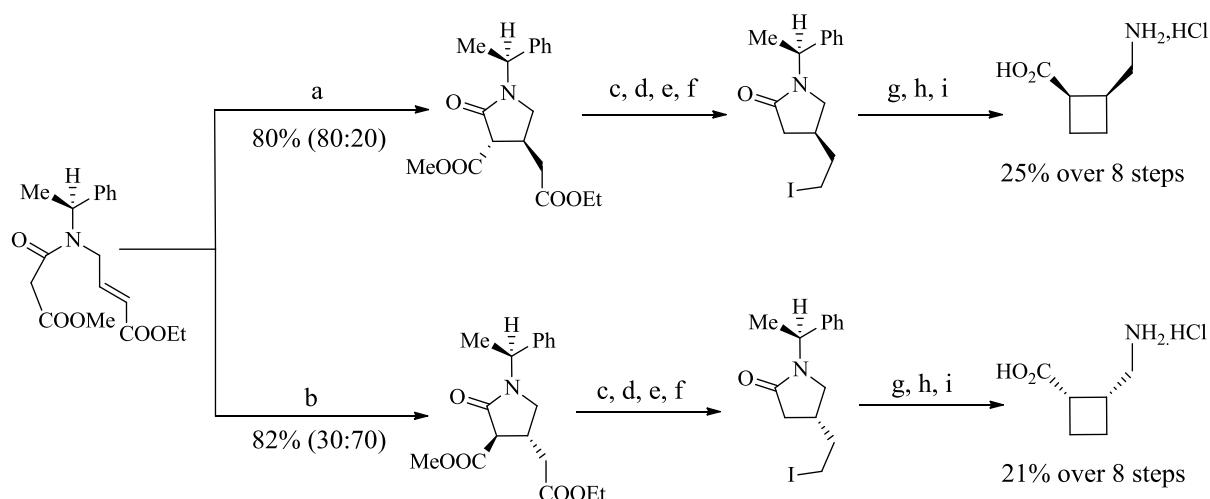


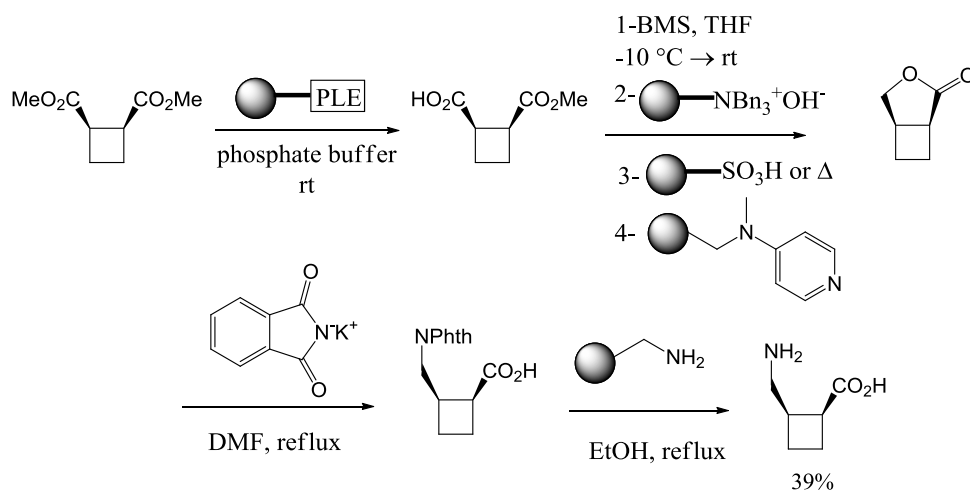
Figure 13: The constrained  $\gamma$ -amino acids of interest: <sup>2,3</sup>CB-GABA and <sup>3,4</sup>CB-GABA

The synthesis of *cis*-<sup>2,3</sup>CB-GABA in enantiomerically pure form was described in 1999 by the Orena group following a lengthy procedure (more than 8 steps), starting from (*S,E*)-ethyl 4-(3-methoxy-3-oxo-*N*-(1-phenylethyl)propanamido)but-2-enoate (see Scheme 18).<sup>97</sup>



Scheme 18: The Orena group's access to both enantiomers of *cis*-<sup>2,3</sup>CB-GABA. Conditions: a) NaH, THF, -78 °C; b) NaOEt, EtOH, -78 °C; c) DMF, NaCl, 80 °C; d) LiBH<sub>4</sub>, THF, 0 °C; e) MsCl, Et<sub>3</sub>N, DMAP, CH<sub>2</sub>Cl<sub>2</sub>, 0 °C; f) NaI, acetone, r.t; g) LiHMDS, THF, -15 °C, 12 h; h) Li-NH<sub>3</sub>, -78 °C i) 1M HCl, 82 °C, 12 h.

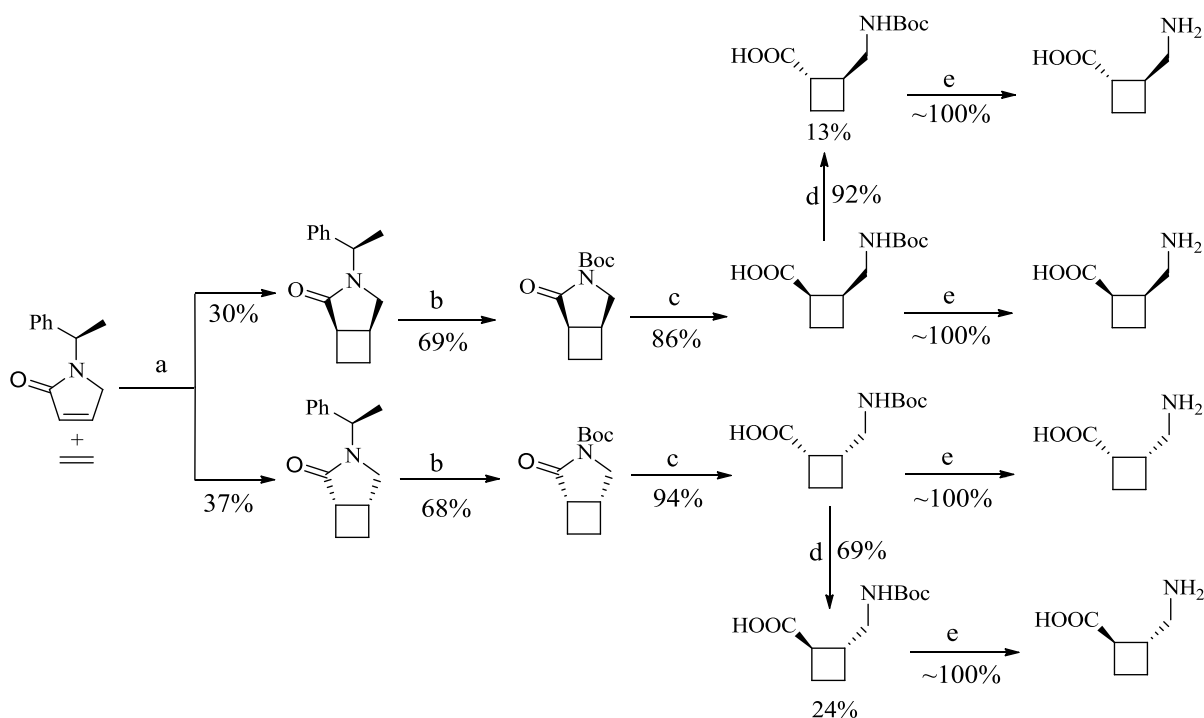
Later, the Ley group used polymer supported enzymes and reagents in order to access only the (1*S*,2*R*) enantiomer of the *cis*-<sup>2,3</sup>CB-GABA starting from (1*R*,2*S*)-dimethyl cyclobutane-1,2-dicarboxylate (see Scheme 19).<sup>98</sup>



PLE: Pig liver enzyme

*Scheme 19: The Ley group's access to (1S,2R)-cis-2,3CB-GABA.*

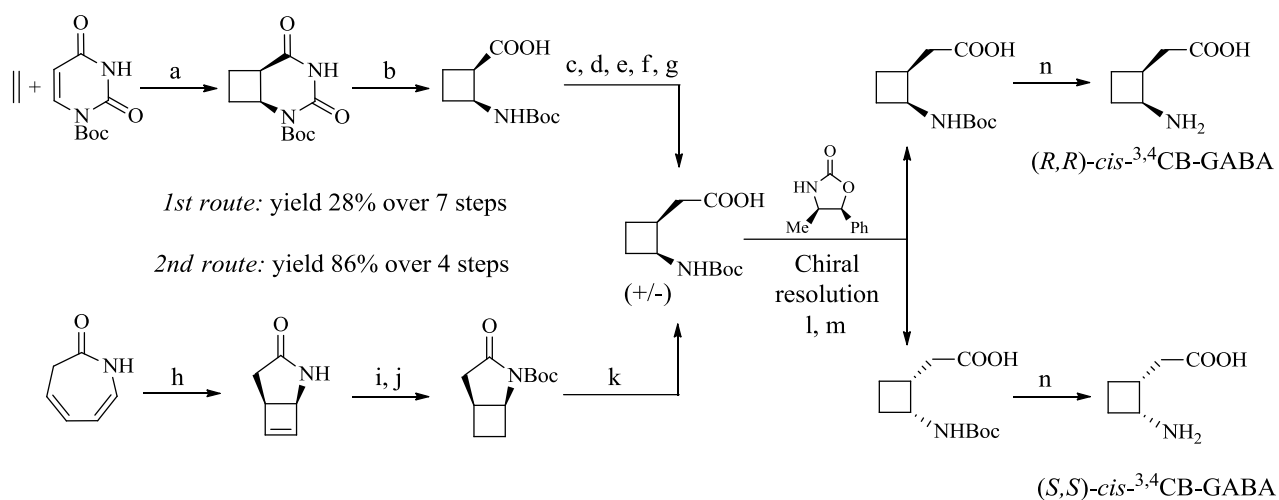
More recently, the Aitken group established a synthetic route that allowed access to both enantiomers of *cis*- and both enantiomers of *trans*-<sup>2,3</sup>CB-GABA.<sup>99, 100</sup> The synthesis began with via a the photochemical [2+2]-cycloaddition reaction of (*R*)-1-(1-phenylethyl)-2,5-dihydro-1*H*-pyrrole with ethylene, which provided the bicyclic photoadduct with an exclusive *cis* geometry and as a mixture of two diastereoisomers which were separated by chromatography. Each of the two compounds obtained was transformed in three steps into *N*-Boc-*cis*-<sup>2,3</sup>CB-GABA in single enantiomer form. In turn, each *cis* derivative was subjected to an epimerization protocol to furnish the corresponding *trans* compound, in enantiomerically pure form (see Scheme 20).



Scheme 20: The Aitken group's access to all four stereoisomers of <sup>2,3</sup>CB-GABA. Conditions: a) *hv*, acetone, 9 h; b) (i) Na, NH<sub>3</sub> (l), *t*-BuOH; (ii) Boc<sub>2</sub>O, DMAP, CH<sub>3</sub>CN; c) (i) LiOH, H<sub>2</sub>O, THF; (ii) H<sub>3</sub>O<sup>+</sup>; d) 6 M NaOH, MeOH, Δ, 16 h e) (i) TFA, CH<sub>2</sub>Cl<sub>2</sub>; ii) Dowex-H<sup>+</sup>

### 1.3.3 Literature synthesis of *cis*- and *trans*-<sup>3,4</sup>CB-GABA

In the literature, access to *cis*- and *trans*-<sup>3,4</sup>CB-GABA, each in racemic form, was described in 1982 by Kennewell and co-workers through a lengthy procedure starting from *cis* and *trans*-cyclobutane-1,2-dicarboxylic acids, respectively.<sup>101</sup> More recently, in order to improve the availability of these conformationally restricted cyclobutane analogues of GABA, our groups jointly reported two complementary synthetic routes that provided practical access to both enantiomers of *cis*-<sup>3,4</sup>CB-GABA (see Scheme 21).<sup>102</sup>



*Scheme 21: The two routes to both enantiomers of cis-<sup>3,4</sup>CB-GABA. Conditions: a) hv, acetone, rt, 4 h; b) NaOH (3M), rt, 14 h; c) DCC, DMAP, MeOH, 0 °C to r.t., 20 h; d) NaBH<sub>4</sub>, EtOH, 1 h, reflux; e) MsCl, Et<sub>3</sub>N, Et<sub>2</sub>O, 24 h, rt; f) NaCN, DMSO, 3 d, < 40 °C; g) NaOH, EtOH, 3.5 h, reflux; h) hv, quartz EtOH, rt, 3 h; i) H<sub>2</sub> Pd/C, EtOH, 16 h, rt; j) Boc<sub>2</sub>O, DMAP, CH<sub>3</sub>CN, 16 h, rt; k) LiOH, THF/H<sub>2</sub>O 16 h, rt; l) (i) PivCl, Et<sub>3</sub>N, THF, 1h, 0 °C; (ii) *n*-BuLi, THF, 1h, -75 °C; m) (i) separation on silica; (ii) LiOH, H<sub>2</sub>O<sub>2</sub>, THF/H<sub>2</sub>O, 16 h, rt n) (i) TFA, CH<sub>2</sub>Cl<sub>2</sub>; ii) Dowex-H<sup>+</sup>*

The first route involved a homologation strategy that started with the photochemical [2+2]-cycloaddition reaction of Boc-uracil with ethylene, which provided a single bicyclic photoadduct with an exclusive *cis* geometry. Basic hydrolysis of this photoadduct led to the known *N*-Boc derivative of ( $\pm$ )-*cis*-2-aminocyclobutanecarboxylic acid.<sup>103</sup> This cyclic  $\beta$ -amino acid derivative was then homologated in five steps to provide the *N*-Boc derivative of ( $\pm$ )-*cis*-<sup>3,4</sup>CB-GABA. The second route started with the known photochemical 4 $\pi$ -electrocyclization of azepinone (see Scheme 21).<sup>102</sup> The photoadduct was then transformed in three steps into the same *N*-Boc derivative of ( $\pm$ )-*cis*-<sup>3,4</sup>CB-GABA that was obtained from the first route. The second route employed fewer steps and had a better overall yield than the first one.

The chiral resolution of ( $\pm$ )-*N*-Boc-*cis*-<sup>3,4</sup>CB-GABA was then described, using (4*S*,5*R*)-4-methyl-5-phenyloxazolidin-2-one as a chiral auxiliary (See Scheme 21).<sup>102</sup> This endeavor required considerable effort; it was first necessary to identify the satisfactory chiral auxiliary, which then had to be prepared synthetically. The resolution protocol itself

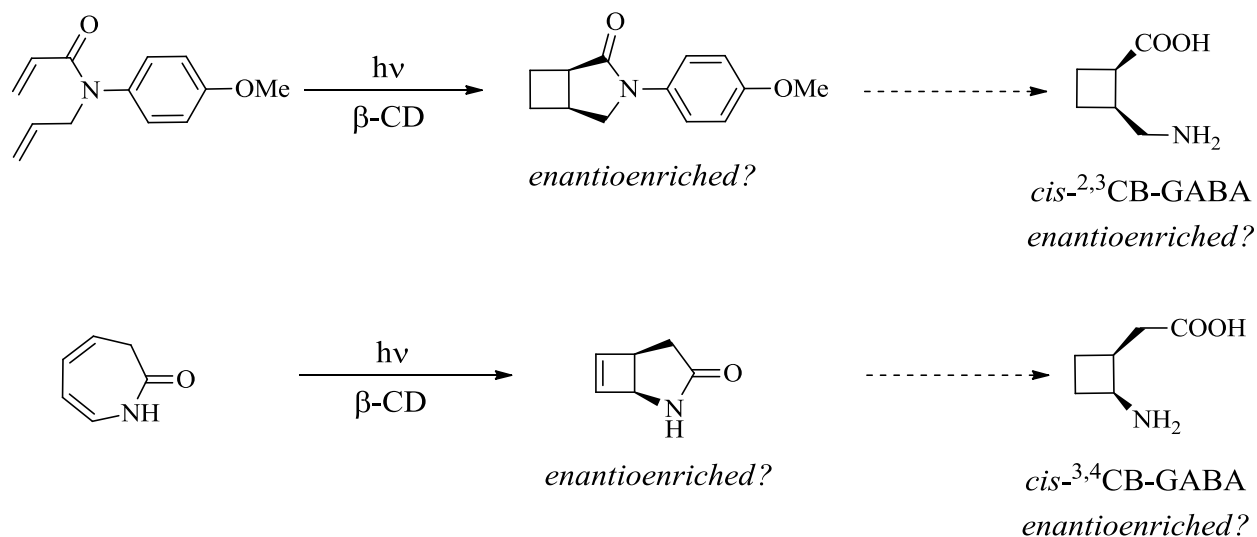
required three steps: coupling of the racemic  $\gamma$ -amino acids derivative with the oxazolidinone, tedious chromatographic separation of the two diastereoisomeric adducts, then cleavage of the chiral oxazolidinone from each, to provide both enantiomers of *N*-Boc-*cis*-<sup>3,4</sup>CB-GABA.

## 1.4 Aims of this project

In this work we sought to explore alternative synthetic strategies which might provide more convenient and/or efficient access to *cis*-<sup>2,3</sup>CB-GABA and *cis*-<sup>3,4</sup>CB-GABA in enantiomerically pure form. It was our intention to use these molecules as building blocks to prepare new mixed peptide sequences and to study these peptides for their foldamer behavior.

We indicated above that photochemical strategies, used in conjunction with covalently attached chiral motifs, can provide access to enantiopure *cis*-<sup>2,3</sup>CB-GABA and *cis*-<sup>3,4</sup>CB-GABA. In these preparations, chiral information is employed either in an “early-stage” role, such as in the synthesis presented in Scheme 20, or in a “late-stage” role, such as in the resolution protocol in Scheme 21. However, in each case the chiral fragment is (temporarily) attached covalently to the requisite  $\gamma$ -amino acid fragment, which implicates the formation of diastereoisomer mixtures at some point in the synthesis and the consequent requirement of diastereoisomeric separation by chromatography.

We considered that the enantioselective synthesis of *cis*-<sup>2,3</sup>CB-GABA and *cis*-<sup>3,4</sup>CB-GABA derivatives warranted study. The clear advantage of this approach would be that the covalent attachment (and subsequent removal) of chiral auxiliaries would not be required, nor would chromatographic separation of diastereoisomeric pairs be necessary. Towards this objective, as a contribution to the growing area of photochirogenesis, we decided to investigate the use of  $\beta$ -CD as a readily-available, chiral supramolecular host for pertinent enantioselective photochemical transformations (see Scheme 22). The intramolecular photochemical [2+2]-cycloaddition of an *N*-allyl *N*-aryl acrylamide in the presence of  $\beta$ -CD might provide access to a bicyclic adduct in enantioenriched form, leading to enantioenriched *cis*-<sup>2,3</sup>CB-GABA. The photochemical  $4\pi$ -electrocyclization of azepinone in the presence of  $\beta$ -CD might provide access to the known bicyclic adduct in enantioenriched form, leading to enantioenriched *cis*-<sup>3,4</sup>CB-GABA.



Scheme 22: The proposed photochirogenic reactions in the presence of  $\beta\text{-CD}$ , leading towards *cis*-<sup>2,3</sup>CB-GABA (top) and *cis*-<sup>3,4</sup>CB-GABA (bottom) in enantioenriched form.

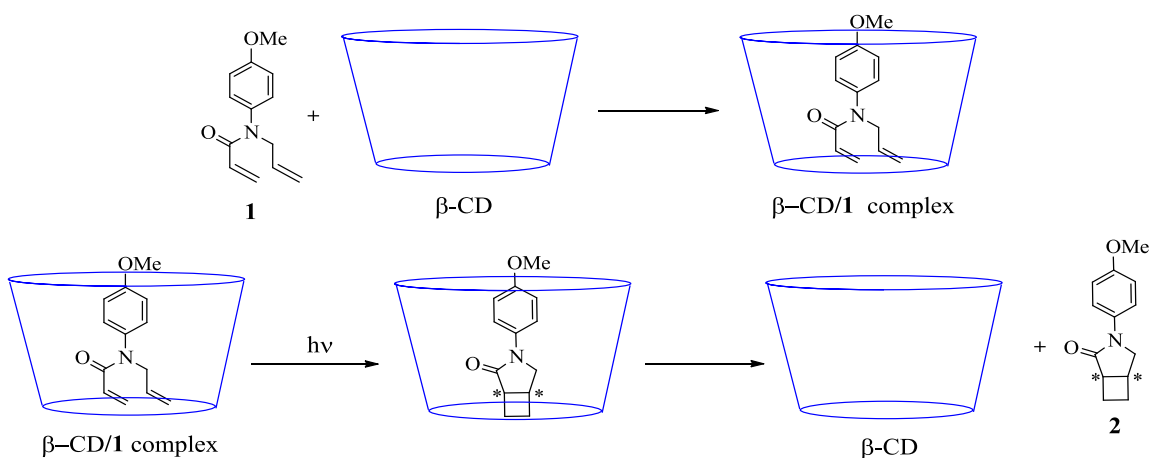
We proposed to use the enantiomerically-pure CB-GABA derivatives obtained above to prepare  $\gamma/\alpha$ -hybrid peptides and study their conformational behavior in solution.

# Chapter 2: The Photochemical Reactivity of *N*-Allyl-*N*-(4-methoxyphenyl)acrylamide

## 2.1 Introduction

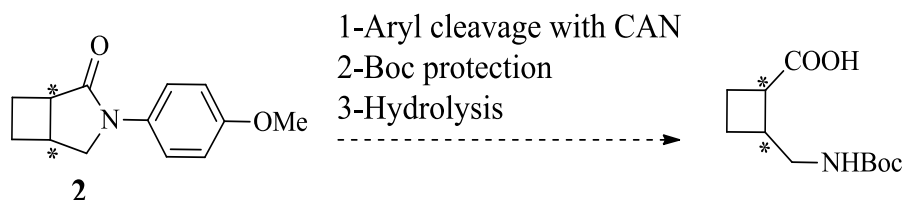
Organic chemists are constantly on the lookout for new methodologies for the synthesis of compounds with biological significance. *N*-allylacrylamide derivatives have been studied for the construction of heterocyclic compounds with multiple stereocenters, of interest as drugs or bioactive reagents, using regioselective ring-closing metathesis reactions (RCM)<sup>104</sup> or palladium-catalyzed tandem cyclization reactions.<sup>105</sup> Enantioselective photochemical cycloaddition reactions of *N*-allylacrylamide derivatives have not been previously studied, but might constitute a “green” synthetic methodology for preparing heterocyclic compounds. Bicyclic lactams, such as the particular intermediate we target below, are of considerable synthetic interest in this respect.

In this chapter we set out to establish a new synthetic access to *cis*-<sup>2,3</sup>CB-GABA derivatives, based on the anticipated enantioselective intramolecular photochemical [2+2]-cycloaddition of an *N*-allylacrylamide derivative hosted inside the chiral cavity of  $\beta$ -CD. The selected *N*-allylacrylamide derivative was *N*-allyl-*N*-(4-methoxyphenyl)acrylamide, **1** (see Scheme 23). The methoxyphenyl group was chosen in order to favor the inclusion of compound **1** inside the hydrophobic (and asymmetric) cavity of the  $\beta$ -CD.



*Scheme 23: The proposed enantioselective intramolecular [2+2]-photocycloaddition of compound 1 in the presence of  $\beta$ -CD.*

In our work, it was expected that, following the [2+2] photocycloaddition, the methoxyphenyl group could be easily removed.<sup>106</sup> Compound **2** should therefore be transformed in only a few steps into the known *N*-Boc protected derivative of *cis*-<sup>2,3</sup>CB-GABA (see Scheme 24).



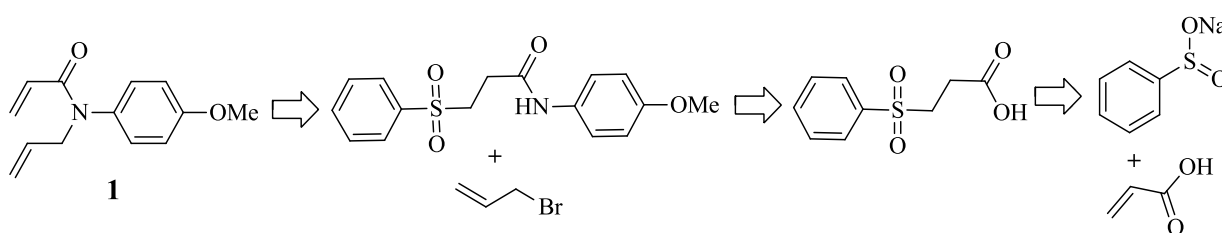
*Scheme 24: Transformation of the anticipated photoadduct 2 into a *cis*-<sup>2,3</sup>CB-GABA derivative.*

Our first objective in this chapter was to synthesize *N*-allyl-*N*-(4-methoxyphenyl)acrylamide. Thereafter, a study of its host-guest interactions with  $\beta$ -CD was envisaged, followed by an assessment of its photochemical reactivity: both alone and in the presence of  $\beta$ -CD. Finally, the transformation of the anticipated cycloadduct to provide enantioenriched *cis*-<sup>2,3</sup>CB-GABA would be carried out.

## 2.2 Results and discussion

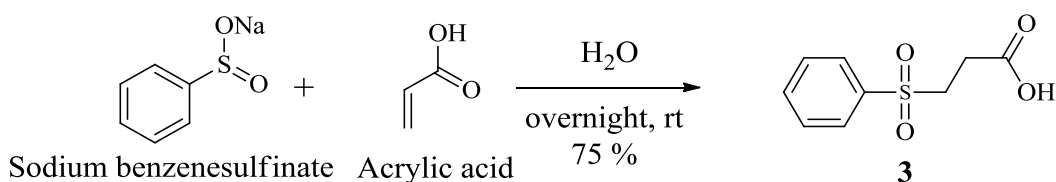
### 2.2.1 Synthesis of *N*-allyl-*N*-(4-methoxyphenyl)acrylamide **1**

A short synthesis of *N*-allyl-*N*-(4-methoxyphenyl)acrylamide **1** has been described, requiring as a starting material the unstable, not readily-available, toxic reagent acryloyl chloride.<sup>104</sup> We preferred to circumvent use of this reagent, and applied instead a variation of the literature procedures described by Bonete,<sup>107</sup> and Wang,<sup>108</sup> following the retrosynthetic approach depicted in Scheme 25.



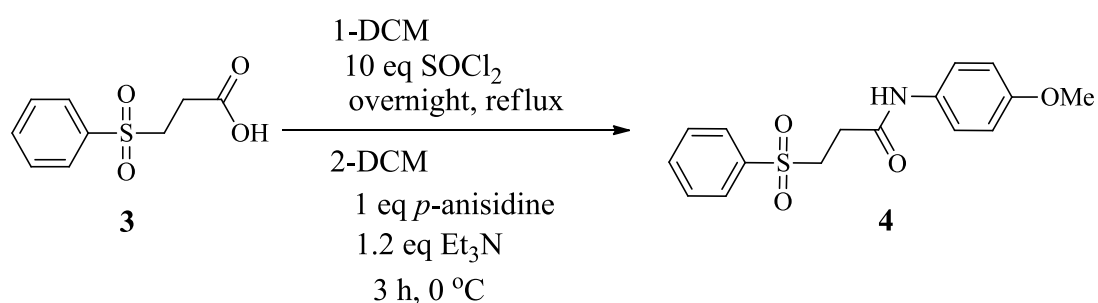
*Scheme 25: Retrosynthetic analysis for the preparation of *N*-allyl-*N*-(4-methoxyphenyl)acrylamide **1**.*

The first step was the Michael addition of benzenesulfinate anion to acrylic acid, performed by stirring the reagents together in water overnight (see Scheme 26). In the literature procedure, 90% ethanol had been used as the solvent, however we encountered solubility problems in various ethanol/water mixtures. The use of water as the solvent greatly simplified the reaction. After the reaction time, the suspension was acidified with 2 M HCl and the desired product, 3-(phenylsulfonyl)propanoic acid **3**, was extracted using diethyl ether. The organic layer was concentrated to give compound **3** as a white solid with a yield of 75%. The product **3** was used in the next step without further purification.



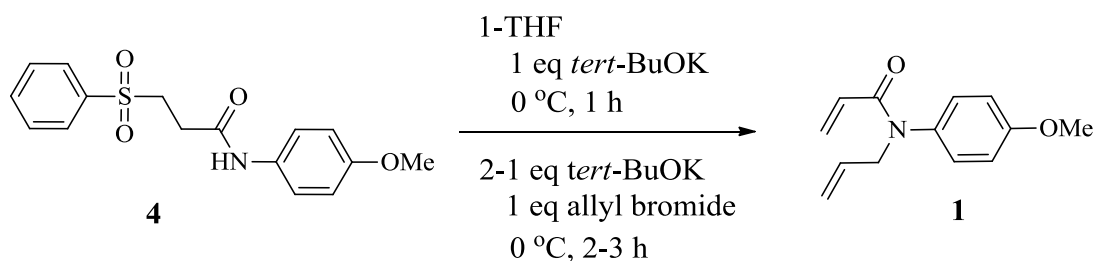
*Scheme 26: Synthesis of 3-(phenylsulfonyl)propanoic acid, **3**, from sodium benzenesulfinate and acrylic acid.*

The second step involved the conversion of the carboxylic acid group of **3** into an acyl chloride by refluxing it overnight with a large excess of thionyl chloride in dry dichloromethane (see Scheme 27). The solvent along with the excess of thionyl chloride were then distilled out under vacuum. The remaining yellowish solid, crude 3-(phenylsulfonyl)proanoyl chloride, was used without isolation or further purification and was reacted with *p*-anisidine in the presence of triethylamine in dry dichloromethane at 0 °C to give *N*-(4-methoxyphenyl)-3-(phenylsulfonyl)propanamide **4** in 85% yield over the two steps. Compound **4** was pure enough to be used in the next step without any purification.



*Scheme 27: The synthesis of N-(4-methoxyphenyl)-3-(phenylsulfonyl)propanamide from 3-(phenylsulfonyl)propanoic acid.*

Making use of the phenylsulfonyl group as leaving group, the third step involved a one pot elimination in the presence of potassium *tert*-butoxide (Scheme 28), followed by addition of allyl bromide in a nucleophilic substitution to give crude compound **1**, *N*-allyl-*N*-(4-methoxyphenyl)acrylamide. The final product was purified by silica gel chromatography, and isolated with an overall yield of 60%.



*Scheme 28: The synthesis of N-allyl-N-(4-methoxyphenyl)acrylamide, 1, from N-(4-methoxyphenyl)-3-(phenylsulfonyl)propanamide, 4.*

It is important to note that compound **1** showed a tendency to polymerize into an insoluble hard solid, so it was important for it not to be in contact with traces of acids, nor be heated above 25 °C while evaporating the solvent after chromatography.

## 2.2.2 The $\beta$ -CD/ *N*-allyl-*N*-(4-methoxyphenyl)acrylamide **1** complex

### 2.2.2.1 Formation of the $\beta$ -CD/**1** complex

Unlike common examples of  $\beta$ -CD complex formation,<sup>109</sup> mixing *N*-allyl-*N*-(4-methoxyphenyl)acrylamide **1** with  $\beta$ -CD in water at a 15 mM concentration, did not result in the formation of a precipitate. In order to prepare a  $\beta$ -CD/**1** complex, we therefore added one equivalent of solid compound **1** to a clear (5 ml, 15 mM, 1 eq) aqueous solution of  $\beta$ -CD. The mixture was heated to 35-40 °C and left to stir for 5 min, during which time **1** dissolved completely. The resulting clear solution was stirred at room temperature for 2 hours then spread on a glass plate and left to evaporate to give a white clear film (see Figure 14).



*Figure 14: The white film (complex) of *N*-allyl-*N*-(4-methoxyphenyl)acrylamide with  $\beta$ -CD.*

### 2.2.2.2 Evidence of complexation by powder X-ray diffraction

In order to confirm the formation of a complex between **1** and  $\beta$ -CD, a powder X-ray diffraction analysis was done. Three samples were compared:  $\beta$ -CD alone, compound **1** alone, and the white film ( $\beta$ -CD/**1** complex), as shown in Figure 17.

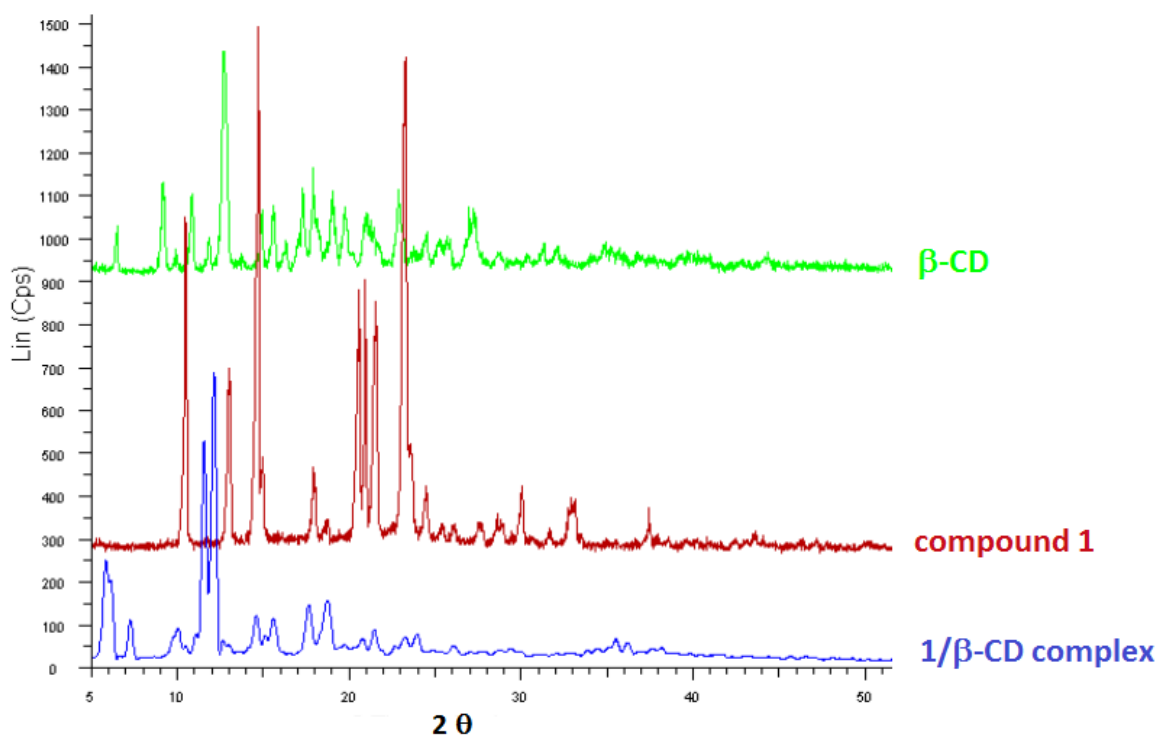


Figure 15: Powder X-ray diffraction spectra of  $\beta$ -CD, compound **1**, and  $\beta$ -CD/**1** complex

The powder X-ray diffraction data obtained for the  $\beta$ -CD/**1** complex film, were different from the data obtained for each component alone. This provides support for the argument that we obtained a genuine complex, rather than a simple physical mixture of the two discrete substances.<sup>110</sup>

### 2.2.2.3 Determination of the complex stoichiometry

Job's method of continuous variation was used to investigate the stoichiometry of the  $\beta$ -CD/**1** complex. Two separate 10 mL (0.9 mmol) mother solutions were prepared in water, one of  $\beta$ -CD and the other of **1**. Specific volumes of each solution were taken and mixed in different proportions to prepare eleven sample solutions (each 2 ml) covering the range of mole ratios  $0 < \chi = \frac{[\text{compound } \mathbf{1}]}{[\text{compound } \mathbf{1}] + [\beta\text{-CD}]} < 1$

$$0 < \chi = \frac{[\text{compound } \mathbf{1}]}{[\text{compound } \mathbf{1}] + [\beta\text{-CD}]} < 1$$

The UV absorbance for each of the eleven sample solutions was recorded at  $\lambda = 228$  nm, and the difference in absorbance ( $\Delta A$ ) between compound **1** alone and in the presence of  $\beta$ -CD multiplied by the molar fraction ( $\chi$ ) was plotted against molar fraction ( $\chi$ ), as shown in Figure 16.

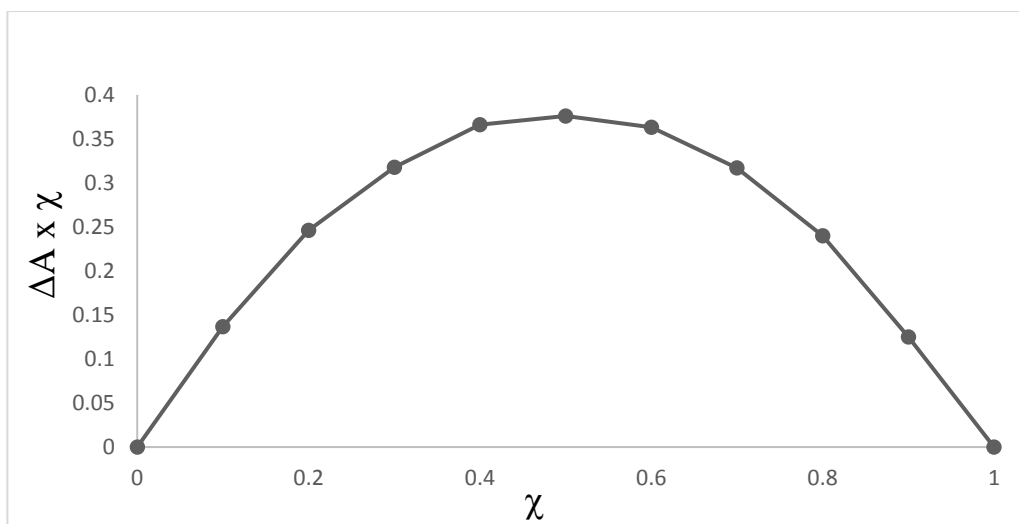


Figure 16: Job's plot of UV absorbance ( $\lambda = 228 \text{ nm}$ ) at different  $\beta\text{-CD}:\mathbf{1}$  molar ratios.

The maximum of the curve at  $\chi = 0.5$  validates a 1:1 stoichiometry in the complex formed upon mixing  $\beta\text{-CD}$  with compound **1** in aqueous solution. The rounded shape of the curvature also provides an indication that the equilibrium constant of the complexation reaction is of low magnitude.<sup>58</sup>

#### 2.2.2.4 1D NMR studies of the $\beta\text{-CD}/\mathbf{1}$ complex

To gain insight into the nature of the interactions between  $\beta\text{-CD}$  and compound **1**, an NMR titration experiment was done. Six different NMR tubes containing a solution of  $\beta\text{-CD}$  in  $\text{D}_2\text{O}$  at 7 mM were prepared. Each tube was prepared with a different equivalence of compound **1** to  $\beta\text{-CD}$  ranging from 0 equivalents in tube 1, to 2 equivalents in tube 6. Figure 17 shows the  $^1\text{H}$  NMR spectra for each tube.

Protons  $\text{H}_3$  and  $\text{H}_5$  of the  $\beta\text{-CD}$  cavity showed a gradual up-field shift with as the amount of compound **1** increased with respect to  $\beta\text{-CD}$ . At a 1:1 ratio, the change in the chemical shift reached 0.15 ppm for  $\text{H}_3$  and 0.2 ppm for  $\text{H}_5$ . On the contrary,  $\text{H}_1$ ,  $\text{H}_2$ ,  $\text{H}_4$  and  $\text{H}_6$  of  $\beta\text{-CD}$ , located outside the cavity, did not show any significant shift change throughout the titration. These observations can be interpreted as showing that compound **1** is being hosted inside the hydrophobic cavity of  $\beta\text{-CD}$ .

The induced shift  $\Delta\delta$ , defined as the difference in the chemical shift of a proton belonging to one molecule, in the presence and absence of another molecule,<sup>64</sup> were calculated by the following equation:  $\Delta\delta = \delta_{(\text{free})} - \delta_{(\text{complexed})}$  and are shown in Table 1. In this convention the positive sign of  $\Delta\delta$  designates an upfield shift.

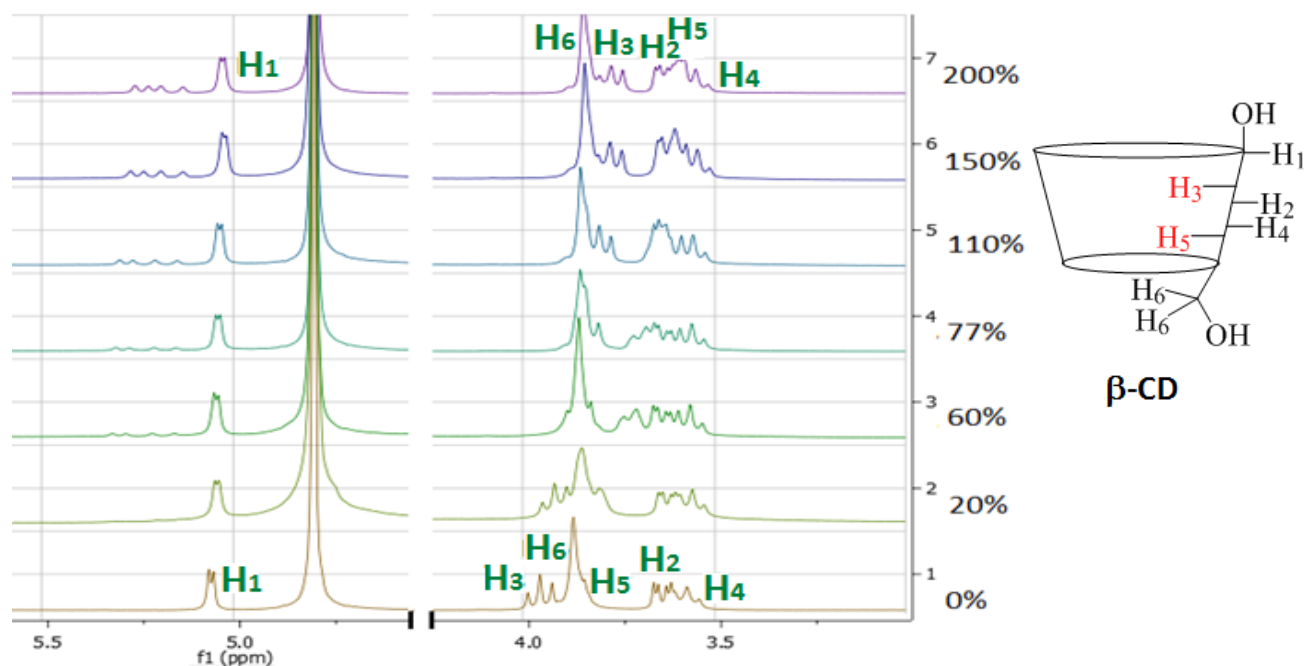


Figure 17:  $^1\text{H}$  NMR (in  $\text{D}_2\text{O}$  solution) of  $\beta\text{-CD}$  showing the shift of  $\text{H}_3$  and  $\text{H}_5$  with each increase in the percentage of compound **1** to  $\beta\text{-CD}$ .

$\beta\text{-CD}$ protons	1	2	3	4	5	6
$\Delta\delta$ (ppm) 0-100%	0.000	0.000	-0.15	0.000	-0.2	0.000

Table 1: The change in chemical shift ( $\Delta\delta$ ) of the  $\beta\text{-CD}$  protons between 0% and 100% of compound **1**.

On the other hand, all protons of compound **1** show a down-field shift except for  $\text{H}_d$  and  $\text{H}_{Ar2}$  which show an up field shift with each increase in the percentage of compound **1** to  $\beta\text{-CD}$ . It's also noteworthy that the multiplicity of  $\text{H}_c$  changes from a doublet in the free compound **1**, to a doublet of doublets in the presence of  $\beta\text{-CD}$  (see figure 18, and table 2).

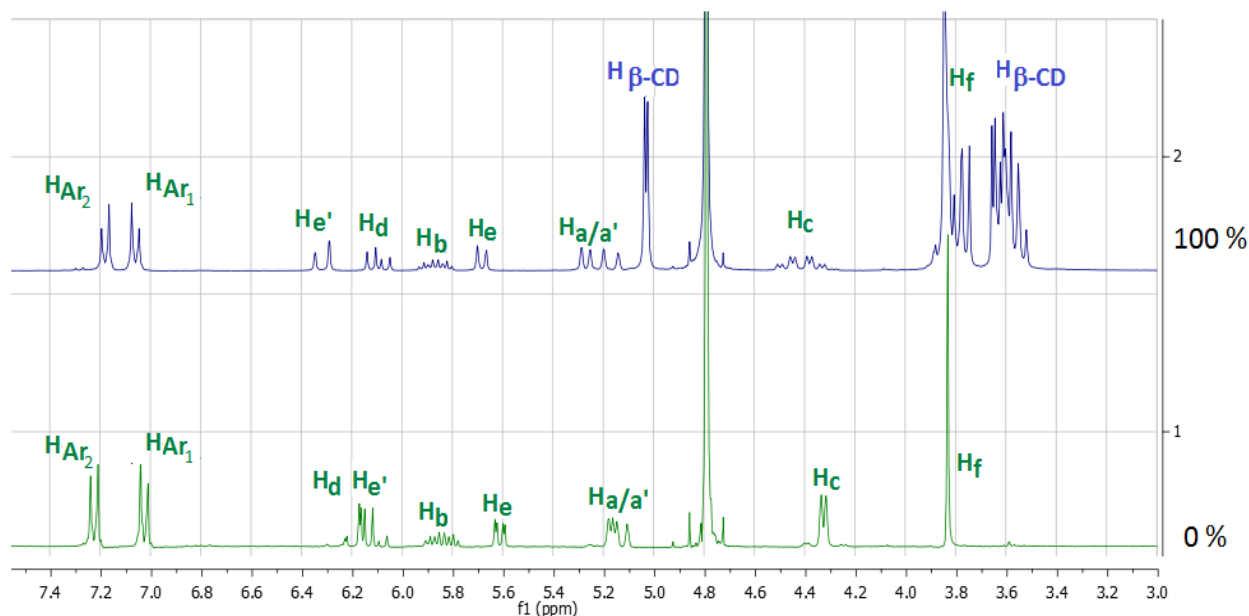
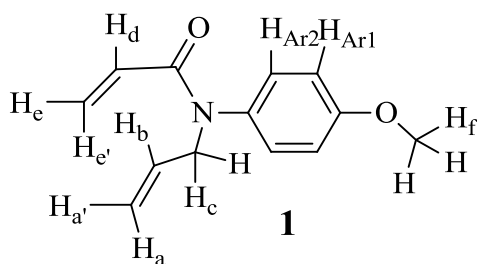


Figure 18:  $^1\text{H}$  NMR (in  $\text{D}_2\text{O}$  solution) of *N*-allyl-*N*-(4-methoxyphenyl)acrylamide (**1**) (bottom), and at 100% of **1** relative to  $\beta\text{-CD}$  (top).

Compound <b>1</b> protons	a	b	c	d	e	e'	f	Ar1	Ar2
$\Delta\delta$ (ppm) 0-100%	0.047	0.031	0.097	-0.009	0.081	0.175	not clear	0.041	-0.040

Table 2: The change in chemical shift ( $\Delta\delta$ ) of *N*-allyl-*N*-(4-methoxyphenyl)acrylamide (**1**) protons between 0% and 100% of compound **1** relative to  $\beta\text{-CD}$ .

The  $^1\text{H}$  NMR titration experiment showed that all the protons of compound **1** and only the inside protons of the  $\beta\text{-CD}$  cavity are affected during the course of the titration, suggesting that compound **1** may be bound, totally or partially, inside the hydrophobic cavity of  $\beta\text{-CD}$ .

By identifying the affected protons, one can have a partial idea about the geometry of the inclusion complex but a ROESY experiment would be needed to more understand the orientation of a guest inside the CD cavity.

### 2.2.2.5 Determination of the binding constant $K_b$

The NMR titration experiment data allowed to establish a linear plot of  $1/\Delta\delta_{H3}$  vs.  $1/[\text{compound } \mathbf{1}]$ , (see Figure 19). The straight line obtained, has a slope of  $1/(K_b \times \Delta\delta_{\text{sat}})$  and an intercept at  $1/\Delta\delta_{\text{sat}}$ , from which the binding constant  $K_b$  for the  $\beta$ -CD/  $\mathbf{1}$  complex was estimated to be 14.7.

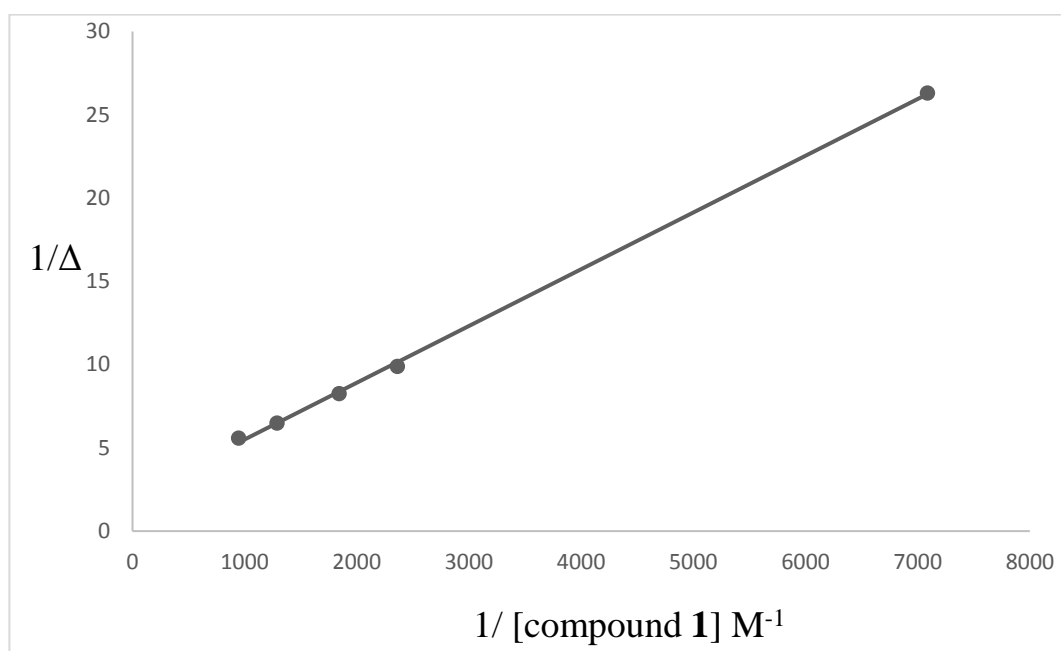


Figure 19: The linear plot of  $1/\Delta\delta_{H3}$  vs.  $1/[\text{N-allyl-N-(4-methoxyphenyl)acrylamide}]$

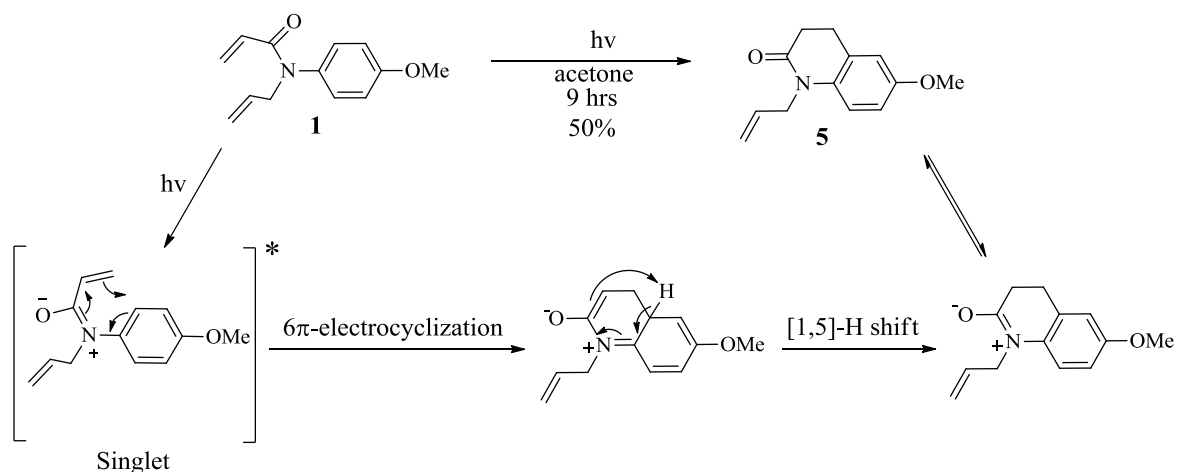
## 2.2.3 The photochemical reactivity of compound $\mathbf{1}$

### 2.2.3.1 Photoreactivity of compound $\mathbf{1}$ in solution, without $\beta$ -CD

Water was the solvent of choice for the photochemical transformation of  $\mathbf{1}$ , taking account of our intention to perform subsequent reactions in the presence of  $\beta$ -CD. However, when a 20 mM solution of  $\mathbf{1}$  in water was introduced into a Pyrex tube then irradiated in a Luzchem (LCZ-4V) reactor fitted with 14 UV-B (303 nm) lamps, no conversion was observed after 15 h of irradiation. The same lack of reactivity was observed when ether was used as the solvent in place of water.

When the reaction was carried out in the same conditions using acetone as the solvent, complete conversion of  $\mathbf{1}$  was achieved after 9 h irradiation. The solvent was evaporated and the crude residue was purified by silica gel column chromatography to give 1-allyl-6-

methoxy-3,4-dihydroquinolin-2(1*H*)-one **5** in a 50% yield. The desired 3-(4-methoxyphenyl)-3-azabicyclo[3.2.0]heptan-2-one **2** was not obtained. (see Scheme 29) NMR analyses and a single crystal X-ray diffraction study confirmed the molecular structure of **5** (see Figure 20). The formation of compound **5** from substrate **1** is the result of a  $6\pi$ -electron cyclization following photochemical excitation, giving a zwitterionic intermediate which undergoes a 1,5-sigmatropic shift to give compound **5**, as illustrated in Scheme 29.



*Scheme 29: The proposed mechanism for the formation of compound 5.*

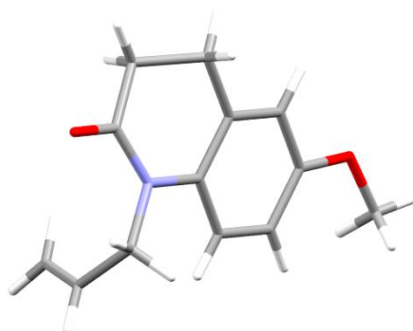
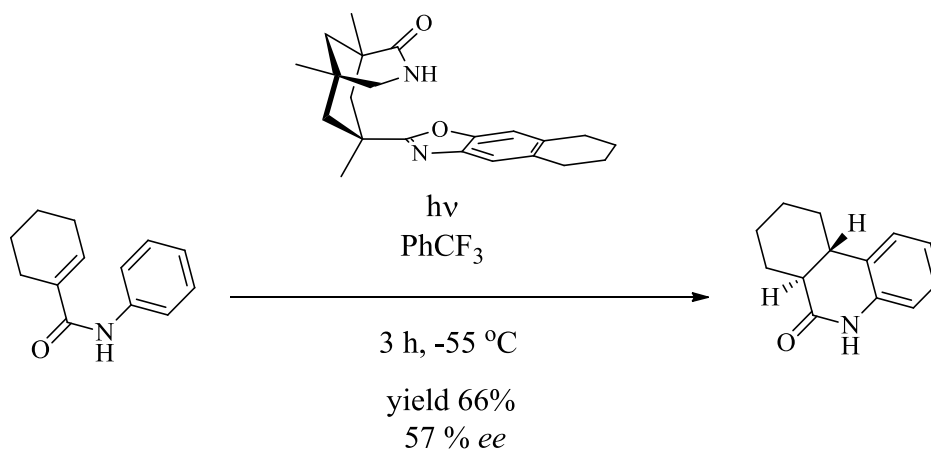


*Figure 20: The X ray crystal structure of compound 5.*

In compound **1** the resonance of the nitrogen lone pair gives the C-N bond of the acrylamide a partial double bond character which establishes a  $6\pi$ -electron system with the methoxyphenyl ring. Upon irradiation, compound **1** moves into a singlet excited state, at this stage there is a competition between a  $6\pi$ -electron conrotatory ring closure, and an evolution of the excited compound **1** into a triplet state. Due to an inefficient inter system

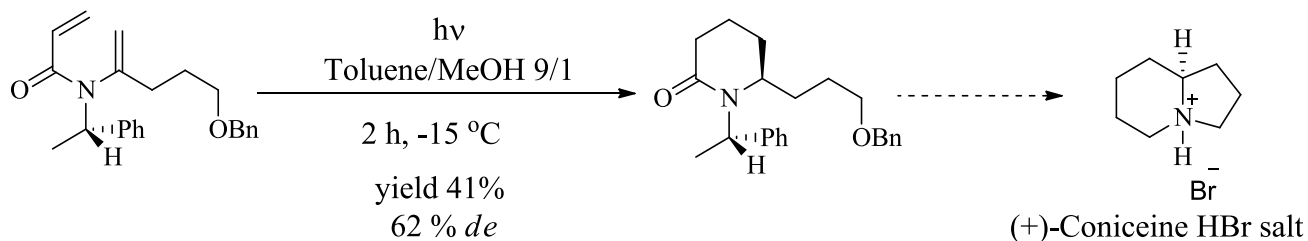
crossing only the latter is observed, favoring the formation of compound **5** over the anticipated compound **2**.

There are literature precedents for photochemical  $6\pi$ -photocyclization reactions of *N*-aryl  $\alpha,\beta$ -unsaturated carboxamides. they have been used to make quinolone or isoquinoline alkanoids derivatives. Enantiodifferentiating  $6\pi$ -photocyclization of *N*-phenylcyclohex-1-enecarboxamide was mediated by chiral template (see Scheme 30).<sup>111</sup>



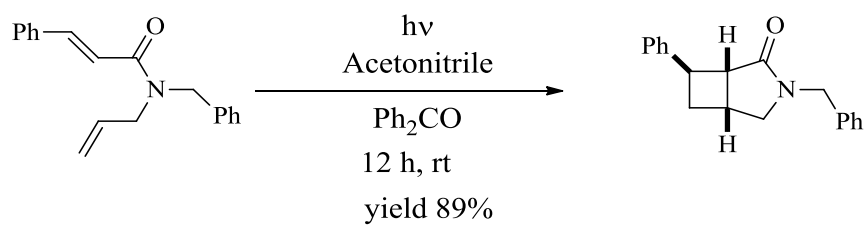
*Scheme 30: Chiral template mediated  $6\pi$ -photocyclization of *N*-phenylcyclohex-1-enecarboxamide.*

Analogously, non-aromatic reductive  $6\pi$ -photocyclization was used as a key step in a the total synthesis of (+)-coniceine as its HBr salt (see Scheme 31).<sup>112</sup>



*Scheme 31: The  $6\pi$ -photocyclization as a key step in the preparation of (+)-coniceine HBr salt.*

Interestingly, the photosensitized photochemical reaction of an *N*-allyl-*N*-benzylacrylamide derivative, which cannot participate in a  $6\pi$ -photocyclization, proceeds smoothly according to a [2+2]-cycloaddition to give a racemic mixture of the photoadduct. (see Scheme 32).<sup>113</sup>



*Scheme 32: The intramolecular [2+2]-cycloaddition N-allyl-N-benzylcinnamamide.*

As far as we are aware, the molecular structure of **1** is the first to provide a formal test case for the competition between the two different photochemical reactivity types, [2+2]-cycloaddition vs.  $6\pi$ -electrocyclization. In the present case, the latter reaction mode prevails.

## 2.3 Conclusion

Following our goal of developing an enantioselective route to *cis*-<sup>2,3</sup>CB-GABA, the objective of this chapter was to obtain compound **2** in enantioenriched form, via an enantioselective [2+2]-photocycloaddition of *N*-allyl-*N*-(4-methoxyphenyl)acrylamide **1** in the chiral environment of the  $\beta$ -CD cavity.

We first adapted a known synthetic procedure to obtain the substrate **1**, then determined the stoichiometry of its complex with  $\beta$ -CD to be 1:1  $\beta$ -CD/**1**. NMR spectroscopic studies suggested the formation of a deep-penetration inclusion complex, but with a relatively weak binding constant, estimated to have a value of  $K_b = 14.7 \text{ M}^{-1}$ .

However, when irradiated in water or ether, compound **1** showed no photoreactivity. Furthermore, in acetone, a photochemical  $6\pi$ -electrocyclization reaction took place, leading to the formation of compound **5**; no photochemical [2+2]-cycloaddition reactivity was in evidence.

At this point, it appeared that appropriate conditions for the proposed enantioselective synthesis were unlikely to be secured. The cumulated difficulties of modest host-guest binding, solvent incompatibility and competitive photochemical reactivity appeared to be insurmountable with our chosen substrate **1**.

It seems likely that a different substrate should be envisaged. The use of a carbamate or benzyl group instead of an aryl group on the nitrogen atom might eliminate the unwanted electrocyclization reactivity and allow the [2+2]-cycloaddition reactivity to prevail, while at the same time bestowing reasonable binding affinity of the substrate in the  $\beta$ -CD cavity (see Figure 21). Never the less, we halted our endeavor to access *cis*-<sup>2,3</sup>CB-GABA for the time being, and turned our attention to study the photochemical reactivity of 1,3-dihydro-2H-azepin-2-one a precursor of *cis*-<sup>3,4</sup>CB-GABA

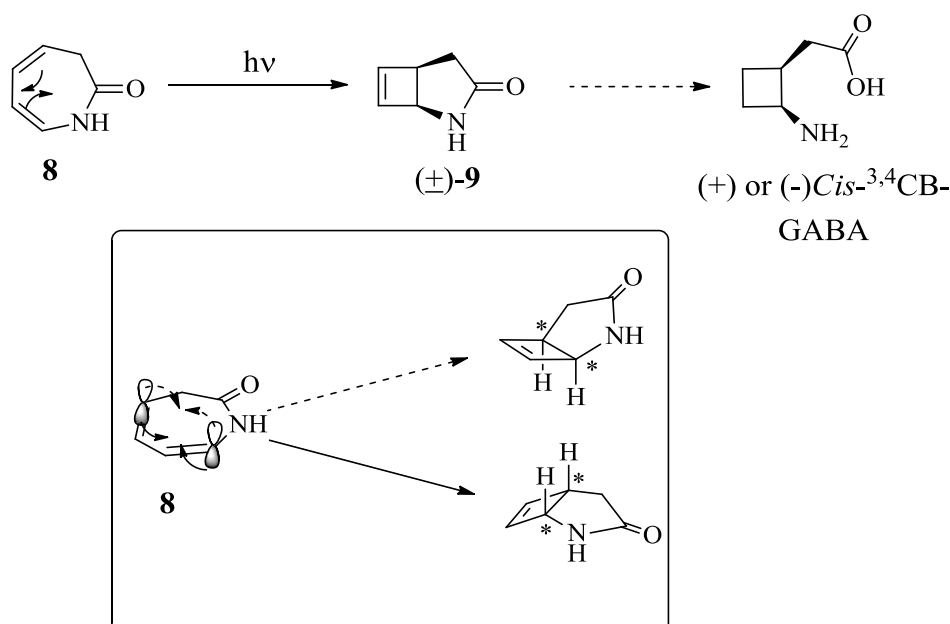


Figure 21: The benzyl (left), and carbamate (right) analogues of compound **1**.

# Chapter 3: The Photochemical Reactivity of 1,3-dihydro-2*H*-azepin-2-one

## 3.1 Introduction

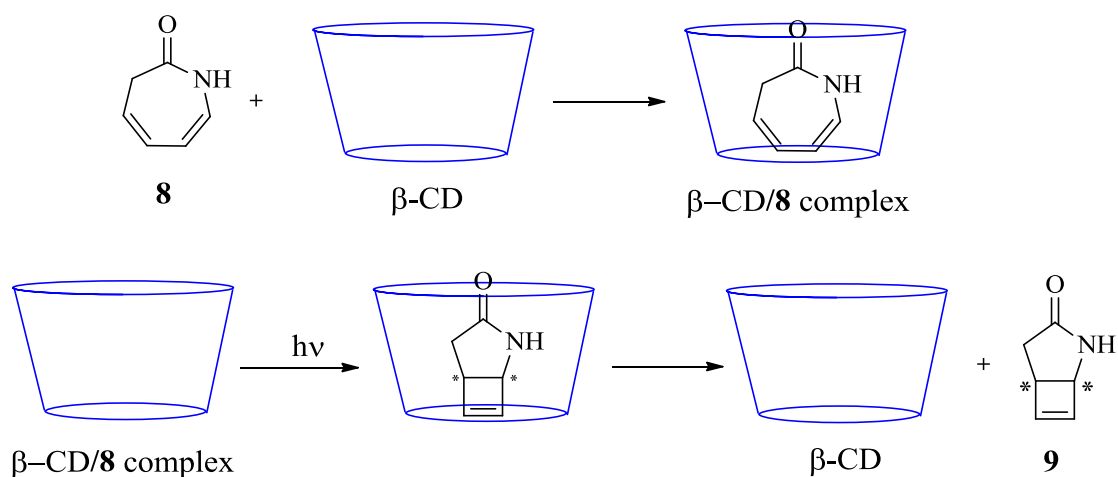
We saw in Section 1.3.3 that the synthesis of *cis*-<sup>3,4</sup>CB-GABA starting from azepinone **8** begins with the photochemical 4π-electrocyclization of the starting compound, during which two stereogenic centers are created (see Scheme 33).



*Scheme 33: The photocyclization reaction of azepinone 8 leading to the formation of the racemic photoadduct 9*

Azepinone **8** has 4 electrons in its  $\pi$  system, which by Woodward–Hoffmann rules would undergo a disrotatory photochemical ring closure. Since the diene system of azepinone **8** is non symmetrical, and because the rotation of the orbitals can go both clockwise and anticlockwise with an equal probability; the photoadduct **9** is formed as a racemic mixture of the two enantiomers (See Scheme 34).

We predict that the presence of  $\beta$ -CD during this 4 $\pi$  electrocyclic ring closure could provide a chiral environment that would favor one topology of the ring closure over the other, thus allowing preferential access to one of the enantiomers (see Scheme 34).



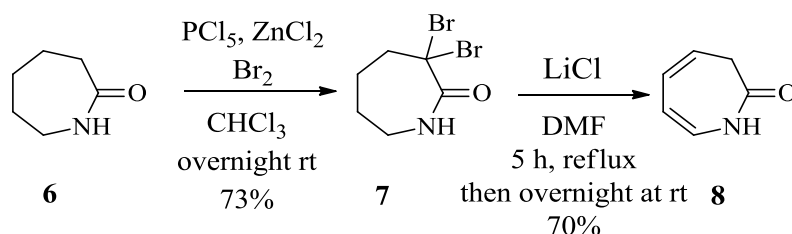
Scheme 34: The proposed enantioselective photoelectrocyclization of azepinone **8** induced by  $\beta$ -CD

In this chapter we first planned to synthesize azepinone **8**, then to study its host-guest interaction with  $\beta$ -CD, followed by a search for the most productive manner of irradiating the complex in terms of chemical yield and *ee* of the bicyclic adduct **9**. Therefrom, following the previously described procedure for the racemate, enantioenriched *cis*-<sup>3,4</sup>CB-GABA could be prepared.

## 3.2 Results and discussion

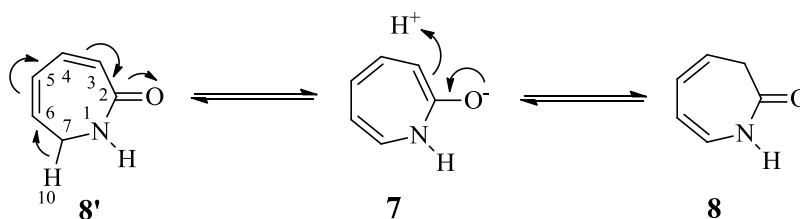
### 3.2.1 Synthesis of azepinone **8**

Azepinone **8** was prepared following the previously reported method,<sup>102</sup> starting from the commercially available caprolactam **6**. (see Scheme 35).  $\alpha$ -Dibromination of caprolactam **6** was carried out in the presence of phosphorous pentachloride, zinc chloride and bromine. The product **7** was isolated in 73% yield and was pure enough to be used without purification. The second step consists of a double elimination of HBr to yield azepinone **8**. This reaction was carried out in the presence of dry lithium chloride in anhydrous DMF at reflux. Azepinone **8** was obtained with 70% yield after chromatography on silica gel.



*Scheme 35: Synthesis of azepinone **8** from caprolactam **6**.*

Formation of the unconjugated compound **8** instead of compound **8'** might be attributed to an excessive ring strain in the latter, due to the sequence of five  $sp^2$  hybridized carbons (C2  $\rightarrow$  C6) with the  $sp^2$  hybridized nitrogen (See Scheme 36).



*Scheme 36: Formation of the more stable azepinone **8**.*

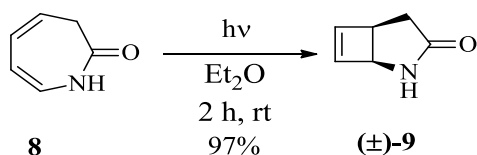
### 3.2.2 Photoelectrocyclization of azepinone **8** in the absence of $\beta$ -CD

The photoelectrocyclization of azepinone **8** in the absence of  $\beta$ -CD was studied both in solution as well as in solid state.

#### 3.2.2.1 Photoelectrocyclization of azepinone **8** in solution

##### 3.2.2.1.1 Photoelectrocyclization of azepinone **8** in ether

The photochemical electrocyclization reaction of **8** was first performed in ether, as previously reported in the literature (See Scheme 37).<sup>102</sup> A solution of azepinone **8** in anhydrous diethyl ether was irradiated for 2-3 h with a 400 W mercury vapor lamp, in a reactor fitted with a quartz filter and cooled by an external water bath. The choice of a quartz filter was made on the basis of a previous analysis of the UV absorbance spectrum of **8** in acetonitrile (0.11 mM), which showed a maximum absorbance at 269 nm, indicating that the molecule has to be in a quartz reactor if we want it to absorb directly. (102)



*Scheme 37: The photochemical cyclization of azepinone **8** to give racemic photoadduct **9**.*

2-Azabicyclo[3.2.0]hept-6-en-3-one **9** was obtained in 97% yield as a brown solid with a very low solubility in ether. As it formed, it stuck on the inner side of the reactor, from which it was collected by scraping it out. The very low solubility of the product precluded further purification, but the  $^1\text{H}$  MNR spectrum and HPLC analysis of the crude product showed a nearly pure compound.

##### 3.2.2.1.2 Photoelectrocyclization of azepinone **8** in water

Since  $\beta$ -CD is not soluble in ether, we tested the photoelectrocyclization of azepinone **8** in water. The reaction time was the same as in ether (2 h) when the same concentration (7.33 mM) was used. With a higher concentration (91 mM) the reaction time was increased to 15 h.

The irradiated reaction mixture was then lyophilized and the crude cyclobutene product ( $\pm$ )-**9** was isolated in a 71% crude yield. Analysis of the crude product by NMR and HPLC showed that it was identical to the sample prepared in diethyl ether. The lower yield in case of water as a solvent is attributed to the loss of product ( $\pm$ )-**9** during the lyophilization process. (see Index, section B )

### 3.2.2.2 Photoelectrocyclization of azepinone **8** in solid state

In the literature, when CDs were used as a chiral hosts, better enantioselectivity was achieved when photochemical transformations were performed in the solid state rather than in solution.<sup>42</sup> For this reason we also tested the photochemical electrocyclization reaction of azepinone **8** in the solid state.

To irradiate azepinone **8** in the solid state, it was first ground into a fine powder then introduced in a quartz tube. The tube was closed and set to rotate in a Rayonet (R-200) reactor, in which it was irradiated until no starting material could be observed by <sup>1</sup>H NMR. The <sup>1</sup>H NMR spectrum of the photoadduct ( $\pm$ )-**9** resulting from the irradiation of azepinone **8** in solid state was identical to that obtained in solution.

The reaction time in the solid state, which could range between 6 and 60 h, depended greatly on the amount and the homogeneity of the solid being irradiated. The more evenly the solid was exposed to the irradiation, the less time it needed for total conversion.

### 3.2.3 Analysis of the enantiomeric excess in photoadduct **9**

Before introducing the  $\beta$ -CD to the reaction mixture, a suitable method has to be established to determine the *ee* of the photoadduct ( $\pm$ )-**9**. We studied the separation of the enantiomers of ( $\pm$ )-**9** by chiral HPLC.

The photoadduct ( $\pm$ )-**9** was passed through a normal phase chiral Lux Cellulose-1 column using a 90/10 hexane/isopropanol eluting mixture at 20 °C and a flow rate of 1.5 ml/min. Under these conditions, the two enantiomers of photoadduct ( $\pm$ )-**9** could be separated with 43 sec of difference in retention time. Figure 22 shows an HPLC chromatogram of photoadduct ( $\pm$ )-**9** prepared by photoelectrocyclization in the absence of  $\beta$ -CD.

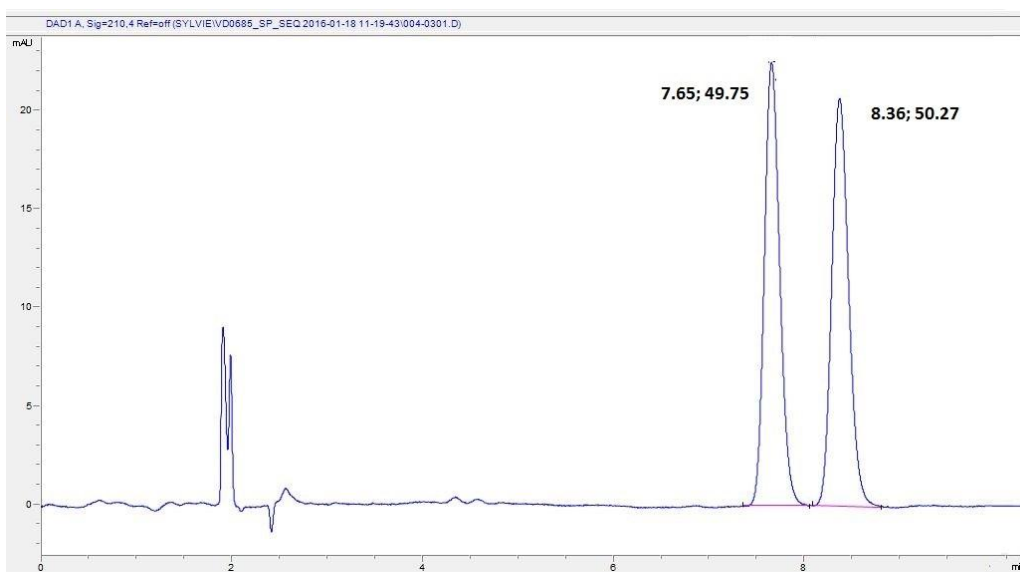


Figure 22: HPLC chromatogram of racemic ( $\pm$ )-**9** on normal phase chiral Lux Cellulose-1.

### 3.2.4 The $\beta$ -CD/azepinone **8** complex

#### 3.2.4.1 Formation of the $\beta$ -CD/azepinone **8** complex:

Both  $\beta$ -CD and azepinone **8** are soluble in water. The  $\beta$ -CD/azepinone **8** complex was prepared by mixing an aqueous solution of the latter with an aqueous solution of  $\beta$ -CD. Upon stirring at room temperature, a white precipitate started to form gradually, and within few minutes, the clear solution turned into a thick “milky suspension” (See Figure 23). It is important to point out that a minimum concentration of about 6 mM, with respect to  $\beta$ -CD, was needed in order for the precipitate to form; and the lower the concentration of the mixture is, the slower the precipitation process became. For this reason, the volume of the final solution was always chosen to have a concentration just less than 15 mM, which is the maximum solubility of  $\beta$ -CD in water at 25 °C.

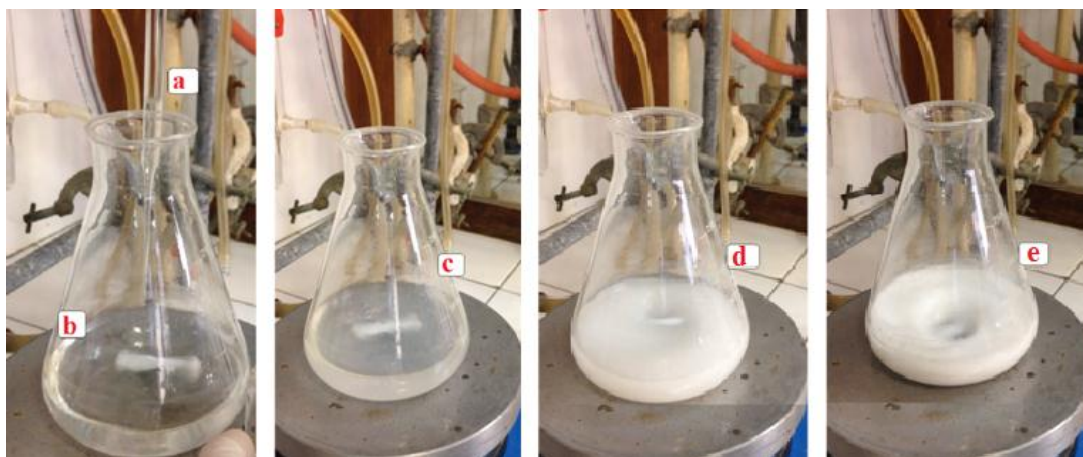


Figure 23: (a) A clear aqueous solution of azepinone **8** at 0.45 M, (b) a clear aqueous solution of  $\beta$ -CD at around 15 mM, (c) the "milky suspension" formed after stirring at room temperature for 30 sec, (d) 1.5 min, (e) 5 min.

### 3.2.4.2 Evidence of complexation by powder X-Ray diffraction

To further validate the existence of complexation between the  $\beta$ -CD and azepinone **8**, powder X-ray diffraction data was obtained for samples of  $\beta$ -CD alone, azepinone **8** alone, and for the white precipitate "complex" obtained from mixing both components in solution (See Figure 24).

The powder X-ray diffraction data obtained for the  $\beta$ -CD/azepinone **8** complex were clearly different from the data obtained for each component alone. This provides further support for the contention that a genuine complex is implicated, rather than a physical mixture of the two discrete substances.

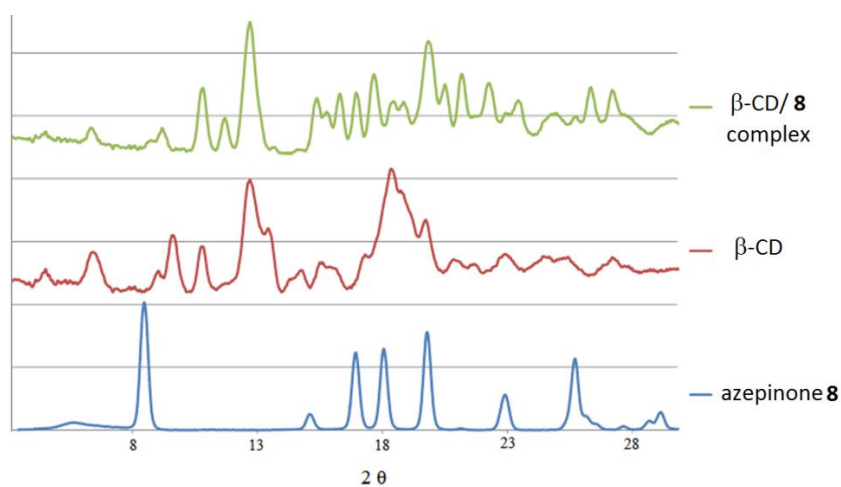


Figure 24: The powder XRD spectra of azepinone **8** vs  $\beta$ -CD vs  $\beta$ -CD /**8** complex.

### 3.2.4.3 Determination of the complex stoichiometry

#### 3.2.4.3.1 The azepinone **8** to $\beta$ -CD ratio in the precipitate

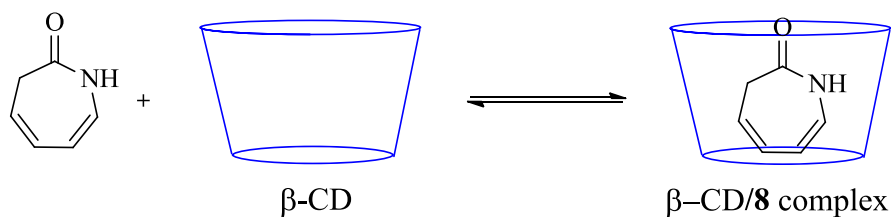
In order to determine the stoichiometry of the formed  $\beta$ -CD/azepinone **8** complex, the “milky suspension” (explained in section 3.2.4.1) was filtered out and the ratio of the azepinone **8** to  $\beta$ -CD in the precipitate was found to be around 1:1, even if more than one equivalent of  $\beta$ -CD was used in the above mentioned complexation procedure. This ratio was calculated by comparing the peak areas in an  $^1\text{H}$  NMR spectrum of the precipitate with a reference equimolar sample of  $\beta$ -CD/azepinone **8**

To further determine the amount of cyclodextrin and lactam in the precipitating solid, the “milky suspension” was filtered and the “uncomplexed” azepinone **8** was extracted out from the aqueous filtrate using ethyl acetate. The organic layer was then concentrated and the aqueous phase was lyophilized to get the uncomplexed  $\beta$ -CD. The masses, summarized in table 3, show that about 70% by mass of  $\beta$ -CD and azepinone **8** are precipitating out in a 1:1 ratio.

Mass of dry $\beta$ -CD used	Mass of dry azepinone <b>8</b> used	Mass of dry precipitating solid complex	Mass of remaining azepinone <b>8</b> extracted from the filtrate	Mass of remaining $\beta$ -CD extracted from the filtrate
1.04 g	100 mg	790 mg	30 mg	321 mg

*Table 3: Distributiun of azepinone **8** and  $\beta$ -CD between the precipitate and the filtrate after complexation.*

In order to see the effect of adding an excess of  $\beta$ -CD on the complexation equilibrium, the starting “milky suspension” described above was charged with two more equivalents of  $\beta$ -CD. The extra amounts of  $\beta$ -CD added were expected to drive the complexation forward, towards the associated  $\beta$ -CD/azepinone **8** form (See Scheme 38).



*Scheme 38: The proposed equilibrium between the free and the associated form of 1,3-dihydro-2H-azepin-2-one **8** and  $\beta$ -CD in solution.*

The charged suspension was filtered and the “uncomplexed” azepinone **8** was extracted out from the aqueous filtrate using ethyl acetate. The organic layer was then concentrated and the aqueous phase was lyophilized. The masses, summarized in table 4, show that about 90% by mass of the starting azepinone **8** is precipitating with  $\beta$ -CD.

Mass of dry $\beta$ -CD used	Mass of dry azepinone <b>8</b> used	Mass of dry residue	Mass of remaining azepinone <b>8</b> extracted from the filtrate	Mass of remaining $\beta$ -CD extracted from the filtrate
3.12 g	100 mg	2.16 g	10 mg	960 mg

So the equilibrium has certainly been shifted toward the formation of the  $\beta$ -CD/ **8** complex.

*Table 4: Distribution of azepinone **8** and  $\beta$ -CD between the precipitate and the filtrate after complexation.*

#### 3.2.4.3.2 The Job’s method of continuous variation:

Job’s method of continuous variation was used to further investigate the stoichiometry of the formed  $\beta$ -CD/azepinone **8** complex. For this, two separate 100 mL ( $4 \cdot 10^{-2}$  mmol) mother aqueous solutions were prepared, one containing  $\beta$ -CD and the other azepinone **8**. Volumes from each solution were then taken and mixed at different proportions to prepare 11 samples (2 mL) covering the range of mole ratios

$$0 < \chi = \frac{[\text{azepinone } \mathbf{8}]}{[\text{azepinone } \mathbf{8}] + [\beta - \text{CD}]} < 1$$

The UV spectra for each of the 11 samples were recorded at  $\lambda = 254$  nm, and the difference in absorbance, ( $\Delta A$ ), between azepinone **8** alone and in the presence of  $\beta$ -CD multiplied by the molar fraction, ( $\chi$ ), was plotted against molar fraction ( $\chi$ ) (see Figure 25).

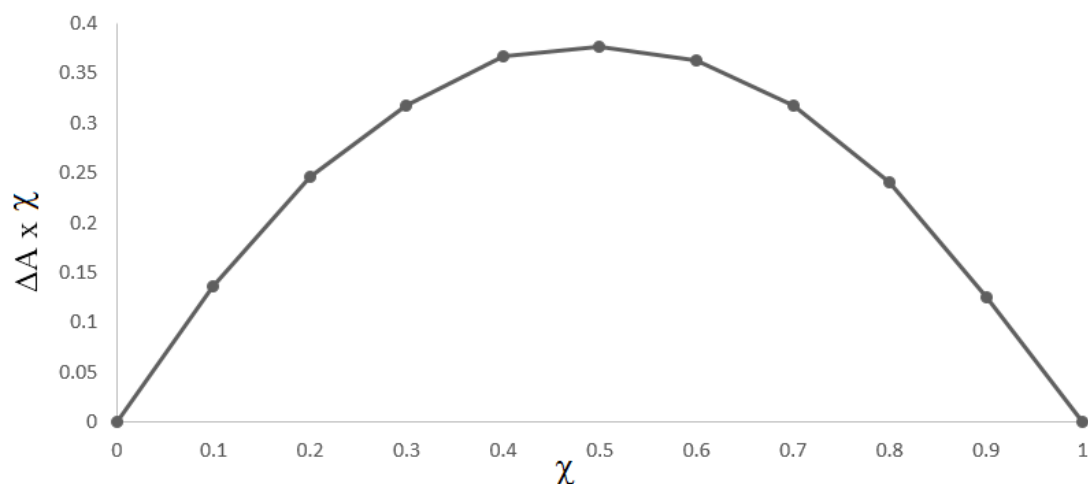


Figure 25: Job's plot of UV absorption ( $\lambda = 254 \text{ nm}$ ) at different  $\beta\text{-CD}$ :azepinone **8** molar ratios.

The position of the maximum of the curve at  $\chi = 0.5$  further validates that the stoichiometry of complex formed upon mixing  $\beta\text{-CD}$  with azepinone **8** in aqueous solution is of a 1:1 stoichiometry. The rounded shape of the curvature also provides an indication that the equilibrium constant of the complexation reaction is expected to be of a low magnitude.<sup>58</sup>

#### 3.2.4.4 1D NMR studies of the $\beta\text{-CD}$ /azepinone **8** complex

Trying to understand the nature of the interactions between azepinone **8** and  $\beta\text{-CD}$ , an NMR titration experiment was done. A 15 mM solution of  $\beta\text{-CD}$  in  $\text{D}_2\text{O}$  was titrated by adding an incremental amount of a  $\text{D}_2\text{O}$  solution of azepinone **8** (10  $\mu\text{l}$  at 73 mM / addition), up to 7 equivalents. The temperature of the experiment was maintained at 40-45  $^\circ\text{C}$  to have a clear solution throughout the experiment.

Protons  $\text{H}_3$  and  $\text{H}_5$  of the  $\beta\text{-CD}$  cavity, showed a gradual up field shift with each addition of the lactam (See Figure 26). At a 1:1 ratio of azepinone **8** to  $\beta\text{-CD}$ , the change in the chemical shift reached 0.03 ppm for  $\text{H}_3$  and 0.07 ppm for  $\text{H}_5$ . On the contrary  $\text{H}_1$ ,  $\text{H}_2$ ,  $\text{H}_4$  and  $\text{H}_6$  of  $\beta\text{-CD}$  that are pointing outside the cavity did not show any significant shift throughout the titration.

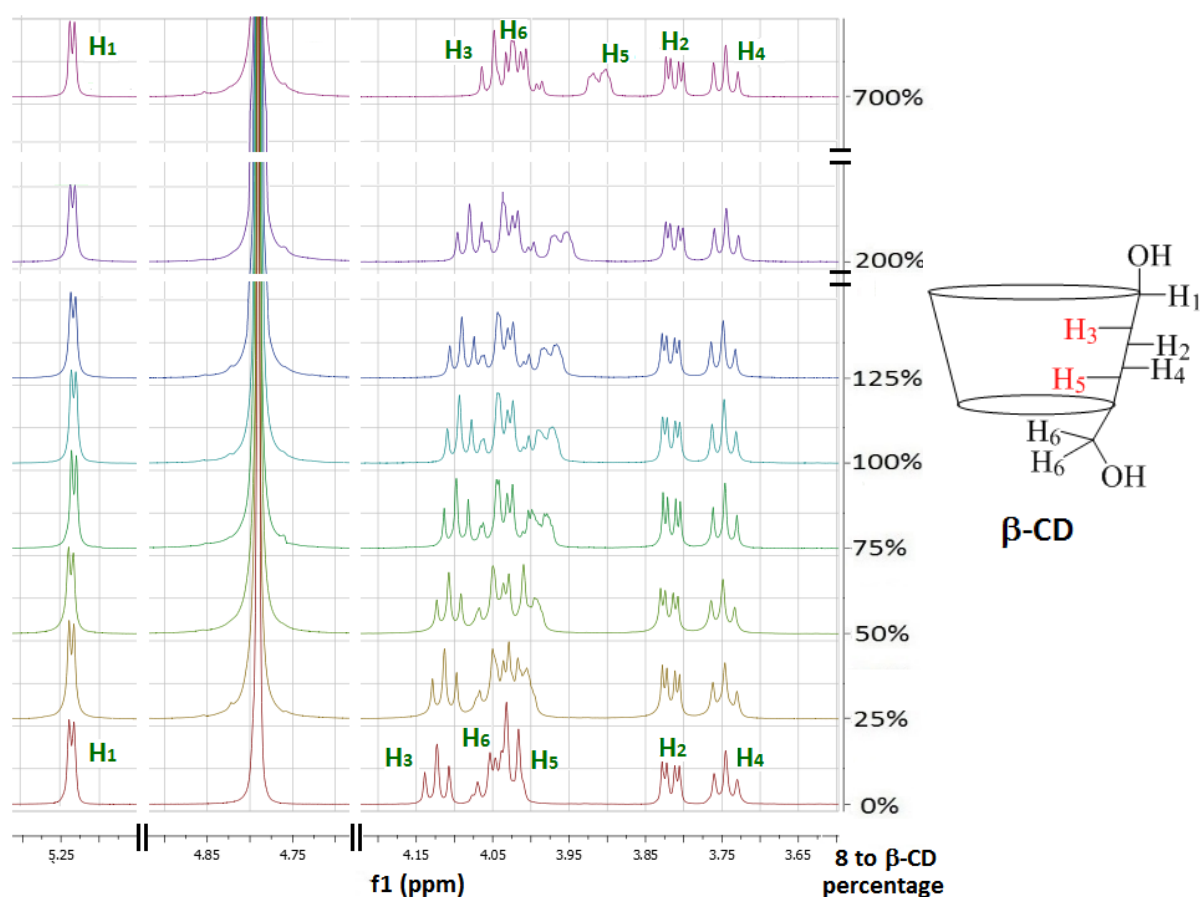


Figure 26:  $^1\text{H}$  NMR of  $\beta\text{-CD}$  showing the shift of  $\text{H}_3$  and  $\text{H}_5$  of the CD with each addition of azepinone **8**.

Further addition of azepinone **8** up to 7 equivalents induces a further increase in the  $\Delta\delta$  values up to 0.064 and 0.012 for  $\text{H}^3$  and  $\text{H}_5$  respectively (see table 5). This increase is almost linear and no significant inflection point could be detected indicating that the complexation of azepinone **8** and  $\beta\text{-CD}$  is a dynamic process of fast exchange between the complexed and the free form of the two molecules relative to the NMR time scale, and the observed chemical shifts at a certain moment are the weighted average of the chemical shifts for the free and complexed form coexisting at that moment.<sup>69</sup> (69) Correia 2002.

$\beta\text{-CD}$ proton	1	2	3	4	5	6
$\Delta\delta$ (ppm) 0-100%	0.000	0.000	0.030	0.000	0.068	0.000
$\Delta\delta$ (ppm) 0-200%	0.000	0.000	0.043	0.000	0.087	0.000
$\Delta\delta$ (ppm) 0-700%	0.000	0.000	0.064	0.000	0.120	0.000

Table 5: The change in chemical shift ( $\Delta\delta$ ) of the CD protons at 100%, 200%, 700% additions of azepinone **8**.

The protons of the azepinone **8** also showed a gradual up field shift throughout the incremental additions. But unlike the inside protons of the CD cavity, the induced shift in the azepinone **8** protons were of a lower magnitude. The most affected lactam protons are H<sub>b</sub>, H<sub>c</sub> and H<sub>d</sub> (See Figure 27 and table 6).

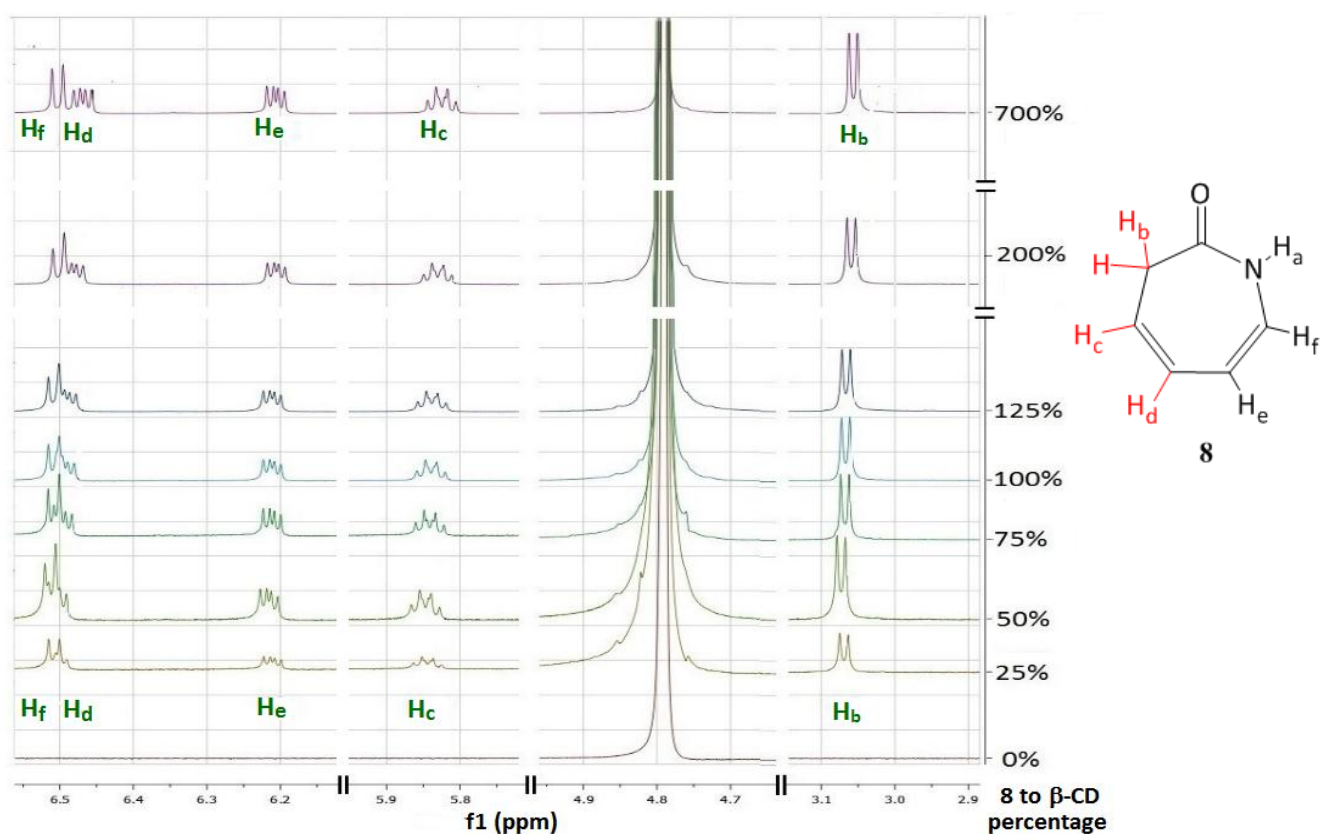


Figure 27: <sup>1</sup>H NMR of azepinone **8** with its incremental additions to a solution of β-CD.

Azepinone <b>8</b> proton	b	c	d	e	f
Δδ (ppm) 25-100%	0.006	0.009	0.013	0.003	0.003
Δδ (ppm) 25-200%	0.010	0.014	0.021	0.005	0.006
Δδ (ppm) 25-700%	0.027	0.034	0.049	0.0186	0.0201

Table 6: The change in chemical shift (Δδ) of the azepinone **8** protons at 100%, 200%, 700% of it relative to β-CD.

<sup>1</sup>H NMR titration experiments showed that the protons inside the β-CD cavity are the ones interacting with azepinone **8**, suggesting that the guest may be bound, totally or partially, inside the hydrophobic cavity. Nevertheless, the absence of an inflection point in the

titration curve with a maximum of variation in the chemical shifts, suggest a fast equilibrium between the associated and the free form of the two molecules.

### 3.2.4.5 Determination of the binding constant $K_b$

Since protons H<sub>3</sub> and H<sub>5</sub> of the  $\beta$ -CD cavity show a chemical shift difference between the free and bound states; one of these protons, H<sub>3</sub> whose NMR signal does not overlap with other protons, could be monitored throughout a titration experiment in which the concentration of the guest azepinone **8** was varied incrementally. The data from such a titration experiment allowed to establish a linear plot of  $1/\Delta\delta_{H3}$  vs.  $1/[\text{azepinone } \mathbf{8}]$  (see figure 28). The straight line obtained, has a slope of  $1/(K_b \times \Delta\delta_{\text{sat}})$  and an intercept at  $1/\Delta\delta_{\text{sat}}$ , from which  $K_b$  was estimated to be 35.4.

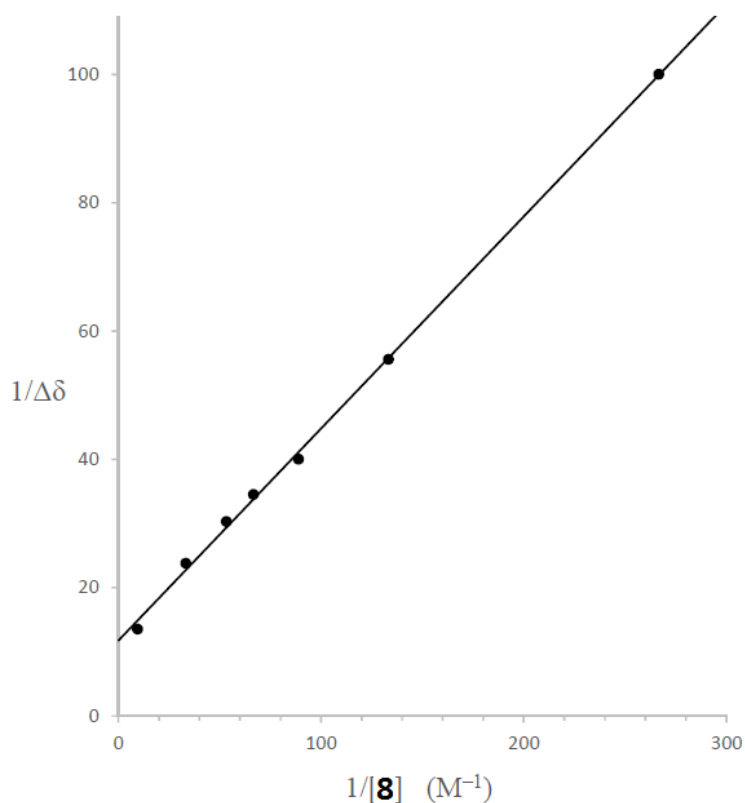


*Figure 28: The linear plot of  $1/\Delta\delta_{H3}$  vs.  $1/[\text{azepinone } \mathbf{8}]$ .*

The relatively low value of  $K_b$  for the  $\beta$ -CD/azepinone **8** complex is in accordance with the shape of the Job's plot curve, which shows a gentle rather than a sharp angular curvature (see section 3.2.4.3.2).

### 3.2.4.6 2D ROESY NMR studies of the complex

Complexation of molecules to CDs usually occurs through non-covalent interactions between the guest molecule and the CD cavity. This is a dynamic process in which the guest molecule continuously associates and dissociates from the host CD. Although in schematic representations a host/guest complex is usually shown as a single entity, the complex is actually composed of a set of species with the depicted complex representing an average structure.<sup>114</sup> In fact, CD complexes have high conformational flexibility, which can accommodate several modes of complexation.<sup>64</sup> This phenomenon is termed multimodal complexation.<sup>29</sup>

In order to investigate the geometry of the formed complex and propose a mode of complexation between the  $\beta$ -CD cavity and azepinone **8**, 2D ROESY NMR experiments were conducted.

A ROESY NMR experiment conducted on an equimolar 1:1  $\beta$ -CD:azepinone **8** mixture in solution at 45 °C (15 mM, D<sub>2</sub>O) showed intermolecular cross peaks only with the inner CD protons (H<sub>3</sub>, H<sub>5</sub>, H<sub>6</sub>), (see Figure 29, and 30), which established inclusion of the guest inside the cavity without any evidence for outside interactions

Azepinone **8** can possibly approach the  $\beta$ -CD from the wide secondary face; this mode of binding is supported by the correlation of all of its protons with H<sub>3</sub> that line up the inner cavity of the CD near the secondary face. The penetration from this face inserts the amide part of the azepinone **8** deep enough inside the cavity, such that all the azepinone **8** protons, except H<sub>d</sub>, are in close proximity to correlate with H<sub>5</sub> far on the other side of the cavity (see Figure 31). H<sub>d</sub>, treated as a “probe hydrogen” never sees H<sub>5</sub>, but still can clearly see H<sub>6</sub> which line up the primary face of the  $\beta$ -CD, suggesting the presence of another mode of complexation in which the penetration of the azepinone **8** occurs from the narrow primary face; but this time the inclusion is not deep enough to put H<sub>d</sub> close contact with H<sub>5</sub>, but only to keep it close to H<sub>6</sub>.

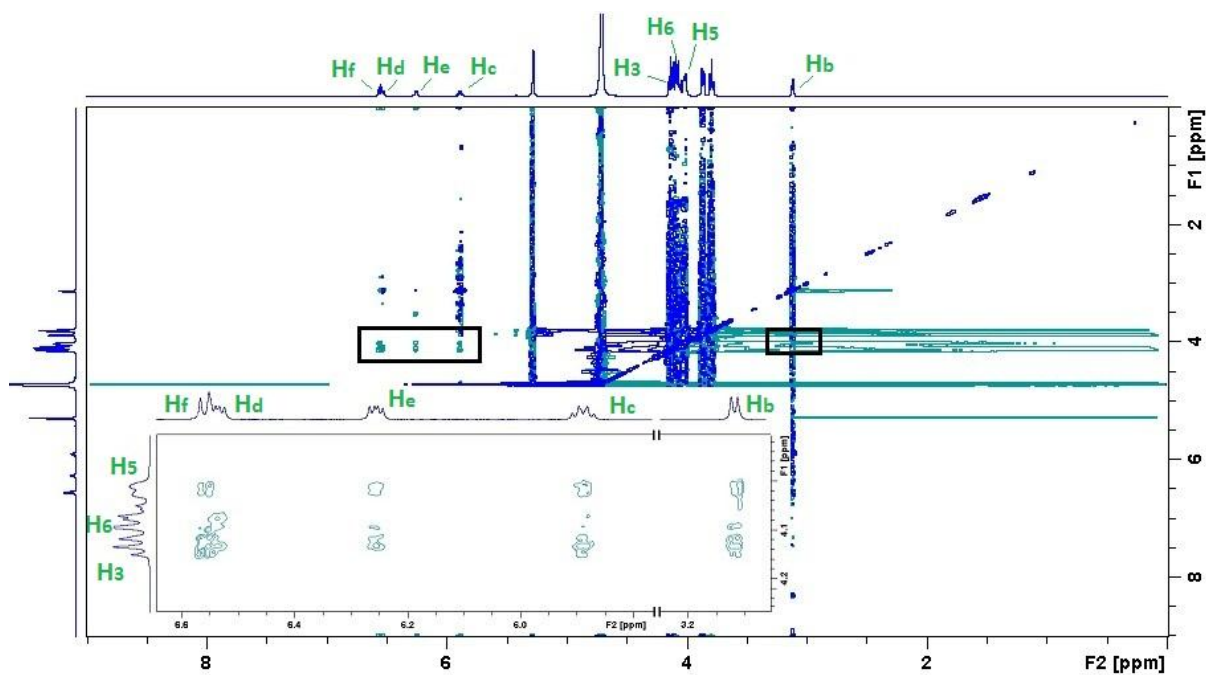


Figure 29: 2D ROESY NMR experiment (600 MHz) of a 1:1 mixture of **8** and  $\beta$ -CD (each 15 mM,  $D_2O$ , 45 °C),

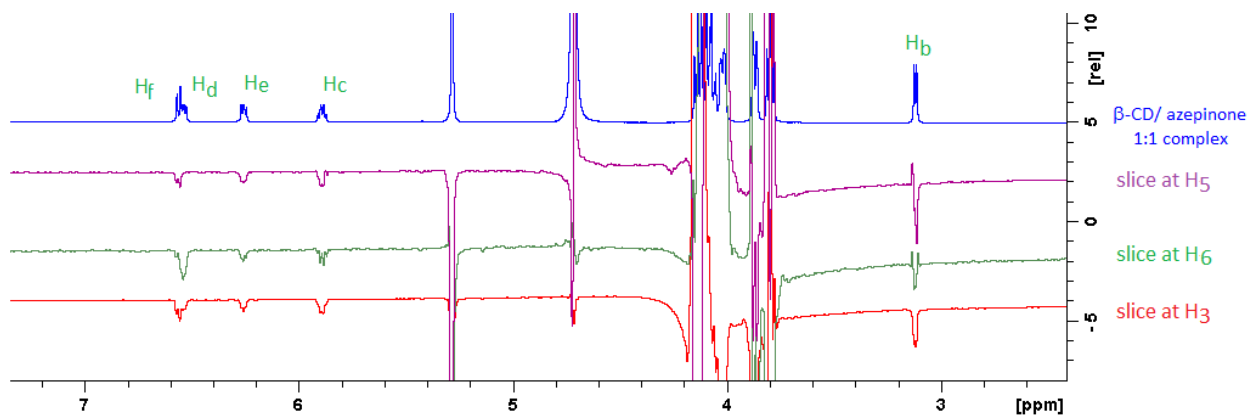
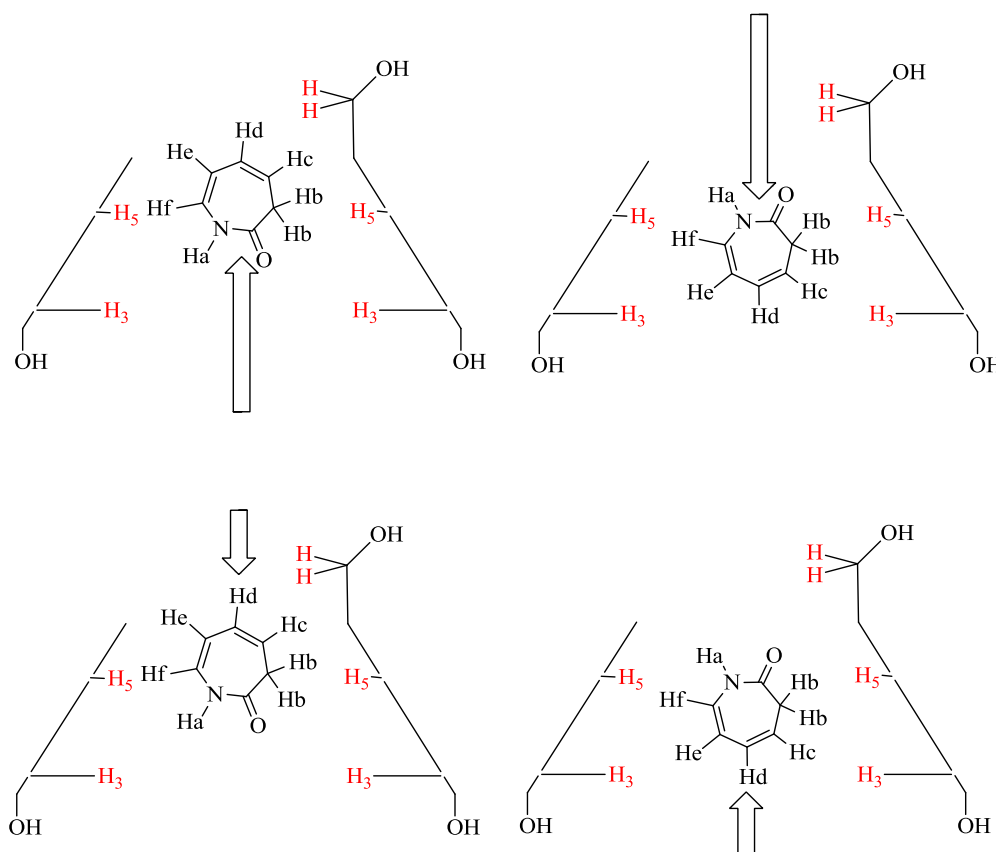


Figure 30: 1D slice of the ROESY from Figure 32, at  $H_5$ ,  $H_6$  and  $H_3$  of the  $\beta$ -CD, aligned with the  $^1H$  proton spectrum.



*Figure 31: The proposed mode of complexation between  $\beta$ -CD and azepinone **8**. Deep penetration of the unsaturated part of azepinone **8** via the two  $\beta$ -CD faces (top left, top right) or a shallow penetration of the amid part of the azepinone from the primary face of  $\beta$ -CD (bottom left) or a deep penetration from the secondary one (bottom right).*

Several selective ROESY experiments are still needed to establish the exact geometry of the azepinone **8** inside the  $\beta$ -CD cavity. Nevertheless, the ROE colorations between the azepinone **8** and the inside protons of the  $\beta$ -CD are clear enough to argue that the azepinone **8** is put in a chiral environment ready for being irradiated.

### 3.2.5 Photoelectrocyclization of azepinone **8** in the presence of $\beta$ -CD

Irradiation of azepinone **8** in the presence of  $\beta$ -CD was either done in fluid or in solid state. Except for one experiment in which the  $\beta$ -CD was manually ground with the lactam without

any solvent, all other experiments started by adding a clear solution of azepinone **8** (30-50 mg in 1 ml of water) to a clear aqueous solution containing the desired equivalents of  $\beta$ -CD. The volume of the final solution was chosen to be at 15 mM with respect to the  $\beta$ -CD. Upon stirring, a white precipitate started to form almost immediately. The formed "milky" suspension was left to stir 2 h at room temperature, and then was treated differently according the desired condition of irradiation (in solution, in suspension, in solid state...).

Our objective was to isolate the resulting bicyclic photoadduct **9** formed by classical extraction methods. But it transpired that this was a major problem.

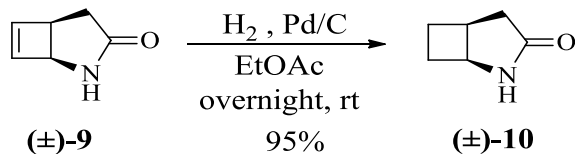
### 3.2.5.1 Recovery of the photoadduct **9**

We first attempted to isolate photoadduct **9** from crude irradiated solid by solid-liquid extraction (Soxhlet) using organic solvents (chloroform, acetone...). Due to the low solubility of **9** in such solvents and probably its interaction with the  $\beta$ -CD molecules, it took several days (up to 30 days) to extract the entire amount of **9** out of the irradiated  $\beta$ -CD/azepinone **8** mixture. The speed of extraction was also dependent on the solvent used. Even though the photoadduct **9** was more soluble in chloroform than in acetone, the latter was better in the continuous extraction process especially if wet acetone was used due to the fact that **9** had a good solubility in water. Due to the prolonged Soxhlet extraction at around 60 °C, the isolated crude **9** was usually a dark viscous oil rather than a light brown solid as it should be. Nevertheless, the  $^1\text{H}$  NMR spectrum and the chiral HPLC chromatogram were identical to the photoadduct **9** prepared by irradiation in ether.

Since it was difficult to isolate all of the photoadduct **9** from the irradiated complex, chiral HPLC analysis was used to determine the *ee* of samples which were partially extracted. The results could not be considered reliable since CDs are known to preferentially hold one enantiomer in their cavity, making the extraction of the other easier.<sup>115</sup> Thus it is possible that the *ee* observed in a partially extracted sample was due to chiral resolution and was not induced during the photochemical reaction. The difficulty in recovering the photoadduct **9** prompted us to seek a more suitable method to access to the bicyclic *cis*-<sup>3,4</sup>CB-GABA precursor.

### 3.2.5.2 Reduction of photoadduct **9**

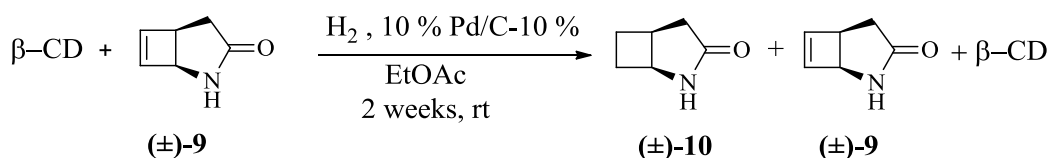
In previous work,<sup>102</sup> it was observed that the reduction of the photoadduct **9** gave a product which had a better solubility in organic solvents (See Scheme 39).



*Scheme 39: Reduction of photoadduct **9** to 2-azabicyclo[3.2.0]heptan-3-one **10**.*

Therefore, we reasoned that if we could reduce the photoadduct **9** in the mixture with  $\beta$ -CD, it would be easier to extract and isolate the reduced derivative **10**.

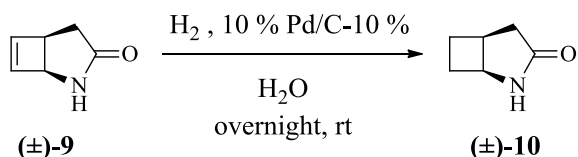
The reduction was first attempted on a suspension of photoadduct **9** and  $\beta$ -cyclodextrin in ethyl acetate with 10% w/w Pd/C-10% under a dihydrogen atmosphere. The presence of  $\beta$ -CD slowed down the reaction, and traces of starting photoadduct **9** were still present even after 2 weeks of stirring at room temperature with a large excess of the catalyst (See Scheme 40).



*Scheme 40: Reduction of photoadduct **9** in EtOAc in the presence of  $\beta$ -CD to give 2-azabicyclo[3.2.0]heptan-3-one **10**.*

Since the irradiated  $\beta$ -CD/photoadduct **9** complex was soluble in water, we supposed that when it went into solution the complex would dissociate giving more free photoadduct **9**. This free form of **9** would be more amenable to reduction.

So the reduction of photoadduct **9** without  $\beta$ -CD was tested in water on an analytical scale. The reaction worked well under a dihydrogen atmosphere in the presence of 10% w/w Pd/C-10%, and only 2-azabicyclo[3.2.0]heptan-3-one **10** could be observed after stirring overnight at room temperature (See Scheme 41).



*Scheme 41: Reduction of photoadduct 9 in water.*

### 3.2.5.3 Analysis of the enantiomeric excess compound (±)-10

To determine the optimal separation conditions of the two enantiomers of (±)-10 on an analytical HPLC system, several tests were done and the most satisfying result was achieved with a normal phase chiral Lux Cellulose-2 column, using a 90/10 hexane/ethanol eluting mixture at 20 °C and a flow rate of 2 ml/min. Under these conditions, the two enantiomers of (±)-10 were separated with 42 sec of difference in retention time. Figure 32 shows a HPLC chromatogram of (±)-10.

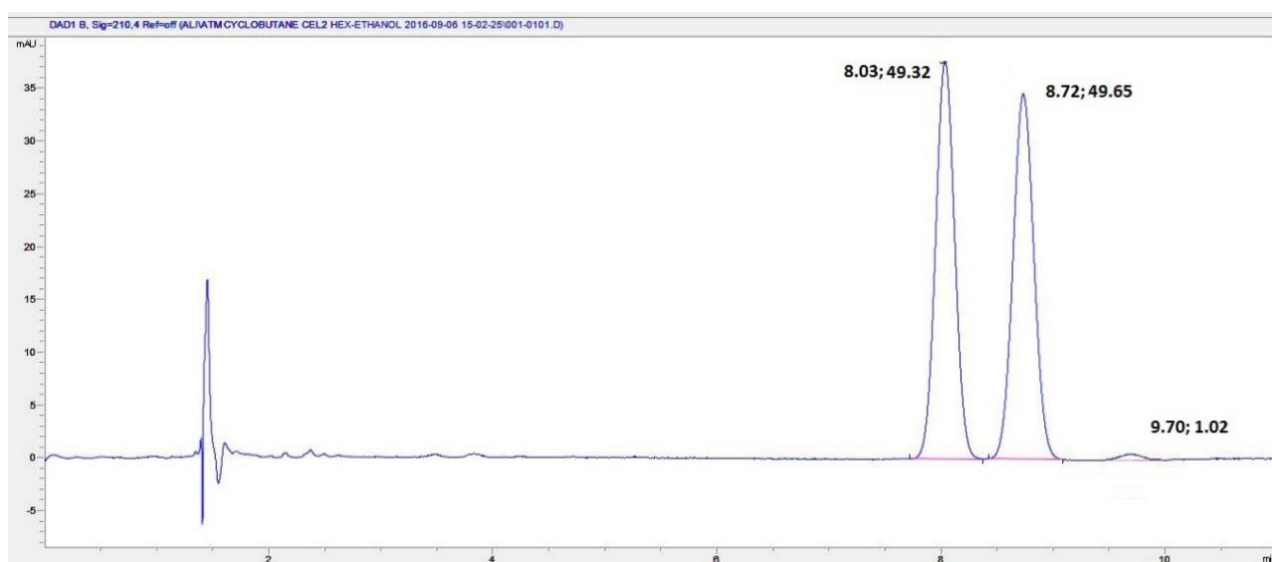
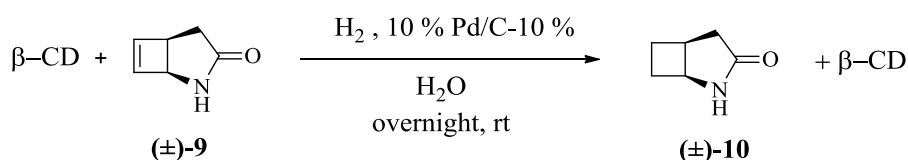


*Figure 32: HPLC chromatogram of (±)-10 showing separation of the two enantiomers.*

The reduction conditions in water were then applied to a crude irradiated  $\beta$ -CD/azepinone **8** complex mixture (See Scheme 42). After stirring overnight, the reaction mixture was filtered to remove the catalyst, and the 2-azabicyclo[3.2.0]heptan-3-one, (±)-10 was completely extracted from the aqueous phase with ethyl acetate. The use of other organic solvents like chloroform, dichloromethane or ether, led to the formation of a hard-to-break emulsion, with  $\beta$ -CD precipitating out in the extraction funnel.



*Scheme 42: Reduction, in water, of photoadduct **9** in the presence of  $\beta$ -CD to give 2-azabicyclo[3.2.0]heptan-3-one, **10**.*

### 3.2.6 Photoelectrocyclization/Reduction of azepinone **8** in presence of $\beta$ -CD

All the following reactions were carried out according to the one-pot method: photoelectrocyclization/reduction

#### 3.2.6.1 Irradiation of $\beta$ -CD/azepinone **8** complex in fluid state

The "milky suspension" obtained by mixing azepinone **8** and  $\beta$ -CD was treated according to the following methods:

##### 3.2.6.1.1 Experiment A: "1:1 Hot solution"

The "milky suspension" described above, containing one equivalent of lactam to  $\beta$ -CD, was heated up to 45-50 °C; at this temperature it turns into a clear solution. It is worth to note that if the solution was cooled back to room temperature the precipitate was observed again.

The suspension was transferred into a quartz tube fitted with a "heating/cooling finger" which is connected to a temperature control system (see Figure 33). The temperature of the mixture was maintained at 45-50 °C. The clear hot solution was then irradiated in a Rayonet reactor until complete conversion of azepinone **8** (2 h). The resulting yellow solution was cooled down to room temperature, and no precipitation was observed.

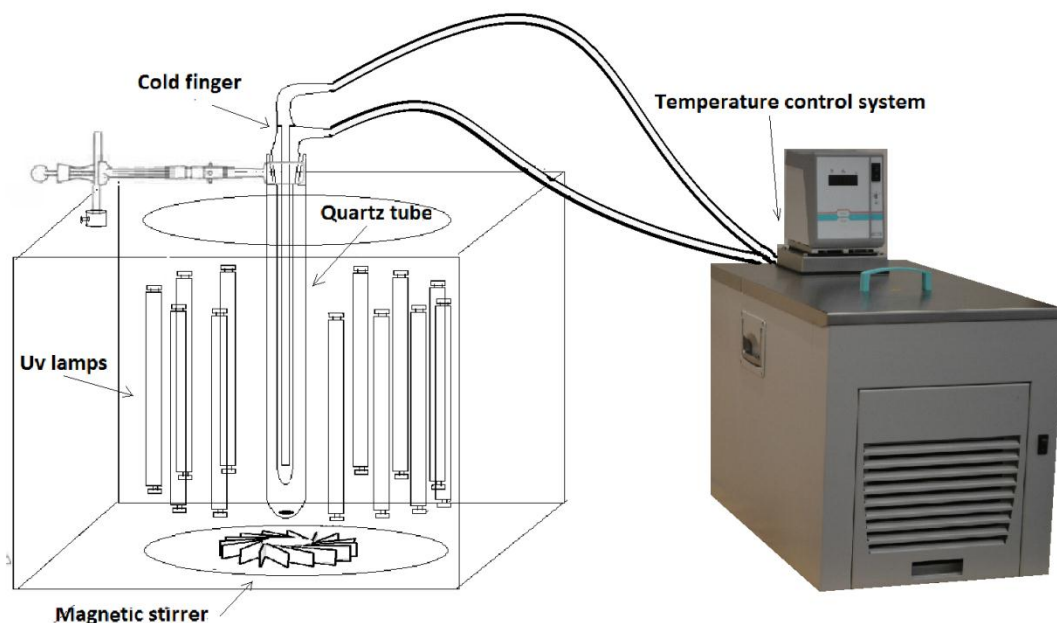


*Figure 33: A schematic draw of the Rayonet reactor (left) showing the reaction tube fitted with a “heating/cooling” finger connected to the temperature control system (right)*

The photoadduct **9** in the irradiated reaction mixture was reduced under a dihydrogen atmosphere in the presence of 10% w/w Pd/C-10%, overnight at room temperature. The reduced product, **10** was then extracted out of the aqueous phase with ethyl acetate. The organic phase was dried over Na<sub>2</sub>SO<sub>4</sub> and the solvent was evaporated under vacuum to give 2-azabicyclo[3.2.0]heptan-3-one **10** as a yellow oil.

The 2-azabicyclo[3.2.0]heptan-3-one **10** from experiment **A** was obtained in 40% crude yield, along with a water soluble solid side product whose <sup>1</sup>H NMR spectrum was not clear enough to identify it. Analysis of the crude **10** by chiral HPLC showed a pure product but no enantiomeric excess (See Figure 34).



*Figure 34: Chromatogram of 10 obtained from Experiment A*

The lack of enantioselectivity when the irradiation was performed on the hot solution agrees with the titration experiment, which showed a weak binding between the host ( $\beta$ -CD) and the guest (azepinone **8**) at this temperature.

As mentioned above by Inoue and coworkers,<sup>36</sup> when  $\beta$ -CD is used as a chiral host in solution, decreasing the temperature could enhance the enantiomeric excess in photochemical reactions. So we attempted the irradiation of the “milky suspension” at low temperature.

### 3.2.6.1.2 Irradiation of 1 $\beta$ -CD/azepinone **8** in Suspension

#### 3.2.6.1.2.1 Experiment B: “1:1 $\beta$ -CD/azepinone **8**, Cold suspension”

The starting “milky suspension” described above, containing one equivalent of azepinone **8** to  $\beta$ -CD was transferred to a quartz tube and the temperature was maintained at 5-8 °C using the temperature control “cold finger”. The cold suspension was then irradiated in a Rayonet reactor. Even at this low temperature, as the reaction proceeded, the suspension slowly turned into a clear yellowish solution. After complete conversion (2 h) the reaction mixture was reduced under a dihydrogen atmosphere, in the presence of 10% w/w Pd/C-10% and the 2-azabicyclo[3.2.0]heptan-3-one **10** was extracted out of the aqueous phase with ethyl acetate after filtration of the Pd/C catalyst.

The 2-azabicyclo[3.2.0]heptan-3-one **10** from experiment **B** was obtained as a yellow oil in 79% crude yield over two steps. Chiral HPLC analysis of the crude product showed a satisfying degree of purity and an *ee* of 38% (See Figure 35).

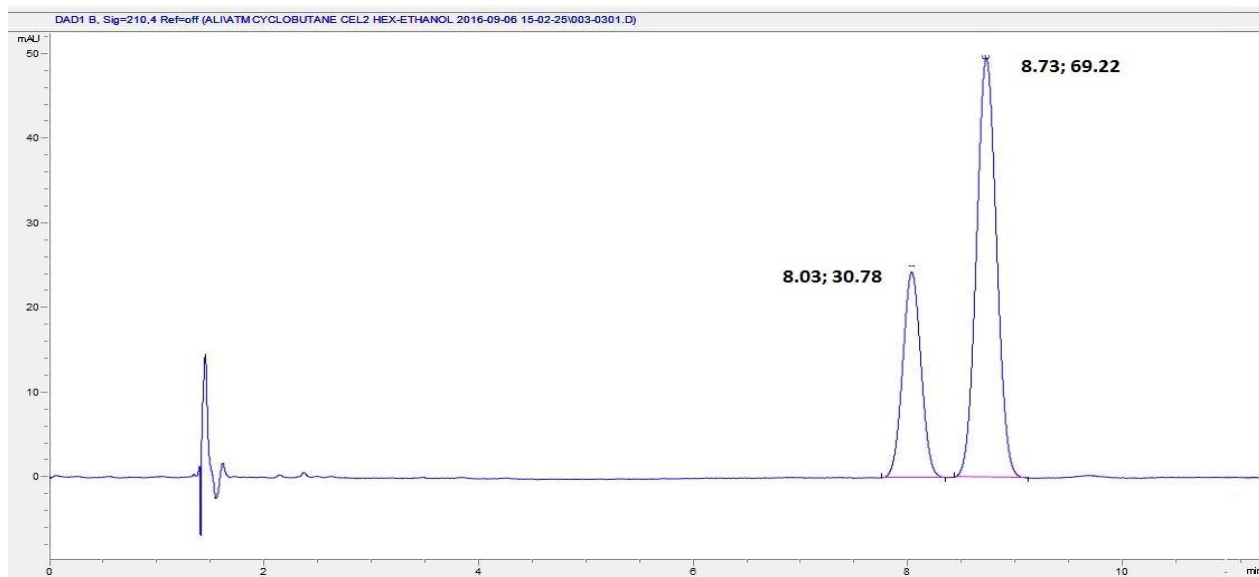


*Figure 35: HPLC chromatogram of enantiomerically enriched 2-azabicyclo[3.2.0]heptan-3-one **10**, obtained from experiment **B**.*

#### 3.2.6.1.2.2 Experiment C: “3:1 $\beta$ -CD/azepinone **8** Cold suspension”

The starting “milky suspension” described above, was charged with two extra equivalents of  $\beta$ -CD. When this 3:1 suspension was cooled to 5-8 °C and irradiated, the time needed for a complete reaction was longer than the other fluid state experiments (3.5 h) due to the presence of a dense CD suspension which made it harder for the light to reach the azepinone.

After irradiation the reaction mixture was transferred to a flask and water was added to dissolve the excess of  $\beta$ -CD. The resulting clear solution was treated with dihydrogen in the presence of 10% w/w Pd/C-10% and 2-azabicyclo[3.2.0]heptan-3-one **10** was then extracted out of the aqueous phase with ethyl acetate.

The 2-azabicyclo[3.2.0]heptan-3-one **10** sample from experiment **C** was obtained as a yellow oil in 75% crude yield over two steps. Chiral HPLC analysis of the crude product showed a satisfying degree of purity and an improved *ee* of 45%, with the same major enantiomer (See Figure 36).

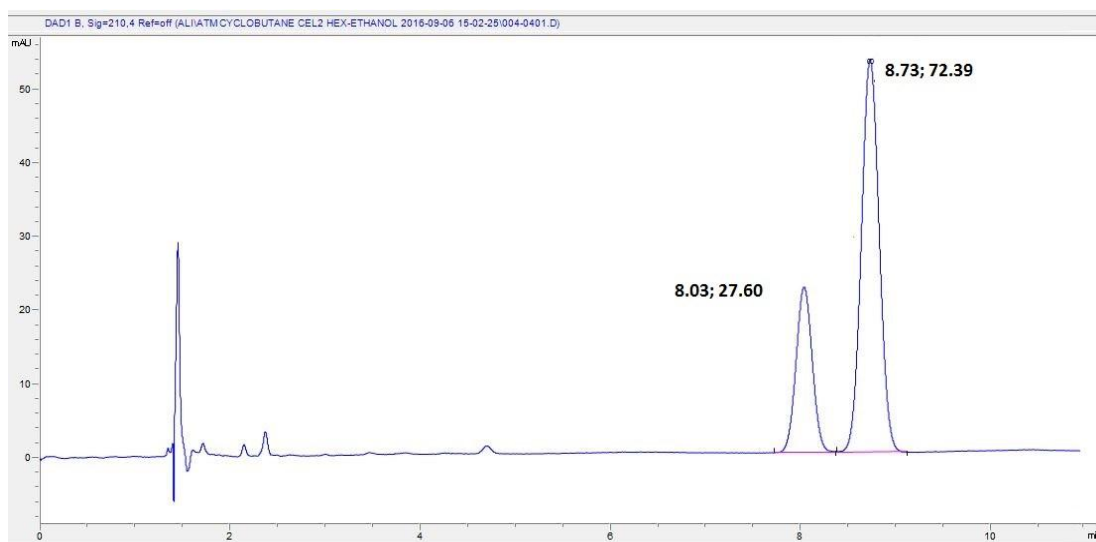


*Figure 36: Chromatogram of enantiomerically enriched 2-azabicyclo[3.2.0]heptan-3-one **10**, obtained from experiment C.*

### 3.2.6.2 Irradiation of $\beta$ -CD/azepinone **8** complex in solid state

As mentioned in literature, the rigidity of the medium is an important parameter for chiral induction during a photochemical reaction;<sup>41</sup> and good enantioselectivity was achieved when  $\beta$ -CD/pyridone complexes were irradiated in the solid state.<sup>42</sup>

#### 3.2.6.2.1 Irradiation of $\beta$ -CD/azepinone **8** complex in solid state powder form

##### 3.2.6.2.1.1 Experiment D: Mechanically ground mixture of $\beta$ -CD and azepinone **8**

One equivalent of azepinone **8** was mechanically ground with  $\beta$ -CD in a mortar. The powder mixture was then transferred to a quartz tube which was then closed and set to slowly rotate while being irradiated inside a Rayonet reactor (See Figure 47).

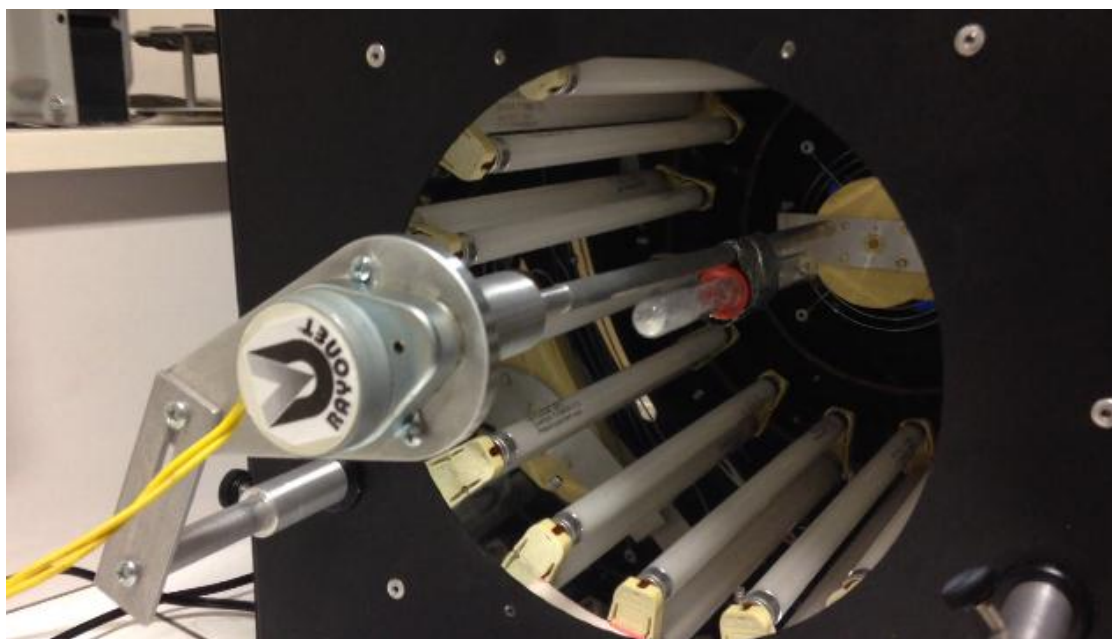


*Figure 37: A photo of the quartz tube containing the solid reactants inside a Rayonet reactor.*

The reaction was followed by  $^1\text{H}$  NMR and when no starting materials could be observed, the irradiated solid was dissolved in water then reduced with dihydrogen in the presence of 10% w/w Pd/C-10%. The 2-azabicyclo[3.2.0]heptan-3-one **10** was extracted from the aqueous phase with ethyl acetate, and the organic layer was concentrated to afford **10** as a yellow oil.

Four experiments were done in these conditions and the crude chemical yield was around 70%, although the *ee* was not constant, varying from 0 to 40%. The variable enantioselectivity suggested that mechanical grinding of azepinone **8** with  $\beta$ -CD does not give a sufficiently homogeneous mixture and thus can not be considered as a reproducible way to prepare the  $\beta$ -CD/azepinone **8** complex.

#### *3.2.6.2.1.2 Experiment E: “ $\beta$ -CD/**8** complex, filtered then irradiated in powder form”*

The  $\beta$ -CD/azepinone **8** milky suspension was filtered out and the solid residue was left to dry in open air, then finely crushed in a mortar.

The fine solid "complex" was introduced into a rotating quartz tube as illustrated in experiment **D** (see Figure 37 section 3.2.6.2.1.1). The rotation of the tube was intended to serve to stir the complex as it was being irradiated, but when performing the experiment, the

finely crushed solid always aggregated into small balls that need to be crushed regularly to achieve complete conversion (See Figure 38).



*Figure 38: Small balls of  $\beta$ -CD/azepinone **8** formed when the complex was irradiated in powder form in a rotating quartz tube.*

To avoid the aggregation, the fine powder was spread on a glass plate and irradiated inside the Rayonet reactor. Even though the exposed area was larger on the plate, the solid was standing still and should be homogenized by agitating it regularly using a spatula, in order to achieve complete conversion. The need for manual agitation rendered the experimental set-up unpractical, especially on larger scale.

The time needed for complete conversion of the starting material during the powder solid state experiments varied largely, from 6 to 60 h depending on the amount of the irradiated solid, its homogeneity and the surface area exposed to the irradiation.

When no starting materials were observed in the  $^1\text{H}$  NMR spectrum, the irradiated solid was dissolved in water to obtain a clear solution and the photoadduct **9** was then reduced with dihydrogen in the presence of 10% w/w Pd/C-10%. The 2-azabicyclo[3.2.0]heptan-3-one **10** was extracted from the aqueous phase with ethyl acetate. The organic phase was dried over  $\text{Na}_2\text{SO}_4$  then concentrated under vacuum to give **10** as a yellow oil.

Crude **10** from experiment **E** was obtained in 71% yield (for two steps) with respect to the amount of azepinone in the irradiated precipitate; the crude product was analyzed by chiral HPLC and showed an *ee* of 36%. The peak at 9.71 min corresponded to caprolactam **6** formed by the reduction of a small amount of the  $\beta$ -CD/azepinone **8** complex which had not been transformed by the electrocyclisation reaction (See Figure 39). No remaining

azepinone **8** was detectable by  $^1\text{H}$  NMR of the reaction mixture. This added further drawbacks to performing the irradiation in powder form.

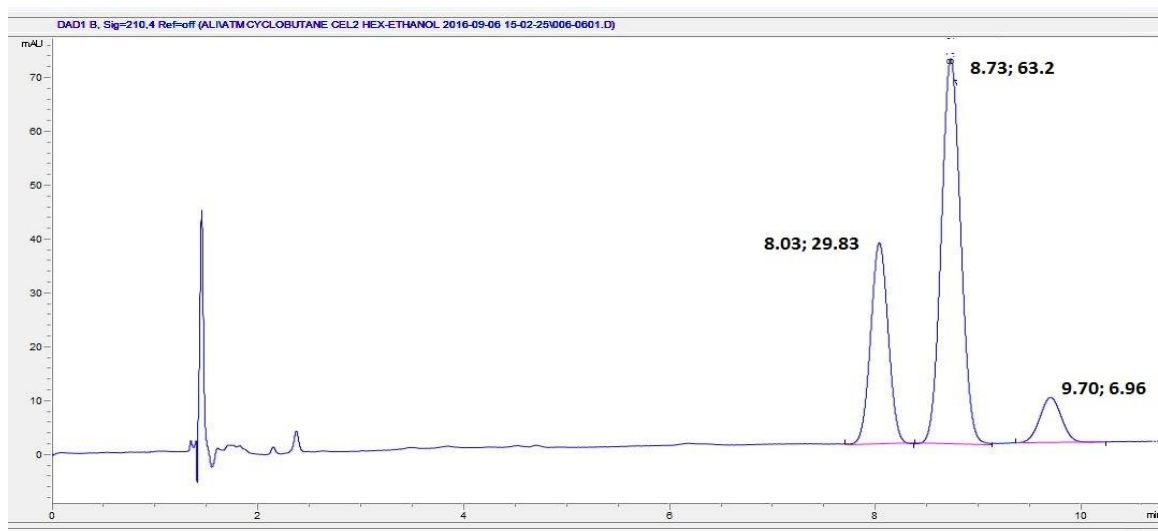


*Figure 39: Chromatogram of enantiomerically enriched 2-azabicyclo[3.2.0]heptan-3-one **10**, obtained from experiment E.*

#### 3.2.6.2.2 Irradiation in thin film form

##### 3.2.6.2.2.1 Experiment F: “1:1 film from 15 mM suspension”

In order to perform the irradiation in a more homogenous solid state and thus decrease the time needed for complete conversion, the starting milky suspension described above was spread on a glass plate and left to dry in open air to give a consistent white film. The film was irradiated directly in the Rayonet reactor (See Figure 40). The reaction course was followed by  $^1\text{H}$  NMR until complete conversion, which was achieved within 5 h. The solid was then dissolved in water to obtain a clear solution and the photoadduct **9** was reduced with dihydrogen in the presence of 10% w/w Pd/C-10%. The resulting 2-azabicyclo[3.2.0]heptan-3-one **10** was then extracted from the aqueous phase with ethyl acetate. The organic phase was dried over  $\text{Na}_2\text{SO}_4$  then concentrated under vacuum to give **10** with a crude yield of 77% over two steps.

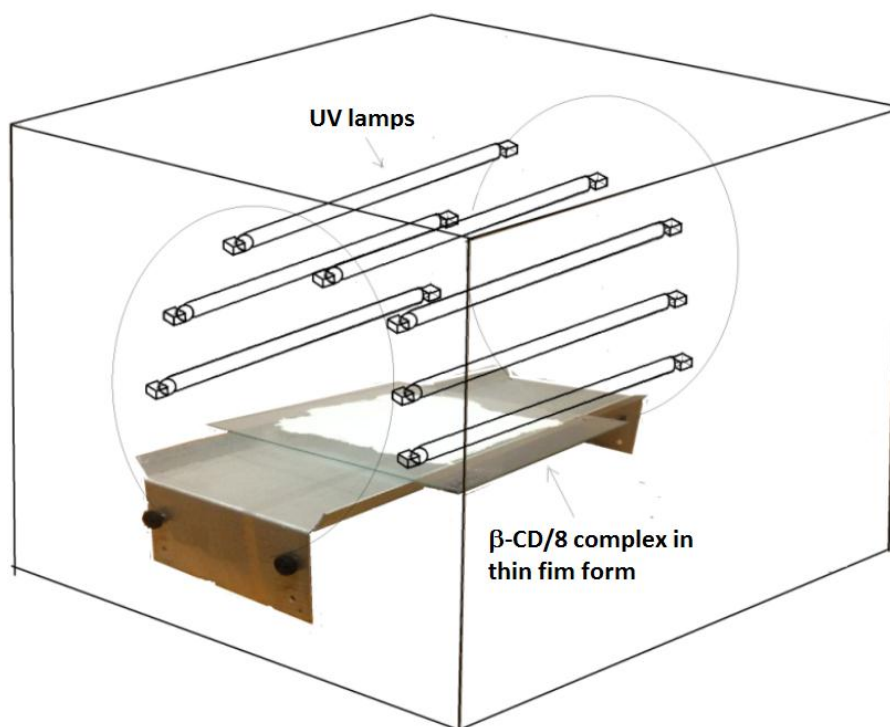


Figure 40: Schematic draw of  $\beta$ -CD/azepinone **8** complex being irradiated as a solid film form inside the Rayonet reactor.

The chiral HPLC analysis of the crude 2-azabicyclo[3.2.0]heptan-3-one **10** showed an *ee* of 41%. A small amount of caprolactam **6** (not detectable by  $^1\text{H}$  NMR) was also observed (see Figure 41).

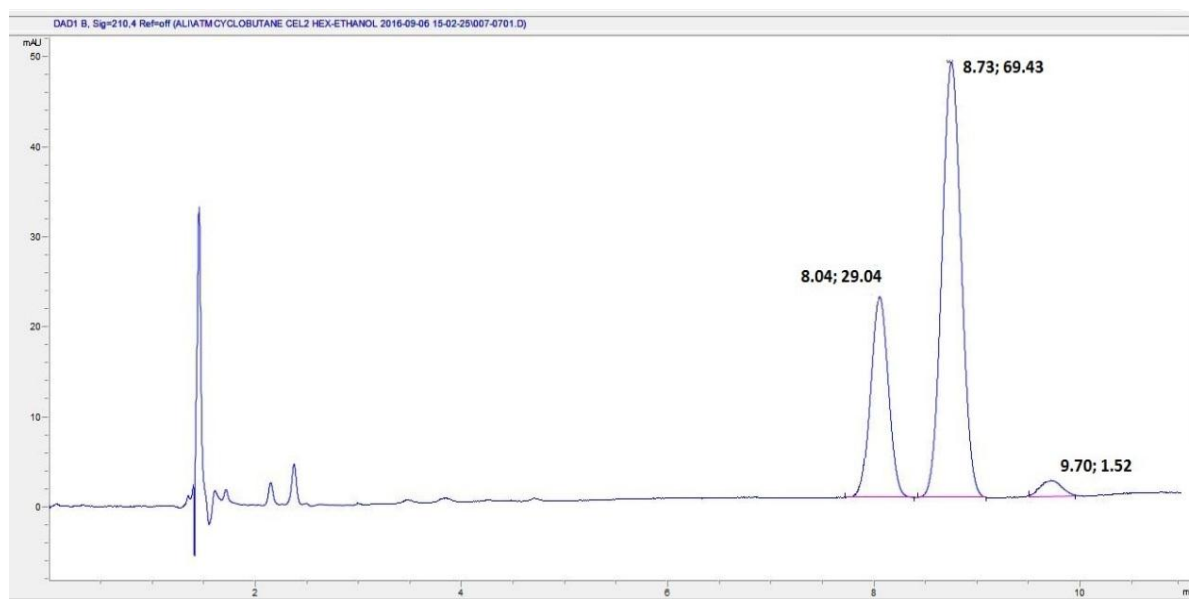


Figure 41: Chromatogram of crude enantiomerically enriched 2-azabicyclo[3.2.0]heptan-3-one **10**, obtained from experiment F.

### 3.2.6.2.2.2 Experiment G: “2:1 film from 15 mM suspension”

To drive the complexation equilibrium forward, two equivalents of  $\beta$ -CD were used in the preparation of the starting milky suspension. The suspension was then spread on a glass plate and left to dry in open air to give a consistent white film. The resulting thin film was irradiated inside the Rayonet reactor for 4-5 hours. The solid was then collected, dissolved in water, and the photoadduct **9** was reduced with dihydrogen in the presence of 10% w/w Pd/C-10%. The resulting 2-azabicyclo[3.2.0]heptan-3-one **10** was then extracted from the aqueous phase with ethyl acetate. The organic phase was dried over Na<sub>2</sub>SO<sub>4</sub> then concentrated under vacuum to give **10** with a yield of 77% over 2 steps. The chiral HPLC analysis of the crude product **10** showed an *ee* of 42%, still accompanied by traces of caprolactam **6** (see Figure 42).

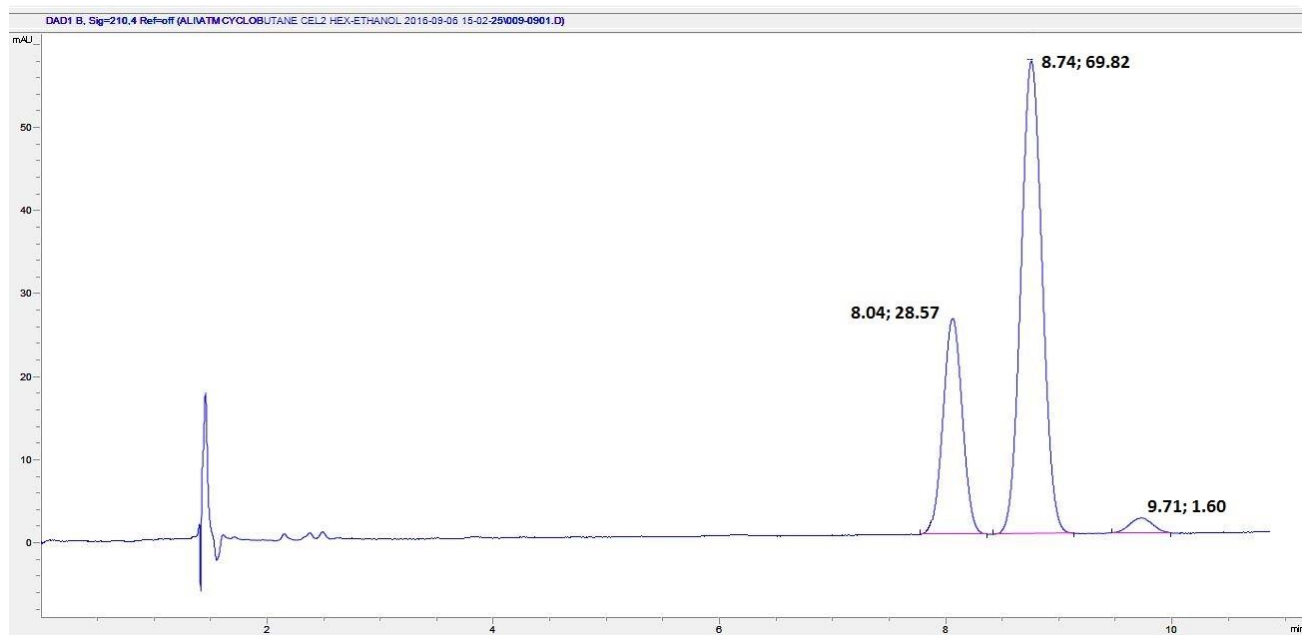


Figure 42: Chromatogram of crude enantiomerically enriched 2-azabicyclo[3.2.0]heptan-3-one **10**, obtained from experiment **G**

### 3.2.6.2.2.3 Experiment H: “1:1 film from 5 mM clear solution”

A 1:1 mixture of  $\beta$ -CD and azepinone **8** prepared in water at a concentration less than 5 mM did not give any precipitate, as we mentioned above. This clear solution was spread on a plate and the water allowed to evaporate. The resulting thin film was irradiated inside the Rayonet reactor. The solid was then collected, dissolved in water, and the photoadduct **9** was reduced with dihydrogen in the presence of 10% w/w Pd/C-10%. The resulting azabicyclo[3.2.0]heptan-3-one **10** was then extracted from the aqueous phase with

ethyl acetate. The organic phase was dried over  $\text{Na}_2\text{SO}_4$  then concentrated vacuum to give **10** with a yield of 78% over 2 steps. The chiral HPLC analysis of the crude product showed an *ee* of 41%. (see Figure 43)



*Figure 43: Chromatogram of the crude enantiomerically enriched 2-azabicyclo[3.2.0]heptan-3-one **10**, obtained from experiment **H**.*

### 3.2.7 The $\beta$ -CD/**8** complex film texture

Although the *ee* values in all three experiments on film type complexes was similar, a change in the texture and consistency of the film was observed when the concentration of  $\beta$ -CD was changed. A film made from a 1:1 mixture of  $\beta$ -CD and azepinone **8** at 15 mM (experiment F) was smooth and could detach itself from the glass plate, whereas at 5 mM (experiment H) the film always stuck to the glass and could only be scraped off (see Figure 44 and 45).

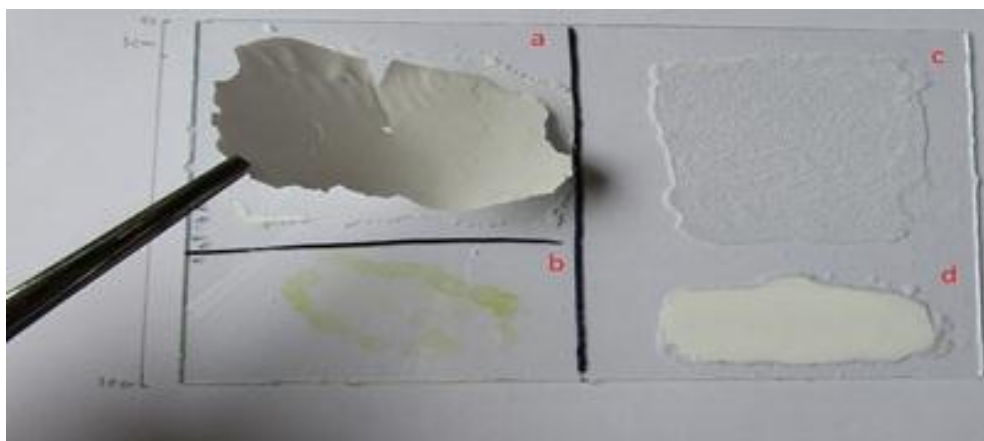


*Figure 44: Photo showing films of; (a) experiment **F**, (b) azepinone 8 alone , (c)  $\beta$ -CD alone, (d) experiment **H**.*



*Figure 45: Photo of 1/1  $\beta$ -CD/azepinone 8 complex film (experiment **F**) as it detaches itself from the glass plate after 2 days (left), and after 4 days (right).*

Moreover, the presence of two equivalents of  $\beta$ -CD at 15 mM (experiment **G**) gave a ragged, crispier, film with clear crystals all over it. Single crystal X-ray diffraction of the crystals showed only  $\beta$ -CD with water inside and outside the cavity (see Figure 49).



*Figure 46: Photo showing film of experiment **G***

### 3.2.7.1 Scanning electron microscopy (SEM) of $\beta$ -CD/azepinone **8** complex films

The solid films of all experiments along with one film made from azepinone **8** alone and another one from  $\beta$ -CD alone, were subjected to analysis by scanning electron microscopy. The pictures showed a well-organized fibrillar morphology in all films, in contrast with azepinone **8** alone and  $\beta$ -CD alone, which each showed only amorphous block structures (See Figure 47).

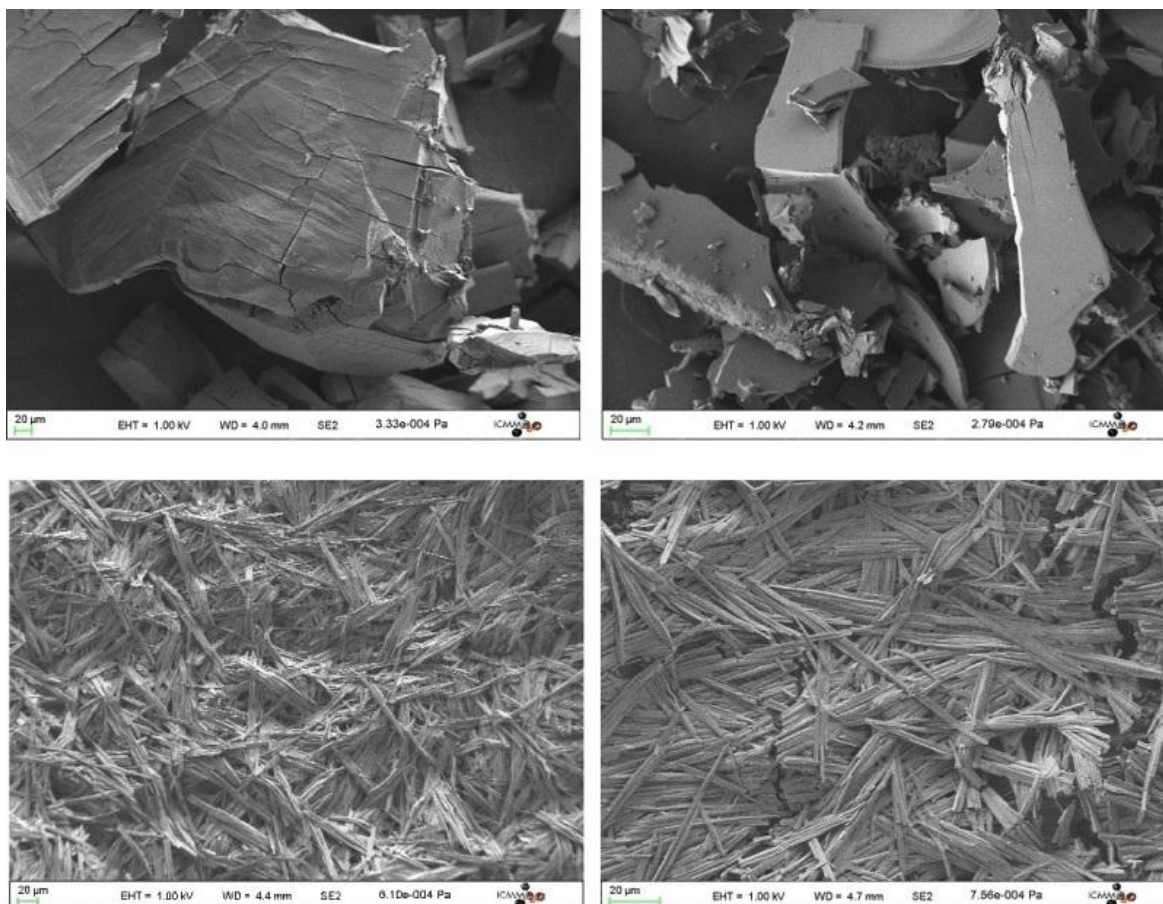
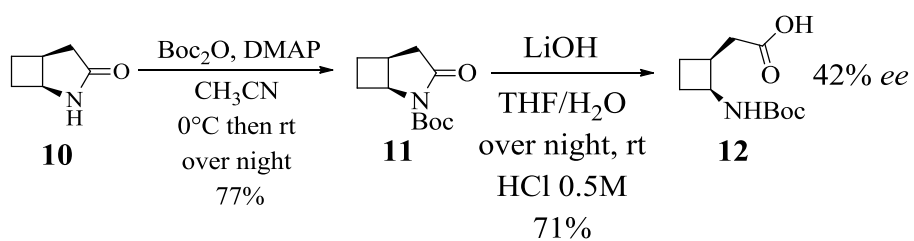


*Figure 47: SEM images of  $\beta$ -CD alone (top left), azepinone **8** alone (top right), film of experiment **G**: before irradiation (bottom left), and after irradiation (bottom right)*

### 3.2.8 The absolute configuration of compound **10**

In all the above-described experiments, the same major enantiomer of **10** was in evidence. To determine the configuration of this predominant enantiomer, a sample of **10** (from experiment G, 42% *ee*) was transformed into the *N*-Boc derivative of *cis*-<sup>3,4</sup>CB-GABA **12** following the known procedure.<sup>102</sup> The sample of **12** thus obtained had an optical rotation value of + 33 (*c* 0.5, CHCl<sub>3</sub>, at 25 °C). The literature value for a sample of (*R,R*)-**12** with

97% *ee* was reported as + 68 (*c* 0.96, CHCl<sub>3</sub>, at 27 °C), indicating that the major enantiomer of **10** had an 1*R*,5*R* absolute configuration (see scheme 43).



*Scheme 43: The chemical transformation of 10 into 12.*

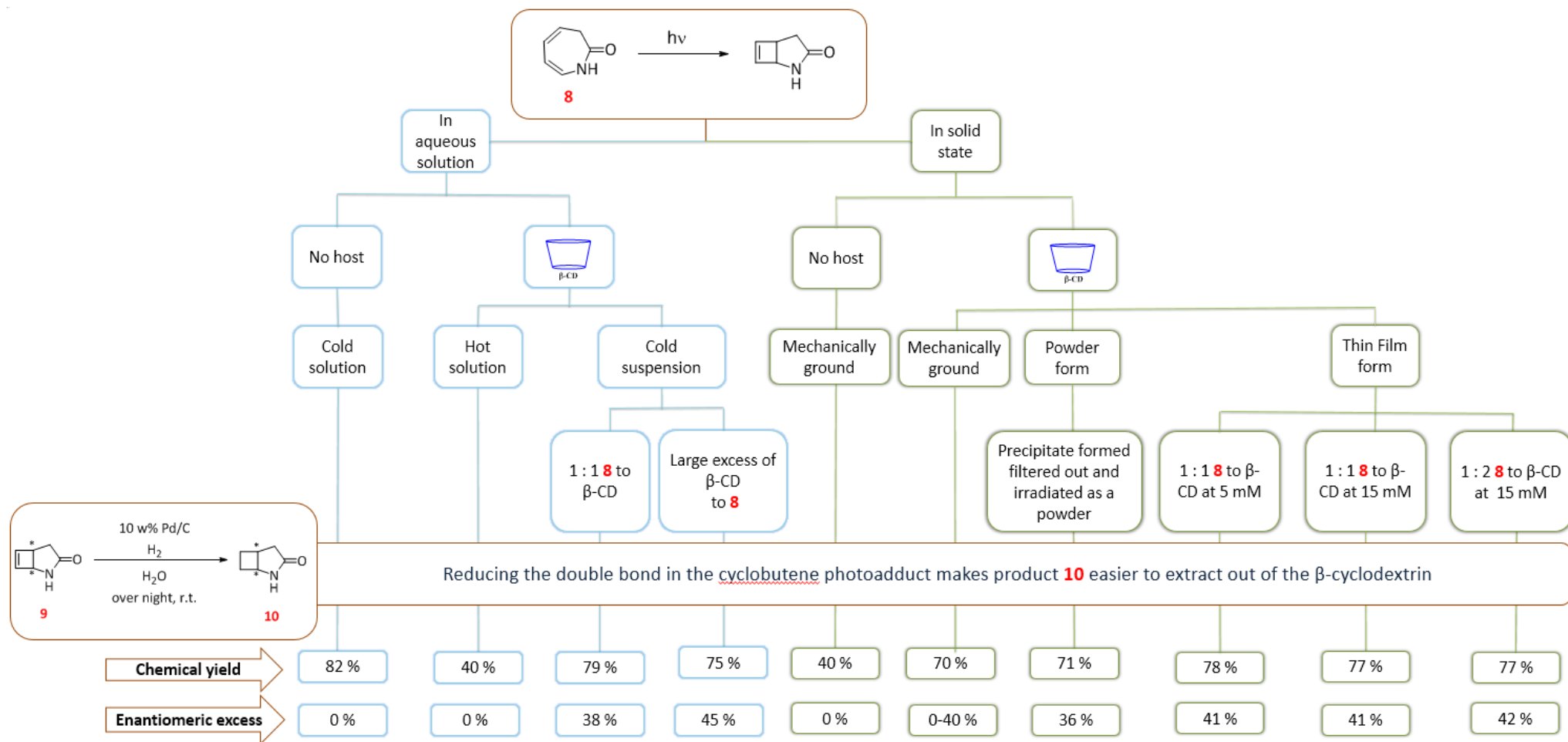


Figure 48: An overall summary of the different methods tested for the enantioselective photocyclization of azepinone **8** in the presence of CD as chiral host. The flowchart shows the corresponding yields over two steps and the measured enantiomeric excess for compound **10**.

### 3.3 Chiral resolution of ( $\pm$ )-*cis*-<sup>3,4</sup>CB-GABA by HPLC

Our efforts to obtain enantiomerically pure *cis*-<sup>3,4</sup>CB-GABA through the enantioselective photoelectrocyclization of azepinone **8** in the presence of  $\beta$ -CD as a chiral host, followed by reduction of the photoadduct, provided samples of 2-azabicyclo[3.2.0]heptan-3-one **10** with 45% *ee* at best.

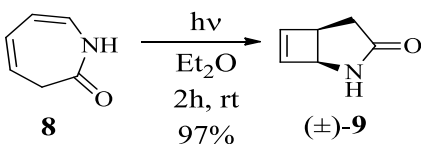
In order to have a more suitable method to access the target amino acid *cis*-<sup>3,4</sup>CB-GABA in enantiomerically pure form, we decided to develop a chiral resolution strategy for its *N*-Boc derivative using semi-preparative HPLC. Such a procedure would have several advantages when compared to the currently employed resolution methodology, which relies on chiral derivatization using an oxazolidinone, as we mentioned before.<sup>102</sup>

#### 3.3.1 Preparation of the Boc protected amino acid ( $\pm$ )-**12**

The multi-step synthesis of the *N*-Boc derivative of racemic *cis*-<sup>3,4</sup>CB-GABA, previously described by our collaborated groups, as we mentioned before.<sup>102</sup> We decided to reproduce this synthesis to obtain ( $\pm$ )-**12** on gram scale.

##### 3.3.1.2 Photoelectrocyclization of azepinone **8** in ether

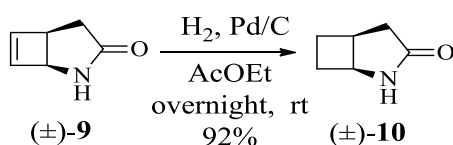
A solution of azepinone **8** was irradiated for 3 h with a 400 W mercury lamp under argon in a reactor fitted with a quartz filter and cooled by an external water/ice bath. The crude product was obtained after evaporation of the solvent, with a yield of 97%, as a brown solid (See Scheme 44). Since the photoadduct ( $\pm$ )-**9** is extremely insoluble in organic solvents, no purification was carried out. The <sup>1</sup>H NMR spectrum in CDCl<sub>3</sub> of the obtained compound ( $\pm$ )-**9** is consistent with the literature.<sup>102</sup>



*Scheme 44: Photocyclization of azepinone 8 in ether*

### 3.3.1.3 Catalytic hydrogenation of photoadduct ( $\pm$ )-**9**

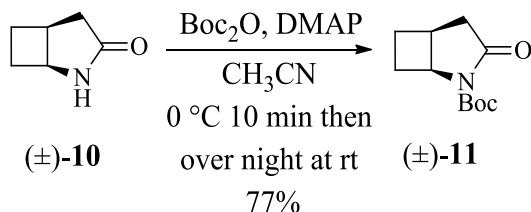
The photoadduct ( $\pm$ )-**9** was reduced overnight in ethyl acetate under dihydrogen, in the presence of 10% w/w Pd/C-10% (See Scheme 45). The reaction mixture was then filtered through Celite, and the filtrate was concentrated under vacuum to obtain the 2-azabicyclo[3.2.0]heptan-3-one ( $\pm$ )-**10** as a yellow solid with a yield of 92%, sufficiently pure to be used in the next step without purification.



*Scheme 45: Catalytic hydrogenation of photoadduct ( $\pm$ )-**9**.*

### 3.3.1.4 Activation of the 2-azabicyclo[3.2.0]heptan-3-one ( $\pm$ )-**10**

*tert*-Butyl 3-oxo-2-azabicyclo[3.2.0]heptane-2-carboxylate ( $\pm$ )-**11** was obtained by reacting 2-azabicyclo[3.2.0]heptan-3-one ( $\pm$ )-**10** with an excess of Boc<sub>2</sub>O in the presence of a catalytic amount of DMAP in acetonitrile at room temperature overnight (See Scheme 46). The reaction mixture was concentrated, and the crude product was purified by flash chromatography on silica. Compound ( $\pm$ )-**11** was obtained as a white solid with a yield of 77%.



*Scheme 46: Protection of 2-azabicyclo[3.2.0]heptan-3-one ( $\pm$ )-**10** with a carbamate group.*



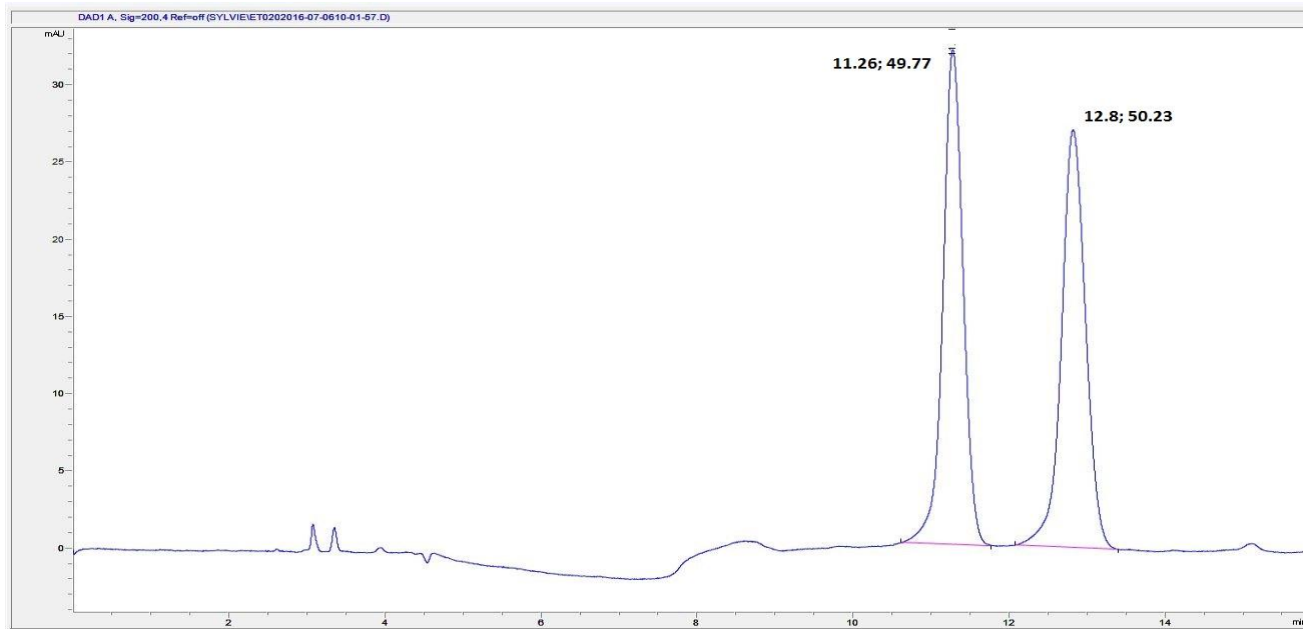


*Figure 49: HPLC chromatogram of racemic **12** showing separation of the two enantiomers on an analytical column.*

These conditions were then applied on a semi-preparative scale, a saturated solution of ( $\pm$ )-**12** in acetonitrile was introduced at a rate of 50  $\mu$ l each 15 min (50  $\mu$ l/injection). The eluted products were collected over three fractions; one that contained the first enantiomer, one that contained the second enantiomer, and a small middle fraction containing both (See Figure 50).

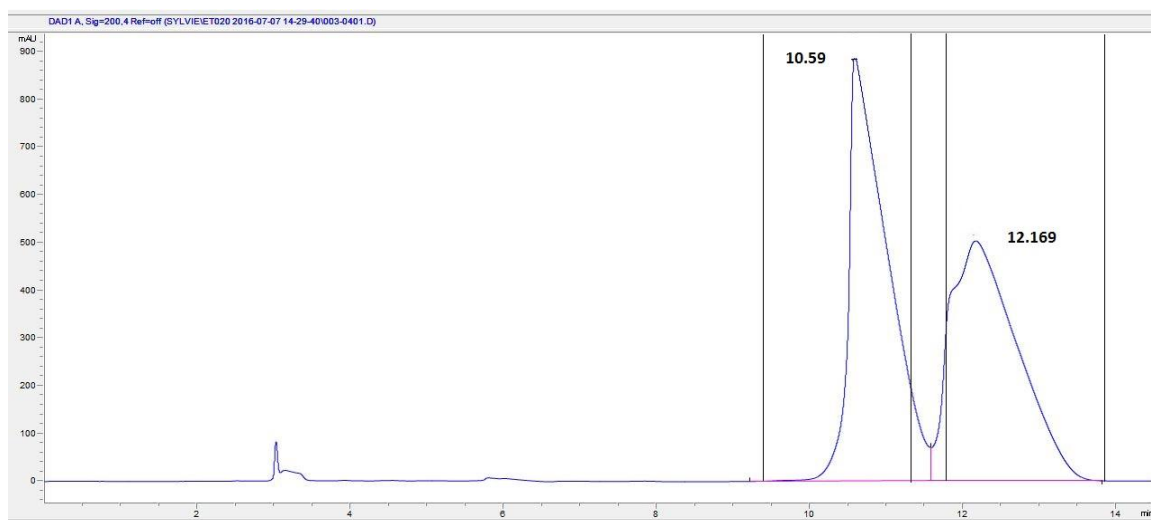


*Figure 50: HPLC chromatogram of racemic **12**, separation of the two enantiomers on a semi-preparative column.*

There were two main drawbacks in the separation of ( $\pm$ )-**12** under these conditions. The first one was that the relatively low solubility of amino acid **12** in acetonitrile, limits the separable amount of product to around 2.5 mg of each enantiomer per hour. The second one was the use of a large amount of water in the eluent which takes several hours to eliminate by lyophilization to obtain the dried products (-)-**12** and (+)-**12**.

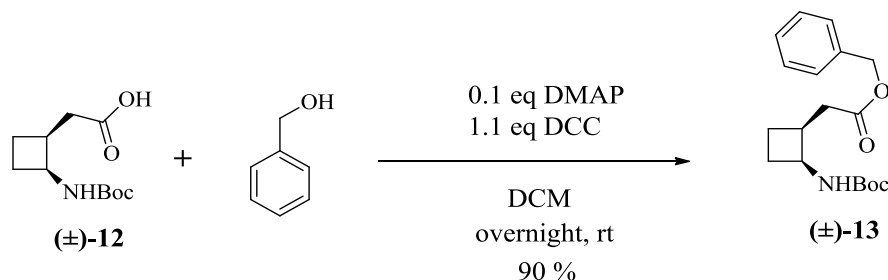
### 3.3.3 Switching to the *N*-Boc benzylic ester ( $\pm$ )-**13**

In order to circumvent these problems, we considered HPLC chiral resolution of the benzylic ester of ( $\pm$ )-**12**. The ester ( $\pm$ )-**13**, (see Scheme 48) was expected to be more soluble in organic solvents, which should improve the rate of the separation. Furthermore, it was proposed that ester ( $\pm$ )-**13** could be resolved using a normal phase column, thus avoiding the use of water as an eluent.

#### 3.3.3.1 Preparation of *N*-Boc benzylic ester ( $\pm$ )-**13**

To obtain ester ( $\pm$ )-**13**, compound ( $\pm$ )-**12** was reacted with one equivalent of benzyl alcohol in the presence of DMAP and DCC in dichloromethane, overnight. The reaction mixture was then

filtered and the filtrate was concentrated under vacuum. The crude product was purified over silica to obtain ( $\pm$ )-**13** as a white solid in 90% yield (see Scheme 50).



*Scheme 48: Synthesis of benzyl ester ( $\pm$ )-13 from ( $\pm$ )-12.*

### 3.3.3.2 Chiral HPLC resolution of *N*-Boc benzylic ester ( $\pm$ )-13

The *N*-Boc protected benzyl ester ( $\pm$ )-**13** was passed through a normal phase chiral Lux Cellulose-2 column using a 97/3 hexane/isopropanol eluting mixture, at 30 °C and a flow rate of 1 ml/min. Under these conditions, the two enantiomers of **13** were separated with a retention time difference of 2.4 min. Figure 51 shows a chromatogram of racemic **13** eluted on an analytical HPLC.



*Figure 51: HPLC Chromatogram of racemic 13, separation of the two enantiomers on an analytical HPLC.*

These conditions were then applied on semi-preparative scale. A 166 mg/ml solution of ( $\pm$ )-**13** in isopropanol was introduced at a rate of 120  $\mu$ l each 17 min (120  $\mu$ l/ injection). The eluted products were collected over three fractions: one that contained the first enantiomer, one that

contained the second enantiomer and a small middle fraction containing the second enantiomer along with traces of the first (See Figure 52).

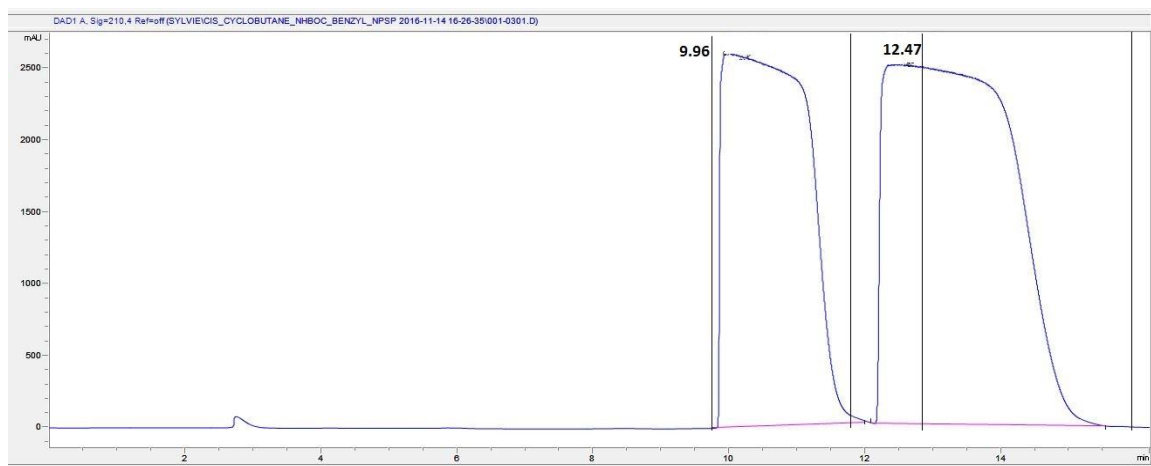


Figure 52: HPLC chromatogram of racemic amino acid ( $\pm$ )-13, separation of the two enantiomers on a semi-preparative column.

At this rate, around 70 mg of ( $\pm$ )-13 was processed per hour, to give 35 mg of the first enantiomer, 24 mg of the second one (see Figure 53), and 11 mg of a middle fraction containing more than 90% of the second enantiomer.

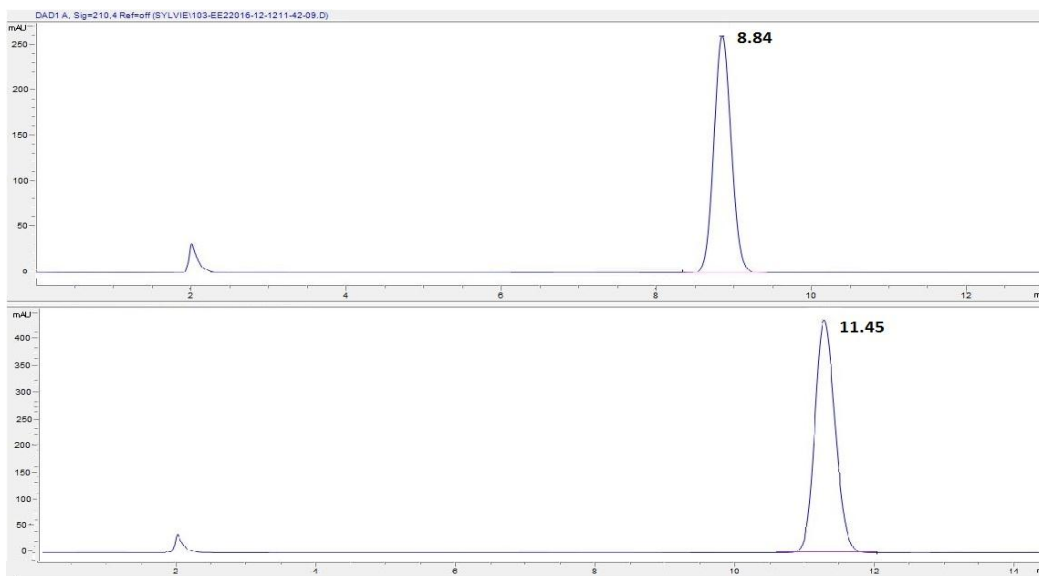


Figure 53: Chromatogram of the pure enantiomers (+)-13 (top) and (-)-13 (bottom)

The absolute configuration of the first enantiomer was determined by x-ray analysis and was found to have a (3*R*,4*R*) configuration. The second enantiomer was thus deduced to be the (3*S*,4*S*) enantiomer (see Figure 54).

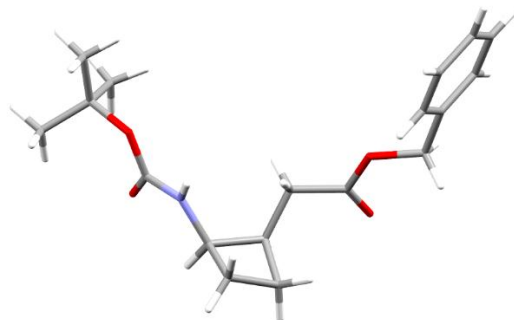


Figure 54: X-ray diffraction structure of the (3*R*,4*R*) enantiomer of the protected (+)-*cis*-<sup>3,4</sup>CB-GABA.

## 3.4 Conclusion

The 2+2 photoelectrocyclization of 1,3-dihydro-2*H*-azepin-2-one (**8**) was studied in the presence of  $\beta$ -CD as a chiral host. The formation of a precipitate upon mixing **8** with  $\beta$ -CD in aqueous solution suggested an interaction between the two components.  $^1\text{H}$  NMR titration experiments were conducted to explore this interaction and showed that the protons inside the  $\beta$ -CD cavity interacted with azepinone **8**, suggesting that the guest was bound, totally or partially, inside the hydrophobic cavity. Nevertheless, the absence of an inflection point in the titration curve with a maximum of variation in the chemical shifts, and a low  $K_b$  value of 35 suggested a fast equilibrium between the associated and the free form of the two molecules.

The photoelectrocyclization reaction of the formed  $\beta$ -CD/azepinone **8** precipitate was performed at different ratios of both components, in hot solution, in cold suspension, in solid powder form, as well as in a solid thin film form. The isolation of the photoadduct **9** from  $\beta$ -CD after the irradiation was not practical so it was reduced into 2-azabicyclo[3.2.0]heptan-3-one **10** in water in the presence of  $\beta$ -CD then extracted in an average chemical yield of 75% over two steps. While no enantiomeric excess was observed in hot solution, up to 45% enantiomeric excess of the (*R,R*) enantiomer could be reached in cold (5-8 °C) suspension and up to 42% in solid form.

The presence of  $\beta$ -CD provided a chiral environment for the photoelectrocyclization of azepinone **8** into photoadduct **9**, and its reaction into 2-azabicyclo[3.2.0]heptan-3-one **10** could be performed on a preparative scale, with a reasonable yield of 75% over two steps, but at best a 45% enantiomerically enriched mixture was obtained.

We established a more suitable method to access both enantiomers of *cis*-<sup>3,4</sup>CB-GABA via a semi-preparative HPLC fitted with a chiral column. The N-Boc benzyl ester derivative ( $\pm$ )-**13** was most amenable to this procedure. The use of semi-preparative HPLC circumvented the long procedure of chiral resolution using an oxazolidinone and provided both enantiomers of *cis*-<sup>3,4</sup>CB-GABA in a conveniently diprotected form.

# Chapter 4: Synthesis and Folding Pattern of $\gamma/\alpha$ -Hybrid Peptides

## 4.1 Introduction

The diversity of protein structures depends on the amino acid polypeptide backbone which can be induced to adopt a very large range of compact conformation. Privileged conformations are often stabilized by short- or long-range non-covalent interactions, leading to well-defined molecular architectures. Substantial progress has been made in establishing peptidomimic architectures, called foldamers, displaying helices, sheets and ribbon shapes.

The folding pattern of homogeneous oligomers of  $\alpha$ ,  $\beta$ , or  $\gamma$  amino acids have been more extensively studied than folding pattern of mixed hybrid  $\alpha/\beta$ ,  $\alpha/\gamma$  and  $\beta/\gamma$ -oligomers of amino acids. The most common regularly-folded architectures are helical: they include the 14-helix and the 9-helix for  $\gamma$ -peptides, the 13-helix and the 11/13-helix for  $\beta,\gamma$ -peptides, the 12-helix and the 12/10-helix for  $\alpha,\gamma$ -peptides.

Many of these secondary structures along with other helical manifolds have been anticipated and simulated by theoretical calculations of systematic conformational analysis.<sup>116, 117</sup> Mixed  $\alpha/\gamma$ -peptides manifolds merit further experimental investigations, to explore if indeed their folded architecture are as suggested by the Hoffman's group theoretical studies.

The Hoffman group<sup>117</sup> suggested through theoretical studies that in a hybrid  $\alpha/\gamma$  peptide a  $\theta$  dihedral angle around  $33^\circ$ , for the  $\gamma$ -amino acid component, is ideal for the formation of a 12/10 helix. The X-ray crystal structure of the *cis*<sup>3,4</sup>CB-GABA, which was synthesized in chapter three, showed that this molecule has an angle  $\theta$  around  $27^\circ$  which makes it a suitable building block for a hybrid  $\alpha/\gamma$ -peptide that could fold into a 12/10 helical secondary structure.

In this chapter we aim to synthesize, characterize, and study the three dimensional folding behavior of mixed  $\alpha/\gamma$ -peptides composed of alternating, enantiomerically pure *cis*<sup>3,4</sup>CB-GABA as the constrained  $\gamma$ -amino acid component and *D*-Alanine (*D*-Ala) as the  $\alpha$ -amino acid component. Two series of mixed  $\alpha/\gamma$ -peptides were studied one that has the (*R,R*)-*cis*<sup>3,4</sup>CB-GABA enantiomer as the  $\gamma$ -amino acid component and one that has the (*S,S*)-*cis*<sup>3,4</sup>CB-GABA enantiomer as the  $\gamma$ -amino acid component.

## 4.1.1 The Three dimensional conformation of polypeptides

In order to understand the three dimensional structure of a given polymer, two essential types of information should be known. The first one is the configuration of the monomer unit itself, and the second, is the relative orientation of the units at each linkage.

### 4.1.1.1 The conformation of the peptide link

In the case of polypeptides, the dimensions of the peptide unit itself has been determined by Pauling and Corey,<sup>119, 120</sup> although slight variations are observed in certain structures, it is established that the peptide link or amid unit form a considerably rigid plane. The origin of this planer organization of the amid unit, is the resonance of the double bond between the carbon-oxygen and carbon-nitrogen positions which leads to a partial double bond character between the O-C-N atoms (see Figure 55).<sup>119</sup> As a consequence, the set of atoms  $C\alpha_n$ -C'-O-NH- $C\alpha_{n+1}$ , starting from one  $\alpha$ -carbon and going to the next  $\alpha$ -carbon atom, forms a planer group.

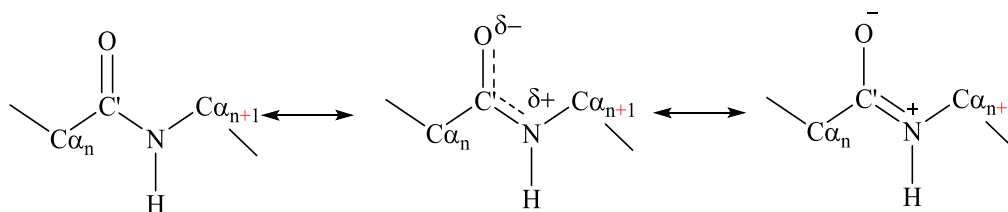
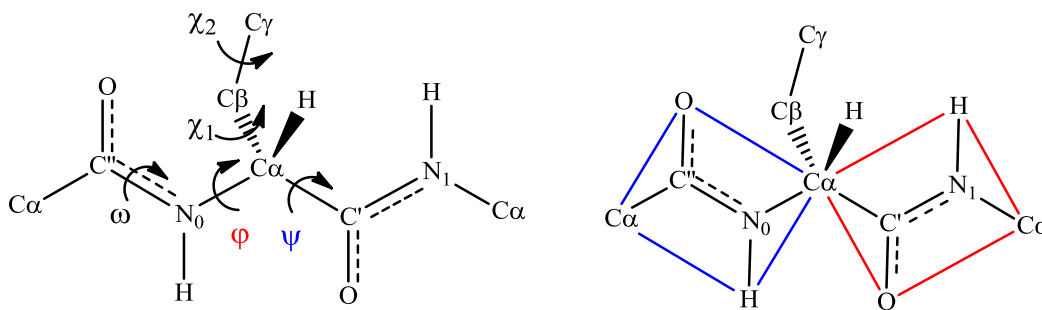


Figure 55: The resonant structures of the peptide unit.

#### 4.1.1.2 The conformation around the peptide bond

When two peptide groups are linked together, it is possible to have a rotation of the planar amid units around the bonds  $N-C\alpha_n$  and  $C\alpha C'$ , and thus the relative configuration of the two groups about the  $C\alpha$  atom can be indicated by two parameters  $\varphi$  and  $\psi$ .<sup>118</sup>

To properly visualize the two rotations around  $C\alpha$ , the two planar amid units are first kept in the same plane, fully stretched with the carbonyls pointing roughly in opposite directions (see Figure 56). Now, the  $O-C''-N_0$  residue (blue) is held in plane, and the other unit (red) as a whole is given a rotation of an angle  $\varphi$  about the  $N_0-C\alpha$  bond, in an anticlockwise sense looking from  $N_0$  towards  $C\alpha$ . This bond,  $N_0-C\alpha$ , is then tightened and the  $O-C''-N_0$  residue (blue) is then rotated through the angle  $\psi$  about the  $C\alpha-C'$  bond, in a clockwise sense, looking from  $C'$  towards  $C\alpha$ . The resulting dipeptide has now a conformation which can be described by the dihedral angles ( $\varphi, \psi$ ).



*Figure 56: The dihedral angles ( $\varphi, \psi, \omega$ , and  $\chi$ ) that describe the conformation of two peptide units.*

This procedure could be further applied for describing the conformation of a complete polypeptide chain containing “n” amino acid residues by first keeping them all stretched in the same plane, and then applying, the series of rotations ( $\varphi_1, \psi_1$ ), ( $\varphi_2, \psi_2$ ). . . up to ( $\varphi_n, \psi_n$ ) at each successive  $\alpha$ -carbon. The obtained set of n pairs of dihedral angles contains the most important information needed for describing the conformation of the backbone for the entire polypeptide chain.<sup>121</sup>

The  $\phi$  and  $\psi$  parameters would be enough to fully describe the conformation of a polypeptide chain only when each peptide unit is considered as an ideal plane with the same dimensions at every  $\alpha$ -carbon. In reality this is never the case, and the dimensions at each peptide unit can vary. In order to compensate for these variations, it is necessary to have further parameters to completely describe the conformation of a polypeptide chain.

To describe the deviation of a peptide unit from being an ideal plane, we need to define the dihedral angle  $\omega$ . It represents a rotation around the peptide bond  $C'-N_1$  and may be defined as the angle between the planes  $C\alpha-C'-N_1$  and  $C'-N_1-C\alpha$  (See Figure 59). Another parameter that affects the overall conformation of a poly peptide chain is denoted by  $\chi$ , which describes the conformation of the atoms in the side chain, and is denoted by a series of dihedral angles  $\chi_1, \chi_2$ , etc., that describe the rotations about the bonds  $(C\alpha-C\beta)$ ,  $(C\beta-C\gamma)$ , etc.

Nevertheless, it is important to realize that, although these  $\phi$ ,  $\psi$ ,  $\omega$ , and  $\chi$  parameters are all needed to describe the exact conformation of a polypeptide chain. The most important parameters are the  $\phi$  and  $\psi$  angles. A good knowledge about the conformation of the polypeptide chain may be obtained from a set of these two dihedral angles.

## **4.1.2 The folding pattern in natural peptides**

### **4.1.2.1 The Ramachandran diagram**

The dihedral angles  $\phi$  and  $\psi$  are both defined over a range of  $[-180^\circ, 180^\circ]$ . The  $\phi, \psi$  values for each amino acid residue can be plotted, with  $\phi$  along the horizontal axis, and  $\psi$  along the vertical one, to produce what is referred as Ramachandran diagram or a  $[\phi, \psi]$  plot. (See Figure 57)

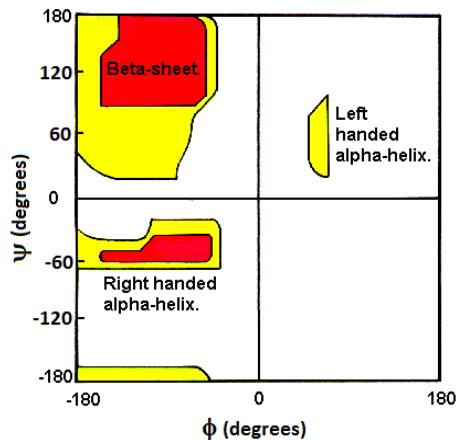


*Figure 57: The Ramachandran plot for all residues, except glycine, with the permitted combinations of torsional angles shown as colored regions.*

The Ramachandran diagram gives a graphical representation of all the possible combinations of dihedral angles  $\phi$  and  $\psi$ . In fact, many of these angle combinations are not allowed due to steric hindrance between atoms.

By looking at a Ramachandran diagram, one can determine the allowed and disfavored torsional angles thereby obtaining an insight into the structural conformation of a given peptide. For instance, the Ramachandran diagram of Figure 57 indicates the different pairs of dihedral angles allowing the formation of  $\alpha$ -helices and  $\beta$ -sheets conformationally accessible in natural proteins.

#### **4.1.2.2 Conformation of natural peptides**

Proteins can have four different structural levels. The most basic one is the linear arrangement of amino acid residues in a polypeptide, which defines its primary structure. Due to stabilizing hydrogen bonds between certain residues, parts of this linear amino acid sequence can assume local structural conformations. These different spatial arrangements define the protein's secondary structure. Peptides secondary structure includes: helices, strands and loops. The folding of a polypeptide into its secondary structure puts some specific amino acids in a close proximity. This can lead to a further folding of the protein into its tertiary structure, which is defined as the overall three-dimensional shape of the entire protein molecule. Some proteins

can show an additional level of organization, when they interact with other proteins and arrange themselves to form an aggregate protein complex called the protein quaternary structure. The final structure of the protein is stabilized by different interaction between its constituents (see Figure 58).<sup>122</sup>

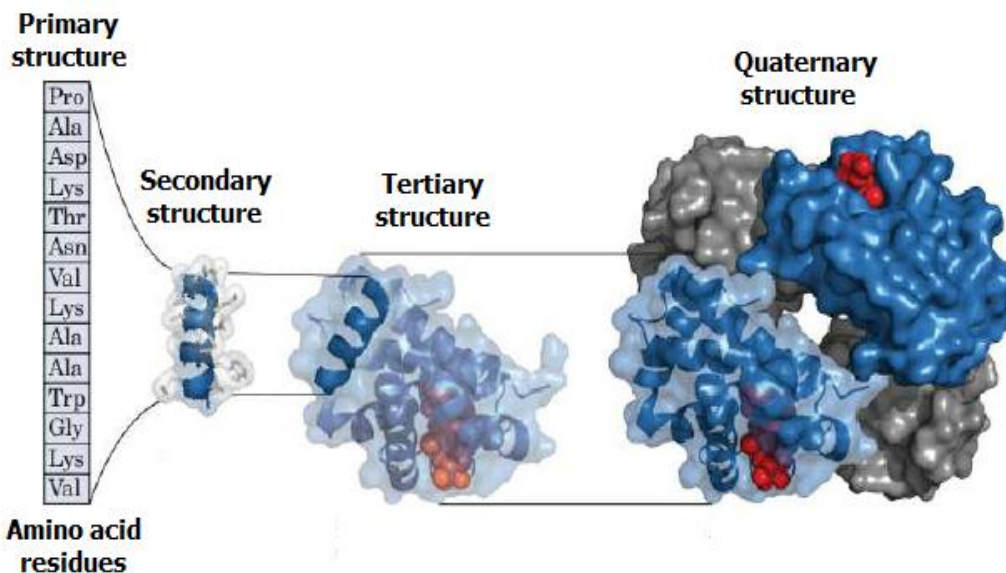


*Figure 58: The Primary, secondary, tertiary, and quaternary structures of protein<sup>122</sup>*

#### 4.1.2.2.1 The $\alpha$ -helix “natural helix”

Helices are the most abundant secondary structures found in globular proteins.<sup>123</sup> They are named p(n)-helix according to the number of atoms (n), and the number of residues (p) for each turn. For example, a 3(10)-helix has 10 atoms and 3 residues per turn.

As mentioned in section 4.1.1.2 above, the secondary structure i.e. the three dimensional folding pattern of a polypeptide is governed by the repeated display of a particular set of backbone dihedral angles  $\phi$  and  $\psi$ . Table 7 shows the ( $\phi$ ,  $\psi$ ) values that define the three types of natural protein helices.

Helix type	$\Phi$	$\Psi$
$\alpha$	$-58^\circ$	$-47^\circ$
$3_{10}$	$-49^\circ$	$-26^\circ$
$\pi$	$-57^\circ$	$-70^\circ$

Table 7: The ( $\phi$ ,  $\psi$ ) values that define the three types of natural protein helices.

The three types of helix whose  $\phi$  and  $\psi$  are presented Table 7, are populated differently in natural proteins.<sup>123, 124</sup> The 3.6(13)-helix also known as the right handed  $\alpha$ -helix was discovered by L. Pauling and is the most abundant helix in natural proteins.<sup>119, 125</sup> About 32-38% of residues are involved in  $\alpha$ -helices. The 3.0(10)-helix also known as the  $3_{10}$ -helix is a rare secondary structure of natural proteins. It accounts for only 3.4% of all residues. The  $3_{10}$ -helices are typically very short structures, found at the beginning or the end of some  $\alpha$ -helices. The  $\pi$ -helix, or 4.4(16)-helix, has been recently discovered and is an extremely rare protein secondary structure that is found at the end of certain  $\alpha$ -helix.<sup>126</sup> The left-handed 3.6(13)-helix and the 2.2(7), 4.3(14) or 4.4(16)-helices, have been predicted but never yet found in natural proteins.<sup>127</sup>

### 4.1.3 The folding pattern in unnatural peptides

During the past few decades, chemists have been inspired by the ability of natural peptides to fold into a well-defined helical secondary structure. These self-organized systems have gained an increasing attention, and have found various applications, like molecular recognition, peptidomimetics, and therapeutics.<sup>128, 129</sup> (**128**) (**129**) The term “foldamers” was first coined by Gellman<sup>130</sup> and defines “oligomers with a strong tendency to adopt a specific conformationally ordered structure in solution, stabilized by a set of noncovalent interactions between nonadjacent monomer units”.<sup>131</sup> These noncovalent interactions include steric repulsions, hydrogen-bonding, electrostatic and  $\pi$ - $\pi$  interactions, coordination to metal ions, as well as solvophobic effects. Out of these interactions, hydrogen-bonding are the most versatile in creating intra-strand connections that could stabilize a well-defined three dimensional structure adopted by an oligomeric peptide chain.<sup>129</sup>

The early studies of Gellman<sup>130, 132</sup> and Seebach<sup>133, 134</sup> and the later contributions of Hofmann<sup>116, 117, 135</sup> have certainly initiated the rapidly evolving field of foldamers. In this context, several homo and hybrid peptides of  $\alpha$ ,  $\beta$ , and  $\gamma$ -amino acids have been studied for their preferential three dimensional folding pattern.

#### 4.1.3.1 Folding pattern in homo-peptides

##### 4.1.3.1.1 $\beta$ -Peptides

$\beta$ -amino acids are homologated analogous of  $\alpha$ -amino acids. The additional backbone carbon inserted between the carboxylic acid and the amino group gives to  $\beta$ -peptides an additional dihedral angle  $\theta$ , and thus a higher conformational flexibility than  $\alpha$ -peptides (see Figure 59). This additional torsional freedom does not prevent the formation of ordered secondary structures in  $\beta$ -peptides.<sup>132, 136</sup>

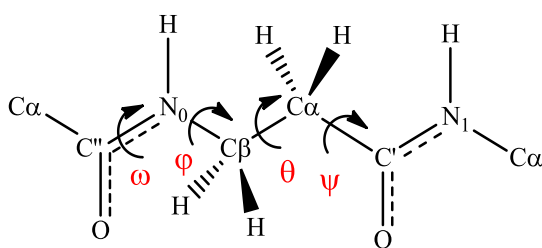


Figure 59: The dihedral angles in a  $\beta$ -peptide.

The Hofmann group<sup>135, 136</sup> predicted via *ab initio* calculations the different types of helices that could be adopted by  $\beta$ -peptide. So far, seven different helices have been experimentally observed (see Figure 60, solid arrows); the 8-,<sup>137</sup> 10-,<sup>138</sup> 10/12-,<sup>139</sup> 12-,<sup>140</sup> 12/10-,<sup>141</sup> 14-,<sup>133</sup> and 18/20-helices.<sup>142</sup>

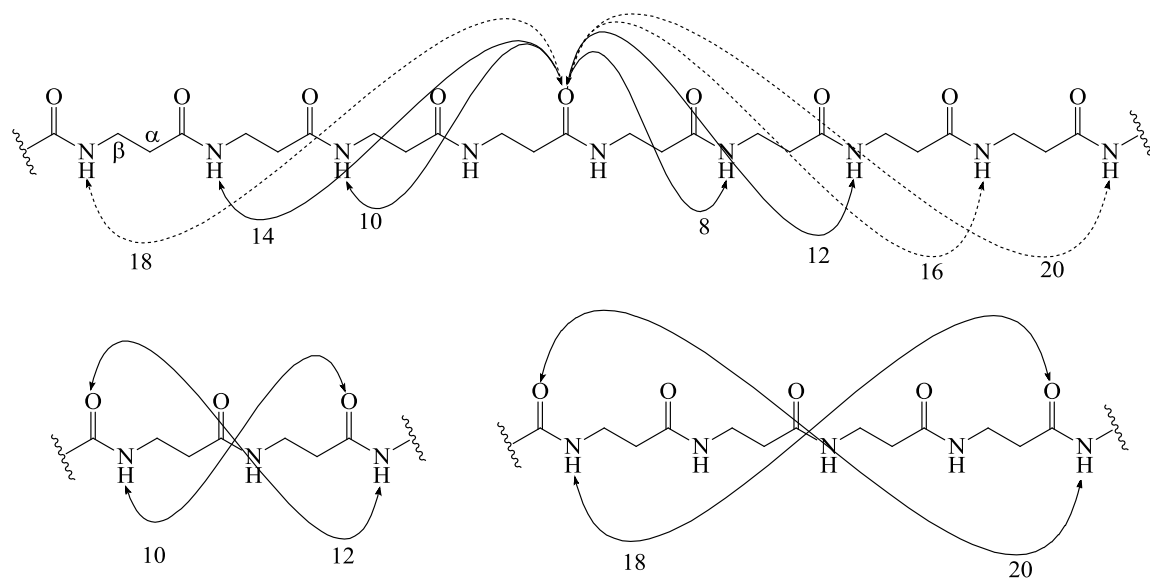


Figure 60: The different types of helices that could be adopted by a  $\beta$ -peptide, as predicted by the Hofmann group. Solid arrows indicate the so far experimentally observed ones.

#### 4.1.3.1.1.1 Example and application of the $\beta$ -Peptides

The 12- and 14-helical structures adopted by  $\beta$ -peptides are the most important ones. The helicity in these two structures is comparable to the one of a native  $\alpha$ -helix (13-helix). This has led researchers to study  $\beta$ -peptides as scaffolds to mimic certain native  $\alpha$ -helices in terms of structure and biological activity.<sup>129</sup>

One example is the 17-residue  $\beta$ -peptide prepared by the Gellman group.<sup>143</sup> Their peptide was composed of (*R,R*)-*trans*-2-aminocyclopentanecarboxylic acid (*trans*-ACPC) and *trans*-4-aminopyrrolidine-carboxylic acid (*trans*-ACP) (see Figure 61). The *trans*-ACP served as a cationic residue giving an amphiphilic property to the formed 12-helix, which was essential to mimic the biological activity of amphiphilic cationic antimicrobial peptides found in nature.

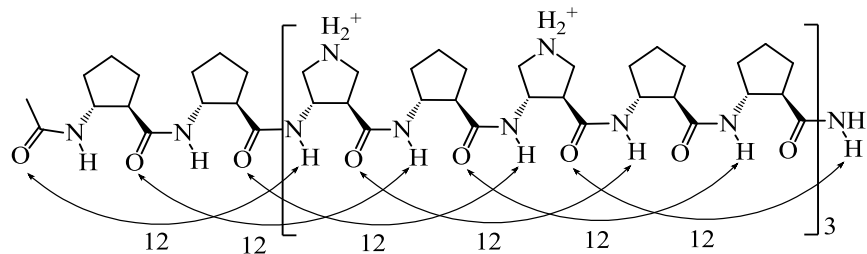


Figure 61: The Gellman's group 12-helix antimicrobial  $\beta$ -peptide.

#### 4.1.3.1.2 $\gamma$ -peptides

$\gamma$ -amino acids are doubly homologated  $\alpha$ -amino acids, the two extra carbons inserted between the carboxylic acid and the amino group gives them two additional dihedral angle  $\theta$ , and  $\zeta$  which makes  $\gamma$ -peptides more flexible than their  $\alpha$ - and  $\beta$ -counterparts (see Figure 62).

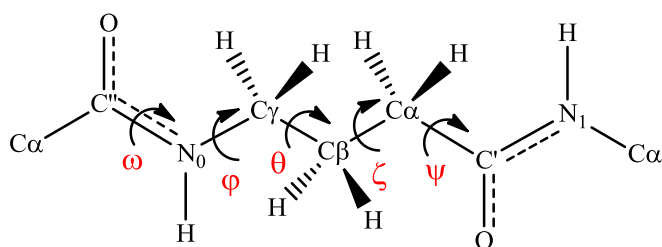


Figure 62: The dihedral angles in a  $\gamma$ -peptide.

The Hofmann group predicted via *ab initio* calculations that a hexamer  $\gamma$ -peptide has the ability to fold into eight different helical secondary structures.<sup>144</sup> So far only the 7-,<sup>145</sup> 9-,<sup>146</sup> and 14-helices<sup>147</sup> have been experimentally observed (see Figure 63, solid arrows). One should note that the folding pattern with a 7-membered pseudocycle arising from intraresidual H-bond formation is viewed as a 7-ribbon rather than a helix due to its small pitch and flattened structure.

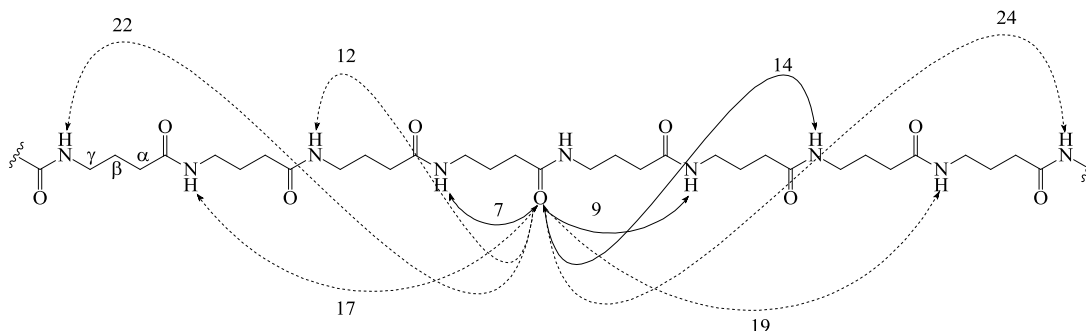


Figure 63: The different types of helices that could be adopted by a  $\gamma$ -peptide, as predicted by the Hofmann group. Solid arrows indicate the so far experimentally observed ones.

#### 4.1.3.1.2.1 Examples and application of the $\gamma$ -peptides

Unlike  $\beta$ -peptides,  $\gamma$ -peptides did not receive any attention in the field of biological applications. The prepared  $\gamma$ -peptides were only a subject of structural and conformational behavior studies. Hanessian<sup>147</sup> and Seebach<sup>148,149, 150</sup> groups independently studied one example of substituted  $\gamma$ -peptides that fold into a stable 14-helix (see Figure 64). The research groups also pointed out the effect of having a substituent at the C-4 position in promoting the formation of a helical structure in  $\gamma$ -peptides. For instance,  $\gamma^4$ ,  $\gamma^{2,4}$ ,  $\gamma^{2,3,4}$ -peptides all adopted a 14-helical structure, whereas  $\gamma^2$ ,  $\gamma^3$ -peptides folded into a flexible, hard to determine structure.

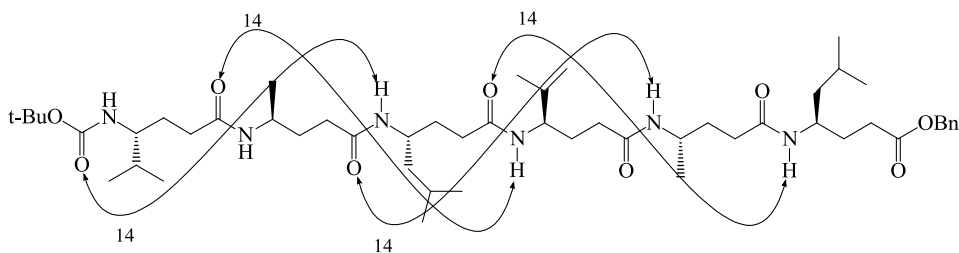


Figure 64: One example of the  $\gamma^4$ -peptides that fold into a stable 14-helix, from Seebach's group.

#### 4.1.3.2 Folding pattern in hybrid peptides

Hybrid peptides include  $\alpha/\beta$ ,  $\alpha/\gamma$ , and  $\beta/\gamma$ -peptides. They have drawn much attention due to their ability to further expand the scope of foldamers in terms of variations in the backbone pattern compared to their homo-peptides counterparts. Furthermore, incorporating unnatural amino acids such as  $\beta$  or  $\gamma$ -amino acids into an  $\alpha$ -peptide sequence with a proteinogenic side chain needed for biological activity, could enhance its *in vivo* proteolytic stability, due to the absence of suitable enzymes. This heterogeneous structure could so allow the peptide to keep its biological function without being easily hydrolyzed by the protease enzymes.<sup>151, 152</sup>

In hybrid peptides, the formed hydrogen-bonding interactions between the non-neighboring amino acids that define their helical structures, could be categorized into three types: hydrogen bonds formed in a backward direction along the sequence, hydrogen bonds formed in a forward direction of the sequence, and hydrogen bonds formed alternately in backward and forward direction (see Figure 65).<sup>116</sup>

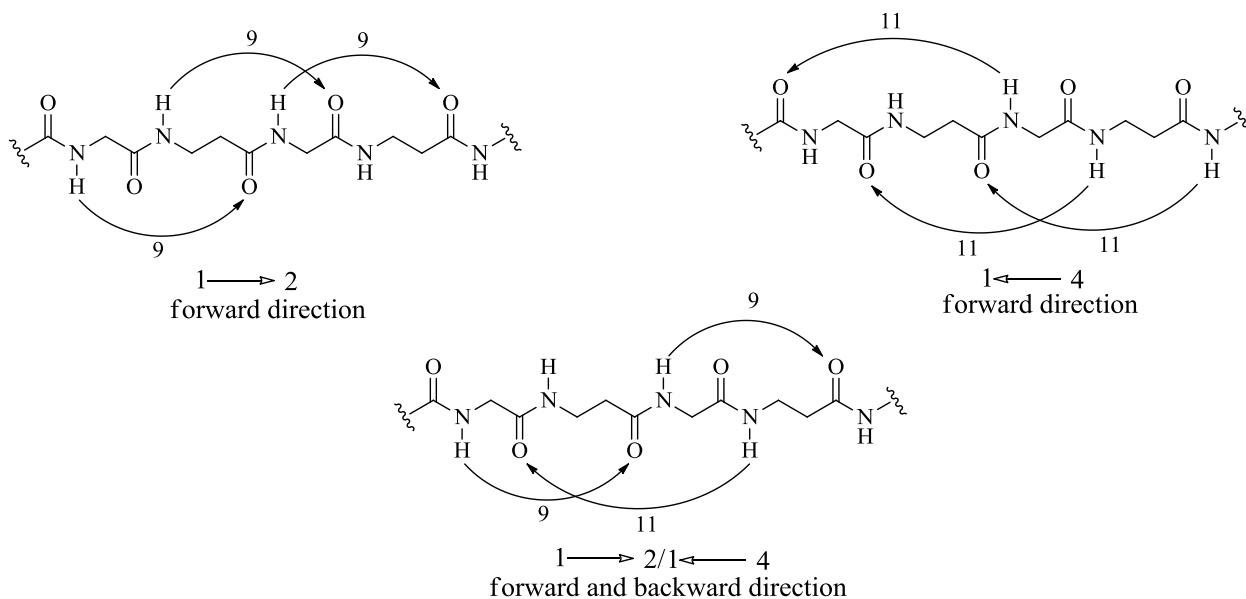


Figure 65: The three possible directions of hydrogen bonding in an  $\alpha/\beta$ -hybrid peptide.

#### 4.1.3.2.1 Mixed $\alpha/\beta$ -peptides

The Hofmann group studied the possible helical secondary structures that could be adopted by a, free of strain,  $\alpha/\beta$ -octapeptide composed of alternating glycine and  $\beta$ -alanine.<sup>116</sup> The authors found via *ab initio* calculations that such a peptide could fold into seven distinct stable helices which are: 9/11-, 11/9-, 11-, 12/13-, 14/15, 16/18- and 18/16-helices.

So far, only the 11/9-,<sup>153</sup> 11-,<sup>154</sup> 12/13-,<sup>155</sup> and 15/14-helices<sup>156</sup> have been experimentally observed.

##### 4.1.3.2.1.1 Examples of $\alpha/\beta$ -peptides and applications

One example of  $\alpha/\beta$ -hybrid peptide, was studied by the Gellman group.<sup>157</sup> The authors were able to design a chimeric peptide composed of an *N*-terminal  $\alpha/\beta$ -fragment and a *C*-terminal  $\alpha$ -fragment. The  $\alpha/\beta$ -fragment which was made of *trans*-ACP and *trans*-ACPC folded into a 15/14-helical structure whereas the  $\alpha$ -fragment composed of proteinogenic amino acids adopted a native  $\alpha$ -helix structure (see Figure 66). This  $\alpha/\beta+\alpha$ -peptide had the ability to bind, with an inhibitory effect, to its target transmembrane protein (Bcl-x<sub>L</sub>). This demonstrates the potential use of specially designed peptide foldamers to inhibit certain protein-protein interactions.

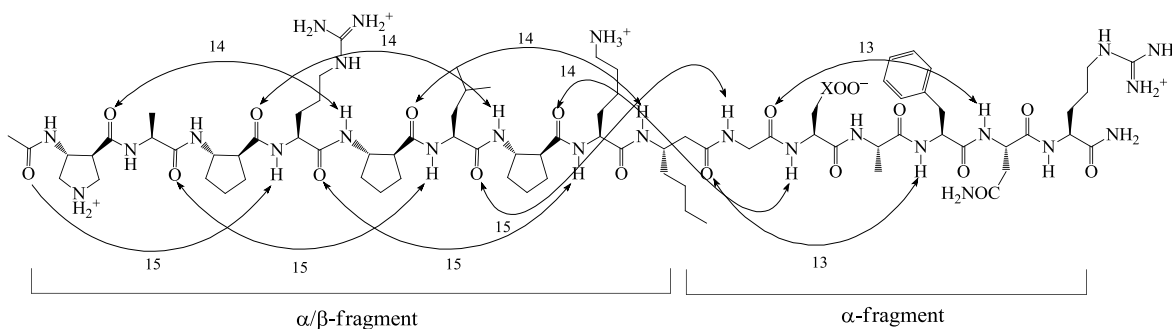


Figure 66: The Gellman's group chimeric  $\alpha/\beta+\alpha$ -peptide.

#### 4.1.3.2.2 Mixed $\beta/\gamma$ -peptides

The  $\beta/\gamma$ -peptides form another class of hybrid peptides, which consist of alternating  $\beta$ - and  $\gamma$ -amino acids.  $\beta/\gamma$ -peptides are interesting due to their ability to adopt helical secondary structures that mimic those of the native  $\alpha$ -peptides, such as the 13- or  $\alpha$ -helix.

The Hofmann group studied via *ab initio* calculations the different possible helical structures which could be adopted by a  $\beta/\gamma$ - octapeptide composed of alternating  $\beta$ -Glycine and GABA.<sup>117</sup> The authors found ten distinct stable helical forms: 11-, 11/13-, 13/11-, 13-,15/16-, 18/17-, 20-, 20/22-, 22/20- and 22-helices. Out of the ten stable helical structures predicted by the Hofmann group, the 11/13-helix has been experimentally observed in solution and the 13-helix has been observed both in solution and in solid state.

Recently the Aitken group were the first to established the ability of  $\beta/\gamma$ -peptide composed of (1*R*,2*R*)-2-aminocyclobutane carboxylic acid (*trans*-ACBC) and GABA, to fold into a 9/8-ribbon, with alternating 9-, 8-hydrogen bonding pseudocycles.<sup>158</sup>

##### 4.1.3.2.2.1 Examples of $\beta/\gamma$ and applications

As mentioned above the  $\beta/\gamma$ -hybrid peptides are important because they are able to fold into a 13-helix similar to the natural  $\alpha$ -helix. The Gellman group,<sup>96</sup> based on the Hoffman group calculations,<sup>117</sup> have designed a  $\beta/\gamma$ -hybrid peptide composed of (*R,R*)-*trans*-ACPC and ethyl-*cis*-2(aminocyclohexane)acetic acid ((*R,R,R*)-EtACHA). The hybrid hexapeptide adopted a regular 13-helix in solution as well as in solid state (see Figure 67).

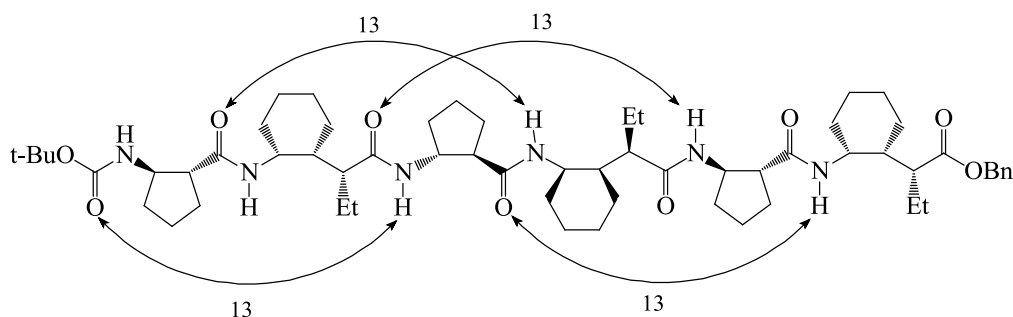


Figure 67 : The Gellman's group  $\beta/\gamma$ -hybrid peptide that folds into a 13-helix.

More recently the Aitken group designed an  $\alpha/\beta/\gamma$ -hybrid peptide using the *trans*-ACBC as the key  $\beta$ -amino acid component and  $\gamma^4$ -amino acids as the  $\gamma$ -amino acid components.<sup>159</sup> The  $\alpha/\beta/\gamma$ -hybrid peptide folded into a 12,13-helix in solution, (see Figure 68) which resembles the native  $\alpha$ -helix, and was able to act as functional and selective  $\alpha$ -helix-mimetic inhibitor of the p53/hDM2 interaction, validating the importance of designed peptide foldamers for applications in the field of protein-protein interactions.

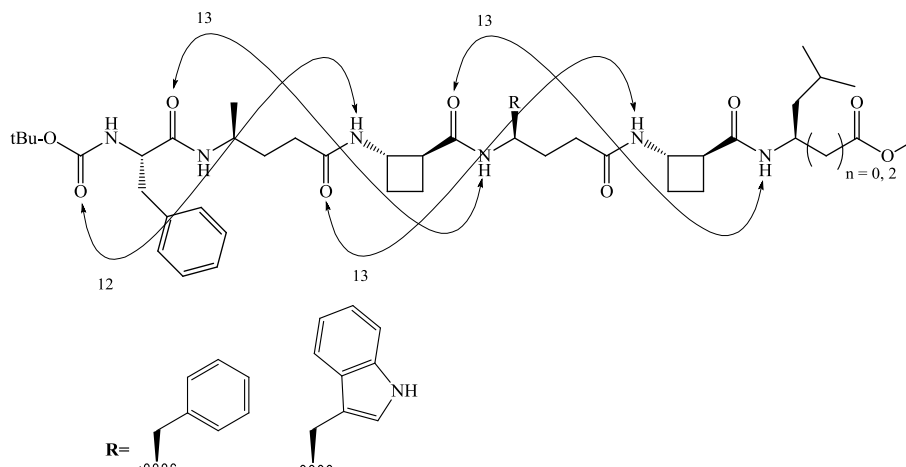


Figure 68: The Aitken's group  $\alpha/\beta/\gamma$ -hybrid peptide that folds into a 13-helix.

#### 4.1.3.2.3 Mixed $\alpha/\gamma$ -peptides

Another class of hybrid peptides,  $\alpha/\gamma$ -peptides, are composed of alternating  $\alpha$ - and  $\gamma$ -amino acids.  $\alpha/\gamma$ -peptides dimer units, with their proteinogenic  $\alpha$ -amino acid component, may properly replace a dipeptide unit in the nonproteinogenic  $\beta$ -peptides.<sup>117</sup> This could open the door to a pool of foldamers having a secondary structure that resembles the folding pattern of  $\beta$ -peptides but with proteinogenic component needed for biological activity.

The Hofmann group studied via *ab initio* calculations the different possible helical structures which could be adopted by an  $\alpha/\gamma$ -octapeptide composed of alternating glycine and GABA.<sup>117</sup> The authors found eleven distinct stable helical forms: 10-, 10/12-, 12/10-, 12-, 15/17-, 18-, 18/20-, 20/18-, 20-, 21/23- and 26-helices. They also suggested that  $\alpha/\gamma$ -hybrid peptides have

helix conformers, which locks like the overall structure of  $\beta$ -peptide helices. Both the most stable 12- and 12/10-helices formed by an  $\alpha/\gamma$ -hybrid peptide showed a very good correspondence with the experimentally found 12- and 12/10-helices of  $\beta$ -peptides with a Root Mean Square Deviation (RMSD) of 0.6 Å, and 0.7 Å respectively (see Figure 69).

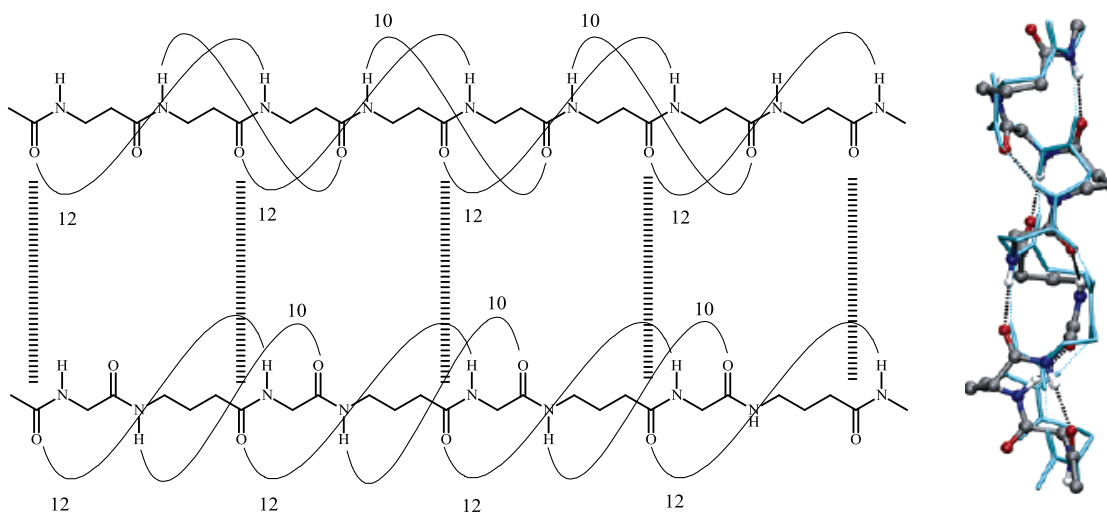


*Figure 69: The resemblance between a theoretically predicted 12/10-helix for a  $\alpha/\gamma$ -hybrid octapeptide (bottom), and that of the experimentally found for a beta peptide (top), with a three dimensional superimposition of both helical structures (right).*

#### 4.1.3.2.3.1 Examples and applications

Out of the eleven stable helical structures predicted by the Hofmann group, the 12-, the 12/10- and most recently the 9- and the 9/12-helix have been experimentally observed in solution and in solid state as illustrated below.

The Balaram group studied  $\alpha/\gamma$ -hybrid peptides composed of alternating  $\alpha$ -aminoisobutyric acid (Aib) and gabapentin (Gpn).<sup>160</sup> The conformational restrictions, imposed by the constrained Aib and Gpn residues on the dihedral angles, allowed the  $\alpha/\gamma$ -nonapeptide to adopt a 12-helical structure in solution but, more interestingly the authors were able to characterize C9, C7, C12, and C17 hydrogen-bonded turns in the crystalline form, in the shorter tetrapeptide;

which emphasizes the fragility of structuration in short oligomers compared to longer ones (See Figure 70).

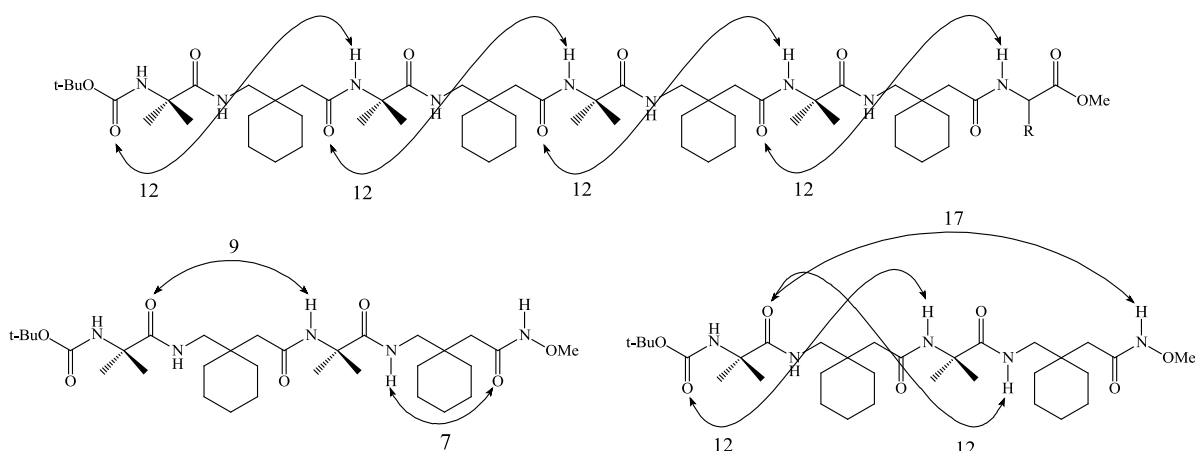


*Figure 70: The folding pattern in the Balaram's group  $\alpha/\gamma$ -hybrid nonapeptide (top), and tetrapeptides (bottom)*

A 12-helix structuration in solution, as well as in crystalline form, was also observed by the Gopi group.<sup>161</sup> An  $\alpha/\gamma$ -peptides composed of alternating  $\alpha$ -aminoisobutyric acid (Aib) and  $\gamma^4$ -phenyl alanine showed a 12-helical structure which was favored by gauche conformation adopted by the dihedral angles  $\theta$ , and  $\zeta$  of the  $\gamma^4$ -phenyl alanine component. Moreover, the obtained 12-helical structure presented a good correlation between its backbone, with its side chain projections, and a native  $\alpha$ -helix (RMSD = 0.8 Å); signifying the possibility of employing specially designed  $\alpha/\gamma$ -peptides for natural peptides mimicry (see Figure 71).

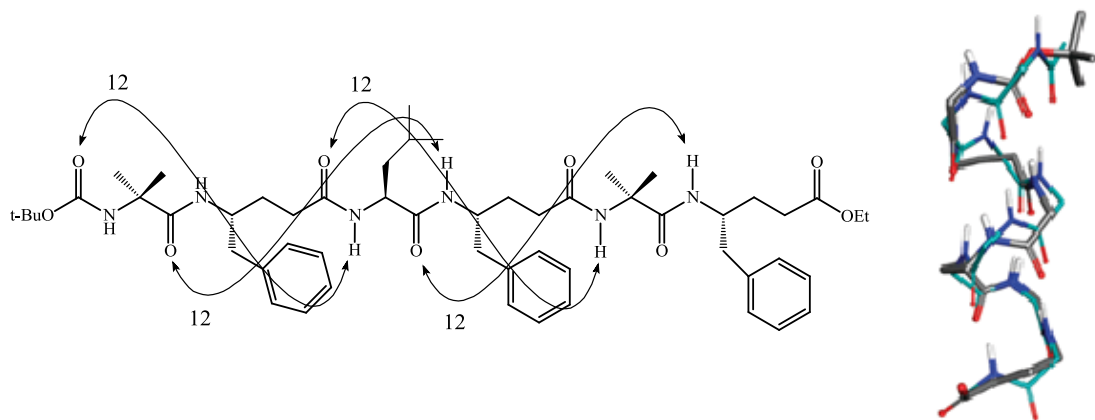


*Figure 71 : The Gopi's group  $\alpha/\gamma$ -hybrid peptide that folds into a 12-helix (left), and a three dimensional superimposition of it with a native  $\alpha$ -helix (right).*

On the other hand the 12/10 secondary helical structure in solution was first reported by the Kunwar's group,<sup>162</sup> the authors prepared a  $\alpha/\gamma$ -hybrid tetrapeptide, composed of alternating L-alanine and C-linked carbo- $\gamma$ -amino acid of D-mannose, whose tetra and hexamers folded into a 12/10-helix in solution (see Figure 72).

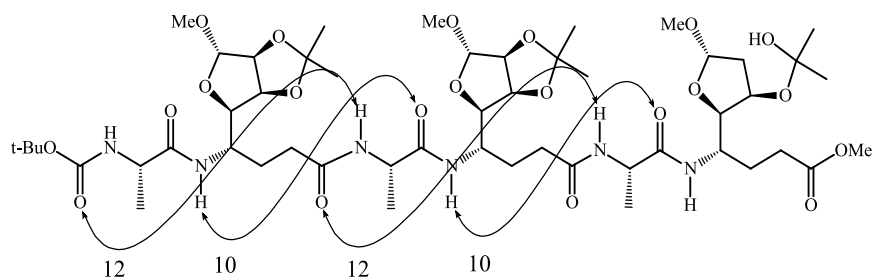


*Figure 72: The Kunwar's group  $\alpha/\gamma$ -hybrid tetrapeptide that folds into a 12/10-helix.*

Similarly, the Gellman's group studied the conformational behavior of a  $\alpha/\gamma$ -hybrid hexapeptide composed of alternating L-alanine and (1*R*,2*R*,3*S*)-2-(1-aminopropyl)-cyclohexanecarboxylic acid (APCH).<sup>163</sup> The conformationally restricted backbone of the (APCH) residue, strongly enforced the formation of a 12/10-helical structure with an alternating direction of the hydrogen bond pattern in solution as well as in crystalline state (see Figure 73).

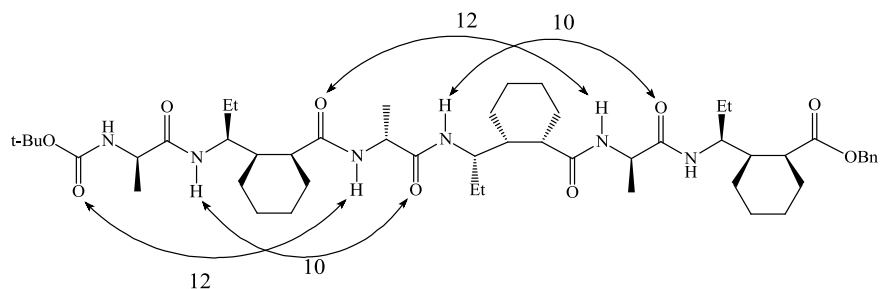


*Figure 73: : The Gellman's group  $\alpha/\gamma$ -hybrid peptide that folds into a 12/10-helix.*

Most recently the Gopi's group reported a 12/10 folding pattern in  $\alpha/\gamma$ -hybrid peptides composed of alternating alanine (Ala), or leucine (Leu), and 4-aminoisocaproic acid (Aic).<sup>164</sup> The authors were able to flip from a 12/10- into a 12-helical structure when the  $\alpha$ -amino acid component was changed into the achiral 1-aminocyclohexane-1-carboxylic acid (Ac<sub>6</sub>c), thus presenting the influence of small structural variations in the  $\alpha$ -amino acid structure on the overall helicity of an  $\alpha/\gamma$ -hybrid peptide. (See Figure 74).

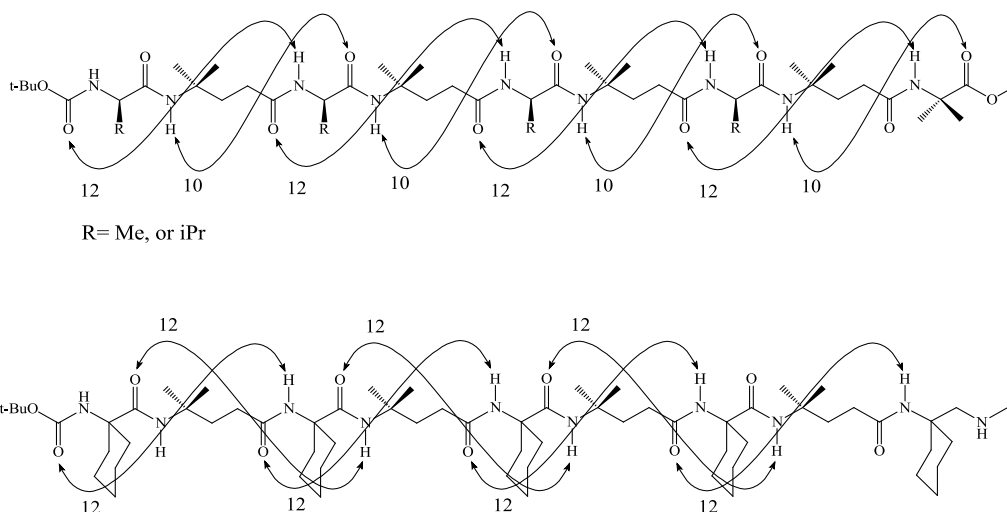


*Figure 74: The Gopi's group  $\alpha/\gamma$ -hybrid peptide that changes its folding pattern from 12/10 (top) into 12 (bottom), with a change in the  $\alpha$ -amino acid side chain substituent.*

Aside from the 12 and the 12/10- helical structuration, The Maillard's group,<sup>165</sup> prepared  $\alpha/\gamma$ -hybrid peptide containing enantiomeric pure 4-amino(methyl)-1,3-thiazole-5-carboxylic acids

(ATCs) as the restricted  $\gamma$ -amino acid component. The authors found that ATCs induced a highly stable 9 pseudocycle (see Figure 75).

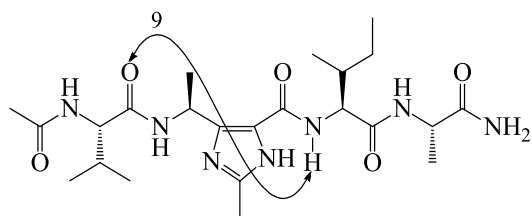


*Figure 75: The Maillard's group peptide that show a 9-membered hydrogen bonding pseudocycle.*

#### 4.1.3.3 Stereochemistry effect on the peptide secondary structure

The stereochemistry of each building block of a peptide sequence has an important effect on the nature and the conformation of the formed secondary structure.<sup>166</sup> For instance, an oligomer composed of alternating homochiral *cis*-1*R*,2*S*-aminocyclopentanecarboxylic acid (*cis*-ACPC) is found to adopt a strand secondary conformation,<sup>167</sup> whereas an alternation of heterochiral 1*R*,2*S*- and 1*S*,2*R*-*cis*-ACPC oligomer folds into a stable 10/12-helix.<sup>139</sup> The change in the relative stereochemistry of amino acid residues changed the secondary structure from a strand to a helix, revealing a profound correlation between the stereochemistry of the amino acid residues and the conformation of the adopted secondary structure (See Figure 76).

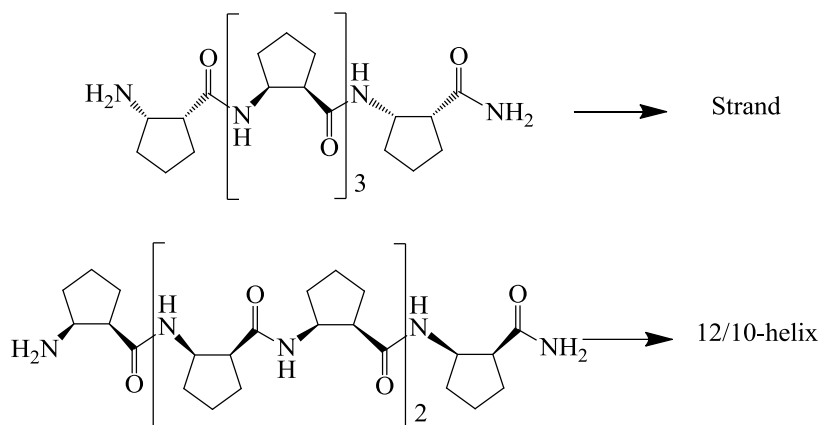


*Figure 76: The effect of changing the chirality of an amino acid component on the over all structuration in an ACPC oligomer.*

Aside from the more popular 12- and the 12/10- helical folding, the Maillard's group<sup>165,168</sup> prepared an  $\alpha/\gamma$ -hybrid peptide, containing enantiomeric pure 4-amino(methyl)-1,3-thiazole-5-carboxylic acids (ATCs) as the restricted  $\gamma$ -amino acid component, (see Figure 77), which showed unique conformational properties resulting from its aromatic ring. These ATC  $\gamma$ -amino acids, having a  $\zeta$  torsion angle locked around  $0^\circ$ , are structurally similar to *Z*-vinylogous  $\gamma$ -amino acids. The ATC acted as a strong turn inducer for folding. The folding pattern depended as well of the absolute configuration of the  $\gamma$ -amino acid. The alternating homochiral (*S*)- $\alpha$ /(*S*)-ATC dipeptide exhibited a C-9 fold while the heterochiral (*S*)- $\alpha$ /(*R*)-ATC dipeptide displayed ribbon structure stabilized by unusual C-9/12 bifurcated hydrogen bonds

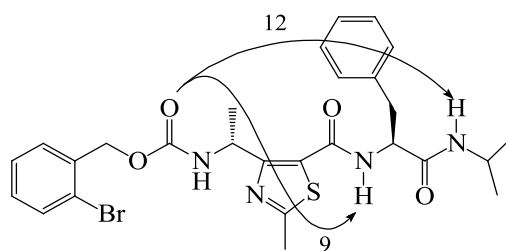


*Figure 77: The 9,12-bifurcated hydrogen bonding pattern recently found by the Maillard's group in  $\gamma/\alpha$ -hybrid peptides.*

#### 4.1.4 Objectives of this work

Studies on  $\alpha/\beta$ -,  $\beta/\gamma$ -, and  $\alpha/\gamma$ -hybrid peptides provided a rich pool of foldamers having helical secondary structures. These foldamers have attractive features, which give them applications in various fields of molecular recognition, peptidomimetics, and therapeutics.<sup>128, 129</sup>

Over the last few years, the Aitken research team has become specialized in the synthesis of unnatural amino acids, especially those incorporating small constrained rings and the development of oligomers based on these building blocks. Oligomers of these constrained amino acids present specific dihedral angles that confer to them the ability to promote stable three dimensional secondary conformations. Even though, there is a lot of theoretical knowledge that correlates between structure of amino acids and peptides folding pattern, a lot remains to be explored experimentally before one can intentionally manipulate the design of a peptide sequence to promote a specific desirable folding pattern in a bottom-up approach.<sup>92, 158</sup>

The *ab initio* theoretical studies done by the Hoffman group suggested that in an  $\alpha/\gamma$ -hybrid peptide a  $\theta$  dihedral angle around  $33^\circ$ , for the  $\gamma$ -amino acid component, is ideal for the formation a 12/10-helix.<sup>117</sup> The crystal structure of the *cis*<sup>3,4</sup>cyclobutane  $\gamma$ -aminobutyric acid (*cis*<sup>3,4</sup>CB-GABA), which was synthesized in chapter three, showed that this molecule has an  $\theta$  angle around  $27^\circ$  (see Figure 78) which makes it a suitable building block for a  $\alpha/\gamma$ -hybrid peptide that could fold into a 12/10-helical secondary structure.

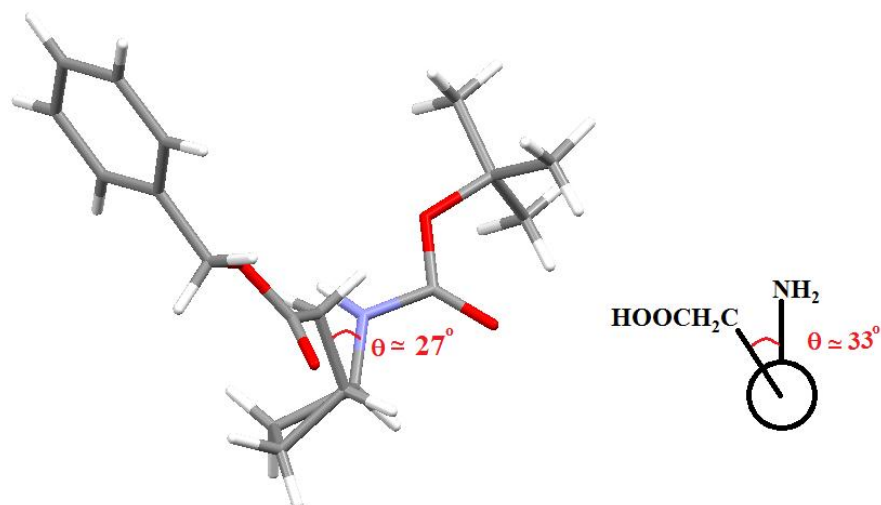


Figure 78: The crystal structure of the *cis*-<sup>3,4</sup>cyclobutane  $\gamma$ -aminobutyric acid (*cis*-<sup>3,4</sup>CB-GABA) (left), the torsional angle needed to obtain a 12/10 helical folding pattern in mixed  $\alpha/\gamma$ -peptides, as predicted by the Hoffman group (right)

In this chapter, we aimed to validate the *cis*-<sup>3,4</sup>CB-GABA as a  $\gamma$ -amino acid component capability to induce a 12/10-helical folding pattern in mixed  $\gamma/\alpha$ -peptides. We also studied the effect of reversing the stereochemistry of the *cis*-<sup>3,4</sup>CB-GABA, on the three dimensional folding pattern of these  $\gamma/\alpha$ -peptides. Thus we synthesized and characterized,  $\gamma/\alpha$ -hybrid peptides composed of alternating, enantiomerically pure either (*S,S*)- or (*R,R*)-*cis*-<sup>3,4</sup>CB-GABA as the constrained  $\gamma$ -amino acid component and D-Alanine (D-Ala) as the  $\alpha$ -amino acid component. The three dimensional folding behavior of these peptides was subsequently studied (see Figure 79).

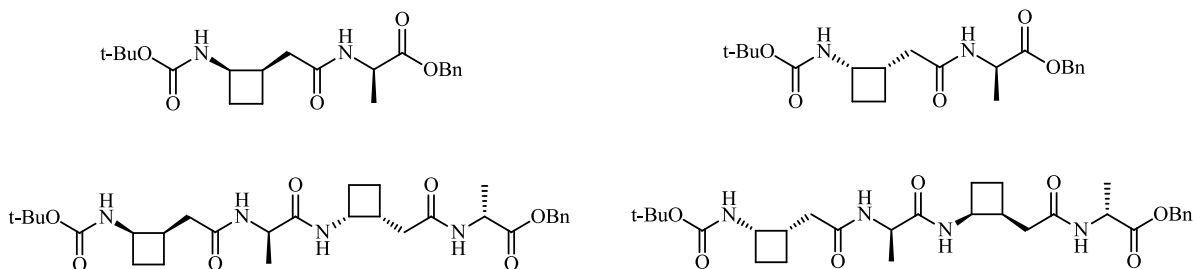


Figure 79: The target  $\gamma/\alpha$ -hybrid peptide, the (*S,S/R*)-series (left), and the (*R,R/R*)-series right.

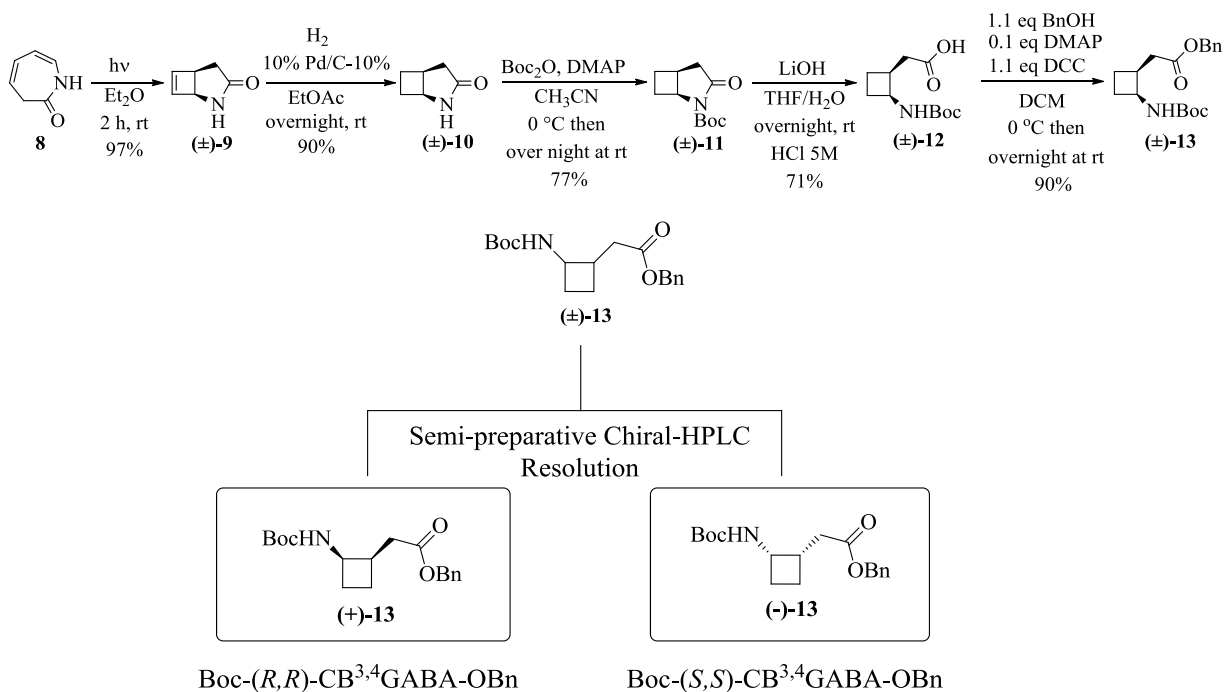
## 4.2. Results and discussion

### 4.2.1 The starting amino acids: Enantiomerically pure protected $\gamma$ - and $\alpha$ -amino acids

The synthesis of mixed  $\gamma/\alpha$ -peptides requires access to enantiomerically pure  $\gamma$ - and  $\alpha$ -amino acid monomers.

#### 4.2.1.1 The enantiomerically pure Boc-*cis*-<sup>3,4</sup>CB-GABA-OBn

The diprotected Boc-*cis*-<sup>3,4</sup>CB-GABA-OBn was prepared in its racemic form following by the semi-preparative Chiral-HPLC separation method as described in chapter three, to obtain both enantiomers in pure form (see Scheme 49).

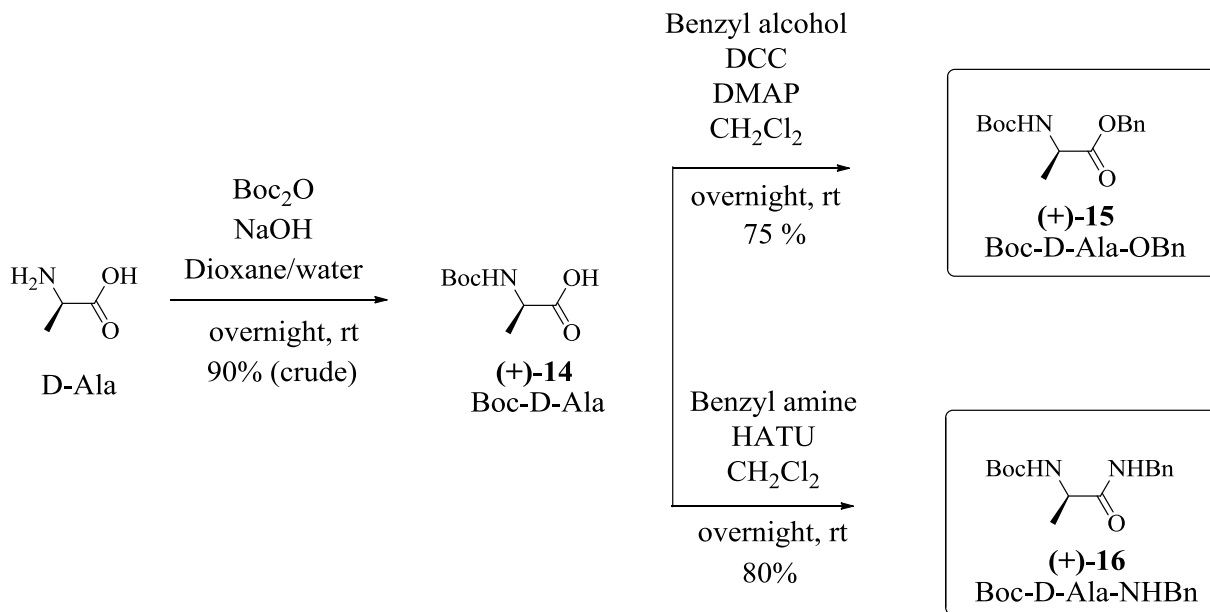


Scheme 49: The synthesis of Boc-*cis*-<sup>3,4</sup>CB-GABA-OBn in its racemic form (top); separation of the two enantiomers via the semi-preparative Chiral-HPLC resolution method (bottom).

#### 4.2.1.2 The Enantiomerically pure D-Alanine

The 12/10 helical structure of a  $\alpha/\gamma$ -peptides, generated by the theoretical calculations of the Hofmann group,<sup>117</sup> suggested that, if we used the (*S,S*)-*cis*<sup>3,4</sup>CB-GABA as the  $\gamma$ -amino acid component and a *R* configuration around the C $\alpha$  of the  $\alpha$ -amino acid component, the  $\alpha$ -amino acid side chain and the cyclobutane ring would be in a plane perpendicular to the helix axis and would not disturb the helical structure formation. On these bases D-Alanine was chosen to be the  $\alpha$ -amino acid component in our studied  $\alpha/\gamma$ -peptides.

The enantiomerically pure Boc-D-Ala-OBn **14** and Boc-D-Ala-NHBn **15** were prepared from commercial D-Ala amino acid, by reacting it with Boc<sub>2</sub>O in the presence of NaOHaq, in dioxane. The resulting “clean” crude Boc-D-Ala was then, either reacted with benzyl alcohol in the presence of DCC and DMAP, to get the benzyl ester Boc-D-Ala-OBn **14** with a 75% yield, or coupled with benzyl amine in the presence of HATU to easily obtain the benzyl amide Boc-D-Ala-NHBn **15** in 80% yield (see Scheme 50).

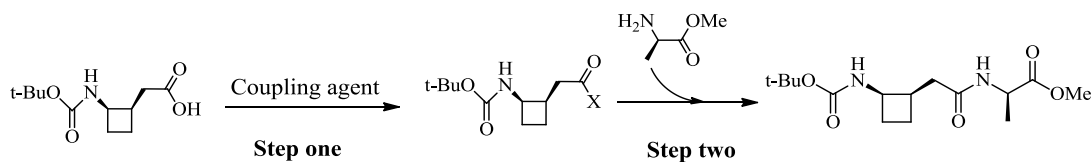


Scheme 50. The synthesis of compounds **15** and **16** from commercial D-Alanine.

## 4.2.2 The general Synthetic method

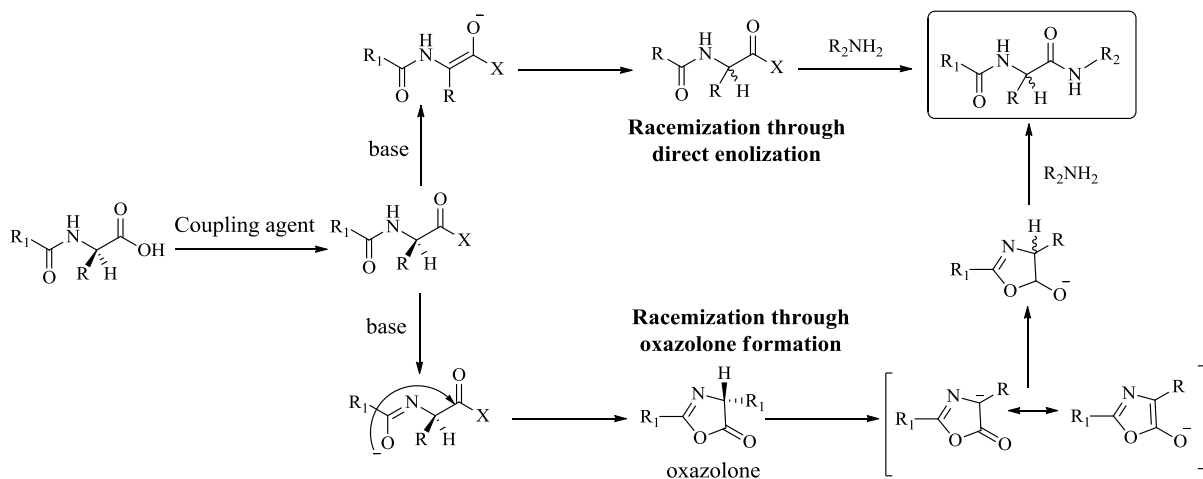
### 4.2.2.1 The activation/ coupling strategy

Peptide synthesis *via* amino acids coupling involves two steps (see Scheme 51). The first step is the activation of the carboxylic acid group of one amino acid residue using a coupling agent. The second step involves the nucleophilic addition of the amino group of the other amino acid derivative at the activated carboxylic acid.



*Scheme 51: The steps of peptide synthesis via amino acid coupling.*

A suitable coupling method has to form peptide bonds in high yields and to maintain the configurational integrity of the carboxylic component.<sup>169,170</sup> Racemization at the  $\alpha$ -carbon usually occurs during the activation of the carboxylic acid function if the amine part is bearing an electron withdrawing group (see Scheme 52).



*Scheme 52: The two possible explanations for the racemization at the  $\alpha$ -carbon during peptide coupling.*

It is important to note that even though our convergent strategy in building up the mixed  $\gamma/\alpha$ -peptides involved an activation of a carboxylic acid group and an amine protected with an electron withdrawing group, no racemization of the D-alanine was observed in any of the synthesized peptides.

#### 4.2.2.2 Choice of the coupling agent

The carboxylic acid activation, first step in peptide coupling, is crucial and one should experiment in order to find the best coupling agent and reaction conditions for a given peptide synthesis. Several coupling reagents are available. For instance, carbodiimide reagents, like DCC, have been used as peptide coupling agents for a long time.

In the recent years, two classes of coupling reagents became popular, the phosphonium type reagents such as BOP, and PyBOP, and the aminium-(uronium) type reagents such as TBTU, HBTU, and HATU (see Figure 80).

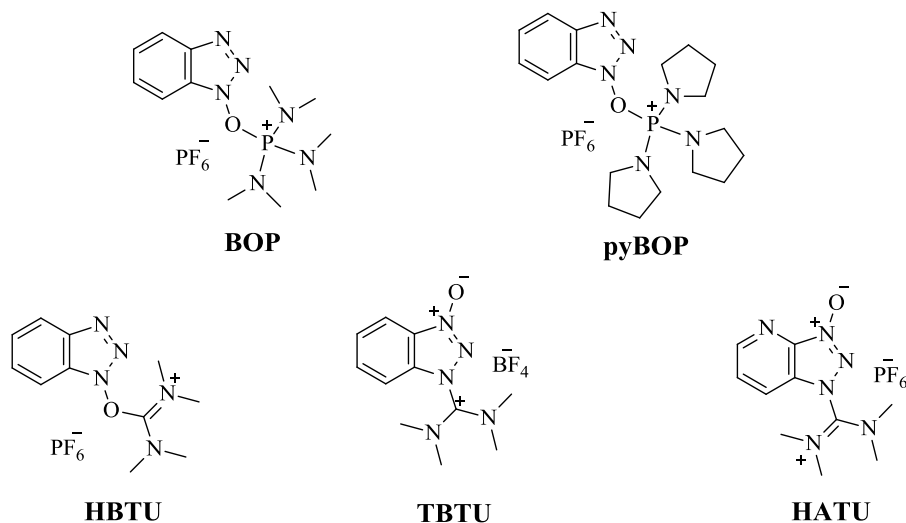
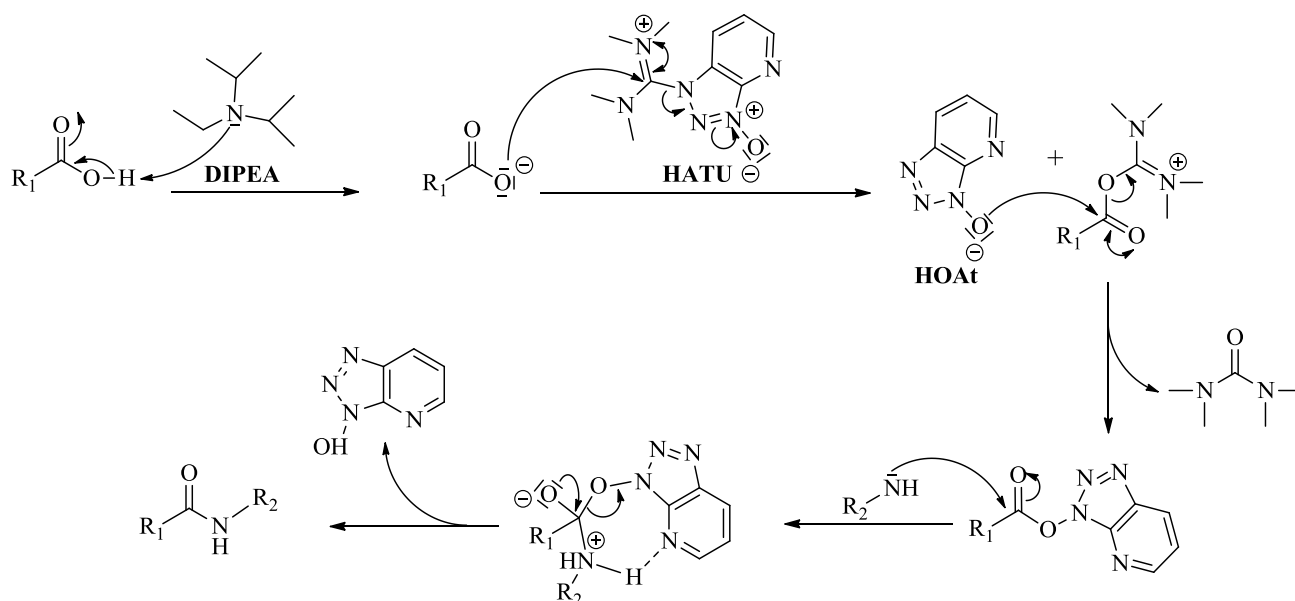


*Figure 80: Examples of the phosphonium (top), and aminium-uronium (bottom) type coupling reagents.*

These compounds achieve high coupling rates accompanied by few undesired side reactions. In contrast with carbodiimide based reagents, activation by these coupling agents require the

presence of a base like diisopropylethylamine (DIPEA) for the activation reaction to proceed (see Scheme 53).<sup>170</sup>



*Scheme 53: The general mechanism of peptide coupling using HATU.*

In our coupling reactions we followed the reaction conditions established previously in our group for  $\beta/\gamma$ -hybrid peptides preparation.<sup>158</sup> Thus we used HATU, as the coupling agent, which was easy to handle and provided high coupling yields, without any unwanted racemization.

The dipeptide coupling reactions were performed by first cleaving the Boc protecting group of the amine partner using TFA in DCM. Then the activation of the carboxylic acid residue of the acid partner, using HATU in the presence of DIPEA, generates the activated carboxylate in a mixture of DCM and DMF. (Scheme 5 below) The DCM/DMF mixture allowed a better dissolution of the HATU, as well as higher order peptides, which have low solubility. The activation of the carboxylic acid residue could be confirmed by the darkening of the reaction mixture (from light brown to dark brown) due to the 1-hydroxy-azaenzine-triazole anion (HOAt) released by HATU (see Scheme 55). Once the activation was complete, within 10 min, a solution of the amine partner, in DCM, with a sufficient amount of DIPEA to neutralize the

excess of TFA, was added to the HATU activated reaction mixture, the resulting reaction mixture was then left to stir at room temperature, under argon, for 24 hours, after which it was purified to give the desired dipeptide.

### 4.2.2.3 Convergent peptide synthesis

The general synthetic strategy we followed in building up the mixed  $\gamma/\alpha$ -peptides was a convergent one. This strategy seems to us more adequate than the linear synthesis of peptides, where the monomers are successively coupled one after the other until the target molecule is reached, with the yield dropping quickly as the number of steps increases. A convergent synthesis is a strategic approach in which fragments of the peptide are first prepared and then combined together to complete the target molecule (see Figure 81). In a convergent strategy, fewer steps than in the linear one are needed to reach the same molecule, thus enhancing the yield and saving time.

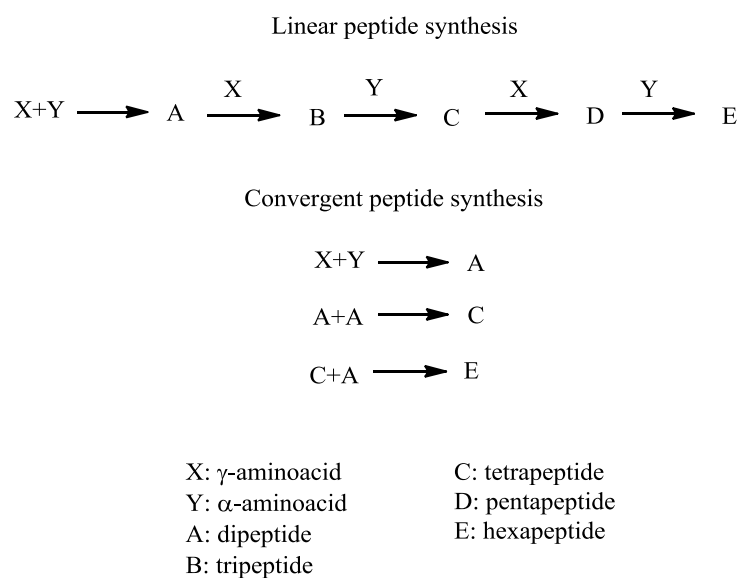
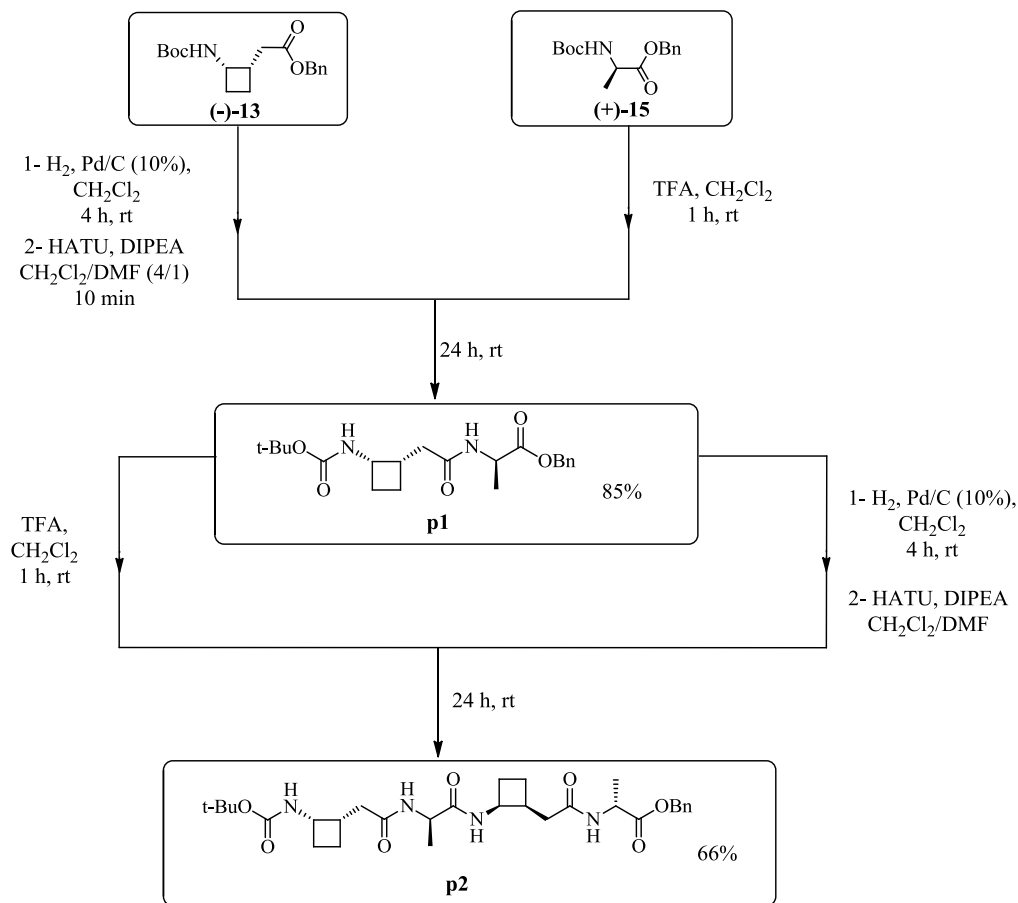


*Figure 81: The linear (top) v.s. the convergent (bottom) strategie for  $\gamma/\alpha$ -hybrid peptide synthesis.*

### 4.2.3 Synthesis of Boc-(*S,S*)-*cis*-<sup>3,4</sup>CB-GABA/(*R*)-Ala-OBn peptides

The synthesis of Boc-[(*S,S*)-*cis*-<sup>3,4</sup>CB-GABA-(*R*)-Ala]<sub>*n*</sub>-OBn peptides **p1** and **p2** was carried out following a convergent strategy, starting from the Boc-(*S,S*)-*cis*-<sup>3,4</sup>CB-GABA-OBn enantiomer (**-**)-**13** as the  $\gamma$ -amino acid partner, and the Boc-D-Ala-OBn (**+**)-**15** as the  $\alpha$ -amino acid partner (see Scheme 54).



*Scheme 54: The convergent synthesis of Boc-[(*S,S*)-*cis*-<sup>3,4</sup>CB-GABA-(*R*)-Ala]<sub>*n*</sub>-OBn peptides **p1** and **p2**.*

#### 4.2.3.1 Synthesis of the Boc-[(*S,S*)-*cis*-<sup>3,4</sup>CB-GABA/(*R*)-Ala]-OBn peptide **p1**

The *C*-terminal benzyl protecting group, of Boc-(*S,S*)-*cis*-<sup>3,4</sup>CB-GABA-OBn was first removed in a quantitative yield by catalytic hydrogenolysis under dihydrogen atmosphere in the presence of 10% Pd-C (10% w/w) for 4 hours to obtain the free acid intermediate (see Scheme 54). The *N*-terminal Boc protecting group of Boc-D-Ala-OBn was cleaved by treatment with a large excess of TFA for 1 hour to give the corresponding amine partner as a TFA salt.

The obtained free acid was then activated with HATU and reacted with the amine partner in the presence of DIPEA for 24 hours at room temperature, under argon, to afford dipeptide **p1** in an 85% yield after purification.

#### 4.2.3.2 Synthesis of the Boc-[(*S,S*)-*cis*-<sup>3,4</sup>CB-GABA/(*R*)-Ala]<sub>2</sub>-OBn peptide **p2**

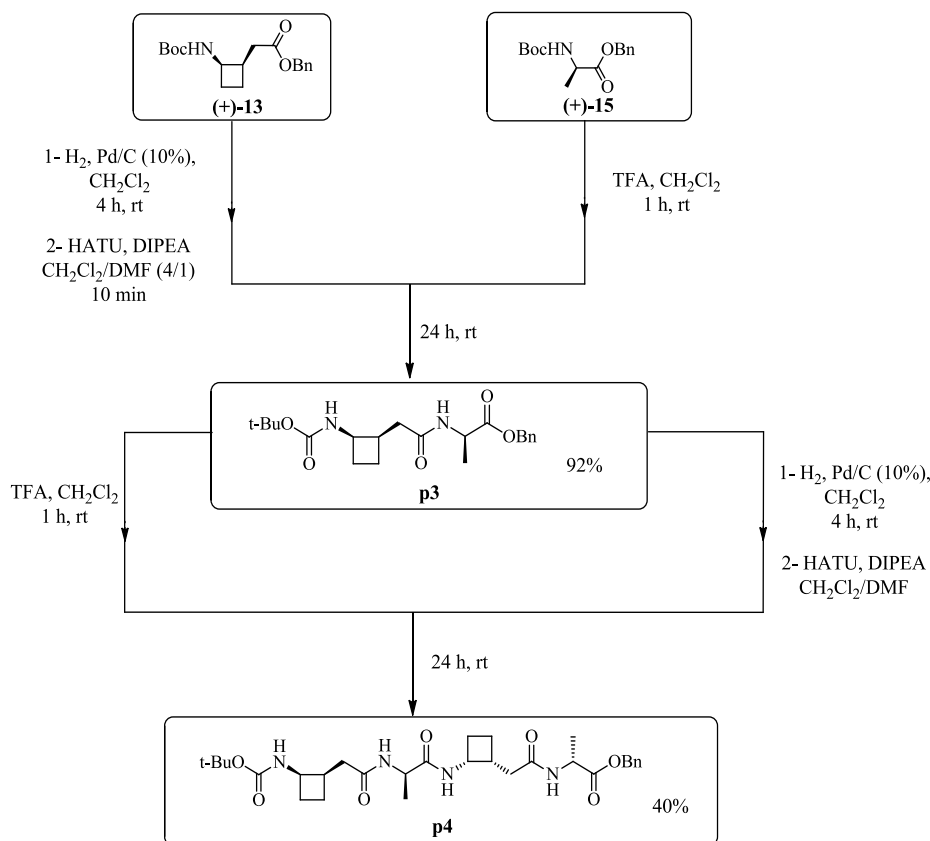
One equivalent of dipeptide **p1** was selectively deprotected at the *N*-terminal with large excess of TFA for 1 hour. Another equivalent of dipeptide **p1** was selectively deprotected at the *C*-terminal by catalytic hydrogenolysis under dihydrogen atmosphere in the presence of 10% Pd-C (10% w/w) for 4 hours. The two monoprotected dipeptides were then mixed together in the presence of excess of DIPEA before HATU was added. The coupling reaction was left to stir for 24 hours, at room temperature, under argon to afford tetrapeptide **p2** in a 66% yield.

In its coupling reaction, the free acid and the free amine partners were mixed together along with enough DIPEA to make the reaction mixture basic before adding the HATU to avoid the risk of racemization of the activated dipeptide (see section 4.2.2.1), by minimizing the time of it being activated without the presence of the nucleophilic amine partner.

#### 4.2.4 Synthesis of Boc-(*R,R*)-*cis*-<sup>3,4</sup>CB-GABA/(*R*)-Ala-OBn peptides

In order to investigate the effect of reversing the stereochemistry of the *cis*-<sup>3,4</sup>CB-GABA component on the three dimensional folding pattern of our  $\alpha/\gamma$ -hybrid peptide, we prepared a di and a tetrapeptide composed of alternating (*R,R*)-*cis*-<sup>3,4</sup>CB-GABA and D-Alanine.

The synthesis of Boc-[(*R,R*)-*cis*-<sup>3,4</sup>CB-GABA-(*R*)-Ala]<sub>n</sub>-OBn peptides **p3** and **p4** was carried out following a convergent strategy, starting from the Boc-(*R,R*)-*cis*-<sup>3,4</sup>CB-GABA-OBn enantiomer (+)-**13** as the  $\gamma$ -amino acid partner, and the Boc-D-Ala-OBn (+)-**15** as the  $\alpha$ -amino acid partner (see Scheme 55).



Scheme 55: The convergent synthesis of Boc-[(*R,R*)-<sup>3,4</sup>CB-GABA-(*R*)-Ala]<sub>n</sub>-OBn peptides **p3** and **p4**.

#### 4.2.4.1 Synthesis of the Boc-(*R,R*)-*cis*-<sup>3,4</sup>CB-GABA-(*R*)-Ala-OBn peptide **p3**

The *C*-terminal benzyl protecting group, of Boc-(*R,R*)-*cis*-<sup>3,4</sup>CB-GABA-OBn was first removed in a quantitative yield by catalytic hydrogenolysis under dihydrogen atmosphere in the presence of 10% Pd-C (10% w/w) for 4 hours to obtain the free acid intermediate (see Scheme 55). The *N*-terminal Boc protecting group of Boc-D-Ala-OBn was cleaved by reaction with a large excess of TFA for 1 hour to give the corresponding amine partner as a TFA salt.

The obtained free acid was activated with HATU and reacted with the amine partner in the presence of DIPEA for 24 hours at room temperature, under argon to afford dipeptide **p3** in a 92% yield. The dipeptide **p3** was selectively deprotected at the *C*-terminal by catalytic hydrogenolysis under dihydrogen atmosphere in the presence of 10% Pd-C10% (w/w) for 4 hours to give its free acid form, **p3-OH**. The analysis of a single crystal of dipeptide **p3-OH** by X-ray diffraction shows no intra residual hydrogen bonding in solid state, but rather an infinite array of intermolecular hydrogen bond interactions implicating three hydrogen bond donors and two acceptors that stack the dipeptide **p3-OH** molecules in an anti-parallel fashion (see Figure 82).

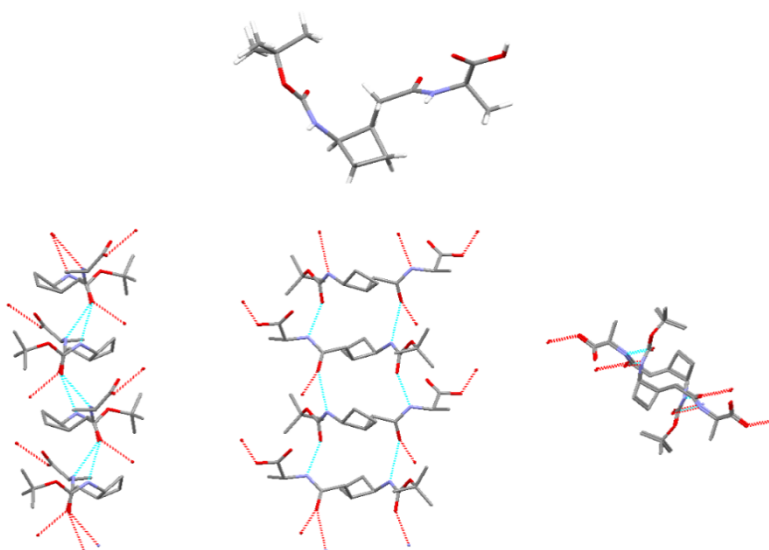


*Figure 82: The X ray crystal structure of peptide **p3-OH** (top), and its intermolecular hydrogen bonding interactions viewed from the side (left), front (middle), and top (right).*

#### 4.2.4.2 Synthesis of the Boc-[(*R,R*)-*cis*-<sup>3,4</sup>CB-GABA-(*R*)-Ala]<sub>2</sub>-OBn peptide **p4**

One equivalent of dipeptide **p3** was selectively deprotected at the *N*-terminal with large excess of TFA for 1 hour. Another equivalent of dipeptide **p3** was selectively deprotected at the *C*-terminal by catalytic hydrogenolysis under dihydrogen atmosphere in the presence of 10% Pd-C (10% w/w) for 4 hours. The two monoprotected dipeptides were then mixed together in the presence of excess of DIPEA before HATU was added. The coupling reaction was left to stir for 24 hours, at room temperature, under argon to afford tetrapeptide **p4** in a 40% yield

The tetrapeptide **p4** exhibited low solubility in organic solvents such as chloroform, and displayed a tendency to form a gel, which made its purification problematic. The preparation of the higher order hexapeptide was subsequently inaccessible. Thus the conformational analysis was performed on the tetrapeptide.

#### 4.2.5 Structural and Conformational analysis in solution

##### 4.2.5.1 General methods for structural and conformational analysis

The linear structure and the three dimensional conformation of the synthesized peptides were studied, in solution, using different experimental and theoretical techniques.

##### 4.2.5.1.1 Structural analysis

The linear structure of the synthesized di- and tetrapeptides was confirmed by a combination of a series of 1D and 2D NMR experiments (<sup>1</sup>H, <sup>13</sup>C, TOXY, COSEY, HSQC, and HMBC). These spectroscopic techniques allowed the unambiguous assignment of all the protons and carbons of the studied peptides, except for some ones, which appeared overlapped with each other.

##### 4.2.5.1.2 DMSO-d<sub>6</sub> NMR titration experiments

DMSO-d<sub>6</sub> NMR titration experiments were done to assign the free and bonded N-H in peptides. Incremental amounts of DMSO-d<sub>6</sub> were successively added to an NMR tube containing a peptide in CDCl<sub>3</sub> (6-7 mM), and the <sup>1</sup>H spectra were recorded after each addition. Addition of

the DMSO-d<sub>6</sub> into the tube increases the polarity of the environment around the peptide. This change in polarity induced a significant change in the chemical shift on the free N-H while it had less effect on the bonded ones.

#### 4.2.5.1.3 Conformational analysis

2D ROESY NMR experiments were used to understand the three dimensional molecular conformation of the synthesized peptides, in solution, by detecting through-space dipolar magnetic interactions known as the Nuclear Overhauser Effect (NOE). By looking at the intramolecular NOE correlations within a peptide molecule, one could gain insight into the overall folding pattern of this peptide.

Here again ROESY was chosen over NOESY due to its better sensitivity in detecting NOE colorations in molecules of molecular masses above 1 KDa (see Section 1.2.3).

#### 4.2.5.1.4 Molecular modeling

Molecular modeling studies for both tetrapeptides (p2 and p4) were performed using a hybrid Monte Carlo Multiple Minima (MCMM). The three dimensional conformational examination was carried out in a chloroform medium using Macromodel 04 from Schrödinger software and the Merck Molecular Force Field (MMFF). Out of the 10 000 conformers that were generated by MCMM, the 100 lowest energy conformers ( $\Delta E=10\text{KJ/mol}$ ) were retained and classified into different conformational families.

The performed molecular modeling was done without any constraints from the experimental data. Thus, the modeling data could be considered as a theoretical tool that is completely independent from experimental one.

#### **4.2.5.2 Determining the linear structure of the peptides p2 and p4**

The linear structure of the tetrapeptides p2 and p4 was confirmed by a combination of a series of 1D and 2D NMR experiments. The chemical shift of the carbamate N-H always relatively more shielded than the other N-Hs was easily attributed. An analysis combination of COSY,

HSQC and HMBC experiments allowed the unambiguous assignment of all the protons and carbons of the studied peptides. A TOXY experiment allowed us to distinguish between the  $\gamma$ - and  $\alpha$ - amino acid protons especially when they appeared to overlap with each other.

#### 4.2.5.2.1 DMSO- $d_6$ titration experiment

The DMSO- $d_6$  NMR titration experiment was performed on  $CDCl_3$  solutions of the tetrapeptides **p2** (1.3 mg/ 0.3 ml, 7.5 mM) and **p4** (1.5 mg/ 0.4 ml, 6.5 mM) at 300 K. The difference in chemical shifts  $\Delta\delta$  of the N-Hs between 0% and 50 or 10% of added DMSO- $d_6$  were determined (see Table 8)

	50% DMSO- $d_6$	10% DMSO- $d_6$	Tetrapeptide <b>p2</b>
$\Delta\delta(\text{NH4})$	1.25	0.73	
$\Delta\delta(\text{NH11})$	1.25	0.73	
$\Delta\delta(\text{NH15})$	0.008	-0.02	
$\Delta\delta(\text{NH22})$	0.75	0.17	
			Tetrapeptide <b>p4</b>
$\Delta\delta(\text{NH4})$	1.42	0.81	
$\Delta\delta(\text{NH11})$	1.40	0.84	
$\Delta\delta(\text{NH15})$	0.39	0.27	
$\Delta\delta(\text{NH22})$	1.38	0.82	

Table 8: The results of the DMSO- $d_6$  NMR titration experiment for tetrapeptides **p2**, and **p4**.

The tetrapeptide **p2** showed two N-H (4 and 11) with relatively high DMSO- $d_6$  titration coefficient (red color) and two N-H with relatively low coefficients (15 and 22) (blue color). The low mobility of N-H 15 and 22 is most likely an indication of their involvement in intramolecular hydrogen bonding.

On the other hand, tetrapeptide **p4** showed three N-H (4, 11, and 22) with relatively high DMSO- $d_6$  titration coefficient (red color) and only one N-H with relatively low coefficients (N-H 15) (blue color). This preliminary observation hints a difference in the preferential folding pattern of the two diastereomeric tetrapeptides in solution, which will be further investigated via two dimensional NMR experiments and molecular modeling.

### 4.2.5.3 Conformational analysis of the peptides **p2** and **p4**

#### 4.2.5.3.1 2D ROESY NMR experiment

2D ROESY NMR experiments were done on a CDCl<sub>3</sub> solution (5 mg/ 0.5 ml) for each of the tetrapeptides **p2** and **p4**. Best ROE colorations were detected when the spinlock parameter during the experiment was set to 400 ms. The most significant ROE correlations and the deduced hydrogen bonding patterns are presented in Figure 83 for tetrapeptide **p2** and in Figure 84 for tetrapeptide **p4**.

The tetrapeptide **p2** generated ROE correlations, which suggest the presence of an alternating 12 and 10-membered pseudocycles, indicating the tendency of this peptide to have a 12/10 helical secondary structure (see Figure 84), which is in accordance with the Hofmann group predictions.<sup>117</sup>

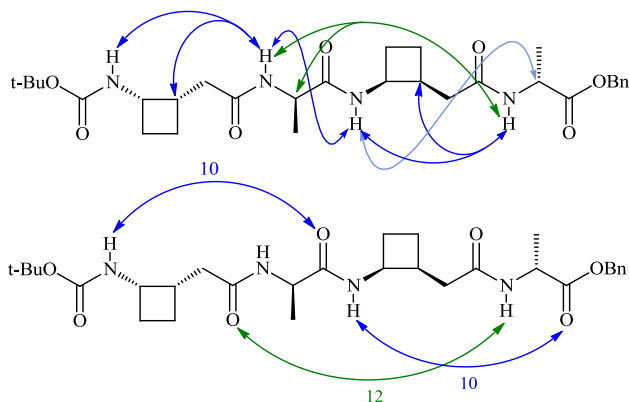
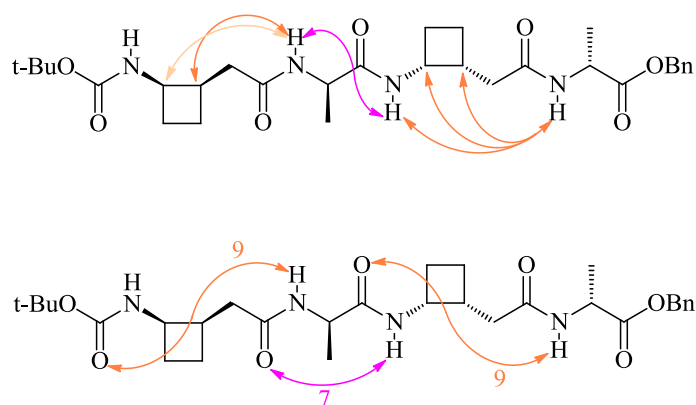


Figure 83: Tetrapeptide **p2** showing ROE correlations characteristic of a 10-membered (blue) and 12-membered (green) hydrogen-bond rings (above) and the overall deduced hydrogen bond pattern (below). The faded colored arrow corresponds to a weak ROE correlation.

Unlike the tetrapeptide **p2**, ROEs correlations observed for the tetrapeptide **p4** do not suggest the presence of a 12/10 folding pattern. They rather indicate the occurrence of an alternating 7- and 9-membered pseudocycles (see Figure 84). This kind of experimentally uncharted, secondary structure results from interactions between adjacent peptide bonds rather than non-

nearest neighbour ones, which is a competitive possibility as suggested by the Hofmann group.<sup>117</sup>



*Figure 84: Tetrapeptide **p4** showing ROE correlations characteristic of a 9-membered (orange) and 7-membered (pink) hydrogen-bond rings (above) and the deduced overall hydrogen bond pattern (below). The fade colored arrow corresponds to a weak ROE correlation.*

#### 4.2.5.3.2 Molecular modeling

An MCMM (Monte Carlo Multiple Minima) calculation was performed on the tetrapeptides **p2** and **p4** to investigate their conformational landscape in chloroform. The lowest energy conformations, were arranged according to the hydrogen-bonded ring systems they form.

Table 9 shows the list of predicted conformations by the MCMM calculations for tetrapeptide **p2** along with their percentage abundance. The discreet, successive hydrogen bonded rings formed between a carbonyl oxygen and an amide hydrogen are separated by a hyphen '-', while the ones implicating a carbonyl oxygen that is bifurcated between two amide hydrogens are separated by a coma ','.

Conformations	Relative abundance of each conformation
[10-12-10]	9.3%
[12-10]	3.5%
[7,7-9]	6.4%
[7,12-10]	25%
[7,7-13-9]	44.4%
[7,7-10]	5%
[7-10]	5.8%
[12-13]	0.6%

Table 9: The list of conformations for tetrapeptide **p2** as predicted by the MCMM calculations

Even though the most abundant conformation is found to be the [7,7-13-9] (44.4%), the lowest energy conformer corresponds to the experimentally found [10-12-10]. The Figure 85 below shows the hydrogen bonding pattern in the most abundant [7,7-13-9] and the lowest energy [10-12-10] conformers as calculated by MCMM.

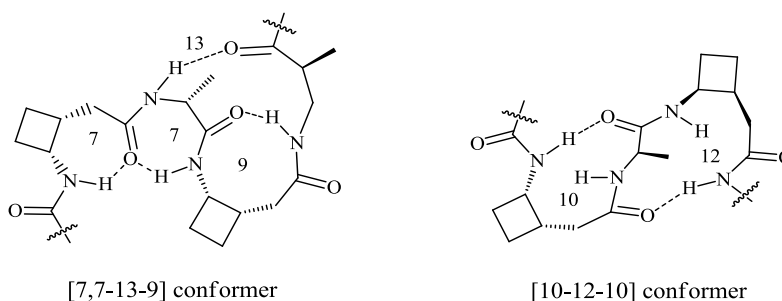


Figure 85: The hydrogen bonding pattern in the most abundant (left), and the lowest energy, also experimentally found (right), conformer of peptide **p2**, as predicted by the MCMM calculations.

On the other hand, for the tetrapeptide **p4** the most abundant conformation is found to be the [9-7,12] (27%), and the lowest energy conformer is the [9,12-9], this conformer is similar to the one recently reported by the Maillard group for  $\alpha/\gamma$ -hybrid peptides containing enantiomeric pure ATCs (See Figure 75, and 77).<sup>165, 167</sup> Such short range H-bonds are reminiscent of the Aitken group for homologous  $\gamma$ -peptides of *cis*-<sup>2,3</sup>CB-GABA, which showed short range consecutive intramolecular 7-membered hydrogen bonds topology in dilute solution;<sup>94</sup> and for

$\beta/\gamma$ -peptide composed of (1*R*,2*R*)-2-aminocyclobutane carboxylic acid (*trans*-ACBC) and GABA, that fold with an alternating 9-, 8-hydrogen bonding pseudocycles.<sup>158</sup>

Table 10 shows the list of predicted conformations by the MCMM calculations of tetrapeptide **p4** along with their percentage abundance.

Conformations	Relative abundance of each conformation
[9,12-9]	7%
[9-7,12]	27%
[15-13-7] <sup>a</sup>	9%
[9-7-9]	15%
[9,12-12]	20%
[7-13-7]	2%
[7,12-10]	3%
[9-12-10]	9%
[10-12-10]	5%
[7-10,7]	2%

Table 10: The list of conformations for tetrapeptide **p4** as predicted by the MCMM calculations. <sup>a</sup>15 and 7 rings are from the same carbonyl

The experimentally found [9-7-9] conformer is the third most abundant (15%) and has the third lowest energy. Figure 89 shows the hydrogen bonding pattern in the most abundant [9-7,12] and the lowest energy [9,12-9] conformers as calculated by MCMM, and the experimentally found [9-7-9] conformer.

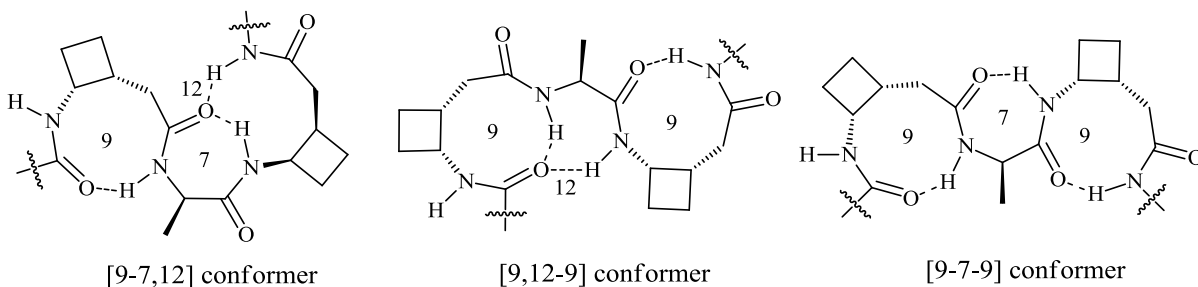
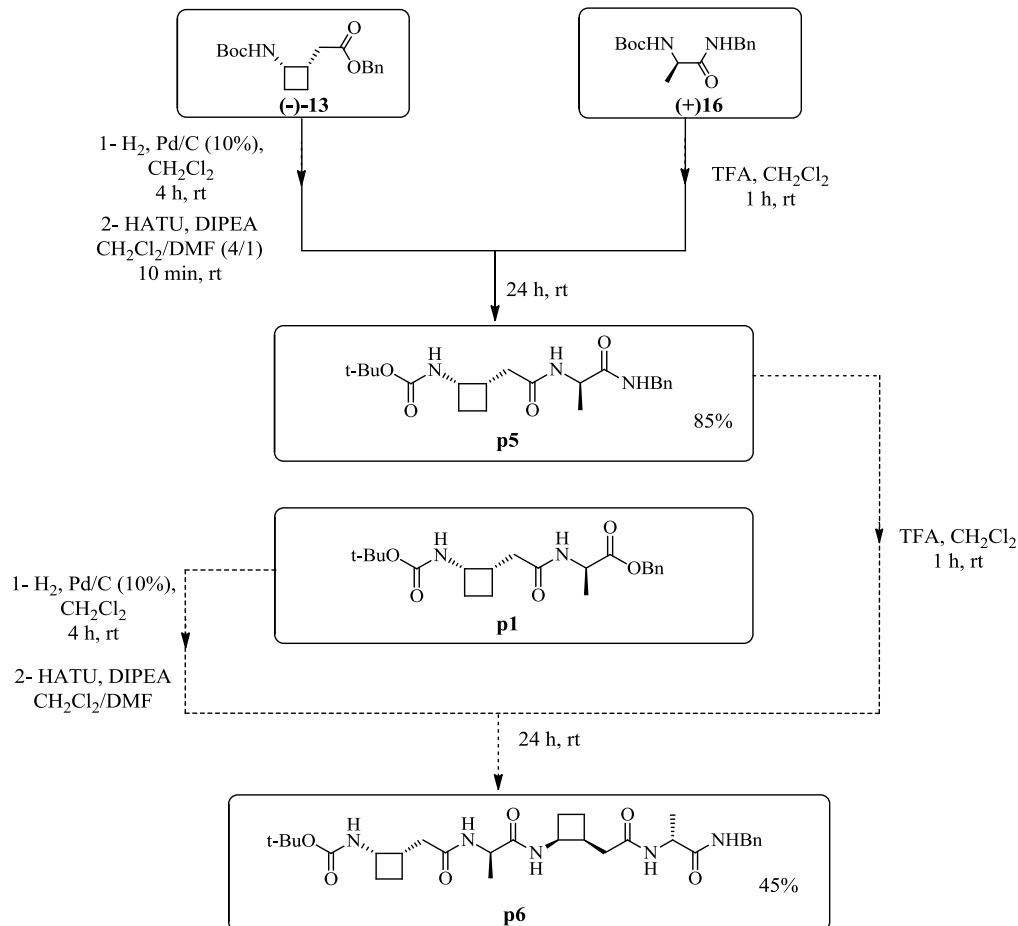


Figure 86: The hydrogen bonding pattern in the most abundant (left), the lowest energy (middle), and the experimentally found (right), conformers of peptide **p4**, as predicted by the MCMM calculations.

#### 4.2.6 Boc-(*S,S*)-*cis*-<sup>3,4</sup>CB-GABA/(*R*)-Ala-NHBn peptides

Having a terminal amide group in a peptide should provide an extra hydrogen bond acceptor, thus increasing the chance of a relatively short tetrapeptide to adopt a well-defined secondary structure. For this, we opted to prepare an analog of the tetrapeptide **p4** with a benzyl amide terminal rather than a benzyl ester.

The synthesis of Boc-[(*S,S*)-*cis*-<sup>3,4</sup>CB-GABA-(*R*)-Ala]<sub>*n*</sub>-NHBn peptides **p5** and **p6** was carried out following a convergent strategy, starting from the Boc-(*S,S*)-*cis*-<sup>3,4</sup>CB-GABA-OBn enantiomer (-)-**13** as the  $\gamma$ -amino acid partner, and the Boc-D-Ala-NHBn (+)-**16** as the  $\alpha$ -amino acid partner (see Scheme 58).



Scheme 56: The convergent synthesis of Boc-[(*S,S*)-<sup>3,4</sup>CB-GABA-(*R*)-Ala]<sub>*n*</sub>-NHBn peptides **p5** and **p6**.

#### 4.2.6.1 Synthesis of the Boc-(*S,S*)-*cis*-<sup>3,4</sup>CB-GABA-(*R*)-Ala-NHBn peptide **p5**

The C-terminal benzyl protecting group of Boc-(*S,S*)-*cis*-<sup>3,4</sup>CB-GABA-OBn was first removed in a quantitative yield by catalytic hydrogenolysis under dihydrogen atmosphere in the presence of 10% Pd-C (10% w/w) for 4 hours to obtain the free acid intermediate. The N-terminal Boc protecting group of Boc-D-Ala-NHBn, was cleaved by treating it with a large excess of TFA for 1 hour to give the corresponding amine partner as a TFA salt.

The obtained free acid was then activated with HATU and reacted with the amine partner in the presence of DIPEA for 24 hours, at room temperature, under argon, to afford dipeptide **p5** in 85% yield. The analysis of a single crystal of dipeptide **p5** by X-ray diffraction shows no intra residual hydrogen bonding in solid state, but rather an infinite array of intermolecular hydrogen bond interactions implicating three hydrogen bond donors and three acceptors that stack the dipeptide **p5** molecules in a parallel fashion (see Figure 87).

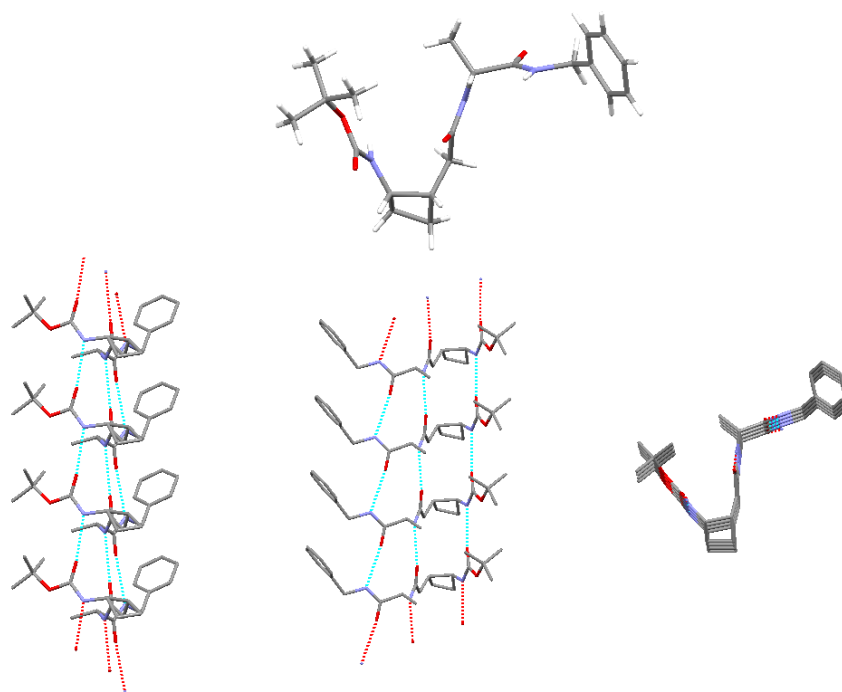


*Figure 87: The X ray crystal structure of peptide **p5** (top), and its intermolecular hydrogen bonding interactions viewed from the side (left), front (middle), and top (right).*



## 4.3 Conclusion

In conclusion two diastereoisomeric  $\gamma/\alpha$ -hybrid tetrapeptides composed of alternating *cis*-<sup>3,4</sup>CB-GABA and D-Alanine were synthesized and fully characterized and their three dimensional folding pattern in solution was investigated. Even though, more conformational analysis including infrared spectroscopy and DFT calculations are still needed to further validate the folding behavior of the two diastereoisomeric  $\gamma/\alpha$ -hybrid tetrapeptides, 2D ROESY NMR experiments and molecular modeling data revealed the tendency of these peptides to fold into a 12/10 helix in solution when the (*S,S*)-*cis*-<sup>3,4</sup>CB-GABA was used as the  $\gamma$ -amino acid component. These experimental results are in correlation with the Hofmann group theoretical calculations.<sup>117</sup> On the other hand when the chirality of the  $\gamma$ -amino acid component was switched to (*R,R*)-*cis*-<sup>3,4</sup>CB-GABA, the peptide showed a tendency to adopt an unprecedented 9/7 folding pattern interpreted by observing the intra residual ROEs colorations displayed by tetrapeptide **p4**.

Despite the fact that the 9/7 folding pattern was only the third abundant one as calculated by the preliminary molecular modeling of **p4** in CDCl<sub>3</sub>, the switching from a 12/10 structuration observed for its diastereomeric analog **p2** emphasizes the importance of the side chain configuration as a tool to design peptides in a deliberate secondary structure.

# Perspective and Overall Conclusion

Our goal in this work was to prepare two cyclobutane-constained  $\gamma$ -amino acids, *cis*-<sup>2,3</sup>CB-GABA and *cis*-<sup>3,4</sup>CB-GABA, in an enantioselective manner, and use these building blocks for the synthesis of  $\gamma/\alpha$ -hybrid peptides that are likely to adopt helical structuration. We focused our interest on a supramolecular photochirogenesis method, adopting  $\beta$ -CD as the chiral guest, since it appeared easily adaptable to our proposed photochemical reactions.

We synthesized *N*-allyl-*N*-(4-methoxyphenyl)acrylamide **1** and assumed its photocycloaddition reaction would lead to the cycloadduct **2**, a precursor of *cis*-<sup>2,3</sup>CB-GABA. The complexation of compound **1** with  $\beta$ -CD was studied by 1D and 2D <sup>1</sup>H NMR experiments which showed diagnostic interactions between protons of both host and guest. The complex was identified as having a 1:1 ( $\beta$ -CD/**1**) ratio and had a low binding constant ( $K_b = 14.7$ ).

A photocyclization reaction test performed with compound **1** (without  $\beta$ -CD) did not lead to the expected photochemical [2+2]-cycloaddition product but gave instead 1-allyl-6-methoxy-3,4-dihydroquinolin-2(1*H*)-one **5**, resulting from a photochemical  $6\pi$ -electrocyclization followed by a 1,5-sigmatropic shift.

Then we turned our attention to the photoelectrocyclization of 1,3-dihydro-2*H*-azepin-2-one **8** in the presence of  $\beta$ -CD which was expected lead to an enantiomerically enriched photoadduct **9**, a precursor of *cis*-<sup>3,4</sup>CB-GABA. The complexation of compound **8** with  $\beta$ -CD was studied by 1D and 2D <sup>1</sup>H NMR experiments which showed diagnostic interactions between protons of both host and guest. The complex was identified as having a 1:1 ( $\beta$ -CD/**8**) ratio and had a moderate binding constant ( $K_b = 35.4$ ).

Irradiation of the  $\beta$ -CD/**8** complex in aqueous solutions, suspensions, or in the solid state, resulted in the electrocyclization of azepinone **8** to give the photoadduct **9**. This later compound had a very low solubility in organic solvent and was immediately reduced in a one-pot reaction into the 2-azabicyclo[3.2.0]heptan-3-one **10** with an yield up to 79% from azepinone **8**. The

highest *ee* of 45% was obtained when the irradiation of the  $\beta$ -CD/**8** complex was performed in suspension form.

Continuing our efforts to have access to (*R,R*) and (*S,S*)-*cis*-<sup>3,4</sup>CB-GABA, we then established a resolution method for the *N*-Boc benzyl ester derivative on a semi-preparative HPLC instrument fitted with a chiral column, which furnished both enantiomers in pure form and on a gram scale.

Enantiomerically pure (-) and (+)-*cis*-<sup>3,4</sup>CB-GABA derivatives were used thereafter to synthesize two diastereoisomeric  $\gamma,\alpha$ -peptides. These hybrid peptides were composed of alternating either (-)-*cis*-<sup>3,4</sup>CB-GABA or (+)-*cis*-<sup>3,4</sup>CB-GABA with *D*-Alanine. Two  $\gamma/\alpha$ -dipeptides, Boc-*S,S*-GABA-*R*-AlaOBn and Boc-*R,R*-GABA-*R*-AlaOBn, as well as two  $\gamma/\alpha$ -tetrapeptides, Boc-(*S,S*-GABA-*R*-Ala)<sub>2</sub>OBn and Boc-(*R,R*-GABA-*R*-Ala)<sub>2</sub>OBn, were prepared by a convergent synthesis and fully characterized.

The conformational analysis of both diastereoisomeric dipeptides by single crystal X-ray diffraction showed no intramolecular interactions but a network of intermolecular hydrogen bonding. 1D and 2D NMR experiments showed that the tetrapeptide, Boc-*S,S*-GABA-*R*-Ala)<sub>2</sub>OBn, adopted a 12/10 helical conformation, whereas its diastereomeric analog, Boc-(*R,R*-GABA-*R*-Ala)<sub>2</sub>OBn, displayed evidence of an unprecedented 7/9 folding pattern in solution.

As a perspective of this work, the [2+2] photocycloaddition of *N*-allyl acrylamide could be favored by the use of a benzyl group on the nitrogen atom in place of an aryl group, thereby suppressing the conjugated  $6\pi$  system responsible of the  $6\pi$ -electrocyclization.

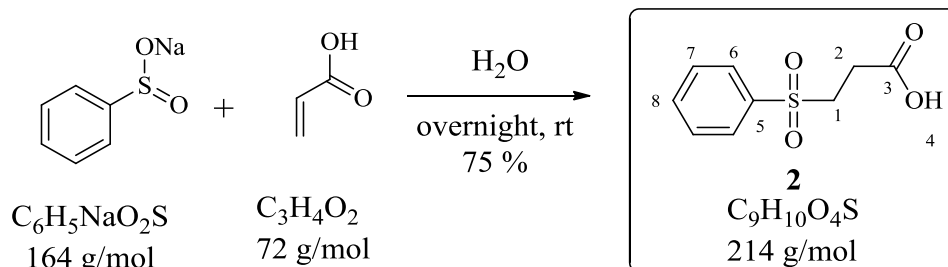
Photochirogenesis using  $\beta$ -CD in the electrocyclization of azepinone **8** could be improved by use of a benzyl or *tert*-butyloxycarbonyl group attached on the nitrogen, to strengthen the  $\beta$ -CD/azepinone complexation.

$\gamma,\alpha$ -tetrapeptides, Boc-(*S,S*-GABA-*R*-Ala)<sub>n</sub>NHBn, could be prepared and their conformational preferences studied, since the amide on the C-terminal is able to provide additional H-bond interactions to enhance folding propensity.



# Experimental Part

## 3-(phenylsulfonyl)propanoic acid [2]



To a stirring solution of sodium benzenesulfinate (4.00 g, 24.39 mmol) in 25 ml distilled water, acrylic acid (1.67 ml, 1 eq.) was added, and the reaction mixture was left to stir overnight. The aqueous solution was then acidified with 2 M HCl and the desired product was extracted with diethyl ether (4 x 25 ml). The organic layer was concentrated under vacuum to obtain the desired product as white solid (3.90 g, 18.29 mmol). The crude product was pure enough to be used in the next step after drying under high vacuum.

**Yield:** 75%

**TLC Rf** (EtOAc): 0.6

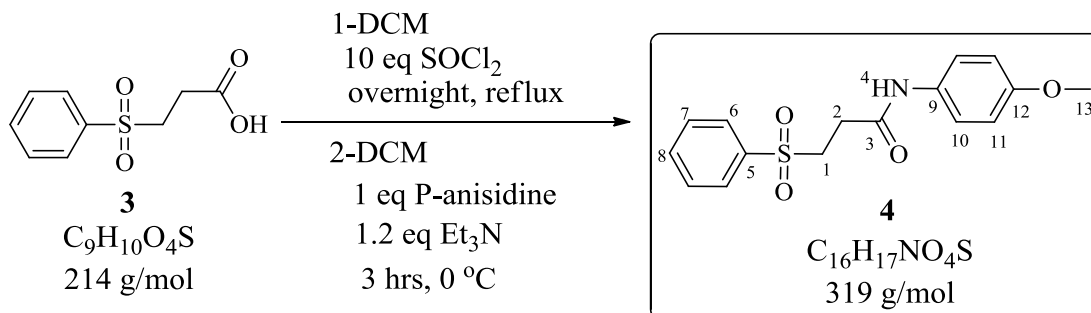
**<sup>1</sup>H NMR (300 MHz, CDCl<sub>3</sub>):** δ = 2.80 (t, 2H, H-2), 3.42 (t, 2H, H-1), 3.76 (s, 3H, H-13), 7.56-7.62 (m, 2H, H-8), 7.66-7.71 (m, 1H, H-9), 7.90-7.94 (m, 2H, H-7)

**<sup>13</sup>C NMR (75 MHz, CDCl<sub>3</sub>):** δ = 27.6 (C-2), 51.3 (C-1), 128.9 (C-6), 129.6 (C-7), 134.3 (C-8), 138.5 (C-5), 175.2 (C-3)

**MP:** 115-116 °C.

**HR-MS:** m/z calcd for [C<sub>9</sub>H<sub>10</sub>O<sub>4</sub>S+Na]<sup>+</sup> 237.0192 ; found 237.0194

### N-(4-methoxyphenyl)-3-(phenylsulfonyl)propanamide [4]



To a solution of **3** (4.00 g, 18.69 mmol) in dry dichloromethane 25 ml, thionyl chloride was added (14 ml, 10 eq.). the reaction mixture was left to reflux overnight. The solvent along with excess thionyl chloride were distilled out under vacuum. The solid residue was left to dry under high vacuum then dissolved in 150 ml dry dichloromethane. The solution was cooled to 0 °C and p-anisidine (2.30 g, 1 eq.) was added followed by trimethylamine (2.5 ml 1.2 eq.). The reaction mixture was left to stir for 3 hours at 0 °C then washed with 1 molar HCl (2 x 20 ml), followed by brine (2 x 20 ml). The organic layer was dried over  $MgSO_4$  and concentrated to half under reduced pressure. To the resulting solution petroleum ether 300 ml was added to precipitate the desired product **4**, which was filtered off over a sintered glass funnel, porosity 3. The crude product was pure enough to be used in the next step. It could also be recrystallized from dichloromethane/ hexane to get clear crystals (5.06 g, 15.88 mmol).

**Yield:** 85%

**TLC Rf** (Hex/EtOAc 2/1): 0.25

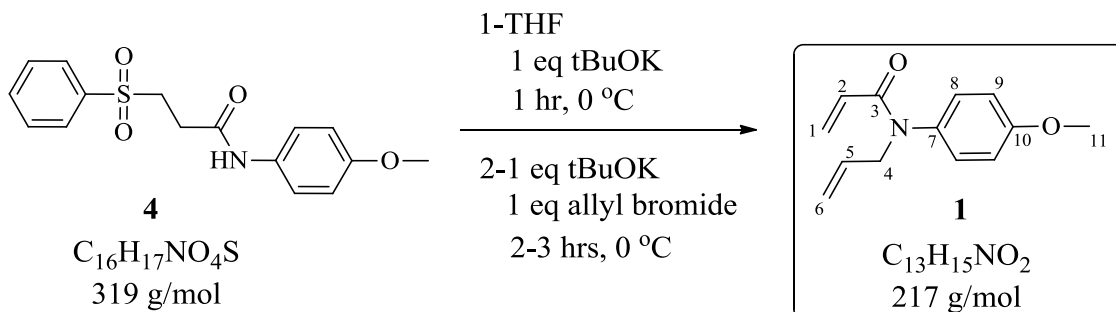
**$^1H$  NMR (500MHz,  $CDCl_3$ ):**  $\delta$  = 2.87 (t, 2H, H-2), 3.55 (t, 2H, H-1), 3.76 (s, 3H, H-13), 6.81 (d, 2H, H-11), 6.32 (d, 2H, H-10), 7.55-7.58 (m, 2H, H-7), 7.65-7.66 (m, 1H, H-8), 7.80 (s, 1H, H-4), 7.93 (d, 2H, H-6).

**$^{13}C$  NMR (125 MHz,  $CDCl_3$ ):**  $\delta$  = 29.8 (C-2), 42.1 (C-1), 55.5 (C-13), 114.2 (C-11), 121.9 (C-10), 128.1 (C-6), 129.6 (C-7), 130.6 (C-8), 134.2 (C-9), 138.7 (C-5), 156.6 (C-12), 166.9 (C-3).

**MP:** 118-119 °C.

**HR-MS:** m/z calcd for [C<sub>16</sub>H<sub>17</sub>NO<sub>4</sub>S+Na]<sup>+</sup> 342.0770 ; found 342.0761

**N-allyl-N-(4-methoxyphenyl)acrylamide [1]**



To a solution of **4** (3.00 g, 9.4 mmol) in 100 ml dry THF, at 0 °C, potassium tertiary butoxide (1.04 g 1 eq.) was added. The reaction mixture was left to stir for 1 hour at 0 °C after which another equivalent of potassium tertiary butoxide was added followed by allyl bromide (0.8 ml, 1eq.) the reaction mixture was left to stir at 0 °C for 3-4 h. The THF was removed under vacuum and ethyl acetate (100 ml) was added. The organic layer was washed with brine (5 x 30 ml). then dried over MgSO<sub>4</sub> and reduced under vacuum. The crude was purified by chromatography on silica (80/20 hexane/EtOAc) to obtain compound **1** as a clear oil. Diethyl ether was added to co-evaporate ethyl acetate and obtain a white solid (1.22 g, 5.6 mmol). Note that the product could polymerize if heated and left as an oil under high vacuum.

**Yield** 60%

**TLC Rf** (PE/EtOAc 7/3): 0.54

**<sup>1</sup>H NMR (300 MHz, CDCl<sub>3</sub>):** δ = 3.82 (s, 3H, H-11), 4.34 (dt, *J* = 6.3 Hz, *J* = 1.3 Hz, 2H, H-4), 5.06-5.15 (m, 2H, H-6), 5.51 (dd, *J* = 10.3 Hz, *J* = 2.1 Hz, 1H, H-1), 5.88 (ddt, *J* = 16.7 Hz, 10.3 Hz, 6.2 Hz, 1H, H-5), 6.03 (dd, *J* = 16.8 Hz, 10.3 Hz, 1H, H-2), 6.36 (dd, *J* = 16.8 Hz, 2.1 Hz, 1H, H-1'), 6.88-6.91 (m, 2H, H-9), 7.05-7.07 (m, 2H, H-8).

**<sup>1</sup>H NMR (300 MHz, D<sub>2</sub>O):** δ = 3.83 (s, 3H, H-11), 4.34 (d, *J* = 5.6 Hz, *J* = 2H, H-4), 5.1-5.18 (m, 2H, H-6), 5.61 (dd, *J* = 9.6 Hz, *J* = 2.4 Hz, 1H, H-1), 5.84 (ddt, *J* = 16.5 Hz, *J* = 11.0 Hz, *J*

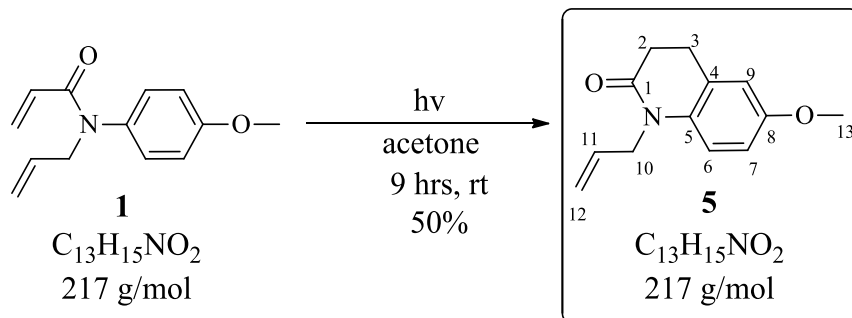
= 5.6 Hz, 1H, H-5), 6.10 (dd,  $J = 17.0$  Hz,  $J = 9.5$  Hz, 1H, H-2), 6.2 (dd,  $J = 17.0$  Hz,  $J = 2.5$  Hz, 1H, H-1'), 7.02 (d,  $J = 8.8$  Hz, 2H, H-9), 7.22 (d,  $J = 8.9$  Hz, 2H, H-9).

**$^{13}\text{C}$  NMR (75 MHz,  $\text{CDCl}_3$ ):**  $\delta = 52.6$  (C-4), 55.6 (C-11), 114.7 (C-9), 118.1 (C-6), 127.7 (C-1), 128.7 (C-2), 129.5 (C-8), 133.1 (C-5), 134.7 (C-10), 159.0 (C-7), 165.7 (C-3)

**MP:** 62-63 °C.

**HR-MS:**  $m/z$  calcd for  $[\text{C}_{13}\text{H}_{15}\text{NO}_2+\text{Na}]^+$  240.0995; found 240.0995

### 1-allyl-6-methoxy-3,4-dihydroquinolin-2(1H)-one [5]



A solution of **1** (44 mg, 0.20 mmol) in 10 ml degassed acetone in a Pyrex tube was irradiated for 9 h inside a Luzchem (LCZ-4V) reactor fitted with 14 UV-B lamps. The solvent was then evaporated under reduced pressure and the crude was purified by chromatography on silica (gradient from 90/10 to 70/30 hexane/EtOAc) to obtain compound **5** as a white solid (22 mg, 0.1 mmol).

**Yield:** 50%

**TLC Rf** (PE/EtOAc 7/3): 0.38

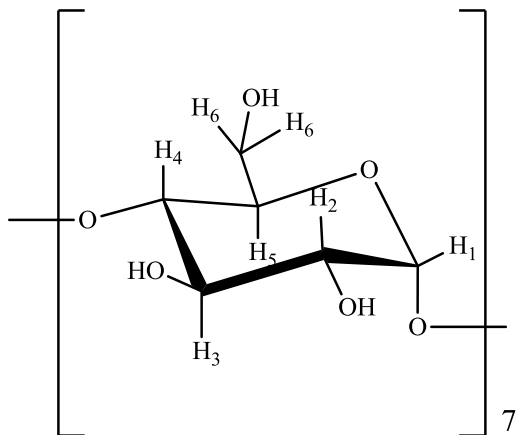
**$^1H$  NMR (300 MHz,  $CDCl_3$ ):**  $\delta$  = 2.67 (dd,  $J$  = 8.7 Hz,  $J$  = 5.8 Hz, 2H, H-2), 2.89 (dd,  $J$  = 8.8 Hz,  $J$  = 5.9 Hz,  $J$  = 2H, H-3), 3.78 (s, 3H, H-13), 4.63-4.41 (m, 2H, H-10), 5.37-5.02 (m, 2H, H-12), 5.88 (ddt,  $J$  = 17.2 Hz,  $J$  = 10.0 Hz, 4.7 Hz, 1H, H-11), 6.79-6.67 (m, 1H, H-9, 1H, H-7), 7.12-6.84 (m, 1H, H-6).

**$^{13}C$  NMR (75 MHz,  $CDCl_3$ ):**  $\delta$  =  $\delta$  25.9 (C-3), 31.9 (C-2), 45.3 (C-10), 55.6 (C-13), 111.9 (C-9 or C-7), 113.9 (C-7 or C-9), 116.41 (C-12), 16.45 (C-6), 128.0 (C-5 or C-4), 132.9 (C-11), 133.5 (C-4 or C-5), 155.4 (C-8), 169.8 (C-1).

**MP:** 59-60 °C.

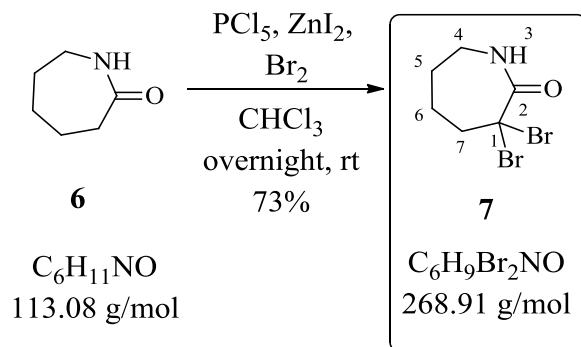
**HR-MS:**  $m/z$  calcd for  $[C_{13}H_{15}NO_2+Na]^+$  240.0995 ; found 240.0994.

## $\beta$ -cyclodextrin ( $\beta$ -CD)



**RMN  $^1\text{H}$  (600 MHz,  $\text{D}_2\text{O}$ ) :**  $\delta = 3.65$  (t,  $J = 9$  Hz, 7H, H-4), 3.73, (dd,  $J = 3.6$  Hz,  $J = 9.9$ Hz, 7H, H-2), 3.92-3.96 (m, 7H, H-5, 14H, H-6), 5.14 (d,  $J = 3.6$ , 6H, H-1)

### 3,3-Dibromoazepan-2-one [7]



A solution of caprolactam **6** (5.00 g, 44.25 mmol) in chloroform (125 mL) was cooled to 4 °C in an ice bath. Phosphorus pentachloride (18.39 g, 89.01 mmol, 2 eq.) was then added followed by dry zinc iodide (0.56 g, 1.75 mmol). Bromine (4.5 mL, 88.5 mmol) was then added slowly over 15 min. The reaction mixture was allowed to warm to room temperature and left to stir overnight. The reaction was quenched with an ice-water mixture (200 mL). The organic layer was separated and washed with water (3 × 100 mL) and with a 0.5 M solution of sodium bisulfite (3 × 100 mL), dried over sodium sulfate, and concentrated under reduced pressure. The crude yellow solid was washed with water to obtain compound **7** as white solid (8.30 g, 30.86 mmol).

**Yield:** 70%.

**TLC R<sub>f</sub>** (PE/EtOAc 50/50): 0.60.

**<sup>1</sup>H NMR (400 MHz, CDCl<sub>3</sub>):**  $\delta$  = 1.67-1.75 (m, 2H, H-6), 1.97 (ddd, J = 8.4, 7.2, 4.7 Hz, 2H, H-5), 2.72-2.75 (m, 2H, H-4), 3.35-3.44 (m, 2H, H-7), 6.59 (bs, 1H, H-3).

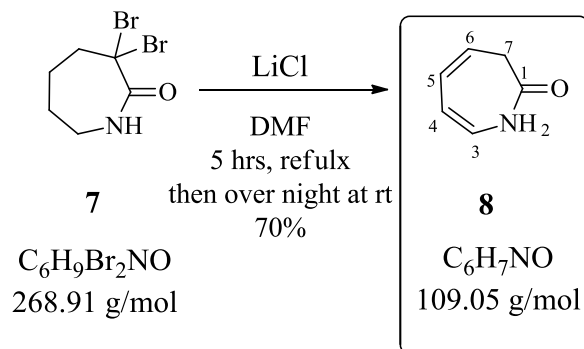
**<sup>13</sup>C NMR (75 MHz, CDCl<sub>3</sub>):**  $\delta$  = 28.3 (C-6), 28.4 (C-5), 42.5 (C-4), 46.0 (C-7), 69.3 (C-1), 168.3 (C-2).

**MP:** 162 °C.

**IR (solid):** (C-Br) 769, (C-C) 1326, (C=O) 1665, (C-H) 2940, (NH) 3090, (NH) 3207  $\text{cm}^{-1}$

**HR-MS:**  $m/z$  calcd for  $[C_6H_9Br_2NO+Na]^+$  291.8943; found 293.8918 (2.5 ppm).

### 2,3-Dihydro-1*H*-azepin-2-one [8]



To a solution of compound **7** (5.80 g, 21.56 mmol) in dry DMF (130 mL), dried anhydrous LiCl (2.71 g, 63.93 mmol) was added. The reaction mixture was heated to reflux under argon atmosphere for 5 h, then left to stir at room temperature overnight. The solvent was then distilled out under reduced pressure. Water 50 ml was added, and the aqueous layer was extracted with  $CH_2Cl_2$  (5 X 50ml). The organic layer was dried over  $Na_2S_2O_4$ , filtered and concentrated to obtain crude **8** as dark brown oil that was purified by flash chromatography on silica (gradient eluent from 80/20 to 50/50 PE/EtOAc). Compound **8** was obtained as yellow solid which was recrystallized from pentane to give white crystals (1.63 g, 14.65 mmol).

**Yield:** 69%.

**TLC  $R_f$**  (PE/EtOAc 50/50): 0.53.

**$^1H$  NMR (360 MHz,  $CDCl_3$ ):**  $\delta$ = 2.91 (d,  $J$  = 6.8 Hz, 2H, H-7), 5.61 (dt,  $J$  = 9.3 Hz,  $J$  = 6.8 Hz, 1H, H-6), 5.84 (dd,  $J$  = 5.1 Hz,  $J$  = 8.9 Hz, 1H, H-4), 6.17-6.23 (m, 1H, H-5, 1H, H-3), 8.17 (bs, 1H, H-2).

**$^1H$  NMR (300 MHz,  $D_2O$ ):**  $\delta$ = 2.79 (d,  $J$  = 6.8 Hz, 2H, H-7), 5.55 (dt,  $J$  = 9.3 Hz,  $J$  = 6.8 Hz, 1H, H-6), 5.94 (dd,  $J$  = 5.3 Hz,  $J$  = 8.9 Hz, 1H, H-4), 6.19 (dd,  $J$  = 5.3 Hz,  $J$  = 9.3, 1H, H-5), 6.25 (d,  $J$  = 9.0 Hz, 1H, H-3).

**UV/Vis ( $CH_3CN$ ):**  $\lambda_{max}$  = 259 ( $\epsilon$  =  $10^4 M^{-1} \cdot cm^{-1}$ ).

**<sup>13</sup>C NMR (75 MHz, CDCl<sub>3</sub>):**  $\delta$  = 37.2 (C-6), 114.2 (C-3), 121.1 (C-1), 125.4 (C-2), 127.6 (C-4), 168.7 (C-7).

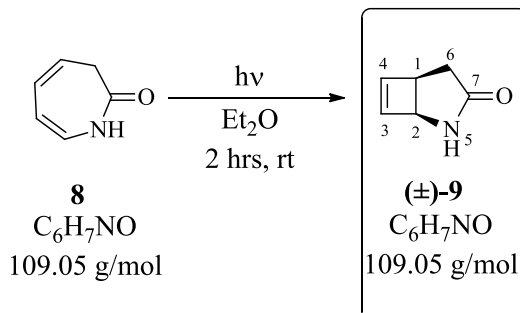
**MP:** 45 °C.

**IR (solid):** (C-C) 1334, (C=O) 1592, (C=C, C=O) 1635 and 1650, (C-H) 2943, (NH) 3083, (NH) 3193 cm<sup>-1</sup>.

**HR-MS:** m/z calcd for [C<sub>6</sub>H<sub>7</sub>NO+H]<sup>+</sup> 110.0600 ; found 110.0604 (-3.3 ppm).

## Photoelectrocyclization of azepinone **8** in ether without $\beta$ -CD:

( $\pm$ )-Cis-2-azabicyclo[3.2.0]hept-6-en-3-one [( $\pm$ )-**9**]



A solution of **8** (200 mg 1.834 mmol) in diethyl ether (250 mL) was degassed with an argon stream in a cylindrical water-cooled reactor during 15 min, and then irradiated for 2 h with a 400 W medium-pressure mercury lamp fitted with a Quartz filter, while the reactor was cooled with an external ice bath. The solvent was evaporated under reduced pressure to obtain crude ( $\pm$ )-**9** (195 mg 1.788 mmol). The crude product was pure enough and was not further purified

**Crude yield:** 97%.

**TLC R<sub>f</sub>** (Et<sub>2</sub>O): 0.11.

**<sup>1</sup>H NMR (300 MHz, CDCl<sub>3</sub>):**  $\delta$  = 2.27 (dd,  $J$  = 17.9 Hz,  $J$  = 3.4 Hz, 1H, H-6), 2.46 (dd,  $J$  = 17.9 Hz,  $J$  = 10.2 Hz, 1H, H-6), 3.56 (dt,  $J$  = 10.2 Hz,  $J$  = 3.4 Hz, 1H, H-1), 4.43-4.44 (m, 1H, H-2), 6.30-6.33 (m, 1H, H-3, 1H, H-4), 7.05 (bs, 1H, H-5).

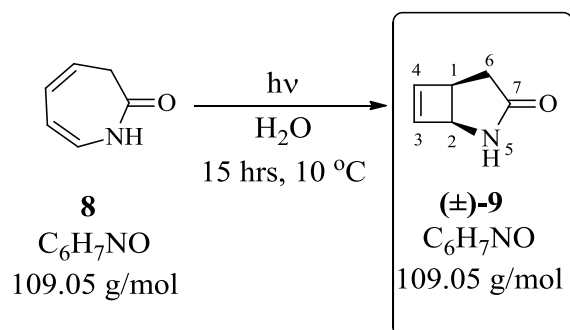
**<sup>13</sup>C NMR (75 MHz, CDCl<sub>3</sub>):**  $\delta$  = 33.7 (C-1), 41.4 (C-2), 57.9 (C-6), 142.3, 142.5 (C-3, C-4), 178.7 (C-7).

**MP:** 75 °C.

**IR** (solid): (C-C) 1250, (C-N) 1302, (C=C) 1645, (C=O) 1676, (C-H), 2961, (NH) 3266 cm<sup>-1</sup>.

**HR-MS:**  $m/z$  calcd for [C<sub>6</sub>H<sub>7</sub>NO+H]<sup>+</sup> 110.600 ; found 110.0599 (1.2 ppm).

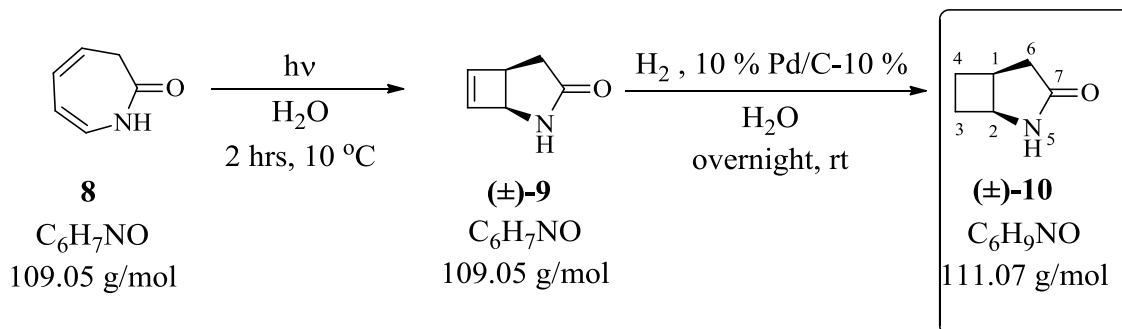
### Photocyclization of azepinone **8** in water without $\beta$ -CD:



A solution of azepinone **8** (500 mg, 4.58 mmol) in 50 ml of ultra-pure water was introduced in a quartz tube and irradiated inside a Rayonet for 15 h at 10°C. The reaction mixture was then lyophilized to obtain crude (±)-**9** (356 mg, 3.26 mmol). The crude product was pure enough and was not further purified. The spectral data were identical to those previously reported on page 145.

**Crude yield:** 71%.

**Preparation of (±)-2-azabicyclo[3.2.0]heptan-3-one (±)-10 by photoelectrocyclisation/reduction.**



A solution of azepinone **8** (50.00 mg, 0.458 mmol) in 30 ml of ultra-pure water, was irradiated in a quartz tube, inside a Rayonet for 2 h at 10 °C. The reaction mixture was then transferred into a round bottom flask and 10% w/w Pd/C-10% were added. The reaction mixture was stirred, without degassing, overnight, at room temperature, under dihydrogen atmosphere. The catalyst was then filtered out and the product (±)-**10** was extracted with ethyl acetate (13 x 40 ml). The organic layer was dried over  $Na_2SO_4$  then concentrated under reduced pressure to obtain crude (±)-**10** (41.70 mg, 0.375 mmol) as a yellow oil. The crude product was of enough purity and no further purification was done.

**Crude yield over 2 steps:** 82%.

**TLC  $R_f$**  (PE/EtOAc 1/1): 0.25.

**$^1H$  NMR (360 MHz,  $CDCl_3$ ):**  $\delta$  = 1.83-2.00 (m, 1H,  $H_3$ , 1H,  $H_4$ ), 2.17 (d,  $J$  = 17.8 Hz, 1H,  $H_6$ ), 2.23-2.33 (m, 1H,  $H_3$ , 1H,  $H_4$ ), 2.57 (dd,  $J$  = 9.1 Hz,  $J$  = 17.8 Hz, 1H,  $H_6$ ), 3.05-3.09 (m, 1H,  $H_1$ ), 4.04-4.07 (m, 1H,  $H_2$ ), 7.20 (bs, 1H,  $H_5$ ).

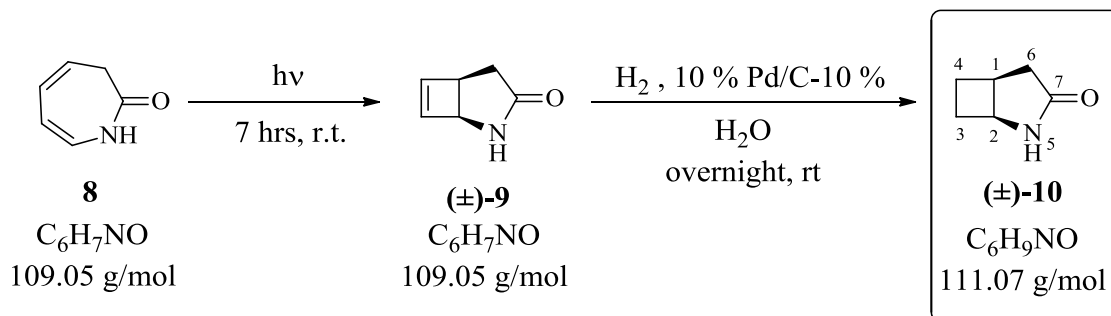
**$^1H$  NMR (300 MHz,  $D_2O$ ):**  $\delta$  = 1.75-1.85 (m, 1H,  $H_3$ , 1H,  $H_4$ ), 2.2 (d,  $J$  = 17.7 Hz, 1H,  $H_6$ ), 2.18-2.35 (m, 1H,  $H_3$ , 1H,  $H_4$ ), 2.51 (dd,  $J$  = 8.7 Hz,  $J$  = 17.7 Hz, 1H,  $H_6$ ), 3.03-3.12 (m, 1H,  $H_1$ ), 4.03-4.12 (m, 1H,  $H_2$ ).

**<sup>13</sup>C NMR (75 MHz, CDCl<sub>3</sub>):** δ=25.2 (C-4), 26.3 (C-3), 33.1 (C-1), 37.1 (C-6), 54.2 (C-2), 179.3 (C-7).

**IR (solid):** (C-C) 1287, (C-N) 1310, (C=O) 1677, (C-H), 2939, (NH) 3237 cm<sup>-1</sup>.

**HR-MS:** m/z Calcd for [C<sub>6</sub>H<sub>9</sub>NO+H]<sup>+</sup> 112.0757; found 112.0761 (-3.5ppm).

### Photoelectrocyclization of azepinone **8** in solid state without $\beta$ -CD:



Azepinone **8** (30.00 mg, 0.275 mmol) was mechanically ground in mortar and introduced in a quartz tube. The tube was closed and set to rotate in a Rayonet in which it was irradiated for 7 h. The crude product was then completely dissolved in ultra-pure water and stirred overnight, without degassing, at room temperature, under dihydrogen atmosphere with 10% w/w Pd/C-10%. The catalyst was then filtered out and the product (±)-**10** was extracted with ethyl acetate (12 x 25 ml). The organic layer was dried over Na<sub>2</sub>SO<sub>4</sub> then concentrated under reduced pressure to obtain crude (±)-**10** (12.22 mg, 0.110 mmol). The crude product was of enough purity and no further purification was done. Spectral data were identical to those previously reported.

**Crude yield over 2 steps: 40%.**

## Photoelectrocyclisation in the presence of $\beta$ -CD:

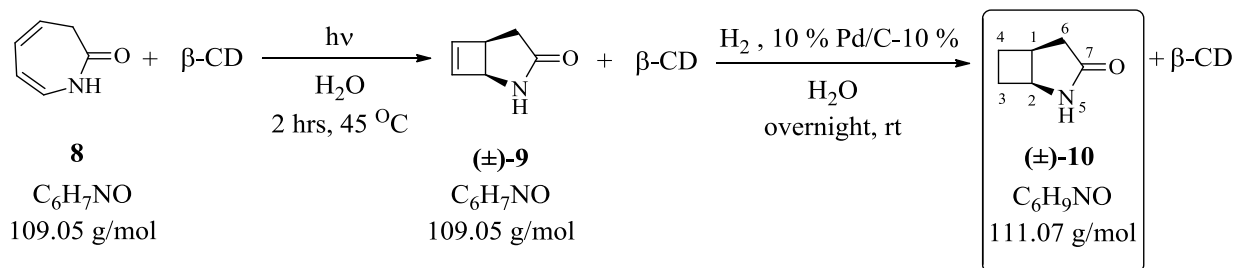
### Photoelectrocyclisation in fluid state:

#### General procedure "I" for irradiation in fluid state:

All experiments in fluid state started by adding a clear aqueous solution of azepinone **8** to a clear aqueous solution containing the desired equivalents dried  $\beta$ -CD. The volume of the final solution was chosen to be just below 15 mM with respect to the host  $\beta$ -CD. Upon stirring, a white precipitate starts to form almost immediately. The suspension was left to stir 2 h at room temperature, and then transferred into a quartz tube fitted with a stirring bar, and a temperature control system (heating cooling finger). The tube was then irradiated inside a in Rayonet RPR-200 equipped with a carousel of 16 lamps [ $\lambda = 254$  nm]. The course of the reaction was followed by  $^1\text{H}$  NMR. When no more starting material azepinone **8** could be detected, the reaction was considered complete. The irradiated solution was then transferred into a round bottom flask and 10% w/w Pd/C-10% were added. The reaction mixture was stirred overnight, at room temperature, under a dihydrogen atmosphere. The catalyst was then filtered out and the aqueous phase was extracted with ethyl acetate until no more **10** could be detected in the aqueous phase by  $^1\text{H}$  NMR.

## Photoelectrocyclisation of $\beta$ -CD/azepinone **8** complex in hot water / reduction

### Experiment A



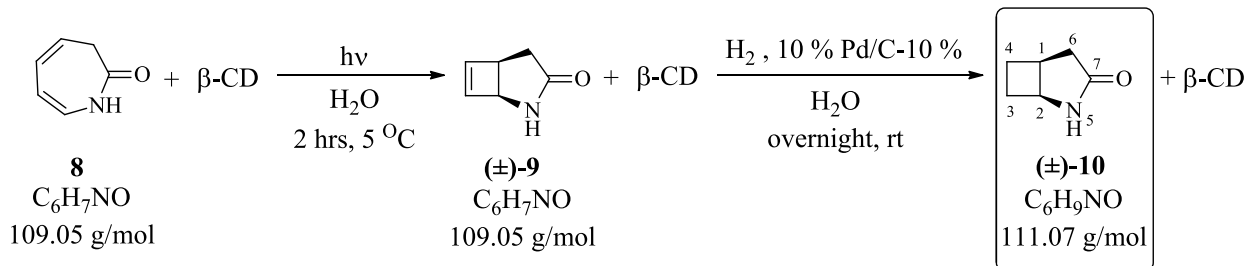
According to general procedure "I" azepinone **8** (50.00 mg, 0.458 mmol) was complexed with 1 equivalent of  $\beta$ -CD (0.52 g, 0.458 mmol) in 31 ml of water. The suspension was transferred to a quartz tube, and then heated up to 45 °C using a temperature control system (heating cooling finger). The hot solution was then irradiated in the Rayonet for 2 hours at 45 °C. The resulting yellowish clear solution was transferred to a flask. The cycloadduct **4** was reduced and extracted from the aqueous phase with ethyl acetate (13 x 40ml). The organic phase was dried over  $Na_2SO_4$  then concentrated under vacuum to obtain crude **10** (12.22 mg, 0.110 mmol). The product was of enough purity and no further purification was done. Spectral data were identical to those previously reported.

**Crude yield:** 40%.

**ee** 0%.

## Photoelectrocyclisation of $\beta$ -CD/azepinone **8** complex in cold water / Reduction

### Experiment B



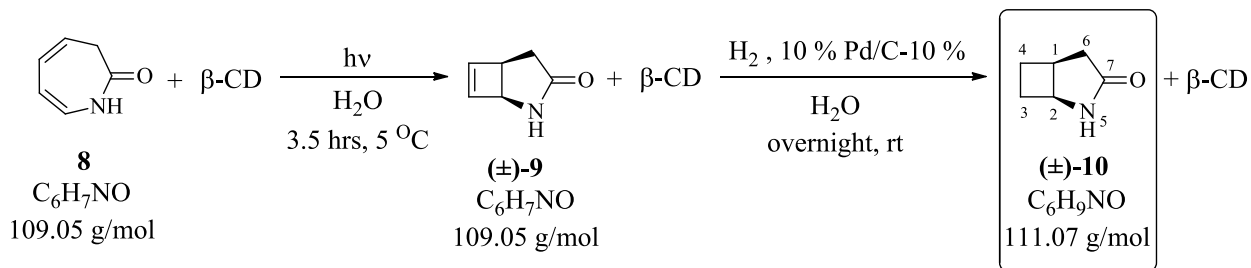
According to general procedure "I" azepinone **8** (30.00 mg, 0.275 mmol) was complexed with 1 equivalent of  $\beta$ -CD (0.32 g, 0.282 mmol) in 19 ml of water. The suspension was cooled to 5 °C, and the cold suspension was irradiated for 2 h at 5 °C. The resulting clear solution was subjected to reduction extracted with ethyl acetate (12 x 25 ml). The organic phase was dried over Na<sub>2</sub>SO<sub>4</sub> then concentrated vacuum to obtain crude **10** (24.01 mg, 0.216 mmol). The crude product was of enough purity and no further purification was done. Spectral data were identical to those previously reported.

**Crude yield:** 79%.

**ee** 38%.

## Photoelectrocyclisation of $\beta$ -CD/azepinone **8** "3/1 complex" in cold water / Reduction

### Experiment C



According to general procedure "I" azepinone **8** (30 mg, 0.275 mmol) was complexed with 1 equivalent of  $\beta$ -CD (0.32 g, 0.282 mmol) in 19 ml of water the suspension was charged with extra 2 equivalents  $\beta$ -CD during the stirring time. The suspension was cooled to 5 °C, and the cold suspension was irradiated for 3.5 hours at 5 °C. The resulting clear aqueous solution was subjected to reduction and extracted with ethyl acetate (12 x 25 ml). The organic phase was dried over Na<sub>2</sub>SO<sub>4</sub> then concentrated under vacuum to obtain crude **10** (23.02 mg, 0.207 mmol). The crude product was of enough purity and no further purification was done. Spectral data were identical to those previously reported.

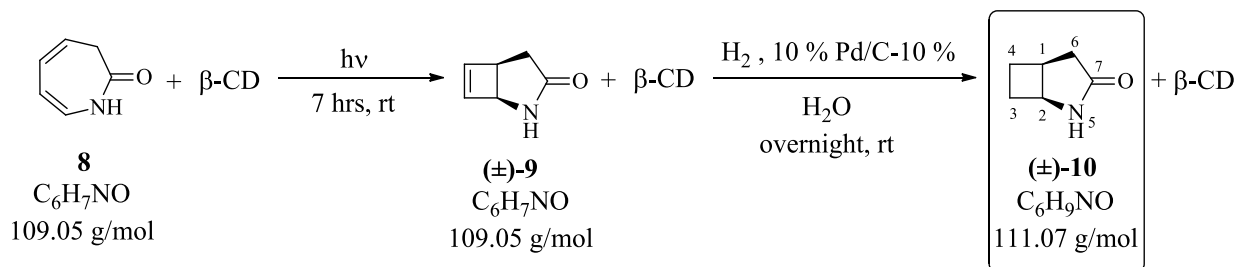
**Crude yield:** 75%.

**ee** 45%.

# Photoelectrocyclisation of $\beta$ -CD/azepinone **8** "3/1 complex" in solid state / Reduction

## Experiment D

### Mechanically ground:



One equivalent of azepinone **8** (30.00 mg, 0.275 mmol) was mechanically ground with  $\beta$ -CD (0.32g, 0.282mmol) in a mortar. The solid was transferred to a quartz tube which was set to slowly rotate while being irradiate inside a Rayonet. When no starting material can be observed by  $^1H$  NMR (7 hours), the irradiated solid was dissolved in ultra-pure water (10 ml) and subjected to reduction. The aqueous phase was extracted with ethyl acetate (12 x 25ml). The organic phase was dried over  $Na_2SO_4$  and concentrated under vacuum to obtain crude **10** (21.30 mg, 0.191 mmol). The crude product was of enough purity and no further purification was done. Spectral data were identical to those previously reported.

**Crude yield:** 70%.

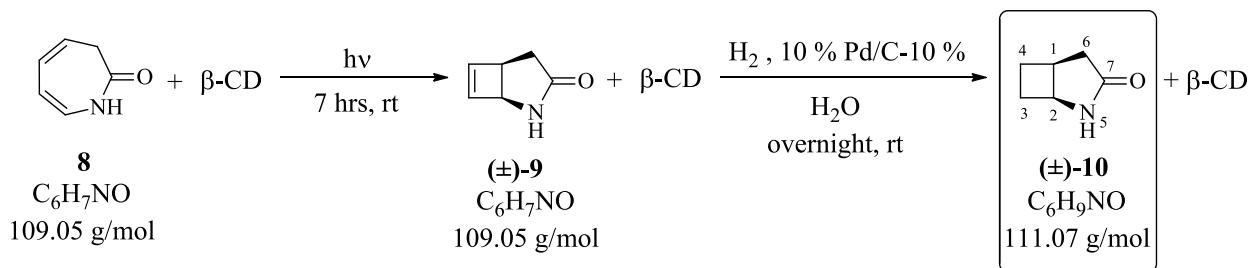
**ee** 0-40%.

### **General procedure "II" for photoelectrocyclisation in solid state / Reduction:**

All of the next experiments in solid state started by adding a clear aqueous solution of azepinone **8** to a clear aqueous solution containing the desired equivalents dried  $\beta$ -CD. The volume of the final solution was always chosen to be just below 15 mM with respect to the host $\beta$ -CD. Upon stirring, a white precipitate starts to form almost immediately. The suspension was left to stir for 2 hours at room temperature, and then treated accordingly to obtain a white solid (powder or film). The resulting solid was irradiated in Rayonet RPR-200 equipped with 16 lamps [ $\lambda = 250$  nm (RPR-3000 Å, Rayonet)]. The course of the reaction was followed by  $^1\text{H}$  NMR. When no more azepinone **8** starting material could be detected, the reaction was considered complete and the irradiated solid was transferred into a round bottom flask, dissolved in ultra-pure water then reduced overnight, at room temp, under dihydrogen atmosphere with 10% w/w of Pd/C-10%. The catalyst was then filtered out and the crude **10** was extracted with ethyl acetate until no more of it could be detected in the aqueous phase by  $^1\text{H}$  NMR.

## Photoelectrocyclisation of $\beta$ -CD/azepinone **8** in powder form / Reduction:

### Experiment E



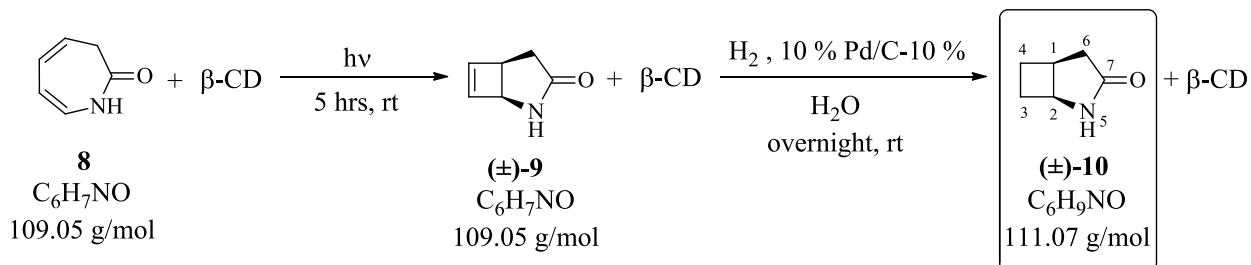
According to general procedure "II" azepinone **8** (50.00 mg, 0.458 mmol) was complexed with 1 equivalent of  $\beta$ -CD (0.52 g, 0.458 mmol) in 31 ml ultra-pure water. The suspension was then filtered on a sintered glass funnel (porosity 3) and washed with 10 ml of ultra-pure water. The uncomplexed azepinone **8** was extracted with ethyl acetate from the filtrate, and 20 mg of it could be recovered. The white complex was dried in air, finely crushed in a mortar and transferred into a quartz tube. The tube was closed and set to rotate inside a Rayonet in which it was irradiated for 20 hours. The irradiated solid was dissolved in ultra-pure water, reduced, and then extracted with ethyl acetate (13 x 40 ml). The organic phase was dried over Na<sub>2</sub>SO<sub>4</sub> and concentrated under vacuum to obtain crude **10** (21.30 mg, 0.191 mmol). The product was of enough purity and no further purification was done. Spectral data were identical to those previously reported.

**Crude yield:** 71% (with respect to the remaining 30 mg in the complex).

**ee** 36%.

**Potoelectrocyclisation of  $\beta$ -CD/azepinone in a 1:1 film, made from a 15 mM suspension /Reduction**

**Experiment F**



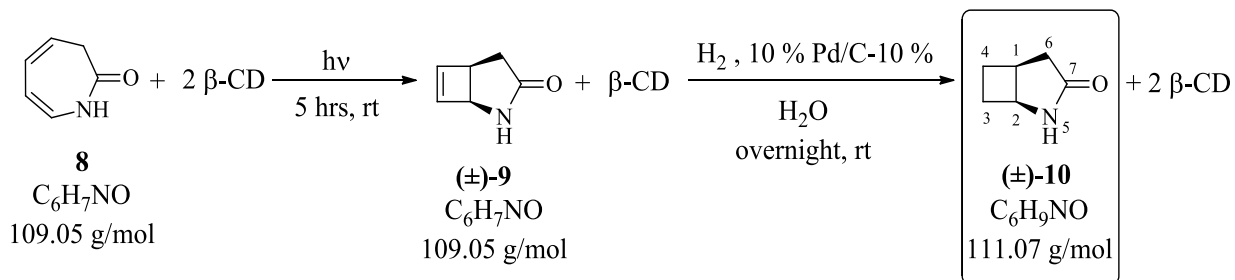
According to general procedure "II" azepinone **8** (50.00 mg, 0.458 mmol) was complexed with 1 equivalent of  $\beta$ -CD (0.52 g, 0.458 mmol) in 31 ml of water the suspension was then spread on a glass sheet and left to dry in open air for 3 days. The film that forms was irradiated in a Rayonet for 5 hours. The irradiated solid was dissolved in ultra-pure water, reduced, and then extracted with ethyl acetate (13 x 40 ml). The organic phase was dried over Na<sub>2</sub>SO<sub>4</sub> then concentrated under vacuum to obtain crude **10** (39.20 mg, 0.323 mmol). The product was of enough purity and no further purification was done. Spectral data were identical to those previously reported.

**Crude yield:** 77%.

**ee** 41%.

## Potoelectrocyclisation of $\beta$ -CD/azepinone **8** in a 2:1 film, made from a 15 mM suspension / Reduction

### Experiment G



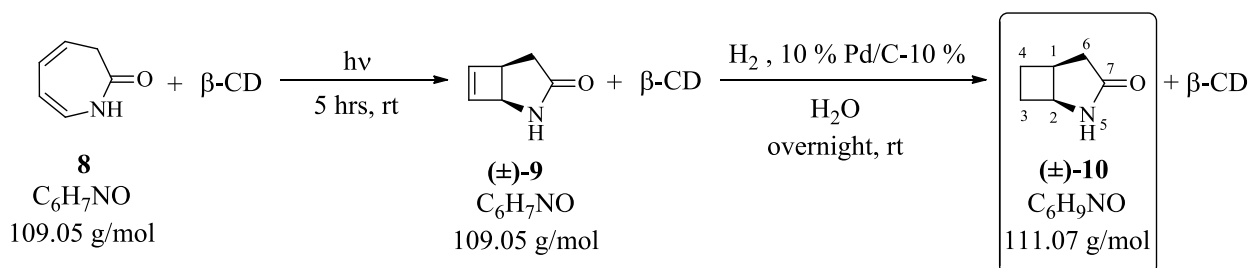
According to general procedure "II" azepinone **8** (33.60 mg, 0.308 mmol) was complexed with 2 equivalents of  $\beta$ -CD (0.702 g, 0.619 mmol) in 41 ml of ultra-pure water. The suspension was then spread on a glass sheet and left to evaporate in open air for 3 days. The film that forms was irradiated in a Rayonet for 5 h. The irradiated solid was put in solution, reduced, and then extracted with ethyl acetate (12 x 30 ml). The organic phase was concentrated under vacuum to obtain crude **10** (26.34 mg, 0.237 mmol). The crude product was of enough purity and no further purification was done. Spectral data were identical to those previously reported.

**Crude yield:** 77%.

**ee** 42%.

**Potoelectrocyclisation of  $\beta$ -CD/azepinone **8** in a 1:1 film, made from a 5 mM solution  
/Reduction:**

### Experiment H

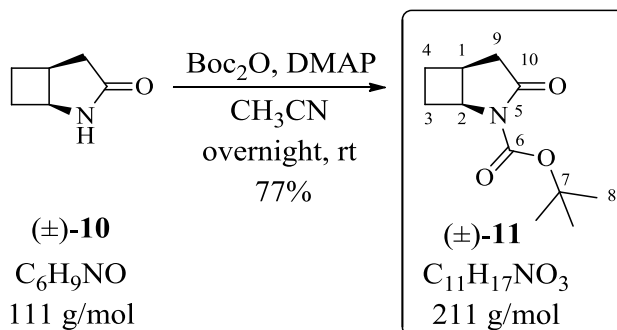


According to general procedure "II" azepinone **8** (30.00 mg, 0.275 mmol) was complexed with 1 equivalent of  $\beta$ -CD (0.32 g, 0.282 mmol) in 55 ml ultra-pure water 5 mM. The clear solution was then spread on glass sheet and left to dry in open air for 3 days. The film that forms was irradiated in a Rayonet for 5 hours. The irradiated solid was solved in ultra-pure water, reduced and then extracted with ethyl acetate (12 x 25 ml). The organic phase was dried over  $Na_2SO_4$  then concentrated under vacuum to obtain crude **10** (23.79 mg, 0.214 mmol). The crude product was of enough purity and no further purification was done. Spectral data were identical to those previously reported.

**Crude yield:** 78%.

**e.e** 41%.

**(±)-*cis*-*tert*-butyl-3-oxo-2-azabicyclo[3.2.0]heptane-2-carboxylate [(±)-11]**



DMAP (52.22 mg, 0.528 mmol, 0.1 eq.) and Boc<sub>2</sub>O (2.41g 11.05 mmol, 2 eq.) were added to a solution of compound (±)-10 (0.614 mg, 5.528 mmol) in acetonitrile (57 mL) at 0 ° C, under argon. The solution was stirred at 0 °C for 5 min and then left to stir over night, at room temperature. The solvent was then evaporated under reduced pressure and the crude product obtained was purified by flash chromatography on silica (gradient from 10/90 to 0/100 PE/Et<sub>2</sub>O). The product (±)-11 was obtained in the form of a white solid (0.853 g 4.042 mmol).

**Yield:** 77%.

**TLC R<sub>f</sub>** (EtOAc/EP 1/1): 0.72.

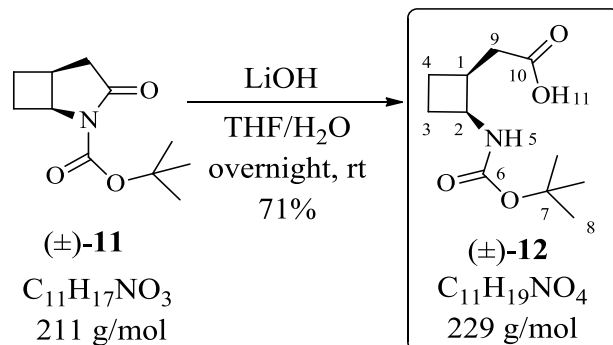
**<sup>1</sup>H NMR (250 MHz, CDCl<sub>3</sub>):** δ = 1.51 (s, 9H, H-8), 1.82-1.92 (m, 1H, H-4), 1.98-2.05 (m, 1H, H-3), 2.25-2.35 (m, 1H, H-4), 2.43 (dd, *J* = 1.8 Hz, *J* = 18.2 Hz, 1H, H-9), 2.43-2.53 (m, 1H, H-3), 2.68 (dd, *J* = 9.1 Hz, *J* = 17.7 Hz, 1H, H-9), 2.93-3.01 (m, 1H, H-1), 4.41-4.45 (m, 1H, H-2).

**<sup>13</sup>C NMR (60 MHz, CDCl<sub>3</sub>):** δ = 25.1 (C-4), 27.8 (C-3), 28.0 (C-8), 28.4 (C-1), 39.5 (C-9), 58.0 (C-2), 82.5 (C-7), 149.7 (C-6), 175.1 (C-10).

**MP:** 51 °C.

**HR-MS:** *m/z* calcd for [C<sub>11</sub>H<sub>17</sub>NO<sub>3</sub>+Na]<sup>+</sup> 234.1101; found 234.1096 (2.2 ppm).

**(±)-cis-2-(2-((*tert*-butoxycarbonyl)amino)cyclobutyl)acetic acid [(±)-12]**



LiOH (4.08g, 9.71 mmol, 10 eq.) was added to a solution of the compound (±)-11 (2.052 g, 9.72 mmol), in a 1/1 THF / H<sub>2</sub>O mixture (30 mL). The reaction mixture was left to stir overnight at room temperature. The THF was evaporated under reduced pressure. The residual aqueous phase was acidified with a solution of HCl (0.5 M) to pH = 1 and then saturated with solid NaCl. It was then extracted with AcOEt (5 x 30 mL). The combined organic phases were dried over MgSO<sub>4</sub>, filtered and concentrated under reduced pressure. The crude product was then purified by flash chromatography on silica (gradient from 50/50 to 0/100 PE/EtOAc). The *N*-Boc protected amino acid (±)-12 was obtained in the form of a white solid (1.58 g, 6.89 mmol).

**Yield:** 71%.

**TLC R<sub>f</sub>** (EP/EtOAc 1/1): 0.28

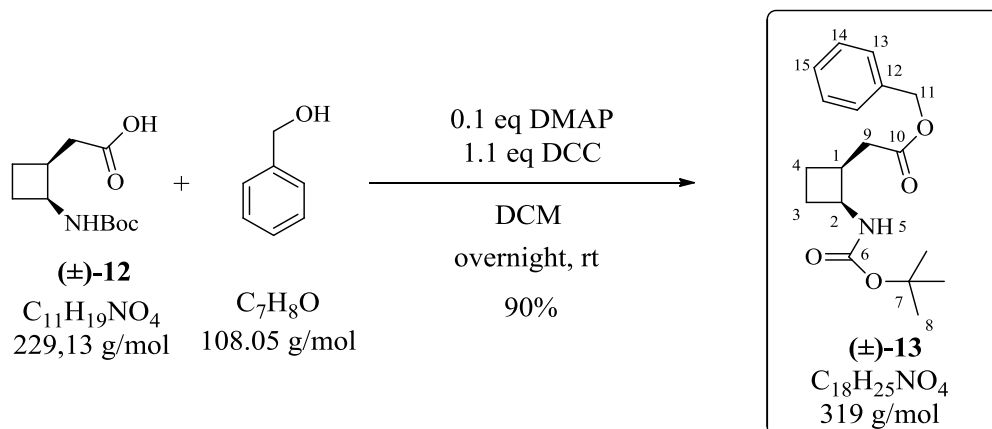
**<sup>1</sup>H NMR (250 MHz, CDCl<sub>3</sub>):** δ = 1.42 (s, 9H, H-8), 1.45-1.62 (m, 1H, H-4), 1.80-2.10 (m, 1H, H-3, 1H, H-4), 2.20-2.50 (m, 1H, H-3), 2.41 (dd, *J* = 15.8 Hz, *J* = 9.0 Hz, 1H, H-9), 2.55 (dd, *J* = 15.8 Hz, *J* = 6.8 Hz, 1H, H-9), 2.78-3.01 (m, 1H, H-1), 4.04-4.30 (m, 1H, H-2), 4.82 (bs, 0.6H, H-5), 6.07 (bs, 0.4H, H-5), 9.71 (bs, 1H, H-11).

**<sup>13</sup>C NMR (90 MHz, CDCl<sub>3</sub>):** δ = 21.2 (C-4), 27.2 (C-3), 28.3 (C-8), 34.2 (C-9), 36.7 (C-1), 46.8 (C-2), 79.4 (C-7), 155.2 (C-6), 177.7 (C-10).

**MP:**117 °C.

**HR-MS:** m/z calcd for [C<sub>11</sub>H<sub>19</sub>NO<sub>4</sub>+Na]<sup>+</sup> 252.1206 ; found 252.1212 (- 2.4 ppm).

**(±)-BenzylCis-2-(2-[[*tert*-butoxy)carbonyl]amino}cyclobutyl)acetate [(±)-13]**



To a stirring solution of amino acid (±)-7(400 mg, 17.46 mmol), and benzyl alcohol (0.185 ml, 1.02 eq.) in dichloromethane (26ml) was added DMAP (21.2 mg, 0.1 eq.). The reaction mixture was then cooled to 0 °C and DCC (400 mg, 1.1 eq.) was added. The reaction mixture was stirred for 10 min at 0 °C overnight at room temperature. The formed precipitate side product was removed by filtration, and the filtrate was concentrated under vacuum. The crude product was then purified by flash chromatography on silica (gradient from 90/10 to 70/30 PE/EtOAc) to obtain (±)-8 (490 mg, 1.53 mmol) as a white solid.

**Yield:** 90%.

**TLC R<sub>f</sub>** (PE/EtOAc 70/30): 0.85.

**<sup>1</sup>H NMR (360 MHz, CDCl<sub>3</sub>):**  $\delta$  = 1.42 (s, 9H, H-8), 1.49-1.57 (m, 1H, H-4), 1.81-1.91 (m, 1H, H-3), 1.95-2.03 (m, 1H, H-4), 2.24-2.37 (m, 1H, H-3), 2.45 (dd,  $J$  = 15.3 Hz,  $J$  = 9.4 Hz, 1H, H-9), 2.55 (dd,  $J$  = 15.3 Hz,  $J$  = 6.4 Hz, 1H, H-9), 2.85-3.02 (m, 1H, H-1), 4.28-4.33 (m, 1H, H-2), 4.82 (d,  $J$  = 6.3 Hz, 0.75H, H-5), 5.11 (s, 2H, H-11), 7.32-7.31 (m, 5H, H-Ar)

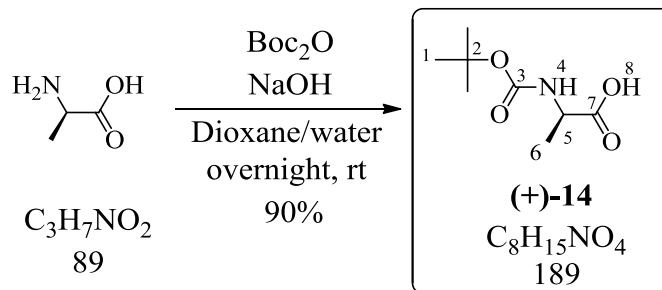
**<sup>13</sup>C NMR (90 MHz, CDCl<sub>3</sub>):** δ = 21.2 (C-4), 27.5 (C-3), 28.4 (C-8), 34.5 (C-9), 37 (C-1), 46.8 (C-2), 66.4 (C-11), 79.4 (C-7), 128.3, 128.7 (C-13, C-14, C-15), 136 (C-12), 155.2 (C-3), 172.8 (C-10).

**HR-MS:** m/z calcd for [C<sub>18</sub>H<sub>25</sub>NO<sub>4</sub>+Na]<sup>+</sup> 342.1683 ; found 342.1676 (2.2 ppm).

**(R,R) enantiomer:**  $[\alpha]_D^{22}$  (C = 0.5; CHCl<sub>3</sub>): 0.342

**(S,S) enantiomer:**  $[\alpha]_D^{22}$  (C = 0.5; CHCl<sub>3</sub>): -0.356

**(R)-2-((tert-butoxycarbonyl)amino)propanoic acid [(+)-14]**



To a solution of D-alanine (1.00 g, 11.2 mmol, 1 eq.) in ultrapure water (25 ml), at 0 °C, were added dropwise NaOH 1 M (22.5 ml) (24.5 mmol, 2 eq.) and a solution of Boc<sub>2</sub>O (3.60 g, 16.5 mmol, 1.5 eq.) in dioxane (25 ml). After the addition, the reaction mixture was left to stir overnight at room temperature. The dioxane was then evaporated under vacuum and the aqueous solution was cooled to 0 °C, and acidified with 1 M HCl to pH = 1. The aqueous layer was then extracted with ethyl acetate (4 x 50 ml) and the combined organic layers were washed with brine, dried over MgSO<sub>4</sub> and concentrated under vacuum to afford crude Boc-(R)-Ala-OH (+)-14 (1.90 g, 10.1 mmol) as white solid. The crude product was pure enough to be used in the next step without any purification.

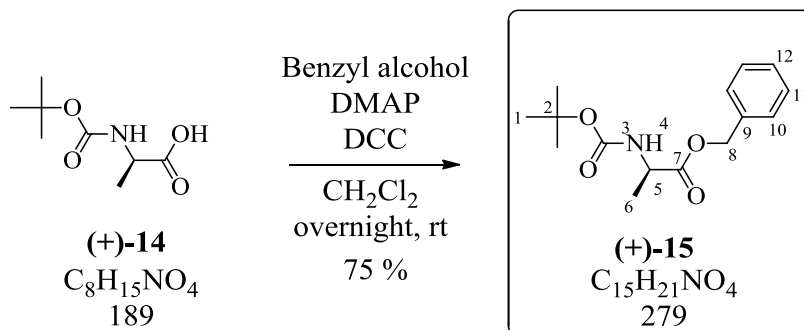
**Crude yield:** 90%

**TLC R<sub>f</sub>** (EtOAc): 0.44

**<sup>1</sup>H NMR (360 MHz, DMSO):** δ = 1.21 (d, *J* = 7.3 Hz, 3H, H-6), 1.37 (s, 9H, H-1), 3.91 (p, *J* = 7.4 Hz, 1H, H-5), 7.10 (d, *J* = 7.6 Hz, 1H, H-4).

**<sup>13</sup>C NMR (75 MHz, DMSO):** δ = 17.07 (C-6), 28.24 (C-1), 48.84 (C-5), 77.95 (C-2), 155.30 (C-3), 174.74 (C-7).

**(R)-benzyl 2-((tert-butoxycarbonyl)amino)propanoate [ (+)-15]**



To a solution of (+)-14 (600 mg, 3.17 mmol, 1eq.), benzyl alcohol (0.33 ml, 1.02 eq.) and DMAP (0.038 mg, 0.1 eq.) in DCM (15 ml) at 0 °C, was added DCC (0.719 g, 1.1eq.). The reaction mixture was warmed to room temperature and left to stir overnight. The solvent was then evaporated to dryness and the crude product was then purified by flash chromatography on silica (8/2 PE/EtOAc) to obtain Boc-(R)-Ala-OBn (+)-15 (663 mg, 2.37 mmol) as a colorless solid.

**Crude yield:** 75%

**TLC Rf** (PE/EtOAc 8/2): 0.44

**$^1H$  NMR (300 MHz,  $CDCl_3$ ):**  $\delta$  = 1.40 (d,  $J$  = 7.2 Hz, 3H, H-6), 1.44 (s, 9H, H-1), 4.32-4.42 (m, 1H, H-5), 5.07 (d, 1H, H-4), 5.15 (d,  $J$  = 12.3 Hz, 1H, H-6), 5.21 (d,  $J$  = 12.4 Hz, 1H, H-6), 7.32-7.46 (m, 5H, H-Ar).

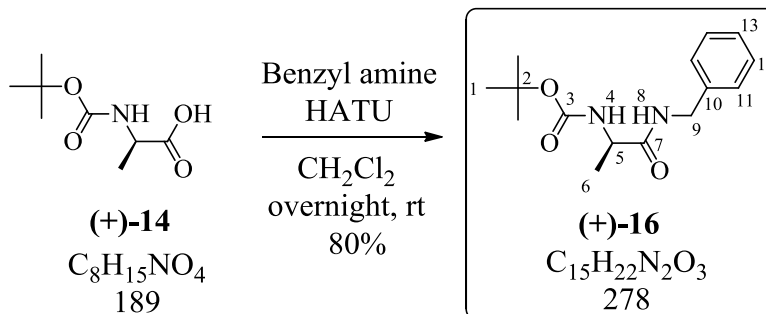
**$^{13}C$  NMR (75 MHz,  $CDCl_3$ ):**  $\delta$  = 18.60 (C-6), 28.27 (C-1), 49.25 (C-5), 66.95 (C-8), 79.81 (C-2), 128.11(C-9), 128.34, 128.56, 135.41(C-9, C-11, C-12), 155.06 (C-3), 173.19 (C-7).

**MP:** 24-25 °C.

**HR-MS:**  $m/z$  calcd for  $[C_{15}H_{21}NO_4+Na]^+$  302.1363 ; found 302.1356.

**$[\alpha]_D^{20}$**  = +13 (c. 0.5 in  $CHCl_3$ )

**(R)-tert-butyl (1-(benzylamino)-1-oxopropan-2-yl)carbamate [(+)-16]**



To a solution of (+)-14 (100 mg, 0.52 mmol, 1eq.), benzyl amine (14  $\mu$ l, 1.02 eq.) and DIPEA (275  $\mu$ l, 1.58 mmol, 3 eq.) in DCM (15 ml) was added HATU (0.72 g, mmol 1.05 eq.). The reaction mixture was stirred for 48 h and the solvent was then evaporated to dryness. Ethyl acetate was added to solubilized the solid products, and the organic layer was then successively washed with a saturated solution of bicarbonate (10 ml), brine, HCl 1M (10 ml), and then brine (10 ml). The organic layer was dried over  $MgSO_4$  then concentrated under vacuum. The crude product was purified by chromatography on flash silica (PE/EtOAc 8/2) to obtain Boc-(R)-Ala-NHBn (+)-16 (117 mg, 0.42 mmol) as a white solid.

**Yield:** 80%

**TLC Rf** (PE/EtOAc 1/3): 0.75

**$^1H$  NMR (360 MHz,  $CDCl_3$ )**  $\delta$ = 1.39 (d,  $J$  = 7.1 Hz, 3H, H-6), 1.41 (s, 9H, H-1), 4.16-4.32 (m, 1H, H-5), 4.44 (s, 2H, H-9), 5.16 (bs, 1H, H-4), 6.76 (bs, 1H, H-8), 7.42 – 7.19 (m, 5H, H-Ar).

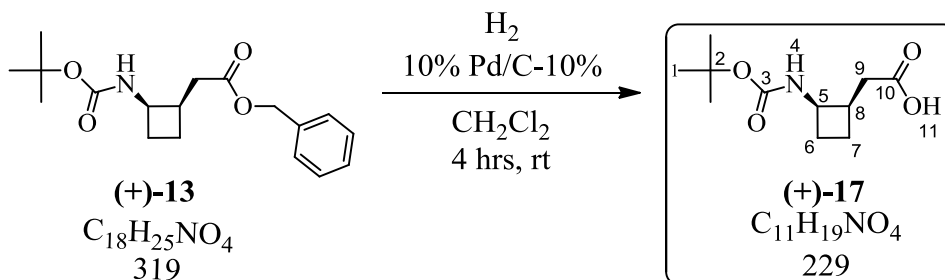
**$^{13}C$  NMR (90 MHz,  $CDCl_3$ ):**  $\delta$ = 18.371 (C-6), 28.27 (C-1), 43.35 (C-9), 50.13 (C-5), 80.13 (C-2), 127.43, 127.56, 128.66, (C-11, C-12, C-13), 138.10 (C-10), 155.59 (C-3), 172.63 (C-7).

**MP:** 104-106  $^{\circ}C$ .

**HR-MS:** m/z calcd for  $[C_{15}H_{22}N_2O_3+Na]^+$  301.1523 ; found 301.1520.

**$[\alpha]_D^{18}$**  = + 24 (c. 0.5 in  $CHCl_3$ )

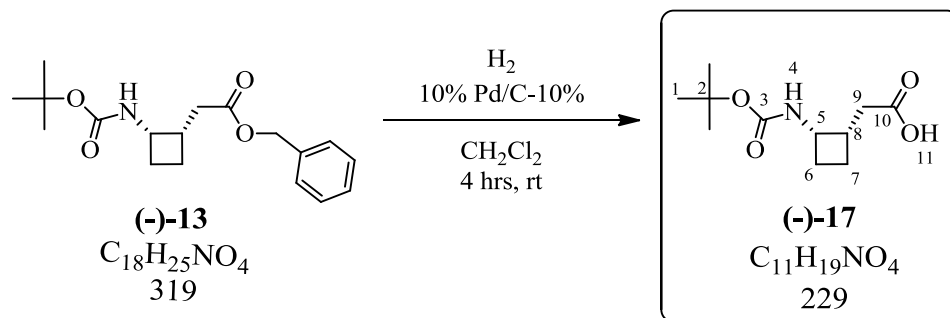
**2-((1*R*,2*R*)-2-((tert-butoxycarbonyl)amino)cyclobutyl)acetic acid [(+)-17]**



To a solution of Boc-(*R,R*)-*cis*-<sup>34</sup>GABA-OBn (+)-**13** (154 mg, 0.48 mmol) in 40 ml of 20/5 DCM/ethyl acetate was added 10% Pd-C (10% w/w) and the black suspension was stirred under dihydrogen atmosphere. When no starting material could be detected by TLC the reaction mixture was filtered (through a PVDF 0.45  $\mu$ m filter) and concentrated under reduced pressure to afford Boc-(*R,R*)-*cis*-<sup>34</sup>GABA-OH (+)-**17** in quantitative yields. The acid (+)-**17** was pure enough to be used in the coupling reactions without any purification.

The analysis is identical to that reported in literature<sup>102</sup>

**2-((1*S*,2*S*)-2-((tert-butoxycarbonyl)amino)cyclobutyl)acetic acid [(-)-17]**



Same procedure than for compound (+)-17

The analysis is identical to that reported in literature<sup>102</sup>

## General procedure “III” for the synthesis of the dipeptides (p1, p3, p5)

### Step one

In flask A, Boc-(*R*)-Ala-OBn, or (Boc-(*R*)-Ala-NHBn for peptide **p5**) (1eq.), was dissolved in dry DCM (4 ml), TFA (30 eq.) was then added, and the reaction mixture was stirred at room temperature. When no Boc-(*R*)-Ala-OBn starting material could be detected by TLC, the reaction was considered complete and the DCM was evaporated under reduced pressure. The excess TFA was co-evaporated with DCM several times, and then left under high vacuum for 2 h. the resulting crude TFA salt was then dissolved in dry DCM, and DIPEA (6 eq., sufficient quantity to reach PH 9) was added and the mixture was left to stir at room temperature.

### Step two

In flask B, Boc-*cis*-<sup>34</sup>GABA-OH (1eq.) was dissolved in a mixture of DCM/DMF (4/1), DIPEA (2 eq.) was then added followed by HATU (1.05 eq.) and the resulting mixture was stirred for 10 min at room temperature during which the color changes from light to dark brown.

### Step three

The content of flask A was then transferred to flask B and the resulting reaction mixture was stirred at room temperature for 24 h. The reaction mixture was concentrated under reduced pressure and toluene was added to co-evapourate DMF. The crude solid was dissolved in Ethyl acetate, or DCM (for **p5**), (50 ml) and successively washed by a saturated bicarbonate solution (20 ml), brine (20 ml), a 1 M HCl solution (20 ml), then brine (20 ml). The organic layer was dried over MgSO<sub>4</sub>, filtered, and concentrated under reduced pressure, and the resulting crude was purified accordingly.

### **General procedure “IV” for the hydrogenolysis of the benzyl ester protecting group**

To a solution of Boc-peptide-OBn in 25 ml DCM/Ethyl acetate (20/5), 10% Pd-C (10% w/w) (125 ml/mmol) was added and the black suspension was stirred under dihydrogen atmosphere; when no Boc-peptide-OBn starting material was detected by TLC the reaction was considered complete. The reaction mixture was filtered through a (PVDF 0.45  $\mu$ m filter), concentrated under reduced pressure to afford Boc-peptide-OH which was of sufficient purity to be used in the coupling reactions.

### **General procedure “V” for the synthesis of the tetrapeptides (p2, p4, p6)**

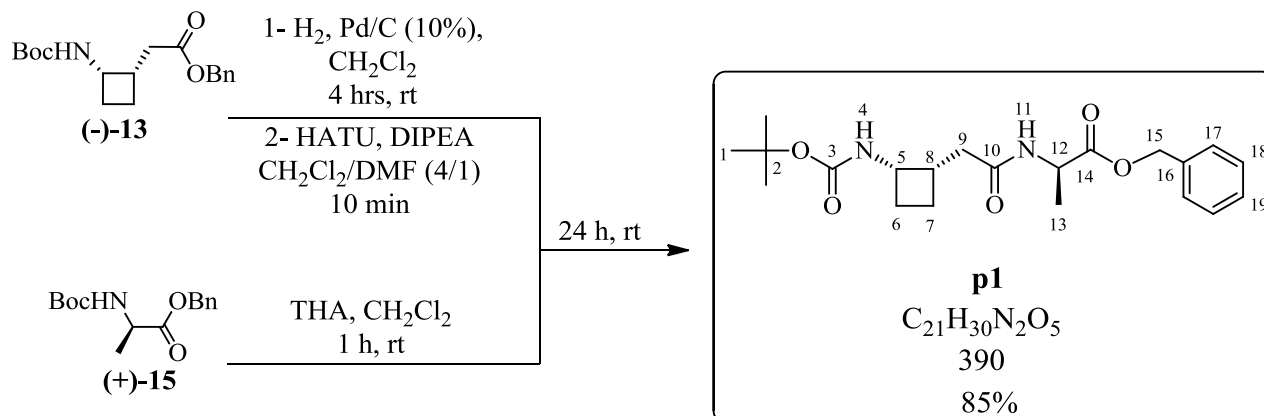
#### **Step one**

In flask A, Boc-peptide-O(or NH)Bn (1 eq.) was dissolved in dry DCM (2 ml), TFA (30 eq.) was then added, and the reaction mixture was stirred at room temperature. When no Boc-peptide-O(or NH)Bn starting material could be detected by TLC, the reaction was considered complete and the DCM was evaporated under reduced pressure. The excess TFA was co-evaporated with DCM several times, and then left under high vacuum for 2 h. the resulting crude TFA salt was then dissolved in dry DCM, and DIPEA (6 eq., sufficient quantity to reach PH 9) was added and the mixture was left to stir at room temperature.

#### **Step two**

In flask B, Boc-peptide-OH (1eq.) and DIPEA (2 eq.) was dissolved in a dry mixture of DCM/DMF (3/1). The content of flask A was then transferred into flask B, then HATU (1.05 eq.) was introduced to the reaction mixture, which was left to stir at room temperature for 24 h during which a precipitate forms. The solvent was removed under reduced pressure and the remaining DMF was co-evaporated with toluene. And the resulting crude was purified accordingly.

### Boc-(*S,S*)-GABA-(*R*)-Ala-OBn [p1]



Following the general procedure “III” dipeptide **p1** was prepared from Boc-(*S,S*)-*cis*-<sup>3,4</sup>GABA-OH (200 mg, 0.87 mmol), DIPEA (152  $\mu$ l, 2 eq.), HATU (348 mg, 1.05 eq.) in a mixture of DCM/DMF (4/1) (4 ml) and the corresponding TFA salt of Boc-(*R*)-Ala-OBn (243 mg, 0.87 mmol), DIPEA (0.91 ml, 6 eq.) in dry DCM (4 ml), overnight. After workup the resulting crude was purified by flash chromatography on silica (6/4 PE/EtOAc) to afford Boc-(*S,S*)-GABA-(*R*)-Ala-OBn **p1** as white solid (289 mg, 0.74 mmol).

**Yield:** 85%

**TLC Rf** (PE/EtOAc 3/2): 0.22

**<sup>1</sup>H NMR (360 MHz, CDCl<sub>3</sub>):**  $\delta$ = 1.41 (d,  $J$  = 7.3 Hz, 3H, H-13, overlapped with H-1) , 1.43 (s, 9H, H-1), 1.55-1.67 (m, 1H, H-7), 1.80-1.93 (m, 1H, H-6), 1.93-2.07 (m, 1H, H-7), 2.29 (dd,  $J$  = 8.0, 14.5 Hz, 1H, H-9), 2.33-2.40 (m, 1H, H-6, overlapped with H-9), 2.46 (dd,  $J$  = 6.8, 14.5 Hz, 1H, H-9), 2.80-2.91 (m, 1H, H-8), 4.20-4.35 (m, 1H, H-5), 4.63 (p,  $J$  = 7.2 Hz, 1H, H-12), 5.15 (d,  $J$  = 12.3 Hz, 1H, H-15), 5.21 (d,  $J$  = 12.3 Hz, 1H, H-15), 5.32 (bs, 1H, H-4), 6.29 (bs, 1H, H-11), 7.30-7.41 (m, 1H, H-Ar),

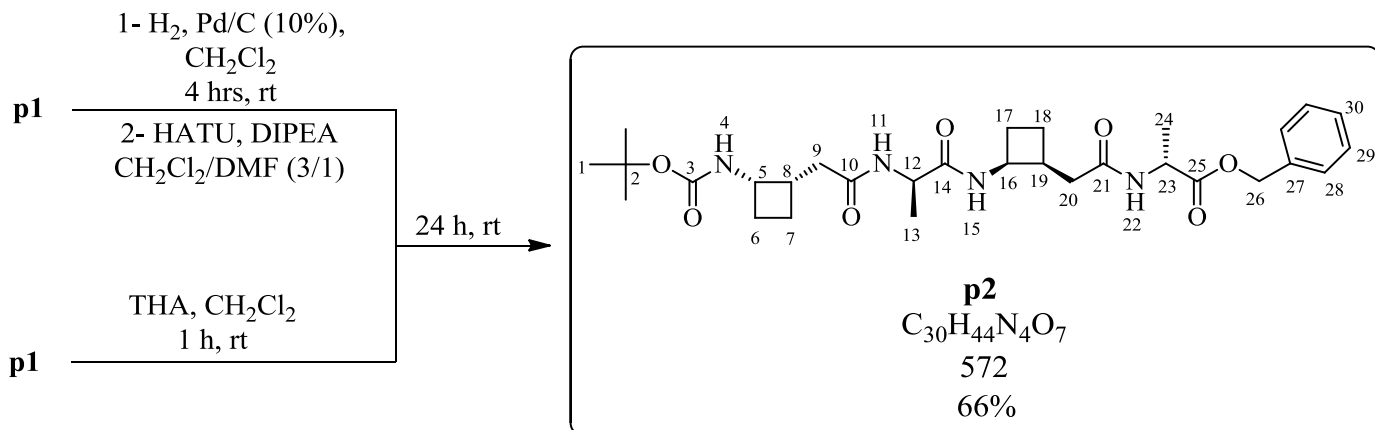
**<sup>13</sup>C NMR (90 MHz, CDCl<sub>3</sub>):**  $\delta$ = 18.3 (C-13), 21.4 (C-7), 27.5 (C-6), 28.3 (C-1), 36.4 (C-9), 37.4 (C-8), 47.3 (C-5), 48.1 (C-12), 67.1 (C-15), 79.3 (C-2), 128.1, 128.4, 128.6, (C-17, C-18, C-19), 135.2 (C-16), 155.4 (C-3), 171.9 (C-10), 172.9 (C-14).

**MP:** 155-157 °C.

**HR-MS:** m/z calcd for  $[\text{C}_{21}\text{H}_{30}\text{N}_2\text{O}_5+\text{Na}]^+$  413.2047 ; found 413.2032

$[\alpha]_D^{25} = +49.6$  (c. 0.23 in MeOH)

## Boc-[(S,S)-GABA-(R)-Ala]<sub>2</sub>-OBn [p2]



Following the general procedure “IV” the benzyl ester of dipeptide **p1** (86 mg, 0.22 mmol) was hydrolysed in 4 h to afford Boc-(S,S)-GABA-(R)-Ala-OH (65 mg, 0.21 mmol) (crude yield 95%)

Following the general procedure “V” peptide **p2** was prepared from Boc-(S,S)-GABA-(R)-Ala-OH (44.60 mg, 0.15 mmol, 1eq.), DIPEA (50 µl, 2 eq.), HATU (60 mg, 1.05 eq.) in a mixture of DCM/DMF (3/1) (2 ml) and the corresponding TFA salt of Boc-(S,S)-GABA-(R)-Ala-OBn (58.0 mg, 0.15 mmol), DIPEA (0.155 ml, 6 eq.) in dry DCM (2 ml), over 24 h. The resulting yellowish crude solid dissolved in DCM (25 ml) and successively washed with a saturated bicarbonate solution (10 ml), brine (10 ml), a 1 M HCl solution (10 ml), then brine (10 ml). The organic layer was dried over MgSO<sub>4</sub>, filtered, and concentrated under reduced pressure. The resulting crude was purified by flash chromatography over silica (gradient eluent of 100/1 to 100/4 DCM/MeOH) to afford Boc-[(S,S)-GABA-(R)-Ala]<sub>2</sub>-OBn **p2** as white solid (57.20 mg, 0.1 mmol).

**Yield:** 66%

**TLC Rf:** (DCM/MeOH / 100/ 4): 0.7

**<sup>1</sup>H NMR (400 MHz, CDCl<sub>3</sub>):** δ= 1.37 (d, *J* = 7.1 Hz, 3H, H-13), 1.43 (s, 9H, H-1), 1.45 (d, *J* = 7.5 Hz, 1H, H-24), 1.68 – 1.57 (m, 1H, H-7), 1.91 – 1.80 (m, 1H, H-6), 2.07 – 1.92 (m, 3H, 1H,

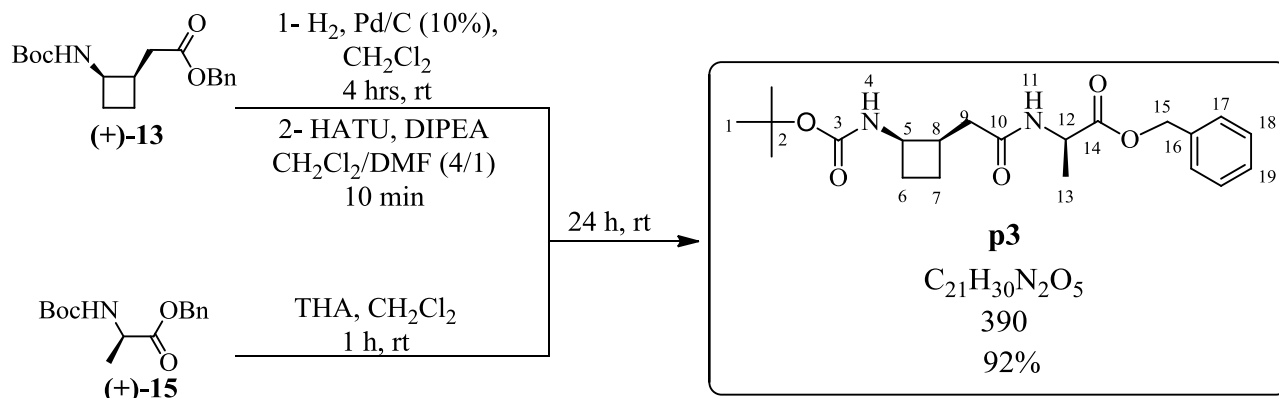
H-7; 1H, H-17; 1H, H-18), 2.41 – 2.12 (m, 6H, 1 H, H-18; 2H, H-20, 1H, H-9; 1H, H-17; 1H, H-6), 2.48 (dd,  $J = 7.6, 14.3$  Hz, 1H, H-9), 2.94 – 2.78 (m, 2H, 1H, H-19; 1H, H-8), 4.33 – 4.18 (m, 2H, 1H, H-5; 1H, H-12), 4.53 (p,  $J = 8.5$  Hz, 1H, H-16), 4.65 (p,  $J = 7.4$  Hz, 1H, H-23), 5.18 (d,  $J = 12.3$  Hz, 1H, H-26), 5.24 (d,  $J = 12.4$  Hz, 1H, H-26), 5.57 (d,  $J = 4.5$  Hz, 1H, H-4), 6.59 (d,  $J = 6.9$  Hz, 1H, H-11), 7.42 – 7.31 (m, 2H, H-Ar), 7.80 (d,  $J = 7.4$  Hz, 1H, H-15), 7.91 (d,  $J = 7.1$  Hz, 1H, H-22).

**$^{13}\text{C}$  NMR (100 MHz,  $\text{CDCl}_3$ ):**  $\delta =$  16.95 (C-24), 17.53 (C-13), 19.81 (C-17 or 18), 21.33 (C-7), 26.68 (C-18 or 17), 27.43 (C-6), 28.41 (C-1), 35.27 (C-20), 36.40 (C-9), 37.65 (C-8 or 19), 37.82 (C-19 or 8), 46.75 (C-16), 47.38 (C-5), 48.15 (C-23), 49.49 (C-12), 67.34 (C-26), 79.33 (C-2), 128.03, 128.41, 128.61 (C-28, 29, 30), 135.25 (C-27), 155.52 (C-3), 172.38 (C-14), 173.07 (C-21), 173.22 (C-10), 175.31 (C-25).

**MP:** 195-197 °C.

**HR-MS:**  $m/z$  calcd for  $[\text{C}_{30}\text{H}_{44}\text{N}_4\text{O}_7+\text{Na}]^+$  595.3102 ; found 595.3095

$[\alpha]_D^{25.3} = -72.76$  (c. 0.5 in  $\text{CHCl}_3$ )

**Boc-(R,R)-GABA-(R)-Ala-OBn [p3]**

Following the general procedure “III” dipeptide **p3** was prepared from Boc-(R,R)-cis-<sup>3,4</sup>GABA-OH (97.0 mg, 0.42 mmol), DIPEA (150  $\mu$ l, 2 eq.), HATU (169 mg, 1.05 eq.) in a mixture of DCM/DMF (4/1) (2 ml) and the corresponding TFA salt of Boc-(R)-Ala-OBn (118 mg, 0.42 mmol), DIPEA (0.45 ml, 6 eq.) in dry DCM (24 ml), overnight. After workup the resulting crude product was purified by flash chromatography on silica (6/4 PE/EtoAc) to afford Boc-(R,R)-GABA-(R)-Ala-OBn **p3** as a white solid (152 mg, 0.39 mmol).

**Yield:** 92%

**TLC Rf** (PE/EtOAc 3/2): 0.22

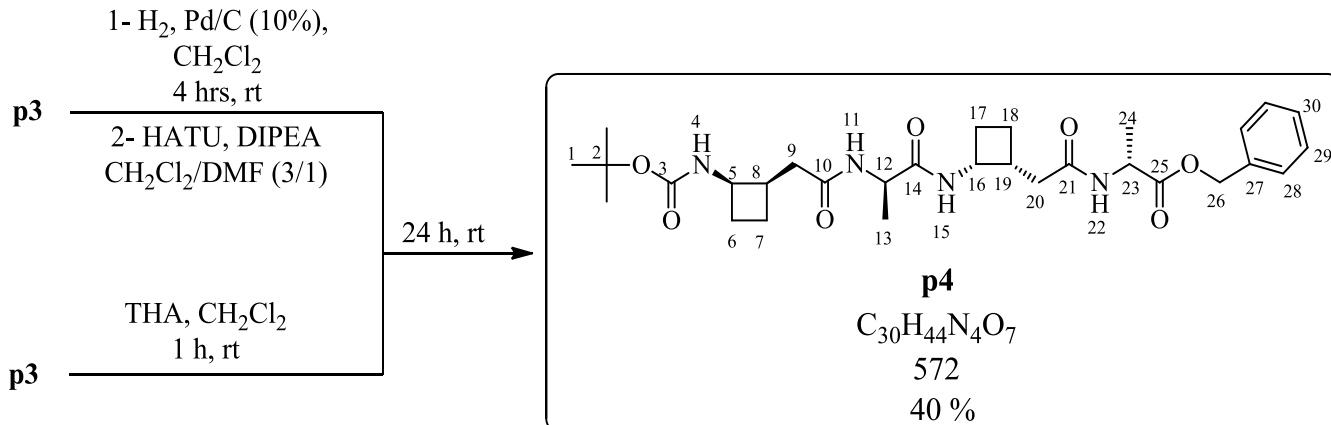
**<sup>1</sup>H NMR (360 MHz, CDCl<sub>3</sub>):**  $\delta$  = 1.42 (d,  $J$  = 7.4 Hz, 3H, H-13), 1.44 (s, 9H, H-1), 1.54-1.66 (m, 1H, H-7), 1.79-1.91 (m, 1H, H-6), 1.92-2.05 (m, 1H, H-7), 2.27 (dd,  $J$  = 14.6, 7.6 Hz, 1H, H-9), 2.27-2.38 (m, 1H, H-6), 2.47 (dd,  $J$  = 14.6, 7.1 Hz, 1H, H-9), 2.77-2.90 (m, 1H, H-8), 4.18-4.33 (m, 1H, H-5), 4.62 (p,  $J$  = 7.3 Hz, 1H, H-12), 5.15 (d,  $J$  = 12.3 Hz, 1H, H-15), 5.21 (d,  $J$  = 12.2 Hz, 1H, H-15), 5.22 (m, 1H, H-4), 6.36 (bs, 1H, H-11), 7.31-7.42 (m, 5H, H-Ar).

**<sup>13</sup>C NMR (90 MHz, CDCl<sub>3</sub>):**  $\delta$  = 18.1 (C-13), 21.7 (C-7), 27.4 (C-6), 28.3 (C-1), 36.4 (C-9), 37.3 (C-8), 47.4 (C-5), 48.1 (C-12), 67.0 (C-15), 79.3 (C-2), 128.1, 128.4, 128.5, (C-17, C-18, C-19), 135.3 (C-16), 155.5 (C-3), 171.9 (C-10), 172.8 (C-14).

**MP:** 145-146 °C.

**HR-MS:** m/z calcd for  $[\text{C}_{21}\text{H}_{30}\text{N}_2\text{O}_5+\text{Na}]^+$  413.2047 ; found 413.2039

$[\alpha]_D^{25} = + 51$  (c. 0.5 in  $\text{CHCl}_3$ )

**Boc-[(R,R)-GABA-(R)-Ala]<sub>2</sub>-OBn [p4]**

Following the general procedure “IV” the benzyl ester of dipeptide **p3** (80 mg, 0.20 mmol) was hydrolysed in 4 h to afford Boc-(R,R)-GABA-(R)-Ala-OH (60 mg, 0.20 mmol) (crude yield 100%)

Following the general procedure “V” peptide **p4** was prepared from Boc-(R,R)-GABA-(R)-Ala-OH (34.0 mg, 0.11 mmol, 1eq.), DIPEA (40 µl, 2 eq.), HATU (45 mg, 1.05 eq.) in a mixture of DCM/DMF (3/1) (2 ml) and the corresponding TFA salt of Boc-(R,R)-GABA-(R)-Ala-OBn (44.1 mg, 0.11 mmol), DIPEA (0.118 ml, 6 eq.) in dry DCM (2 ml), over 24 h. The resulting yellowish crude solid was washed with water and filtered on a sintered glass funnel (size 4), the residue was washed with ether, dried under vacuum then purified by flash chromatography over silica (gradient eluent of 100/1 to 100/4 DCM/MeOH) to afford Boc-[(R,R)-GABA-(R)-Ala]<sub>2</sub>-OBn as white solid (25.2 mg, 0.044 mmol).

**Yield:** 40%

**TLC Rf** (DCM/MeOH 100/4): 0.7

**<sup>1</sup>H NMR (400 MHz, CDCl<sub>3</sub>):** δ= 1.36 (d, *J* = 6.7 Hz, 3H, H-13) ,1.42 (d, *J* = 7.1 Hz, 3H, H-24 covered by H-1), 1.43 (s, 9H, H-1), 1.53-1.70 (m, 2H, 1H, H-7; 1H, H-18), 1.78-1.94 (m, 1H, H-6), 1.94-2.12 (m, 3H, 1H, H-7; 1H, H-17; 1H, H-18 ), 2.21-2.41 (m, 4H, 1H, H-9; 1H, H-6; 1H, H-17; 1H, H-20), 2.41-2.57 (m, 2H, 1H, H-20; 1H, H-9), 2.82-3.01 (m, 2H, 1H, H-8; 1H,

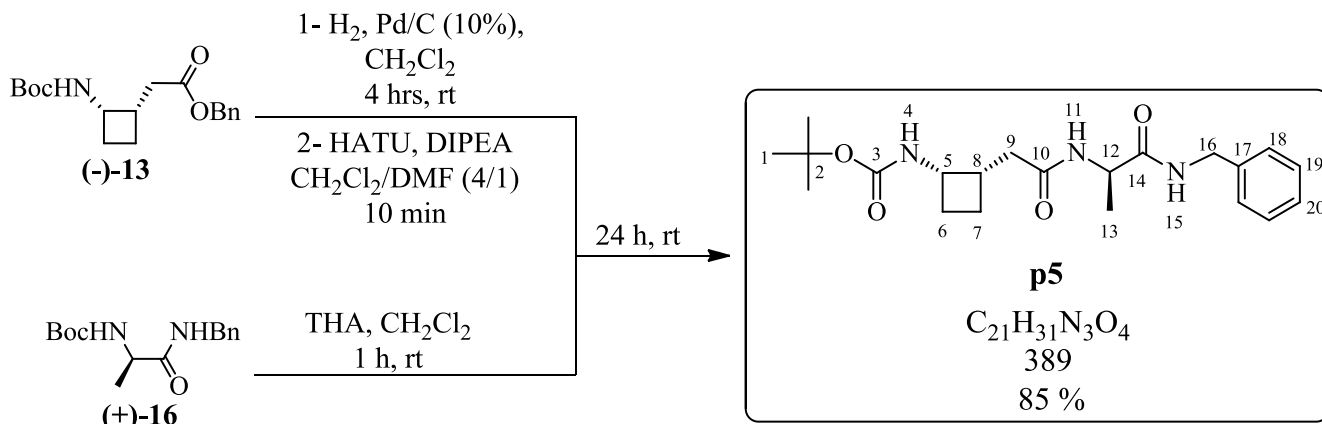
H-19) 4.15-4.34 (m, 1H, H-5), 4.34-4.52 (m, 2H, 1H, H-12; 1H, H-16), 4.55-4.69 (m, 1H, H-23), 5.15 (d,  $J = 12.4$  Hz, 1H, H-26), 5.21 (d,  $J = 12.4$  Hz, 1H, H-26), 5.29 (d,  $J = 5.6$  Hz, 1H, H-4), 6.37 (d,  $J = 12.0$  Hz, 1H, H-211), 6.81 (d,  $J = 12.4$  Hz, 1H, H-22), 7.30-7.42 (m, 5H, H-Ar), 7.65 (d,  $J = 11.2$  Hz, 1H, H-15).

**$^{13}\text{C}$  NMR (100 MHz,  $\text{CDCl}_3$ ):**  $\delta = 17.8$  (C-24), 18.48 (C-13), 22.1 (C-7 and 18), 27.0 (C-17), 27.3 (C-6), 28.3 (C-1), 36.6 (C-9, or 20), 36.8 (C-9, or 20), 37.1 (C-8, or 19), 37.3 (C-19 or 8), 46.8 (C-16), 47.7 (C-5), 48.2 (C-23), 49.3 (C-12), 67.1 (C-26), 79.4 (C-2), 128.15, 128.4, 128.6 (C-28, C-29, C-30), 135.3 (C-27), 155.6 (C-3), 172.0 (C-14), 172.3 (C-10 or 21), 172.4 (C-21, or 10), 173.1 (C-25).

**MP:** 204-207 °C.

**HR-MS:**  $m/z$  calcd for  $[\text{C}_{30}\text{H}_{44}\text{N}_4\text{O}_7+\text{Na}]^+$  595.3102 ; found 595.3079

$[\alpha]_D^{25} = -35$  (c. 0.5 in  $\text{CHCl}_3$ )

**Boc-(S,S)-GABA-(R)-Ala-NHBn [p5]**

Following the general procedure “III” dipeptide **p5** was prepared from Boc-(S,S)-*cis*-<sup>3,4</sup>GABA-OH (50.0 mg, 0.22 mmol), DIPEA (75  $\mu$ l, 2 eq.), HATU (87 mg, 1.05 eq.) in a mixture of DCM/DMF (4/1) (2 ml), and the corresponding TFA salt of Boc-(R)-Ala-NHBn (60.7 mg, 0.22 mmol), DIPEA (0.23 ml, 6 eq.) in dry DCM (24 ml), overnight. After workup the resulting crude was purified by flash chromatography over silica (1/3 PE/EtOAc) to obtain Boc-(S,S)-GABA-(R)-Ala-NHBn **p5** as white solid (72.2 mg, 0.18 mmol).

**Yield:** 82%

**TLC Rf** (PE/EtOAc 1/3): 0.53

**<sup>1</sup>H NMR (400 MHz, CDCl<sub>3</sub>):**  $\delta$ = 1.40 (d,  $J$  = 7.0 Hz, 1H, H-13), 1.43 (s, 2H, H-1), 1.51-1.62 (m, 1H, H-7) 1.78-1.90 (m, 1H, H-6), 1.90-2.03 (m, 1H, H-7), 2.24 (dd,  $J$  = 7.7, 14.5Hz, 1H, H-9), 2.28 -2.39 (m, 1H, H-6, overlapped with H-9), 2.45 (dd,  $J$  = 7.1, 14.5Hz, 1H, H-9), 2.76-2.87 (m, 1H, H-8), 4.18-4.30 (m, 1H, H-5), 4.41 (d,  $J$  = 6.8 Hz, 1H, H-16), 4.44 (d,  $J$  = 7.0 Hz, 1H, H-16), 4.50 (p,  $J$  = 7.1 Hz, 1H, H-12), 5.19 (s, 1H, H-4), 6.44 (d,  $J$  = 6.4 Hz, 1H, H-11), 6.71 (s, 1H, H-15), 7.22-7.35 (m, 1H, H-Ar).

**<sup>13</sup>C NMR (63 MHz, CDCl<sub>3</sub>):** δ= 18.06 (C-13), 21.72 (C-7), 27.37 (C-6), 28.37 (C-1), 36.48 (C-9), 37.41 (C-8), 43.49 (C-16), 47.55 (C-5), 48.87 (C-12), 127.46, 127.58, 128.67 (C-18, 19, 20), 137.99 (C-17), 155.55 (C-3), 172.13 (C-10 or 14), 172.35 (C-14, or 10).

**MP:** 196-197 °C.

**HR-MS:** m/z calcd for [C<sub>21</sub>H<sub>31</sub>N<sub>3</sub>O<sub>4</sub>+Na]<sup>+</sup> 412.2207 ; found 412.2201

**[α]<sub>D</sub><sup>26</sup>** = - 7.7 (c. 0.5 in CHCl<sub>3</sub>)



# Index

## A- Determination of the binding constant $K_b$ for a 1:1 complex

The equilibrium constant,  $K$ , for a complex formation between a host (H) and a guest (G) can be formulated from the general equilibrium reaction:



when the stoichiometry of the formed  $\beta$ -cyclodextrin/ guest complex is 1:1, the desired equilibrium or binding constant  $K_b$  is given by:

$$K_b = \frac{[HG]}{[H][G]} \quad (1)$$

Where  $[G]$  is the concentration of free guest,  $[H]$  is the concentration of free host, i.e. ( $\beta$ -CD), and  $[HG]$  the concentration of the formed host/guest complex.

Because the complexation process is a dynamic equilibrium, the individual concentration of each species is not readily measurable. Instead of measuring separate concentrations, a well-known approach to determine the molecular binding constant, is to generate the binding curve and then to extract  $K$  via a regression analysis.<sup>65</sup>

To apply this approach, we need to define the total guest concentration  $[H]_t$ , which is always equal to the concentration of the host in the free form added to the concentration of the Host in the bound form, equation (2):

$$[H]_t = [H] + [HG] \quad (2)$$

In addition, we have the expression that indicates the fraction of the host that is bound  $X_b$ , which is the concentration of the bound host at a given time divided by the total concentration of the host at that time:

$$X_b = \frac{[HG]}{[H]_t} \quad (3)$$

Substituting equations (2) and (3) in equation (1) and rearranging for  $X_b$ , we obtain equation (4) which is known as the binding isotherm:<sup>66</sup>

$$X_b = \frac{K[G]}{1+K[G]} \quad (4)$$

In order for equation (4) to be useful,  $X_b$  needs to be described in terms of a measurable property whose magnitude varies as a function of the amount of Host bound, i.e. complex formation.<sup>65</sup>

One of the most common properties whose variation could be studied as a function complex formation is the NMR shift of specific protons located on the host or the guest molecules.

So we first need to relate  $X_b$  to the chemical shift variation of a specific proton on the host or the guest. To be able to establish such a relation one should be aware that the rates of complex formation and dissociation are usually faster than the NMR time scale, and the observed signals are actually an average between the chemical shifts in the free and the bound form of the host and the guest molecules.<sup>29</sup>

Thus if  $\delta_H$  is the chemical shift of the monitored proton in the free state, and  $\delta_{HG}$  is the chemical shift of the same proton in the bound state, then the observed chemical shift,  $\delta_{obs}$ , is given by:<sup>66</sup>

$$\delta_{obs} = X_f\delta_H + X_b\delta_{HG} \quad (5)$$

In equation (5)  $X_f$  and  $X_b$  represent the fraction of the host in the free and bound form respectively. Now since  $X_f + X_b = 1$  equation (5) could be written as

$$\delta_{obs} = X_b(\delta_{HG} - \delta_H) + \delta_H \quad (6)$$

Rearranging equation 6 for  $X_b$  we obtain equation (6')

$$X_b = \frac{\delta_{\text{obs}} - \delta_H}{\delta_{\text{HG}} - \delta_H} \quad (6')$$

The expression  $\delta_{\text{obs}} - \delta_H$  represents the variation in the chemical shift of the monitored proton  $\Delta\delta$ , and the  $\delta_{\text{HG}} - \delta_H$  represents the maximum change in chemical shift which is attained at saturation  $\Delta\delta_{\text{sat}}$ . using this notation equation 6' becomes:

$$X_b = \frac{\Delta\delta}{\Delta\delta_{\text{sat}}} \quad (6'')$$

Substituting equation 6'' into equation 4 we get:

$$\Delta\delta = \frac{\Delta\delta_{\text{sat}} K [G]}{1 + K[G]} \quad (7)$$

The reciprocal of equation 7 gives:

$$\frac{1}{\Delta\delta} = \frac{1}{\Delta\delta_{\text{sat}} K [G]} + \frac{1}{\Delta\delta_{\text{sat}}} \quad (8)$$

A plot of  $1/\Delta\delta$  vs  $[G]$  establishes a straight line whose slop is directly related to the value of  $K$  (see Figure 88).

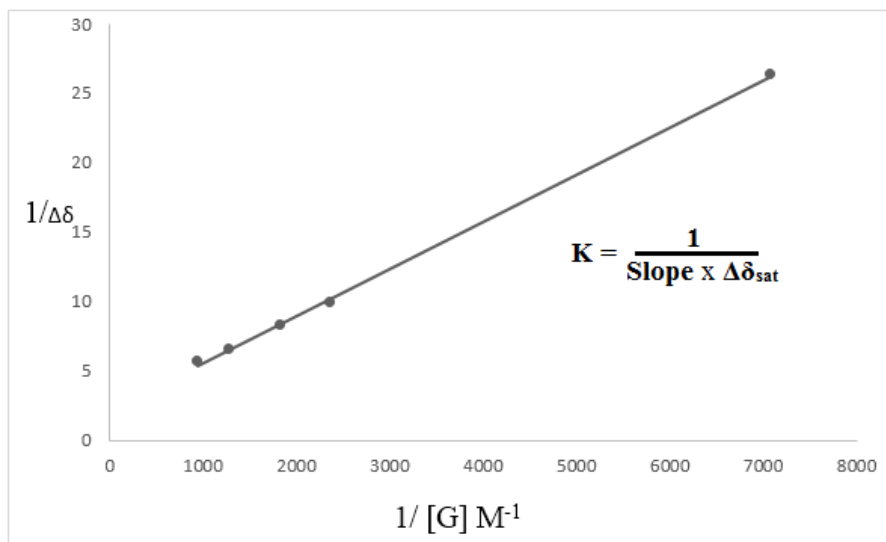


*Figure 88: A plot of  $1/\Delta\delta$  vs  $[G]$ .*

**B-** In a subsequent control reaction, we observed that up to half the amount of cyclobutene product ( $\pm$ )-**9** was lost when an equimolar solution of this compound and  $\beta$ -CD in water was lyophilized for 3 days.

## Summary in French (Résumé français)

# Nouvelles Transformations Enantioselective Induites par une Cyclodextrine: Applications pour la Preparation de Blocs de Construction Moléculaire d' Intérêt Biologique

Thèse de doctorat de l'Université Libanaise et de l'Université Paris-Saclay, préparée à  
l'Université Paris Sud

École doctorale n°571 sciences chimiques : molécules, matériaux, instrumentation  
et biosystèmes (2MIB)

Ecole doctorale des sciences et technologie de l'Université Libanaise (EDST)

Spécialité de doctorat: Chimie

Thèse présentée et soutenue à Beyrouth, le 5 Juil 2018, par

**M. Ali Taher Mansour**

## Introduction

La majorité des molécules naturelles et biologiquement actives ont une configuration bien définie en lien avec leur fonction moléculaire. Il est étonnant de voir comment les organismes vivants ont la capacité de choisir ou de biosynthétiser de manière sélective un seul énantiomère d'une molécule donnée. Les chimistes cherchent depuis toujours à imiter les systèmes biologiques; ainsi, la *synthèse asymétrique* de composés organiques est devenue un terrain de prédilection pour la recherche. La préparation énantiosélective de molécules revêt également

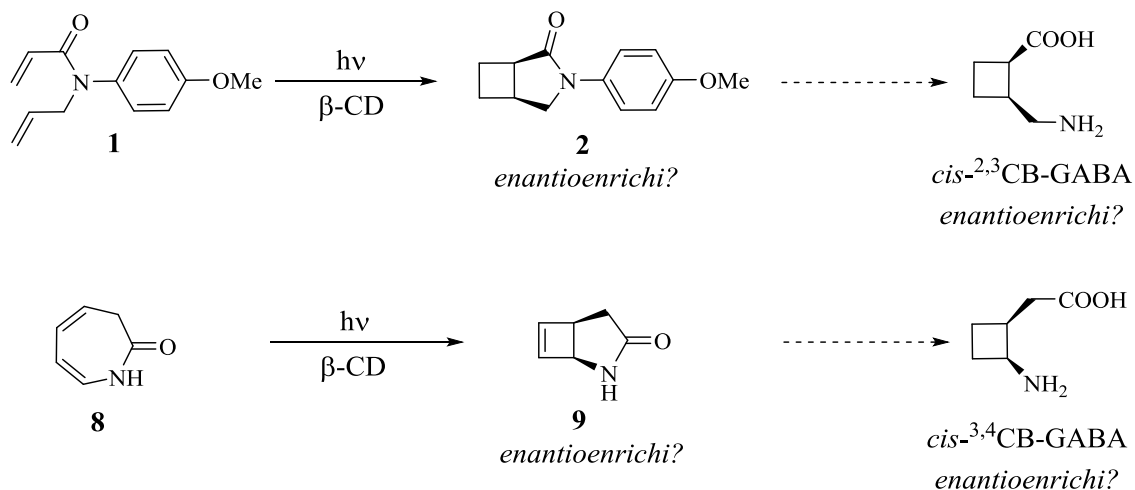
une importance industrielle, en raison du besoin de molécules stéréochimiquement pures dans le domaine de la médecine et de la science des matériaux.

Au cours des dernières décennies, la synthèse asymétrique de composés organiques a été traditionnellement réalisée par des transformations catalytiques ou enzymatiques, et un large éventail de méthodes a été développé pour obtenir un contrôle stéréochimique sur diverses transformations chimiques. La photochimie s'est révélée être un outil polyvalent en synthèse organique et fait l'objet d'une attention encore plus grande aujourd'hui, car elle est considérée comme une méthode de préparation de nouveaux matériaux dans un contexte «respectueux de l'environnement», appelé chimie verte. Néanmoins, les transformations photochimiques asymétriques ne sont pas très largement étudiées. Le terme «photochirogénèse» est assez récent. Elle a été inventée en 1996 et est conceptuellement synonyme de «photochimie asymétrique» ou «photochimie chirale», l'accent étant mis sur la création d'une chiralité moléculaire via l'utilisation d'un photon.

La recherche en matière de photochirogénèse a fait de grands progrès quantitatifs et qualitatifs grâce aux nouvelles méthodologies développées pour contrôler les processus impliqués. Il est essentiel pour obtenir un contrôle stéréochimique d'une réaction photochimique, de s'assurer que la molécule «substrat» réside déjà dans un environnement chiral pendant l'étape d'excitation. À cet égard, la photochirogénèse peut être facilement divisée en deux catégories principales. Le premier comprend les réactions dans lesquelles la chiralité est transférée à une molécule réactive par la présence d'un substituant chiral, lié de manière covalente ou ionique au réactif. Avec une telle approche, la chiralité peut être induite par l'interaction intramoléculaire entre le centre chiral, agissant comme un «auxiliaire chiral», et le fragment réactif. La deuxième catégorie, la photochirogénèse supramoléculaire, peut être décrite comme une interaction hôte-invité entre le réactif, en tant qu'invité, et une molécule hôte qui fournit un environnement chiral pour que la réaction photochimique se déroule de manière asymétrique. Ici, la chiralité est transférée d'une molécule à une autre par le biais d'interactions intermoléculaires entre le substrat et une molécule voisine possédant certaines propriétés chirales.

## L'objectif de ce travail

Dans ce travail, nous avons cherché à explorer la possibilité d'utiliser la photochimie supramoléculaire asymétrique comme stratégie de synthèse alternative pouvant fournir un accès plus rapide et / ou plus efficace au *cis*-<sup>2,3</sup>CB-GABA et au *cis*-<sup>3,4</sup>CB-GABA sous une forme énantiomériquement pure. Nous envisagions ensuite d'utiliser ces molécules comme éléments de base pour la préparation de nouvelles séquences de peptides mixtes et d'étudier le comportement de repliement en trois dimensions de ces peptides. Nous avons envisagé la synthèse énantiosélective des dérivés du *cis*-<sup>2,3</sup>CB-GABA et de *cis*-<sup>3,4</sup>CB-GABA. L'avantage évident de cette approche énantiosélective étant d'éviter l'utilisation d'un auxiliaire chiral pour effectuer la résolution des composés racémiques. Pour atteindre cet objectif, afin de contribuer à la croissance de la photochirogène, nous avons décidé d'étudier l'utilisation de la  $\beta$ -cyclodextrine ( $\beta$ -D) en tant qu'hôte supramoléculaire chiral, facilement disponible pour les transformations photochimiques énantiosélectives (Schéma a). La cycloaddition intramoléculaire [2 + 2] photochimique du *N*-allyl-*N*-arylacrylamide **1** en présence de  $\beta$ -CD pourrait donner accès à un adduit bicyclique **2** sous forme énatio-enrichie précurseur du *cis*-<sup>2,3</sup>CB-GABA. D'autre part, La  $4\pi$ -électrocyclisation photochimique de l'azépinone **8** en présence de  $\beta$ -CD pourrait donner accès au produit bicyclique **9** sous forme énatio-enrichie, pouvant conduire au *cis*-<sup>3,4</sup>CB-GABA.



Scheme a: Réactions photochirogéniques proposées en présence de  $\beta$ -CD, pouvant conduire au *cis*-<sup>2,3</sup>CB-GABA (en haut) et au *cis*-<sup>3,4</sup>CB-GABA (en bas) énantiorenrichis

## La réactivité photochimique du *N*-Allyl-*N*-(4-méthoxyphényl)acrylamide.

Nous avons commencé ce projet en étudiant la réactivité photochimique du *N*-allyl-*N*-(4-méthoxyphényl) acrylamide **1**. Les chimistes organiciens sont constamment à la recherche de nouvelles méthodologies pour la synthèse de composés d'importance biologique tels que les dérivés du *N*-allylacrylamide. Ces dérivés ont déjà été préparés pour la construction de composés hétérocycliques à stéréocentres multiples, présentant un intérêt en tant que médicaments ou réactifs bioactifs, par réactions de métathèse à cycle fermé régiosélectives (RCM) ou par réactions de cyclisation tandem catalysées par le palladium. Les réactions de cycloaddition photochimiques énantiosélectives de dérivés de *N*-allylacrylamide n'ont pas encore été étudiées, mais pourraient constituer une méthode de synthèse «verte» pour la préparation de composés hétérocycliques. Les lactames bicycliques, tels que l'intermédiaire particulier **2** que nous ciblons ci-dessous, présentent un intérêt synthétique considérable à cet égard

Nous avons donc entrepris d'établir un nouvel accès synthétique au dérivé *cis*-<sup>2,3</sup>CB-GABA, sur la base de la cycloaddition photochimique intramoléculaire énantiosélective [2 + 2] d'un dérivé de *N*-allylacrylamide inclu dans la cavité chirale d'une  $\beta$ -CD. Le dérivé de *N*-allylacrylamide sélectionné était le *N*-allyl-*N*-(4-méthoxyphényl) acrylamide **1** (schéma b). Le groupe méthoxyphényle a été choisi afin de favoriser l'inclusion du composé **1** dans la cavité hydrophobe et asymétrique de la  $\beta$ -CD.

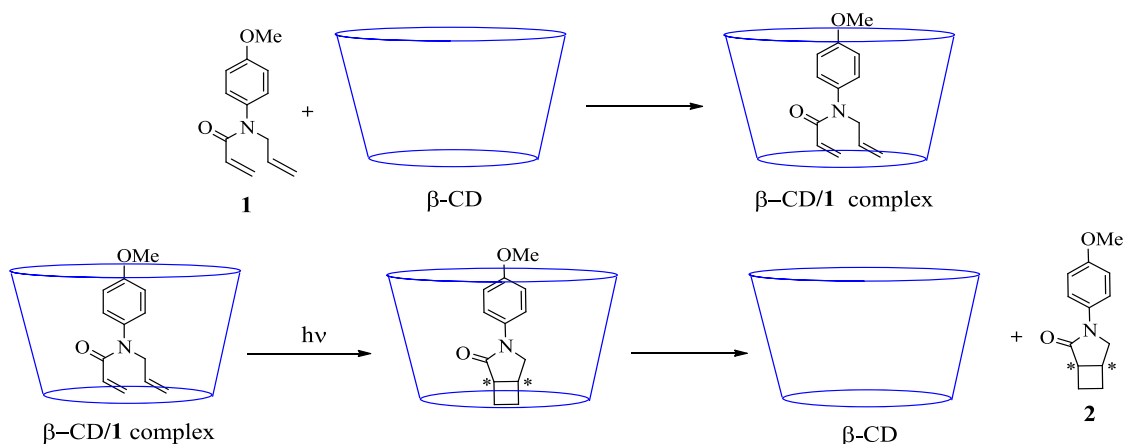
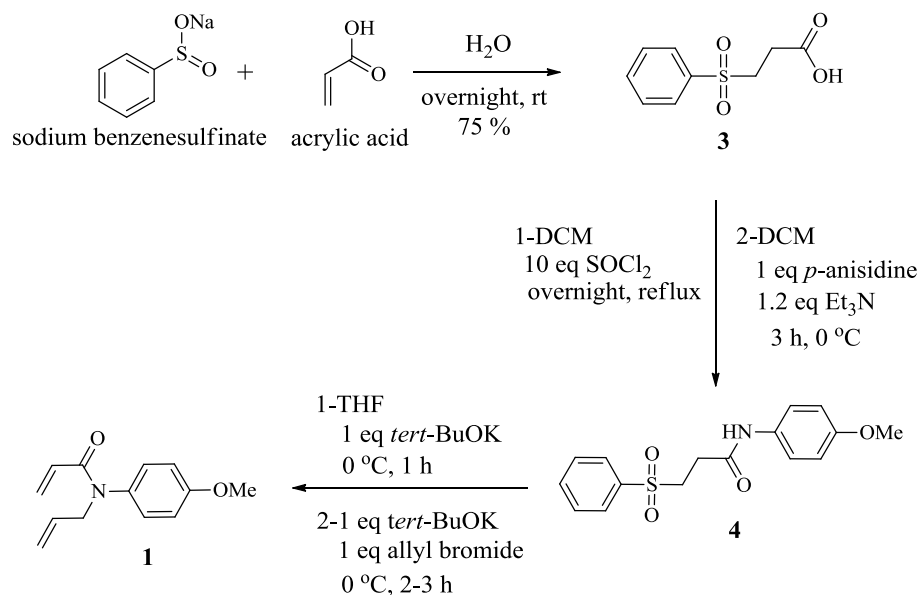


*Schéma b: Photocycloaddition [2+2] intramoléculeire énantiosélective du composé **1** en présence de  $\beta$ -CD.*

## La synthèse du *N*-allyl-*N*-(4-méthoxyphényl)acrylamide **1**

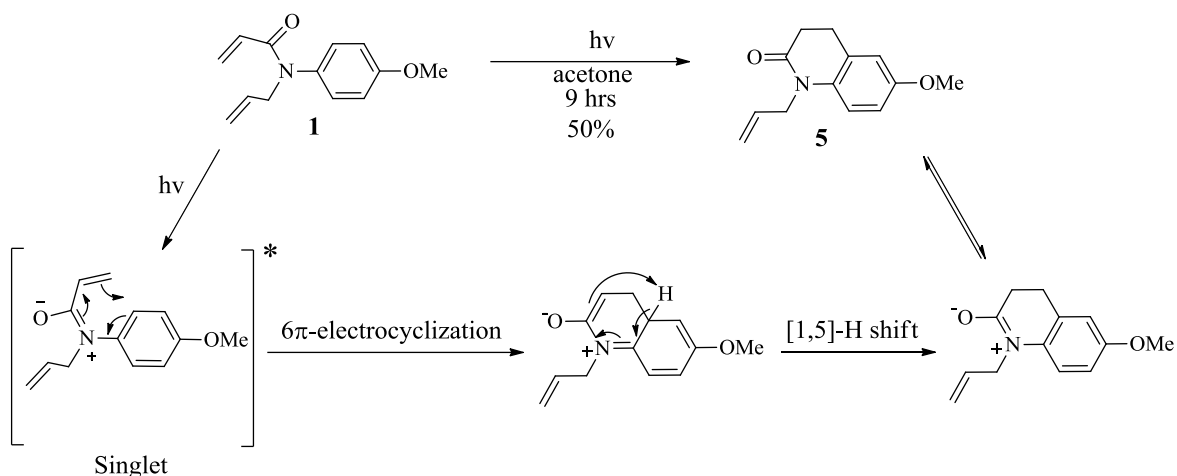
La synthèse du composé **1** a tout d'abord consisté en une addition de Michael du benzènesulfonate de sodium sur l'acide acrylique, conduisant au composé **3** avec un rendement de 75% (Schéma 3). L'acide carboxylique **3** a ensuite été converti en chlorure d'acyle avant de le faire réagir avec la *p*-anisidine pour donner le *N*-(4-méthoxyphényl)-3-(phénylsulfonyl)propanamide **4** avec un rendement de 85% sur les deux étapes. L'élimination du groupe phénylsulfonyl du composé **4** a été effectuée dans un processus « one pot » avec l'allylation de l'azote amidique pour donner le *N*-allyl-*N*-(4-méthoxyphényl)acrylamide **1** (Schéma c).



*Scheme c: Synthèse du N-allyl-N-(4-méthoxyphényl)acrylamide **1**, à partir du benzenesulfonate de sodium et de l'acide acrylique*

## La réactivité photochimique du composé **1**

Avec le composé **1** en main, nous avons étudié sa photoréactivité. L'eau était le solvant de choix pour la transformation photochimique de **1**, en tenant compte de notre intention d'effectuer des réactions ultérieures en présence de  $\beta$ -CD. Cependant, L'exposition aux rayons UV du composé **1** n'a donné lieu à aucune réaction. D'autre part, lorsque la réaction a été effectuée dans l'acétone, une conversion complète de **1** a été observée, mais le 3-(4-méthoxyphényl)-3-azabicyclo [3.2.0] heptan-2-one désiré **2** n'a jamais été obtenu. Au lieu de cela, une électrocyclisation- $6\pi$  suivi d'un réarrangement 1,5-sigmatropique s'est produite, pour conduire au composé **5** dont la structure a été validée par analyse par diffraction aux rayons X. (Schéma d, figure a).



*Schema a: Mécanisme proposé pour la formation du composé 5.*

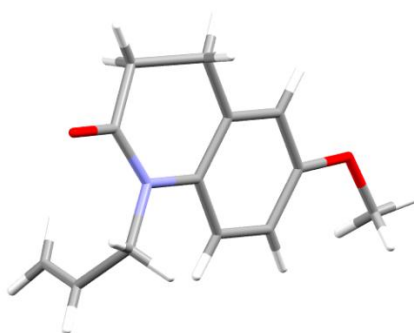


*Figure a: Structure par diffraction aux rayons X du composé 5.*

Dans le composé **1**, le doublet non-liant de l'azote associé avec la partie acryloyle et le cycle aromatique donne lieu à un système à 6 électrons  $\pi$  délocalisables. Lors de l'irradiation, le composé **1** entre dans un état excité singulet. À ce stade, il existe une compétition entre une fermeture de cycle conrotatoire à 6 électrons  $\pi$  et une évolution du composé **1** vers un état triplet. En raison d'un échange intersystème inefficace, on n'observe que le premier de ces deux phénomènes, conduisant à la formation du composé **5** vis à vis composé **2**. À ce stade, il est apparu que les conditions appropriées pour la synthèse énantiosélective proposée n'était probablement pas réunies. Les difficultés cumulées de l'interaction faible hôte-invité, de l'incompatibilité des solvants et de la réactivité photochimique compétitive semblaient insurmontables avec le substrat **1** que nous avons choisi. Il semble évident qu'un substrat différent devrait être envisagé. L'utilisation d'un groupe carbamate ou benzyle au lieu d'un

groupe aryle sur l'atome d'azote pourrait éliminer la réactivité indésirable à l'électrocyclisation et permettre à la cycloaddition [2 + 2] de prévaloir, tout en conférant une affinité de liaison raisonnable du substrat dans la cavité  $\beta$ -CD (Figure b). Néanmoins, nous avons suspendu nos efforts pour accéder au *cis*-<sup>2,3</sup>CB-GABA pour le moment et avons concentré notre attention sur la réactivité photochimique de la 1,3-dihydro-2H-azépine-2-one **8** précurseur du *cis*-<sup>3,4</sup>CB-GABA.

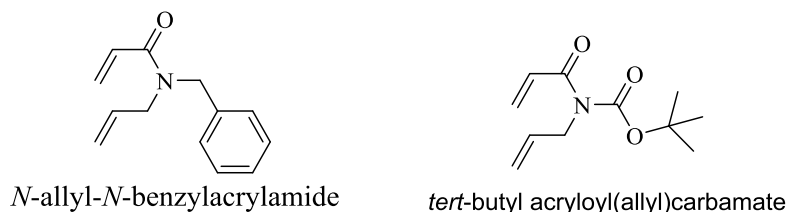


*Figure b: Analogues benzyl (left), and carbamate (right) analogues of compound 1.*

## La réactivité photochimique de la 1,3-dihydro-2H-azépine-2-one **8**

Dans cette partie du projet de recherche, nous avons cherché à établir un accès synthétique aux dérivés du *cis*-<sup>3,4</sup>CB-GABA, sur la base de l'électrocyclisation photochimique intramoléculaire énantiosélective du composé **8** en présence de  $\beta$ -CD.

Nous supposons que la présence de  $\beta$ -CD au cours de cette électrocyclisation  $4\pi$  pourrait fournir un environnement chiral qui favoriserait une topologie de fermeture du cycle par rapport à l'autre, permettant ainsi un accès préférentiel à l'un des énantiomères (schéma e).

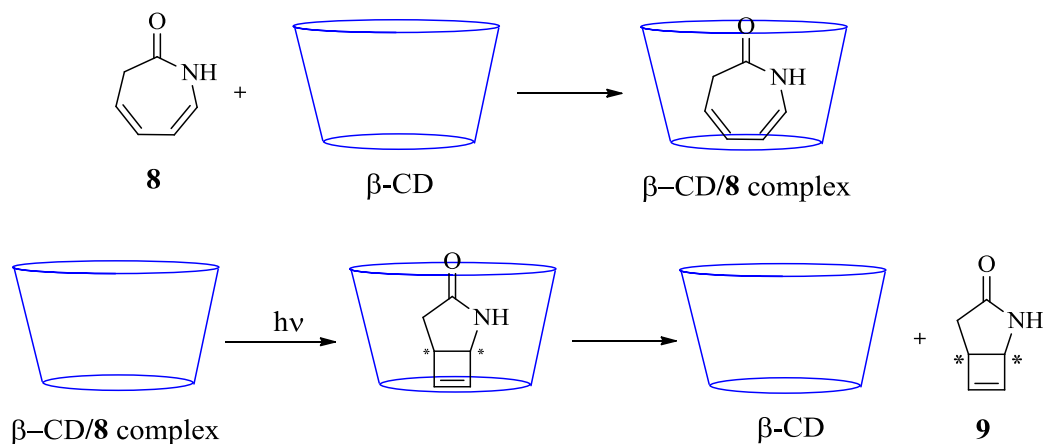
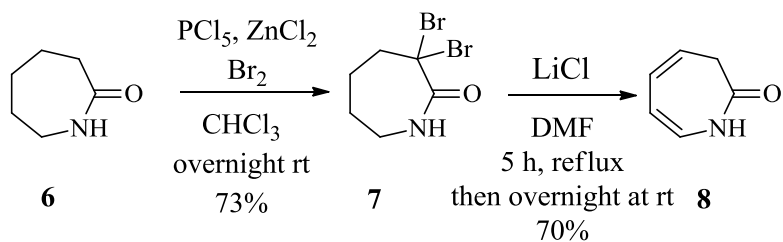


*Schéma e: Photoélectrocyclisation énantiosélective de l'azépinone 8 induite par la  $\beta$ -CD*

Dans ce chapitre, nous avons d'abord planifié la synthèse de l'azépinone **8**, l'étude de l'interaction hôte-invité **8**/ $\beta$ -CD, les meilleurs conditions d'irradiation du complexe en termes de rendement chimique et d'excès énantiomérique en produit **9**. Par la suite, le *cis*-<sup>3,4</sup>CB-GABA énantioériquement enrichi pourraient être préparés en suivant le mode opératoire décrit pour la forme racémique.

## La synthèse de l'azépinone **8**

L'azépinone **8** a été préparée selon un procédé précédemment décrit. Elle est ainsi obtenue par la dibromation du caprolactame **6** commercial conduisant au composé **7** avec un rendement de 73%, qui par double élimination de HBr produit l'azépinone **8** avec 70% de rendement (schéma f).



*Schema f: Synthèse de l'azépinone 8 à partir du caprolactame 6*

## Préparation et caractérisation du complexe $\beta$ -CD / **8**

La  $\beta$ -CD et l'azépinone **8** sont solubles dans l'eau. Le complexe  $\beta$ -CD / azépinone **8** a été préparé en mélangeant une solution aqueuse de cette dernière avec une solution aqueuse de  $\beta$ -CD. Sous agitation à la température ambiante, un précipité blanc se forme pour conduire à une «suspension laiteuse» épaisse. Il est important de souligner qu'une concentration minimale d'environ 6 mM par rapport à la concentration de  $\beta$ -CD, est nécessaire pour que le précipité se forme; et plus la concentration du mélange est faible, plus le processus de précipitation est lent. Pour cette raison, le volume de la solution finale a toujours été choisi pour avoir une concentration juste inférieure à 15 mM, ce qui correspond à la solubilité maximale de la  $\beta$ -CD dans l'eau à 25 °C.

L'apparition d'un précipité lors du mélange du lactame **8** avec la  $\beta$ -CD suggère la présence d'une interaction entre ces deux composés. Cela a été validé par l'analyse du précipité par diffraction aux rayons X sur poudre (PXRD). Les données obtenues pour le complexe  $\beta$ -CD / **8** étaient effectivement différentes de celles du lactame **8** et de la  $\beta$ -CD seules. Nous avons ainsi eu une indication supplémentaire de l'implication d'un véritable complexe, plutôt que d'un mélange physique de deux substances distinctes (Figure c).

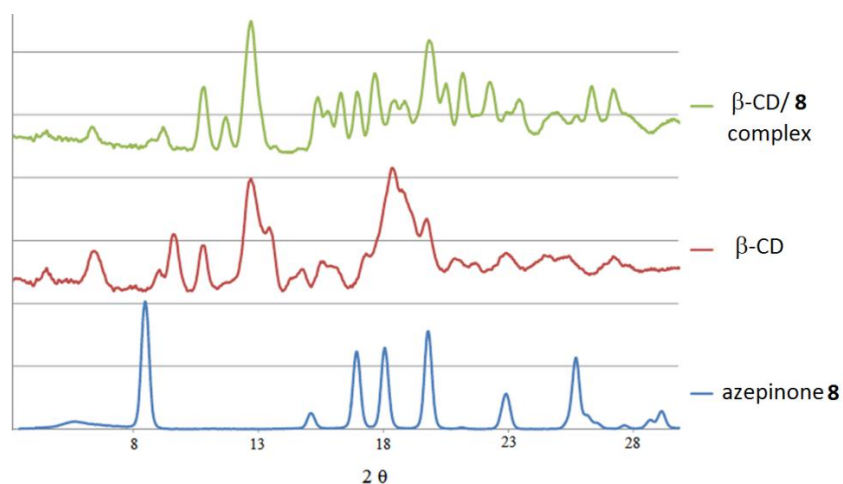
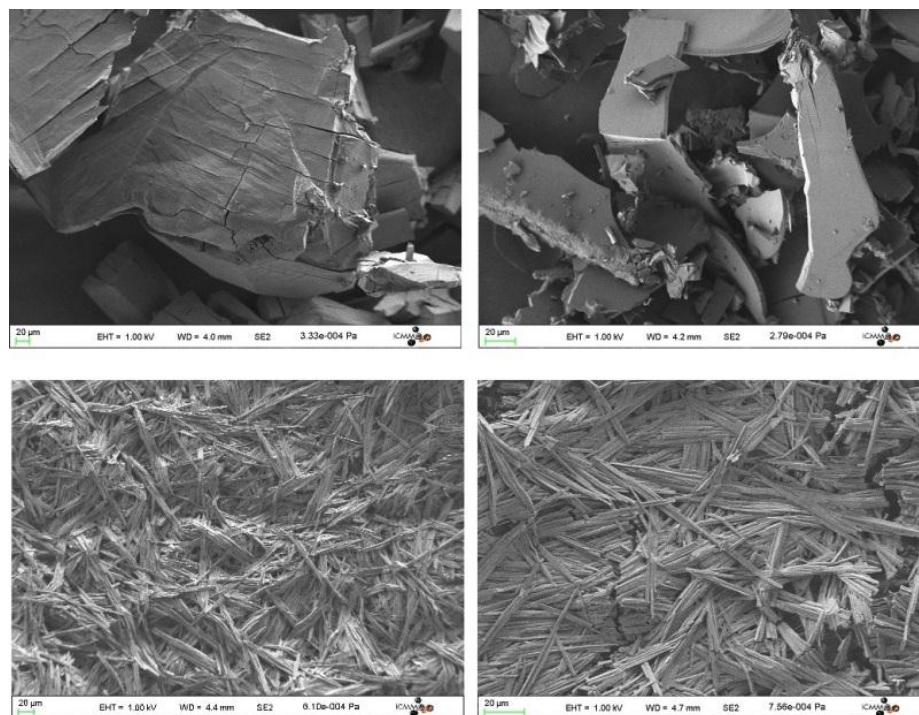


Figure c: Spectre PXRD de l'azépinone **8** vs  $\beta$ -CD vs complexe

La microscopie électronique à balayage (MEB) a également été utilisée pour valider la formation d'un complexe entre la  $\beta$ -CD et l'azépinone **8**. Les images en MEB ont montré une morphologie fibrillaire bien organisée pour le complexe, contrairement à l'azépinone **8** seule et à la  $\beta$ -CD seule, qui n'ont montré que des structures amorphes (Figure d).  $\beta$ -CD /**8**.



*Figure d: Images MEB de la  $\beta$ -CD seule (en haut à gauche), de l'azépinone **8** seule (en haut à droite), du complexe  $\beta$ -CD/**8** avant irradiation (en bas à gauche), et après irradiation (en bas à droite).*

La stœchiométrie du complexe a ensuite été évaluée par spectroscopie UV en utilisant la méthode de variation continue. Une représentation graphique de l'évolution de l'absorption à 254 nm pour des solutions aqueuses de composition molaire relative variée a suggéré la formation d'un complexe dans un rapport molaire de 1: 1, comme illustré à la figure e.

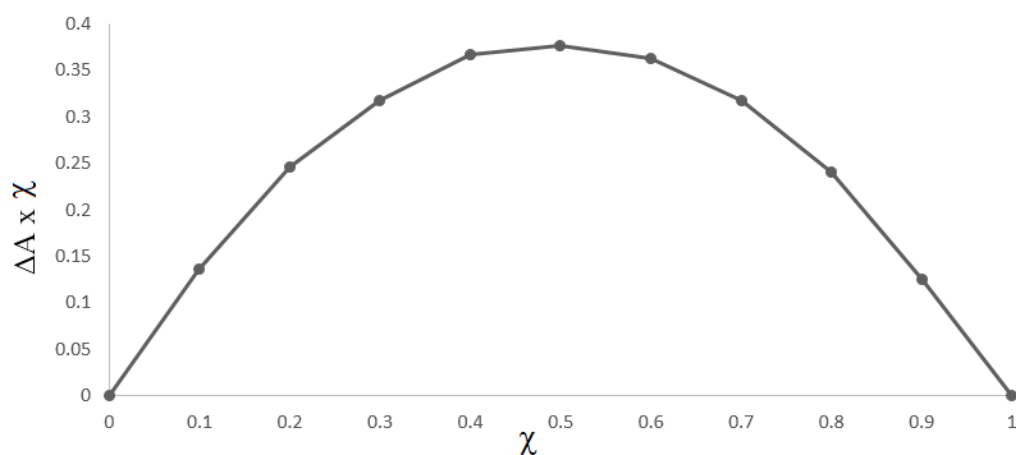


*Figure e: Job's plot de l'absorption UV ( $\lambda = 254 \text{ nm}$ ) d'une solution  $\beta$ -CD:azépinone **8** à différents rapports molaires.*

Nous avons, par la suite, effectué des mesures spectroscopiques pour étudier le comportement du complexe en solution. Une expérience de titrage par RMN  $^1\text{H}$  a été réalisée dans laquelle la variation des déplacements chimiques des protons de la  $\beta$ -CD était mesurée avec l'augmentation progressive de la concentration en l'azépinone **8**. Les signaux correspondants aux protons H1, H2, H4 et H6, situés à l'extérieur de la cavité  $\beta$ -CD, ne présentaient aucun changement significatif. Par contre, les signaux correspondants aux protons H3 et H5, orientés vers l'intérieur de la cavité, présentaient un décalage vers les champs forts, avec des variations  $\Delta\delta$  de 0,03 et 0,07 ppm, respectivement, pour un rapport  $\beta$ -CD :**8** de 1: 1, suggérant la présence d'un complexe d'inclusion à pénétration profonde (Figure f).

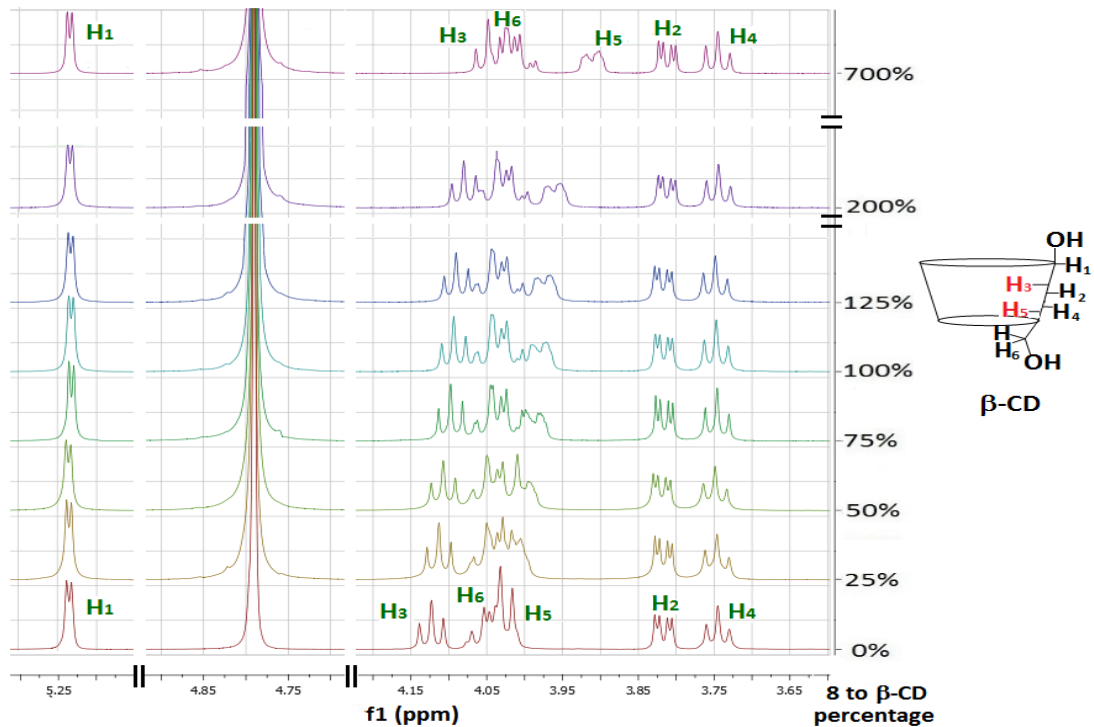


*Figure f: Spectres RMN <sup>1</sup>H de la β-CD montrant la variation de déplacement chimique de H<sub>3</sub> et H<sub>5</sub> avec chaque addition d'azépinone 8*

Les données de titrage par RMN <sup>1</sup>H pour le proton H<sub>3</sub> de la β-CD, ont également été utilisées pour évaluer la constante de liaison, en utilisant l'équation de Benesi – Hildebrand. La valeur de K<sub>b</sub> a été estimée à 35,4 (Figure g).

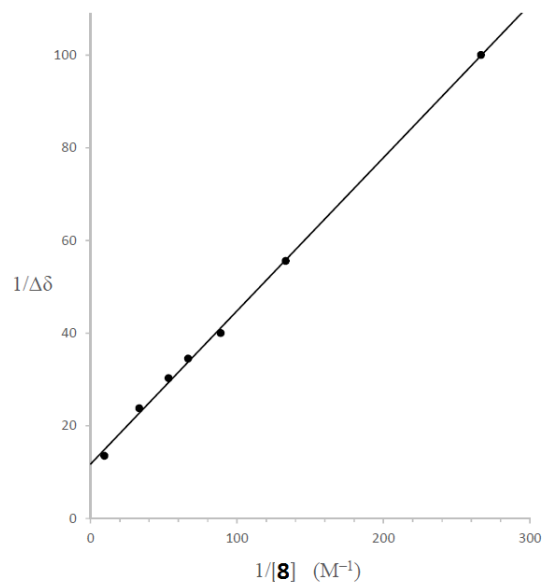


*Figure g: variation de  $1/\Delta\delta_{H3}$  en fonction de  $1/[\text{azépinone } \mathbf{8}]$ .*

La formation d'un complexe d'inclusion a également été validée par une expérience RMN 2D ROESY, réalisée sur une solution équimolaire de  $\beta$ -CD / **8** dans du  $D_2O$  à  $40^\circ C$ . nous avons pu observer la présence de taches de corrélation, impliquant les protons vinyliques H4, H5, H6, H7 de l'azépinone **8** et les protons internes H3 et H5 de la  $\beta$ -CD (Figure h).

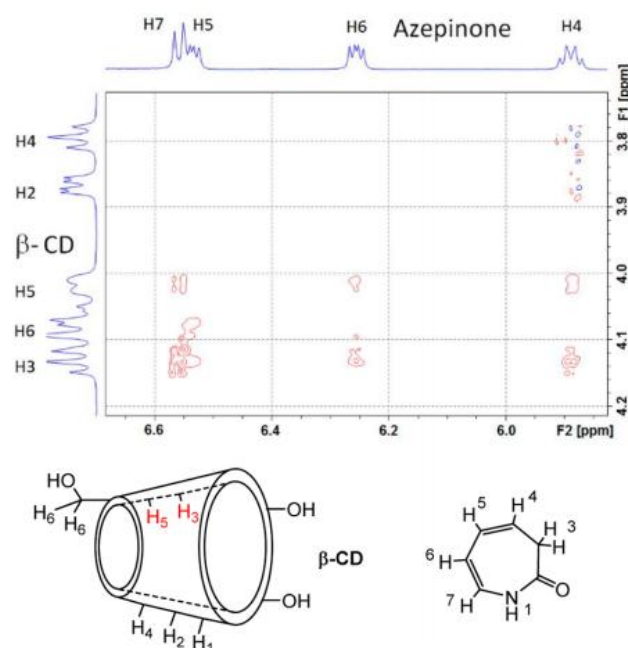


Figure h: Agrandissement du spectre RMN ROESY à 600 MHz d'une solution 1:1 de  $\beta$ -CD/**8** (15 mM in  $D_2O$ , 40 °C) (en haut).  $\beta$ -CD (en bas à gauche) et lactame **8** (en bas à droite).

## Photoélectrocyclisation de l'azépinone **8** en présence de $\beta$ -CD

Nous avons ensuite irradié le complexe  $\beta$ -CD / azépinone **8**. La réaction de photoélectrocyclisation a été réalisée avec différentes proportions hôte/invité, en solution à chaud, en suspension à froid, sous forme de poudre solide, ainsi que sous forme de film mince solide. L'isolation du photocycloadduit **9** (Schéma 9), après l'irradiation s'est avérée très délicate. Ce dernier a donc été réduit en 2-azabicyclo[3.2.0]heptan-3-one **10** dans un processus « one pot ». Le produit **10** a ainsi été obtenu avec un rendement de 75% sur deux étapes.

Aucune énantiosélectivité n'a été observée lors des réactions effectuées sur le complexe  $\beta$ -CD/**8** en solution. L'irradiation du complexe  $\beta$ -CD/**8** 1:1 à l'état solide en suspension dans l'eau ou en film mince, suivies d'une hydrogénation catalytique « one pot », a fourni le (1*R*,5*R*)-2-

azabicyclo[3.2.0]heptan-3-one **10** avec des rendements allant jusqu'à 79% et avec excès énantiomériques allant jusqu'à 45%. (Schéma h, Tableau a).

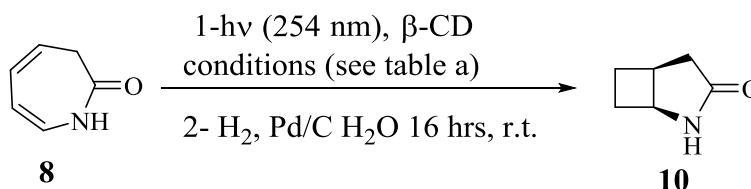


*Schéma h: Préparation du composé 10 à partir du composé 4*

Entrée	Conditions d'irradiation <sup>a</sup>	état <sup>b</sup>	Rdt <b>10</b> (%)	ee <b>10</b> (%)
1	A, 45 °C, 2 h	solution	40	0
2	A, 20 °C, 2 h	solution <sup>c</sup>	65	0
3	A, 5 °C, 2 h	suspension	79	38
4	A, 5 °C, 2 h	suspension <sup>d</sup>	75	45
5	B, 25 °C, 7 h	poudre <sup>e</sup>	70	0-40 <sup>f</sup>
6	B, 25 °C, 20 h	poudre	71	36
7	C, 25 °C, 5 h	film	77	41
8	C, 25 °C, 5 h	film <sup>g</sup>	77	42
9	C, 25 °C, 5 h	film <sup>c</sup>	78	41

*Tableau a: (a): Pour le détail des conditions A, B and C, voir la partie expérimentale; (b): tous les échantillons ont été préparés à partir d'une solution aqueuse de 8 and de β-CD (1:1 ratio) à 15 mM, sauf indication contraire; (c): les concentrations de 8 et de la β-CD étaient de 4 mM (1:1 ratio); (d): addition de 2 équivalents de β-CD solide; (e): les deux réactifs ont été mélangés directement, sans solvant ; (f): Pour 3 expériences identiques, les ee étaient de 0%, 29% and 40%; (g): La concentration de 8 était de 7.5 mM (1:2 ratio).*

## La configuration absolue du composé **10**

Toutes les expériences décrites ci-dessus ont conduit au même énantiomère majoritaire de **10**. Pour déterminer la configuration de cet énantiomère majoritaire, un échantillon de **10** (avec ee = 42%) a été transformé en dérivé *N*-Boc **12** du *cis*-<sup>3,4</sup>CB-GABA, selon une procédure déjà décrite. La mesure du pouvoir rotatoire du composé **12** a donné une valeur  $[\alpha]_D + 33$  (c 0,5, CHCl<sub>3</sub> à 25°C). Dans la littérature l'énantiomère (*R,R*)-**12** (ee = 97%) présente une valeur  $[\alpha]_D + 68$  (c 0,96, CHCl<sub>3</sub> à 27°C). Nous avons ainsi pu déduire que l'énantiomère majoritaire de **10** avait une configuration absolue (*1R,5R*) (Schéma i).

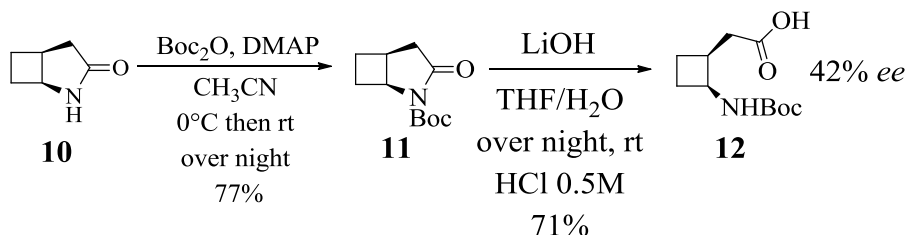


Schéma i: Transformation de **10** en **12**.

## Dédoublément du ( $\pm$ )-*cis*-<sup>3,4</sup>CB-GABA par HPLC

Nos tentatives pour obtenir du *cis*-<sup>3,4</sup>CB-GABA énantiomériquement pur par la photoélectrocyclisation énantiosélective de l'azépinone **8** en présence de  $\beta$ -CD en tant qu'hôte chiral, suivis d'une réduction du photoadduct, ont fourni des échantillons de 2-azabicyclo[3.2.0]heptan-3-one **10** avec un excès énantiomérique au maximum de 45%.

Afin de disposer d'une méthode d'accès plus appropriée à l'acide aminé cible *cis*-<sup>3,4</sup>CB-GABA sous une forme énantiomériquement pure, nous avons développé une stratégie de dédoublement de son dérivé racémique *N*-Boc **12** en utilisant une HPLC semi-préparative (Figure i). Une telle procédure présenterait plusieurs avantages par rapport à la méthode déjà décrite et qui repose sur la dérivatisation à l'aide d'une oxazolidinone chirale, comme nous l'avons mentionné précédemment.

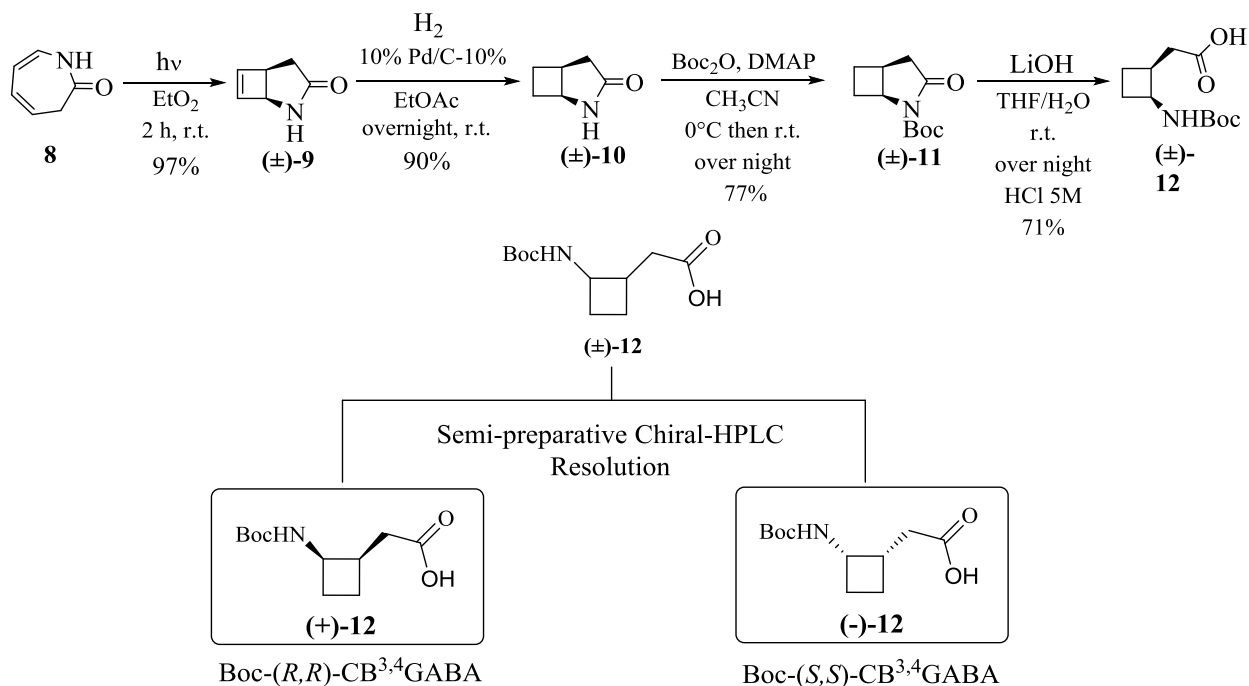


Figure i: Dédoublément par HPLC semi-préparative du N-Boc-cis-<sup>3,4</sup>CB-GABA 12 racémique.

L'acide ( $\pm$ )-12 a pu être dédoublé grâce à une colonne Lux Cellulose-3 chirale, mais en raison de sa faible solubilité dans l'éluant, la séparation à l'échelle semi-préparative n'était pas efficace.

Afin de contourner ce problème, nous avons effectué le dédoublément de l'ester benzylique ( $\pm$ )-13, qui présentait une plus grande solubilité dans les solvants organiques (Schéma j).

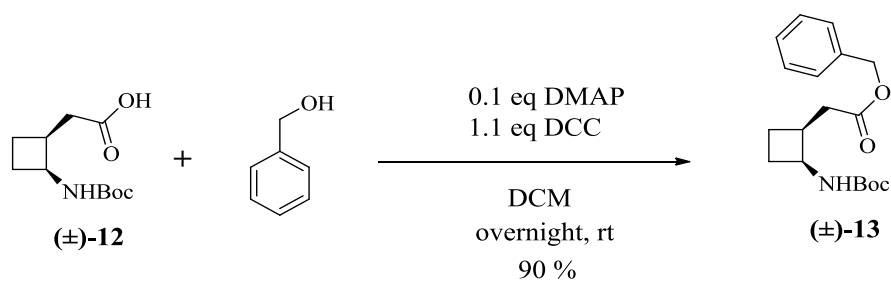


Schéma j: Synthèse de l'ester benzylique ( $\pm$ )-13 à partir de ( $\pm$ )-12

L'ester benzylique ( $\pm$ )-**13** a été dédoublé sur une colonne Lux Cellulose-2 chirale en phase normale. La figure j montre le chromatogramme en HPLC analytique de ( $\pm$ )-**13**.

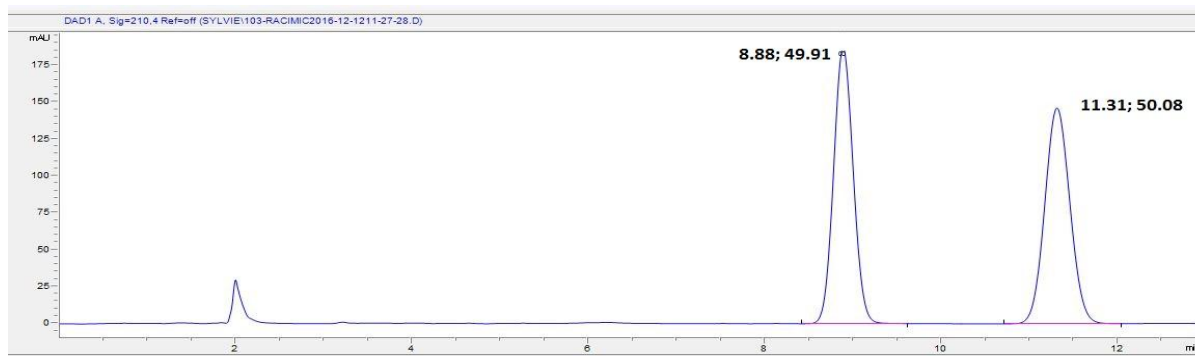


Figure j: Chromatogramme en HPLC analytique de ( $\pm$ )-**13**

Nous avons pu ainsi obtenir des fractions pures de chaque énantiomère de l'ester **13**, comme le montre les chromatogrammes ci-dessous (Figure k).

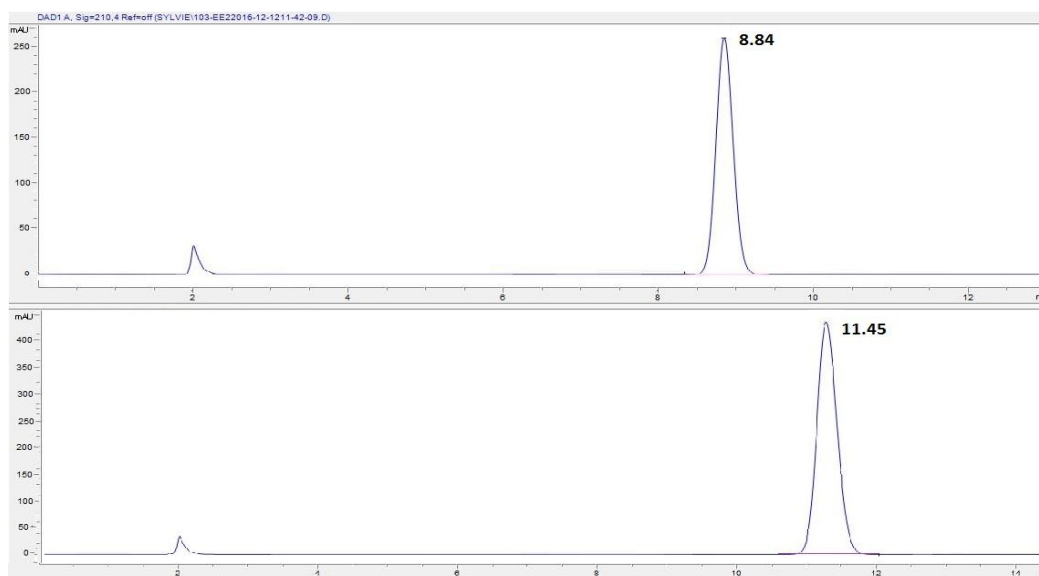


Figure k: Chromatogramme des énantiomères (+)-**13** (en haut) and (-)-**13** (en bas) purs.

La configuration absolue de l'énantiomère (+)-**13** a été déterminée par analyse par diffraction des rayons X comme étant ( $3R,4R$ ). Nous avons donc déduit que l'énantiomère (-)-**13** était de configuration ( $3S,4S$ ) (Figure l).

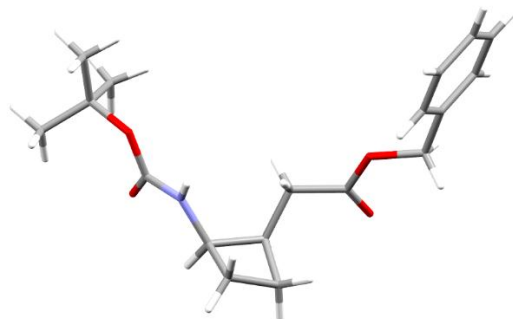


Figure l: Structure par diffraction aux rayons X du (+)-(3R,4R)-**13**.

## Synthèse et structuration des peptides hybrides $\alpha/\gamma$

Au cours des dernières années, le groupe du Pr. Aitken s'est spécialisé dans la synthèse d'acides aminés non naturels, contraints par un cyclobutane, et la préparation d'oligomères à partir de ces blocs de construction. Les oligomères de ces acides aminés contraints présentent des angles dièdres spécifiques qui leur confèrent la capacité de favoriser des structurations secondaires stables en trois dimensions. Bien que de nombreuses connaissances théoriques établissent une corrélation entre la structure des acides aminés et le schéma de repliement des peptides, il reste encore beaucoup à explorer expérimentalement avant de pouvoir établir une séquence peptidique afin d'anticiper un repliement spécifique dans une approche « bottom-up ».

Les études théoriques *ab initio* effectuées par le groupe d'Hoffman ont suggéré que, dans un peptide hybride  $\alpha/\gamma$ , un angle dièdre  $\theta$  d'environ  $33^\circ$ , sur le  $\gamma$ -amino acide, était idéal pour la formation d'une hélice 12/10. Sur la structure de l'ester (+)-(3R,4R)-**13**, nous avons pu mesurer un angle  $\theta$  d'environ  $27^\circ$  (Figure m), ce qui en faisait un bloc de construction approprié pour un peptide  $\alpha/\gamma$  qui pourrait se structurer en hélice 12/10.

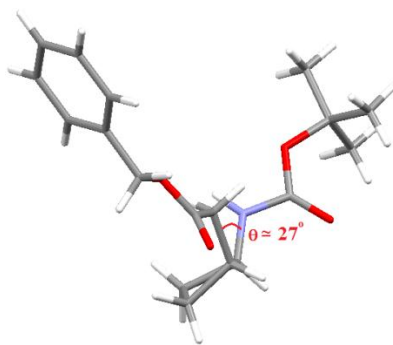


Figure m: Structure cristalline du (+)-(3R,4R)-13 with the  $\theta$  value.

Ayant les deux énantiomères du *cis*-<sup>3,4</sup>CB-GABA en mains nous avons voulu voir l'effet de la stéréochimie du  $\gamma$ -aminoacide sur le repliement d'un peptide  $\alpha/\gamma$ . Nous avons donc synthétisé et caractérisé des peptides hybrides  $\alpha/\gamma$  composés d'alternativement de la D- Alanine avec soit du (*3S,4S*)-, soit (*3R,4R*)-*cis*-<sup>3,4</sup>CB-GABA. La structuration tridimensionnelle de ces peptides a ensuite été étudiée.

## Procédure générale de synthèse des peptides hybrides $\gamma/\alpha$ .

Nous avons débuté la synthèse des peptides cibles via une approche convergente impliquant le couplage de la D-alanine et l'un des énantiomères du *cis*-<sup>3,4</sup>CB-GABA en présence de l'agent de couplage HATU.

Le dipeptide obtenu a ensuite été partitionné en deux ; une partie a été sélectivement déprotégée à l'extrémité *N*-terminale en présence de TFA, l'autre partie a été déprotégée sélectivement à l'extrémité *C*-terminale par hydrogénation catalytique en présence de Pd-C. Les deux dipeptides monoprotégés ont ensuite été couplés en présence de DIPEA et d'HATU pour conduire au tétrapeptide correspondant (Schéma k).

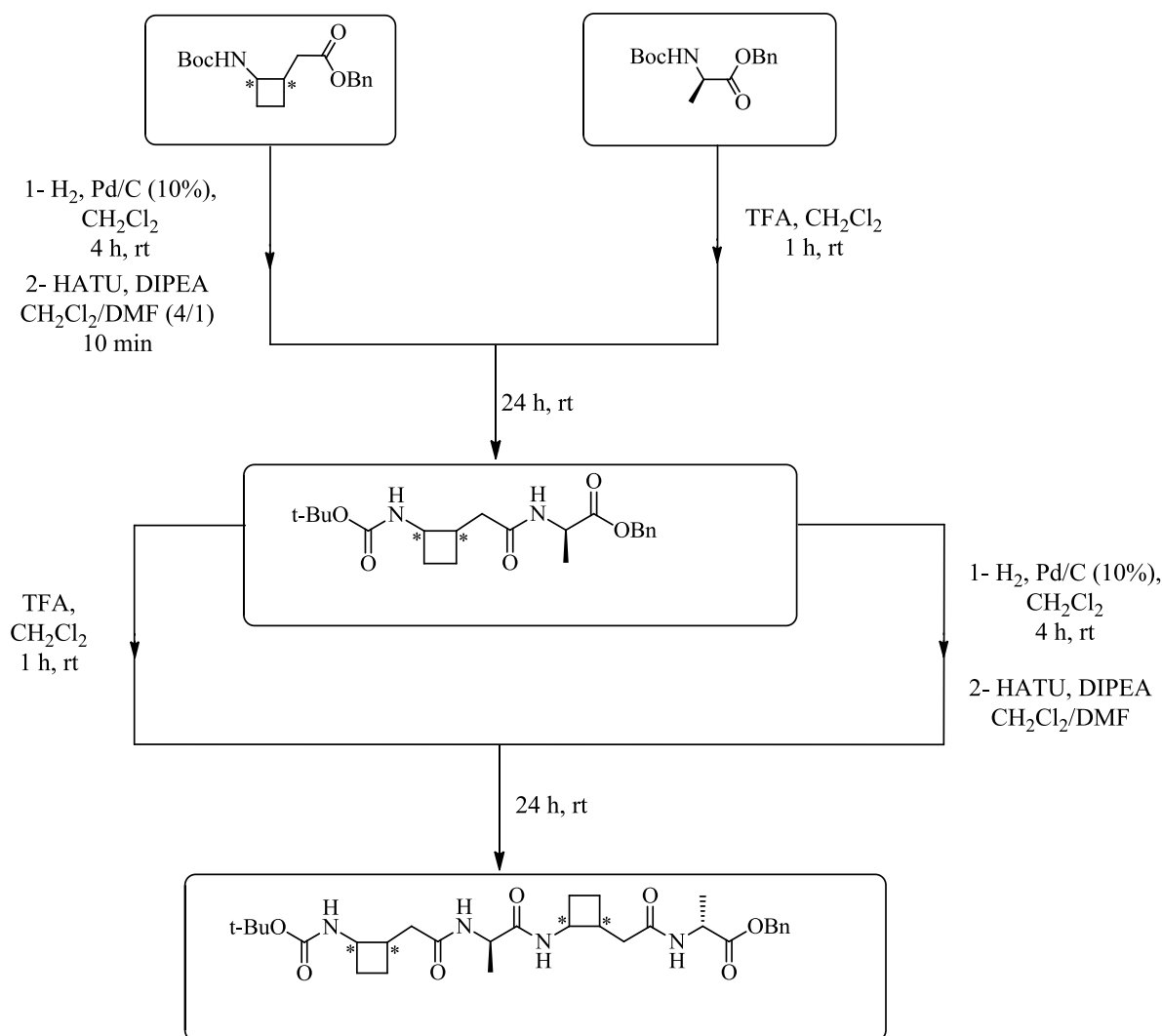


*Schéma k: Schéma général de la synthèse convergente des Boc-cis-<sup>3,4</sup>CB-GABA-(R)-Ala]<sub>n</sub>-OBn di- and tetra-peptides.*

## Analyses Structurale et Conformationnelle en solution

Par cette approche, les deux  $\gamma/\alpha$ -dipeptides, Boc-*S,S*-GABA-*R*-AlaOBn et Boc-*R,R*-GABA-*R*-AlaOBn, ainsi que les deux  $\gamma/\alpha$ -tetrapeptides, Boc-(*S,S*-GABA-*R*-Ala)<sub>2</sub>OBn et Boc-(*R,R*-GABA-*R*-Ala)<sub>2</sub>OBn, ont été préparés et par la suite entièrement caractérisés (Figure o).

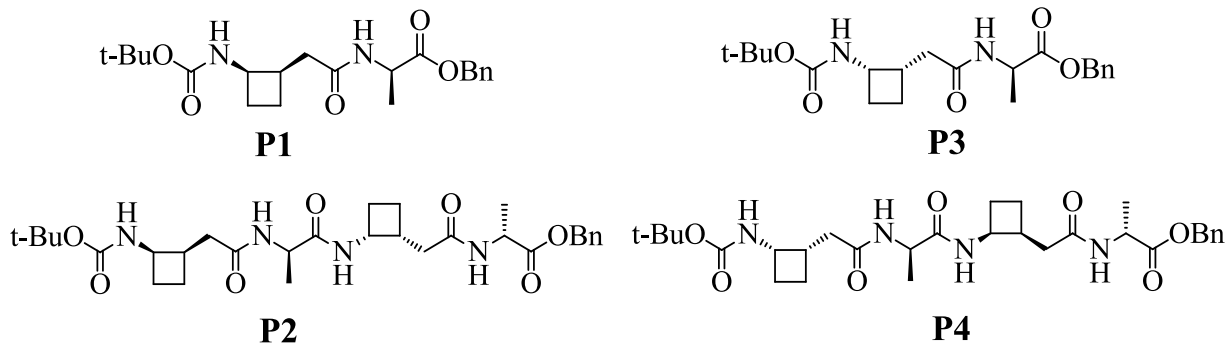


*Figure o: Les quatre peptides hybrides  $\gamma/\alpha$  préparés, en série (S,S/R) (à gauche), en série (R,R/R) (à droite).*

Aucune liaison hydrogène intramoléculaire n'a pu être mise en évidence sur les deux séries de dipeptides. La structure par diffraction aux rayons X montre, elle, un réseau de liaisons hydrogènes intermoléculaires assurant un empilement parallèle pour le dipeptide **p3** et antiparallèle pour **p1** (Figure p and q).

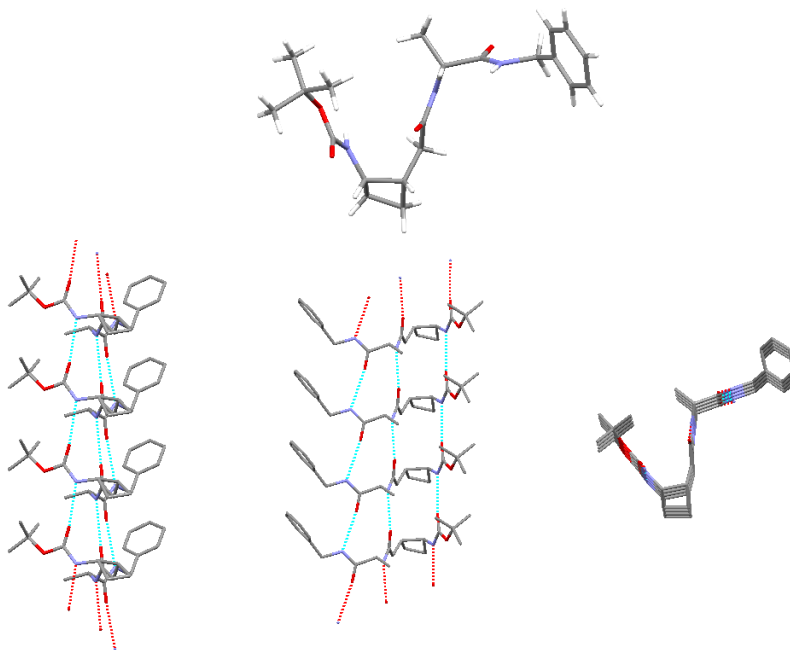


*Figure p: Structure par diffraction aux rayons X du peptide **p3** (enhaut), réseau de liaisons hydrogène intermoléculaires, vue de côté (à gauche), de face (au milieu), de dessus (à droite).*

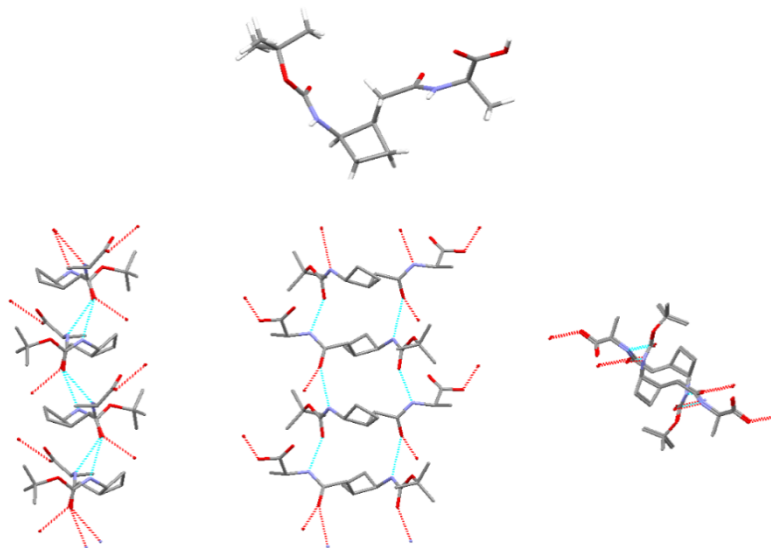


Figure q: Structure par diffraction aux rayons X du peptide **p1** (enhaut), réseau de liaisons hydrogène intermoléculaires, vue de côté (à gauche), de face (au milieu), de dessus (à droite).

Des expériences de NMR 2D ROESY ont été effectuées sur les tetrapeptides **p2** et **p4**. Les corrélations ROE visibles pour le tetrapeptide **p2** suggèrent la présence d'une alternance de pseudocycles à 12 et 10-atomes indiquant une tendance de ce peptide à adopter une structure secondaire hélicoïdale 12/10 en accord avec les prédictions d'Hoffmann(Figure r).

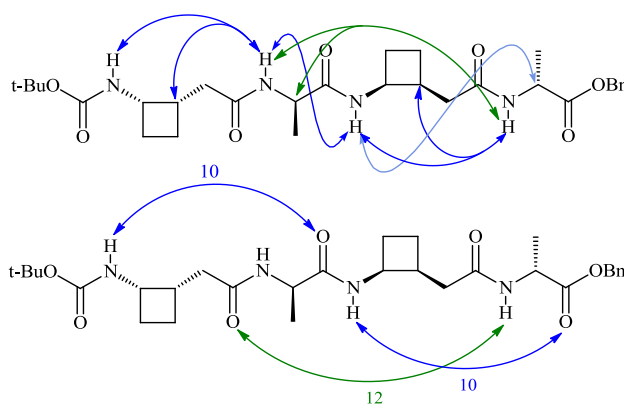
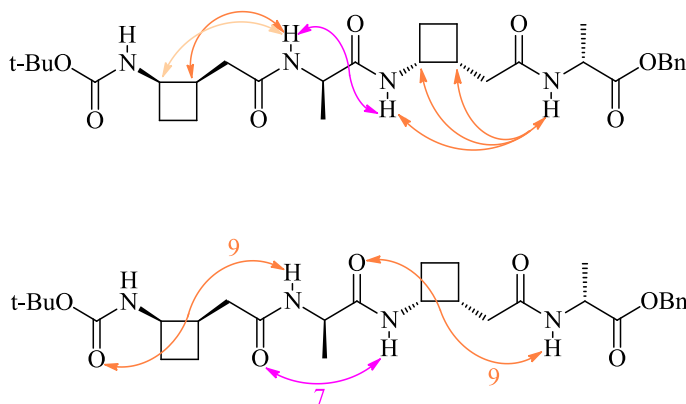


Figure r: Corrélations ROE caractéristiques sur le tetrapeptide **p2** (en haut) montrant la présence de pseudocycles (en bas) à 10 atomes (bleu) et à 12 atomes (vert). la flèche bleu claire correspond à une corrélation ROE faible.

Contrairement au tetrapeptide **p2**, les corrélations ROE observées pour le tetrapeptide **p4** ne suggèrent pas la présence d'une hélice 12/10, mais plutôt la présence d'une alternance de pseudocycles 7/9 (Figure s). Ce type de structuration, qui n'a pas été décrite à ce jour et qui résulte d'interactions entre des liaisons peptidiques adjacentes, est une structuration compétitive suggérée par Hofmann.



*Figure s: Corrélations ROE caractéristiques sur le tetrapeptide **p4** (en haut) montrant la présence de pseudocycles (en bas) à 9 atomes (orange) et à 7 atomes (rose). La flèche orange claire correspond à une corrélation ROE faible.*

## Conclusion et Perspective

Le but de ce travail était de préparer les deux  $\gamma$ -amino acides cyclobutaniques contraints, *cis*-<sup>2,3</sup>CB-GABA et *cis*-<sup>3,4</sup>CB-GABA, par une transformation énantiosélective et de les utiliser comme blocs de construction pour la synthèse de peptides hybrides  $\gamma/\alpha$ , susceptibles d'adopter une structuration hélicoïdale. La cyclodextrine a été choisie comme molécule hôte afin d'induire cette chirogénèse supramoléculaire lors de la formation du cyclobutane par voie photochimique.

Dans ce but nous avons synthétisé le *N*-allyl-*N*-(4-méthoxyphényl) acrylamide **1** afin de le soumettre à une réaction de photocycloaddition [2+2] pouvant mener au lactame bicyclique **2**, précurseur du *cis*-<sup>2,3</sup>CB-GABA. La complexation du composé **1** avec la cyclodextrine a été

évaluée grâce à des expériences en NMR  $^1\text{H}$ , 1D et 2D qui ont montré des interactions significatives entre les protons de l'hôte et de l'invité. Le ratio **1**/CD du complexe a été identifié comme étant de 1:1 avec une faible constante de complexation  $K_b=14.7$ .

La photocycloaddition réalisée sur le composé **1**, en l'absence de  $\beta$ -cyclodextrine n'a pas conduit au produit de cycloaddition photochimique [2 + 2] attendu, mais au 1-allyl-6-méthoxy-3,4-dihydroquinoléine-2(1H)-one **5**, résultant d'une électrocyclisation  $6\pi$  photochimique suivie d'un réarrangement sigmatropique 1,5.

D'autre part, nous avons étudié la photoélectrocyclisation de la 1,3-dihydro-2H-azépine-2-one **8** en présence de  $\beta$ -cyclodextrine, pouvant mener à un photocycloadduit **9** énantiomériquement enrichi, précurseur du *cis*- $^{3,4}$ CB- GABA. La complexation du composé **8** avec la  $\beta$ -cyclodextrine a été évaluée par des expériences en NMR  $^1\text{H}$  1D et 2D 1H RMN qui ont montré des interactions significatives entre les protons de l'hôte et de l'invité. Le complexe a été identifié comme présentant un rapport 1: 1 ( $\beta$ -CD / **8**) et une constante de complexation modérée ( $K_b=35,4$ ).

L'irradiation du complexe  $\beta$ -CD / **8** en solutions aqueuses, en suspensions dans l'eau ou à l'état solide, a provoqué l'électrocyclisation de l'azépinone **8** pour donner le photocycloadduit **9**. Ce dernier ayant une très faible solubilité dans les solvants organiques, à été immédiatement réduit par une hydrogénation « one-pot » en 2-azabicyclo[3.2.0]heptan-3-one **10** avec des rendements allant jusqu'à 79% à partir de l'azépinone **8**. L'excès énantiomérique le plus élevé (45%) a été obtenu lorsque l'irradiation a été réalisée sur le complexe  $\beta$ -CD / **8** en suspension dans l'eau.

Poursuivant nos efforts pour accéder au (*R, R*)- et (*S, S*)-*cis*- $^{3,4}$ CB-GABA, nous avons établi une méthode de dédoublement de son dérivé *N*-Boc ester benzylique **13** racémique, par HPLC semi-préparative équipé d'une colonne chirale. Par cette technique nous avons pu obtenir les deux énantiomères sous forme pure et à l'échelle du gramme.

Les dérivés énantiomériquement purs (-)- et (+)-*cis*- $^{3,4}$ CB-GABA ont ensuite été utilisés pour la synthèse deux séries de peptides diastéréoisomères. Ces peptides hybrides étaient composés d'une alternance de (-)-*cis*- $^{3,4}$ CB-GABA ou de (+)-*cis*- $^{3,4}$ CB-GABA et de D-Alanine. Deux  $\gamma/\alpha$ -

dipeptides, Boc-*S,S*-GABA-*R*-AlaOBn **p3** et Boc-*R,R*-GABA-*R*-AlaOBn **p1**, ainsi que deux  $\gamma/\alpha$ -tétrapeptides, Boc-(*S,S*-GABA-*R*-Ala)<sub>2</sub>OBn **p4** et Boc-(*R,R*-GABA-*R*-Ala)<sub>2</sub>OBn **p3** ont été préparés selon une synthèse convergente, et entièrement caractérisés.

L'analyse de cristaux des deux dipeptides diastéréoisomères, par diffraction des rayons X, n'a révélé aucune interaction intramoléculaire, mais un réseau de liaisons hydrogène intermoléculaires. Des expériences de RMN 1D et 2D ont montré qu'en solution, le tétrapeptide Boc-(*S,S*-GABA-*R*-Ala)<sub>2</sub>OBn **p4**, adopte une conformation en hélice 12/10, alors que son diastéréoisomère Boc-(*R,R*-GABA-*R*-Ala)<sub>2</sub>OBn **p3**, présente une structuration inédite en hélice 7/9.

Une des perspectives de ce travail, est d'obtenir la photocycloaddition [2+2] du *N*-allylacrylamide. Cette réaction pourrait être favorisée en remplaçant le groupement aryl (*p*MeO-phényle) par un groupement benzyle sur l'atome d'azote de l'amide, le système conjugué à 6 électrons  $\pi$  responsable de l'électrocyclisation n'étant plus là.

La complexation  $\beta$ -CD / azépinone **8** pourrait être renforcée par l'utilisation d'un groupement benzyle ou *tertio*-butyloxycarbonyle sur l'atome d'azote et ainsi améliorer l'énantiosélectivité lors de l'électrocyclisation de l'azépinone **8**.

Des  $\gamma/\alpha$ -tétrapeptides, Boc-(*S,S*-GABA-*R*-Ala)<sub>n</sub>NHBn, pourraient être préparés et leurs préférences conformationnelles étudiées, car l'hydrogène de la fonction amide C-terminale pourrait fournir une liaison hydrogène supplémentaire, pouvant renforcer une structuration secondaire.



# Bibliography

1. Guijarro, A.; Yus, M. *The origin of chirality in the molecules of life*; RSC Publishing: Cambridge, 2009.
2. Avalos, M.; Babiano, R.; Cintas, P.; Jiménez, J. L.; Palacios, J. C. *Chemical Reviews* **1998**, *98*, 2391-2403.
3. Noyori, R. *Angew. Chem. Int. Ed.* **2002**, *41*, 2008-2022.
4. Gotor, V.; Alfonso, I.; García-Urdiales, E. *Asymmetric Organic Synthesis with Enzymes*; Wiley-VCH Verlag GmbH & Co. KGaA: Germany, 2008.
5. Hoffmann, N. *Chem. Rev.* **2008**, *108*, 1052-1103.
6. Bach, T.; Hehn, J. P. *Angew. Chem. Int. Ed.* **2011**, *50*, 1000-1045.
7. Cole, E. E.; Oelgemöller, M. Solar Photochemistry from the Beginnings of Organic Photochemistry to the Solar Production of Chemicals. In *CRC Handbook of Organic Photochemistry and Photobiology*, 3rd ed.; CRC Press: Boca Raton, 2012; Chapter 10, Vol. 1, pp 237-248.
8. Griesbeck, A.; Oelgemöller, M.; Ghetti, F. *CRC Handbook of Organic Photochemistry and Photobiology*, 3rd ed.; CRC Press: Boca Raton, 2012; Vol. 1.
9. Inoue, Y. *Chem. Rev.* **1992**, *92*, 741-770.
10. Brimiouille, R.; Lenhart, D.; Maturi, M. M.; Bach, T. *Angew. Chem. Int. Ed.* **2015**, *54*, 2-21.
11. Hammond, G. S.; Cole, R. S. *J. Am. Chem. Soc.* **1965**, *87*, 3256-3257.
12. Inoue, Y.; Yamasaki, N.; Yokoyama, T.; Tai, A. *J. Org. Chem.* **1992**, *57*, 1332-1345.
13. Maeda, R.; Wada, T.; Mori, T.; Kono, S.; Kanomata, N.; Inoue, Y. *J. Am. Chem. Soc.* **2011**, *133*, 10379-10381.
14. Yan, Z.; Wu, W.; Yang, C.; Inoue, Y. *Supramol. Catal.* **2015**, *2*, 9-24.
15. Griesbeck, A. G.; Kramer, W.; Lex, J. *Angew. Chem. Int. Ed.* **2001**, *40*, 577-579.
16. Chen, C.; Chang, V.; Cai, X.; Duesler, E.; Mariano, P. S. *J. Am. Chem. Soc.* **2001**, *123*, 6433-6434.
17. Scheffer, J. R.; Wang, K. *Synthesis* **2001**, *8*, 1253-1257.
18. Yang, C.; Inoue, Y. *Chem. Soc. Rev.* **2014**, *43*, 4123-4143.
19. Ramamurthy, V.; Sivaguru, J. *Chem. Rev.* **2016**, *116*, 9914-9999.
20. Tanaka, K.; Fujiwara, T.; Urbanczyk-Lipkowska, Z. *Org. Lett.* **2002**, *4*, 3255-3257.

21. Müller, C.; Bauer, A.; Bach, T. *Angew. Chem. Int. Ed.* **2009**, *48*, 6640–6642.
22. Mayr, F.; Brimioulle, R.; Bach, T. *J. Org. Chem.* **2016**, *81*, 6965–6971.
23. Szejtli, J. *Cyclodextrin Technology*; Kluwer Academic Publishers: Dordrecht, 1988.
24. Szejtli, J. *Chem. Rev.* **1998**, *98*, 1743–1754.
25. Tee, O. S. *Adv. Phys. Org. Chem.* **1994**, *29*, 1–85.
26. Davis, M. E.; Brewster, M. E. *Nat. Rev. Drug Discov.* **2004**, *12*, 1023–1035.
27. Loftsson, T.; Duchene, D. *Int. J. Pharm.* **2007**, *329*, 1–11.
28. Biwer, A.; Antranikian, G.; Heinzle, E. *Appl. Microbiol. Biotechnol.* **2002**, *6*, 609–617.
29. Dodziuk, H., Ed. *Cyclodextrins and Their Complexes*; Wiley-VCH: Weinheim, 2006.
30. Mori, T.; Weiss, R. G.; Inouec, Y. *J. Am. Chem. Soc.* **2004**, *126*, 8961–8975.
31. Rao, V. P.; Turro, N. J. *Tetrahedron. Lett.* **1989**, *30*, 4641–4644.
32. Ramamurthy, V. *Tetrahedron.* **1986**, *42*, 5753–5839.
33. Furutani, A.; Katayama, K.; Uesima, Y.; Ogura, M.; Tobe, Y.; Kurosawa, H.; Tsutsumi, K.; Morimoto, T.; Kakiuchi, K. *Chirality* **2006**, *18*, 217.
34. Vízvárdi, K.; Desmet, K.; Luyten, I.; Sandra, P.; Hoornaert, G.; Van der Eycken, E. *Org. Lett.* **2001**, *3*, 1173–1175.
35. Fleck, M.; Yang, C.; Wada, T.; Inoue, Y.; Bach, T. *Chem. Commun* **2007**, 822–824.
36. Nakamura, A.; Inoue, Y. *J. Am. Chem. Soc.* **2005**, *127*, 5338–5339.
37. Fukuhara, G.; Mori, T.; Wada, T.; Inoue, Y. *J. Org. Chem.* **2006**, *71*, 8233–8243.
38. Yang, C.; Fukuhara, G.; Nakamura, A.; Origane, Y.; Fujita, K.; Yuan, D. -Q.; Mori, M.; Wada, T.; Inoue, Y. *J. Photochem. Photobiol. A* **2005**, *173*, 375–383.
39. Vizitiu, D.; Walkinshaw, C. S.; Gorin, B. I.; Thatcher, G. R. J. *J. Org. Chem.* **1997**, *62*, 8760–8766.
40. Takeshita, H.; Kumamoto, M.; Kouno, I. *Bull. Chem. Soc. Jpn* **1980**, *53*, 1006–1009.
41. Koodanjeri, S.; Joy, A.; Ramamurthy, V. *Tetrahedron* **2000**, *56*, 7003–7009.
42. Shailaja, J.; Karthikeyan, S.; Ramamurthy, V. *Tetrahedron Lett.* **2002**, *43*, 9335–9339.
43. Kaliappan, R.; Ramamurthy, V. *J. Photochem. Photobiol. A* **2009**, *207*, 144–152.
44. Inoue, Y.; Kosaka, S.; Matsumoto, K.; Tsuneishi, H.; Hakushi, T.; Tai, A. *J. Photochem. Photobiol. A: Chem.* **1993**, *71*, 61–64.
45. Inoue, Y.; Wada, T.; Sugahara, N.; Yamamoto, K.; Kimura, K.; Tong, L.-H.; Gao, X.-M.; Hou, Z.-J.; Liu, Y. *J. Org. Chem.* **2000**, *65*, 8041–8050.
46. Li, G.; Wang, Z.; Lu, R.; Tang, Z. *Tetrahedron. Lett.* **2011**, *52*, 3097–3101.

47. Luo, L.; Liao, G.-H.; Wu, X.-L.; Lei, L.; Tung, C.-H.; Wu, L.-Z. *J. Org. Chem.* **2009**, *74*, 3506–3515.
48. Nakamura, A.; Inoue, Y. *J. Am. Chem. Soc.* **2003**, *125*, 966-972.
49. Yang, C.; Ke, C.; Liang, W.; Fukuhara, G.; Mori, T.; Liu, Y.; Inoue, Y. *J. Am. Chem. Soc.* **2011**, *133*, 13786-13789.
50. Wei, X.; Wu, W.; Matsushita, R.; Yan, Z.; Zhou, D.; Chruma, J. J.; Nishijima, M.; Fukuhara, G.; Mori, T.; Inoue, Y.; Yang, C. *J. Am. Chem. Soc.* **2018**, *140*, 3959-3974.
51. Connors, K. A. *Chem. Rev.* **1997**, *97*, 1325-1357.
52. Ali, S. M.; Maheshwari, A.; Asmat, F. *Quim. Nova* **2006**, *29*, 685-688.
53. Ivanov, P. M.; Salvatierra, D.; Jaime, C. *J. Org. Chem.* **1996**, *61*, 7012-7017.
54. Herkstroeter, W. G.; Martic, P. A.; Farid, S. *J. Chem. Soc. Perkin Trans. II* **1984**, 1453-1457.
55. Linde, G. A.; Laverde Jr, A.; Colauto, N. B. Changes to Taste Perception in the Food Industry. In *Handbook of Behavior, Food and Nutrition*; Preedy, V. R., Watson, R. R., Martin, C. R., Eds.; Springer Science & Business Media, 2011; Chapter 8, Vol. 1, pp 99-18.
56. Tošner, Z.; Aski, S. N.; Kowalewski, J. *J. Incl. Phenom. Macrocycl. Chem.* **2006**, *55*, 59-70.
57. Fielding, L. *Tetrahedron* **2000**, *56*, 6151-6170.
58. Renny, J. S.; Tomasevich, L. L.; Tallmadge, E. H.; Collum, D. B. *Angew. Chem. Int. Ed.* **2013**, *52*, 2–18.
59. Thakkar, A. L.; Demarco, P. V. *J. Pharm. Sci* **1971**, *60*, 652–653.
60. Demarco, P. V.; Thakkar, A. L. *J. Chem. Soc. D* **1970**, *0*, 2-4.
61. Sun, D.-Z.; Li, L.; Qui, X.-M.; Liu, F.; Yin, B.-L. *Int. J. Pharm.* **2006**, *316*, 7–13.
62. Schneider, H.-J.; Hacket, F.; Rüdiger, V.; Ikeda, H. *Chem. Rev.* **1998**, *98*, 1755-1785.
63. Thordarson, P. *Chem. Soc. Rev.* **2011**, *40*, 1305-1323.
64. Fernandes, C. M.; Carvalho, R. A.; da Costac, S. P.; Veiga, F. J. B. *Eur. J. Pharm. Sci.* **2003**, *18*, 285–296.
65. Ramstad, T.; Hadden, C. E.; Martin, G. E.; Speaker, S. M.; Teagarden, D. L.; Thamann, T. J. *Int. J. Pharm* **2005**, *296*, 55-63.
66. Connors, K. A. *Binding constants. In: the measurement of molecular complex stability*; John Wiley & Sons, 1987.
67. Dodziuk, H.; Koźmiński, W.; Ejchart, A. *Chirality* **2004**, *16*, 90-105.
68. Cruz, J. -R.; Becker, B. A.; Morris, K. F.; Larive, C. K. *Magn. Reson. Chem.* **2008**, *46*,

838–845.

69. Correia, I.; bezzenine, N.; Ronzani, N.; Platzer, N.; Beloeil, J. -C.; Doan, B. -T. *J. Phys. Org. Chem.* **2002**, *15*, 647–659.
70. Forgo, P.; D'Souza, V. T. *Carbohydr. Res.* **1998**, *306*, 473-478.
71. Korytkowska-Walach, A.; Dubrawska, B.; Śmiga-Matuszowicz, M.; Bieg, T. *J. Mol. Struct.* **2016**, *1127*, 532-538.
72. Riaz, N. N.; M, F.; Ahmad, M. M. *Med. Chem.* **2017**, *7*, 302-307.
73. Gajcy, K.; Lochński, S.; Librowski, T. *Curr. Med. Chem.* **2010**, *17*, 2338-2347.
74. Boistel, J.; Fatt, P. *J. Physiol.* **1958**, *144*, 176-191.
75. Owens, D. F.; Kriegstein, A. R. *Nat. Rev. Neurosci.* **2002**, *9*, 715-727.
76. Wong, C. G.; Bottiglieri, T.; Snead, O. C. *Ann. Neurol.* **2003**, *54*, S3-S12.
77. Egerton, A.; Modinos, G.; Ferrera, D.; McGuire, P. *Transl. Psychiatry* **2017**, *7*, 1-10.
78. Mandal, P. K.; Kansara, K.; Dabas, A. *J. Alzheimers Dis.* **2017**, *1*, 43-45.
79. Froestl, W. *Future Med. Chem.* **2011**, *3*, 163-175.
80. Ordóñez, M.; Catiuela, C. *Tetrahedron: Asymmetry* **2007**, *18*, 3–99.
81. Levandovskiy, I. A.; Sharapa, D. I.; Shamota, T. V.; Rodionov, V. N.; Shubina, T. E. *Future Med. Chem.* **2011**, *3*, 223-241.
82. Johnston, G. A. R. *Neurochem. Res* **2016**, *41*, 476-480.
83. Johnston, G. A. R.; Curtis, D. R.; Beart, P. M.; Game, C. J. A.; McCulloch, R. M.; Twitchin, B. *J. Neuroche.* **1975**, *24*, 157-160.
84. Falch, E.; Hedegaard, A.; Nielsen, L.; Jensen, B. R.; Hjeds, H.; Krogsgaard-Larsen, P. *J. Neurochem.* **1986**, *47*, 898-903.
85. Ng, C. K. L.; Kim, H.-L.; Gavande, N.; Yamamoto, I.; Kumar, R. J.; Mewett, K. N.; Johnston, G. A. R.; Hanrahan, J. R.; Chebib, M. *Future Med. Chem.* **2011**, *3*, 197-209.
86. Czuczwar, S. J.; Patsalos, P. N. *CNS Drugs* **2001**, *15*, 339-350.
87. Gu, Y.; Huang, L.-Y. M. *Pain* **2001**, *93*, 85-92.
88. Jehle, T.; Lagrèze, W. A.; Blauth, E.; Knröle, R.; Schnierle, P.; Lücking, C. H.; Feuerstein, T. J. *Naunyn-Schmiedebergs Arch Pharmacol* **2000**, *362*, 74-81.
89. Vasudev, P. G.; Chatterjee, S.; Shamala, N.; Balaram, P. *Chem. Rev.* **2011**, *111*, 657–687.
90. Bouillère, F.; Thétiot-Laurent, S.; Kouklovsky, C.; Alezra, V. *Amino Acids* **2011**, *41*, 687–707.
91. Guo, L.; Zhang, W.; Guzei, I. A.; Spencer, L. C.; Gellman, S. H. *Org. Lett.* **2012**, *14*, 2582-2585.

92. Grison, C. M.; Robin, S.; Aitken, D. J. *Chem. Commun.* **2016**, 52, 7802-7805.
93. Jones, C. R.; Qureshi, M. K. N.; Truscott, F. R.; Hsu, S.-T. D.; Morrison, A. J.; Smith, M. D. *Angew. Chem. Int. Ed.* **2008**, 47, 7099-7102.
94. Awada, H.; Grison, C. M.; Charnay-Pouget, F.; Baltaze, J. -P.; Brisset, F.; Guillot, R.; Robin, S.; Hachem, A.; Jaber, N.; Naoufal, D.; Yazbeck, O.; Aitken, D. J. *J. Org. Chem.* **2017**, 82, 4819-4828
95. Farrera-Sinfreu, J.; Zaccaro, L.; Vidal, D.; Salvatella, X.; Giralt, E.; Pons, M.; Albericio, F.; Royo, M. *J. Am. Chem. Soc.* **2004**, 126, 6048-6057.
96. Guo, L.; Almeida, A. M.; Zhang, W.; Reidenbach, A. G.; Choi, S. H.; GuzeI, L. A.; Gellman, S. H. *J. Am. Chem. Soc.* **2010**, 132, 7868-7869.
97. Galeazzi, R.; Mobbili, G.; Orena, M. *Tetrahedron* **1999**, 55, 261-270.
98. Baxendale, I. R.; Ernst, M.; Krahnert, W.-R.; Ley, S. V. *Synlett.* **2002**, 10, 1641-1644.
99. André, V.; Vidal, A.; Ollivier, J.; Robin, S.; Aitken, D. J. *Tetrahedron Lett.* **2011**, 52, 1253-1255.
100. André, V.; Gras, M.; Awada, H.; Guillot, R.; Robin, S.; Aitken, D. J. *Tetrahedron* **2013**, 69, 3571-3576.
101. Kennewell, P. D.; Matharu, S. S.; Taylor, J. B.; Westwood, R.; Sammes, P. G. *J. Chem. Soc. Perkin Trans. 1* **1982**, 2553-2562.
102. Awada, H.; Robin, S.; Guillot, R.; Yazbeck, O.; Naoufal, D.; Jaber, N.; Hachem, A.; Aitken, D. J. *J. Eur. J. Org. Chem.* **2014**, 7148-7171.
103. Declerk, V.; Aitken, D. J. *Amino Acids* **2011**, 41, 587-595.
104. Benedetti, E.; Lomazzi, M.; Tibiletti, F.; Goddard, J.-P.; Fensterbank, L.; Malacria, M.; Palmisano, G.; Penoni, A. *Synthesis* **2012**, 44, 3523-3533.
105. Yip, K.-T.; Yang, M.; Law, K.-L.; Zhu, N.-Y.; Yang, D. *J. Am. Chem. Soc.* **2006**, 128, 3130-3131.
106. Annadi, K.; Wee, A. G. H. *Arkivoc* **2014**, vi, 108-126.
107. Bonete, P.; Nájera, C. *J. Org. Chem.* **1994**, 59, 3202-3209.
108. Wang, E.-C.; Huang, K.-S.; Lin, G.-W.; Lin, J.-R.; Hsu, M.-K. *J. Chin. Chem. Soc.* **2001**, 48, 83-90.
109. Hedges, A. R. *Chem. Rev.* **1998**, 98, 2035-2044.
110. Mangolim, C. S.; Moriwaki, C.; Nogueira, A. C.; Sato, F.; Baesso, M. L.; Neto, A. M.; Matioli, G. *Food Chem.* **2014**, 153, 361-370.
111. Bach, T.; Grosch, B.; Strassner, T.; Herdtweck, E. *J. Org. Chem.* **2003**, 68, 1107-1116.
112. Hjelmggaard, T.; Gardette, D.; Tanner, D.; Aitken, D. J. *Tetrahedron: Asymmetry* **2007**, 18,

- 671-678.
113. Denisenko, A. V.; Druzhenko, T.; Skalenko, Y.; Samoilenko, M.; Grygorenko, O. O.; Zozulya, S.; Mykhailiuk, P. K. *J. Org. Chem.* **2017**, *82*, 9627-9636.
  114. Stella, V. J.; Rao, V. M.; Zannou, E. A.; Zia, V. *Adv. Drug Deliv. Rev* **1999**, *36*, 3–16.
  115. Amharar, Y.; Grandeury, A.; Sanselme, M.; Petit, S.; Coquerel, G. *Ann. Pharm. Fr.* **2010**, *68*, 212-217.
  116. Baldauf, C.; Günther, R.; Hofmann, H. -J. *Biopolymers* **2006**, *48*, 408-413.
  117. Baldauf, C.; Günther, R.; Hofmann, H. -J. *J. Org. Chem.* **2006**, *71*, 1200-1208.
  118. Ramachandran, G. N.; Ramakrishnan, C.; Sasisekharan, V. *J. Mol. Biol.* **1963**, *7*, 95-99.
  119. Pauling, L.; Corey, R. B.; Branson, H. R. *Proc. Natl. Acad. Sci.* **1951**, *37*, 205-211.
  120. Pauling, L.; Corey, R. B. *Proc. Natl. Acad. Sci.* **1953**, *39*.
  121. Ramachandran, G. N.; Sasiekhara, V. *Adv. Protien Chem.* **1968**, *23*, 283-438.
  122. Rashid, M. A.; Khatib, F.; Sattar, A. *CoRR* **2015**, *abs/1510.02775*, 1-23.
  123. Barlow, D. J.; Thornton, J. M. *J. Mol. Biol.* **1988**, *201*, 601-619.
  124. Creighton, T. E. *Proteins: Structures and Molecular Properties*; W.H. Freeman & Co Ltd, 1992.
  125. Eisenberg, D. *Proc. Natl. Acad. Sci.* **2003**, *100*, 11207-11210.
  126. Fodje, M. N.; Al-Karadaghi, S. *Protien Eng.* **2002**, *15*, 353-358.
  127. Donohue, J. *Proc. Natl. Acad. Sci. U.S.A.* **1953**, *39*, 470.
  128. Fosgerau, K.; Hoffmann, T. *Drug. Discov. Today* *20*, 122-128.
  129. Hecht, S., Huc, I., Eds. *Foldamers: Structure, Properties, and Applications*; WILEY-VCH Verlag GmbH & Co. KGaA: Weinheim, 2007.
  130. Appella, D. H.; Christianson, L. A.; Karle, I. L.; Powell, D. R.; Gellman, S. H. *J. Am. Chem. Soc.* **1996**, *118*, 13071-13072.
  131. Hill, D. J.; Mio, M. J.; Prince, R. B.; Hughes, T. S.; Moore, J. S. *Chem. Rev.* **2001**, *101*, 3893-4011.
  132. Gellman, S. H. *Acc. Chem. Res.* **1998**, *31*, 173-180.
  133. Seebach, D.; Overhand, M.; Kühnle, F. N. M.; Martinoni, B. *Helv. Chem. Acta.* **1996**, *79*, 913-941.
  134. Seebach, D.; Matthews, J. L. *Chem. Commun.* **1997**, *0*, 2015-2022.
  135. Möhle, K.; Günther, R.; Thormann, M.; Sewald, N.; Hofmann, H. -J. *Biopolymers* **1999**, *50*, 167-184.

136. Günther, R.; Hofmann, H. -J. *J. Phys. Chem. B* **2001**, *105*, 5559-5567.
137. Abele, S.; Seiler, P.; Seebach, D. *Helv. Chem. Acta* **1999**, *82*, 1559-1571.
138. Hetényi, A.; Mándity, I. M.; Martinek, T. A.; Tóth, G. K.; Fülöp, F. *J. Am. Chem. Soc.* **2005**, *127*, 547-553.
139. Martinek, T. A.; Mándity, I. M.; Fülöp, L.; Tóth, G.; Vass, E.; Hollósi, M.; Forró, E.; Fülöp, F. *J. Am. Chem. Soc.* **2006**, *128*, 13539-13544.
140. Fernandes, C.; Faure, S.; Pereira, E.; Théry, V.; Declerck, V.; Guillot, R.; Aitken, D. J. *Org. Lett.* **2010**, *12*, 3606-3609.
141. Rueping, M.; Schreiber, J. V.; Lelais, G.; Jaun, B.; Seebach, D. *Helv. Chem. Acta* **2002**, *85*, 2577-2593.
142. Szolnoki, É.; Hetényi, a.; Mándity, I. M.; Fülöp, F.; Martinek, T. A. *Eur. J. Org. Chem.* **2013**, *17*, 3555-3559.
143. Porter, E. A.; Weisblum, B.; Gellman, S. H. *J. Am. Chem. Soc.* **2002**, *124*, 7324-7330.
144. Baldauf, C.; Günther, R.; Hofmann, H. -J. *Helv. Chim. Acta* **2003**, *86*, 2573-2588.
145. Kothari, A.; Qureshi, M. K. N.; Beck, E. M.; Smith, M. D. *Chem. Commun* **2007**, 2814-2816.
146. Sharma, G. V. M.; Jayaprakash, P.; Narsimulu, K.; Sankar, A. R.; Reddy, K. R. *Angew. Chem. Int. Ed.* **2006**, *45*, 2944-2947.
147. Hanessian, S.; Luo, X.; Schaum, R.; Michnick, S. *J. Am. Chem. Soc.* **1998**, *120*, 8569-8570.
148. Hintermann, T.; Hintermann, K.; Jaun, B.; Seebach, D. *Helv. Chem. Acta* **1998**, *81*, 983-1002.
149. Seebach, D.; Brenner, M.; Rueping, M.; Schweizer, B.; Jaun, B. *Chem. Commun* **2001**, 207-208.
150. Seebach, D.; Brenner, M.; Rueping, M.; Jaun, B. *Chem. Eur. J.* **2002**, *8*, 573-584.
151. Pilsl, L. K. A.; Reiser, O. *Amino Acids* **2011**, *41*, 709-718.
152. Hintermann, T.; Seebach, D. *Chimia* **1997**, *50*, 244-247.
153. Srinivasulu, G.; Kumar, S. K.; Sharma, G. V. M.; Kunwar, A. C. *J. Org. Chem.* **2006**, *71*, 8395-8400.
154. Schmitt, M. A.; Choi, S. H.; Guzei, L. A.; Gellman, S. H. *J. Am. Chem. Soc.* **2005**, *127*, 13130-13131.
155. De Pol, S.; Zorn, C.; Klein, C. D.; Zerbe, O.; Reiser, O. *Angew. Chem. Int. Ed.* **2004**, *43*, 511-514.
156. Choi, S. H.; Guzei, I. A.; Gellman, S. H. *J. Am. Chem. Soc.* **2007**, *129*, 13780-13781.

157. Sadowsky, J. D.; Fairlie, W. D.; Hadley, E. B.; Lee, H. -S.; Umezawa, N.; Nikolovska-Coleska, Z.; Wang, S.; Huang, D. C. S.; Tomita, Y.; Gellman, S. H. *J. Am. Chem. Soc.* **2007**, *129*, 139-154.
158. Grison, C. M.; Robin, S.; Aitken, D. J. *Chem. Commun.* **2015**, *51*, 16233-16236.
159. Grison, C. M.; Miles, J. A.; Robin, S.; Wilson, A. J.; Aitken, D. J. *Angew. Chem. Int. Ed.* **2016**, *55*, 11096–11100.
160. Chatterjee, S.; Vasudev, P. G.; Ananda, K.; Raghothama, S.; Shamala, N.; Balaram, P. J. *Org. Chem.* **2008**, *73*, 6595–6606.
161. Bandyopadhyay, A.; Jadhav, S. V.; Gopi, H. N. *Chem. Commun.* **2012**, *48*, 7170–7172.
162. Sharma, G. V. M.; Jadhav, V. B.; Ramakrishna, K. V. S.; Jayaprakash, P.; Narsimulu, K.; Subash, V.; Kunwar, A. C. *J. Am. Chem. Soc.* **2006**, *128*, 14657-14668.
163. Giuliano, M. W.; Maynard, S. J.; Almeida, A. M.; Guo, L.; Guzei, I. A.; Spencer, L. C.; Gellman, S. H. *J. Am. Chem. Soc.* **2014**, *136*, 15046–15053.
164. Misra, R.; Raja, K. M. P.; Hofmann, H. -J.; Gopi, H. N. *Chem. Eur. J.* **2017**, *23*, 16644-16652.
165. Legrand, B.; Mathieu, L.; Lebrun, A.; Andriamanarivo, S.; Lisowski, V.; Masurier, N.; Zirah, S.; Kang, Y. K.; Martinez, J.; Maillard, L. T. *Chem. Eur. J.* **2014**, *20*, 6713-6720.
166. Mándity, I. M.; Wéber, E.; Martinek, T. A.; Olajos, G.; Tóth, G. K.; Vass, E.; Fülöp, F. *Angew. Chem. Int. Ed.* **2009**, *48*, 2171-2175.
167. Martinek, T. A.; Tóth, G. K.; Vass, E.; Hollósi, M.; Fülöp, F. *Angew. Chem. Int. Ed.* **2002**, *41*, 1718-1721.
168. Bonnel, C.; Legrand, B.; Simon, M.; Martinez, J.; Bantignies, J. -L.; Kang, Y. K.; Wenger, E.; Hoh, F.; Masurier, F.; Maillard, L. T. *Chem. Eur. J.* **2017**, *23*, 17584-17591.
169. Al-Warhi, T. I.; Al-Warhi, H. M. A.; El-Faham, A. *J. Saudi Chem. Soc.* **2012**, *16*, 97-116.
170. El-Faham, A.; Albericio, F. *Chem. Rev.* 2011, *111*, 6557-6602.

**Titre :** Nouvelles transformations énantiosélectives dirigées par des cyclodextrines: Applications pour la préparation de briques moléculaires d'intérêt biologique

**Mots clés :**  $\beta$ -Cyclodextrine, photochirogénèse supramoléculaire, foldamères, analogue du GABA, résolution chirale CLHP, couplage de peptide.

**Résumé :** Le but de ce travail était la préparation de dérivés cyclobutaniques du GABA optiquement purs et leur utilisation dans la préparation de  $\gamma/\alpha$ -peptides pouvant adopter une structure tridimensionnelle bien définie. Pour cela, deux stratégies ont été développées. La première consistait en l'utilisation de la  $\beta$ -Cyclodextrine comme hôte supramoléculaire chirale lors de cyclisations photochimiques énantiosélectives. La tentative de cyclisation [2+2] intramoléculaire du N-allyl-N-(4-methoxyphenyl)acrylamide n'a conduit qu'à un  $\delta$ -lactame issu d'une électrocyclisation  $6\pi$ . L'électrocyclisation de la 1,3-dihydro-2H-azepin-2-one nous a permis d'obtenir le  $\gamma$ -lactame bicyclique précurseur du (+)-cis-3,4CB-GABA avec un excès énantiomérique de 45%. La deuxième stratégie était basée sur une synthèse racémique du N-Boc-cis-3,4CB-GABA suivi d'une séparation des deux

énantiomères par CLHP semi-préparative avec une colonne chirale.

Les (-) et (+)-cis-3,4CB-GABA optiquement purs ont ainsi été obtenu à l'échelle du gramme. Ces deux énantiomères (-) et (+)-cis-3,4CB-GABA ont ensuite été utilisés pour la préparation de deux séries de peptides mixtes- $\gamma/\alpha$ , diastéréoisomères [(S,S/R) et (R,R/R)] à courtes chaînes contenant alternativement le cis-3,4CB-GABA et le D-Alanine. L'analyse des conformations des dipeptides des deux séries par Diffraction des Rayons X, n'a montré aucune interaction intramoléculaire mais plutôt un assemblage de liaisons d'hydrogène intermoléculaires entre les molécules du dipeptide. D'autre part, les études RMN 1D et 2D (en solution) ont montré que le térapeptide des séries (S,S/R) pourraient avoir une structure hélicoïdale 12/10, tandis que son analogue diastéréoisomères des séries (R,R/R), a montré, en solution, une nouvelle structure sous forme de ruban 7/9.

**Title :** New Enantioselective Transformations Induced by Cyclodextrins: Applications in the Preparation of Molecular Building Blocks of Biological Interest

**Keywords :**  $\beta$ -Cyclodextrin, supramolecular photochirogenesis, foldamers, GABA analogue, HPLC chiral resolution, peptide coupling.

**Abstract :** This work revolves around the synthesis of enantiomerically pure cyclobutane derivatives of GABA, and their use in the preparation of hybrid  $\gamma/\alpha$ -peptides that could adopt a well-defined three dimensional secondary structure. In this aim we developed two strategies. The first one employed native  $\beta$ -Cyclodextrin as a supramolecular chiral host to achieve enantiodifferentiating photochemical cyclizations. Attempting to perform an intramolecular [2+2] cyclization of N-allyl-N-(4-methoxyphenyl)acrylamide, we only obtained a  $\delta$ -lactam resulting from a  $6\pi$ ; electrocyclization, whereas the electrocyclization of 1,3-Dihydro-2H-azepin-2-one allowed access to a 45% enantiomerically enriched bicyclic  $\gamma$ -lactam precursor of (+)-cis-3,4CB-GABA. The second strategy was based on a racemic synthesis of N-Boc-cis-3,4CB-GABA followed by a separation of the two enantiomers using a semi-preparative HPLC

fitted with a chiral column. This allowed access to optically pure (-) and (+)-cis-3,4CB-GABA, on a gram scale. Furthermore, the enantiomerically pure (-) and (+)-cis-3,4CB-GABA, were used to synthesize, and fully characterize two series [the (S,S/R) and the (R,R/R)] of short diastereomeric hybrid  $\gamma/\alpha$ -peptides composed of alternating cis-3,4CB-GABA and D-Alanine. Analysis of the conformational behavior of the dipeptides from both series by X-Ray diffraction on a single crystal, showed no intramolecular interactions but rather an array of intermolecular hydrogen bonding between the dipeptide molecules. On the other hand, a series of 1D and 2D NMR experiments showed that the tetrapeptide of the (S,S/R)-series could attain a 12/10 helical structuration, whereas its diastereomeric analog of the (R,R/R)-series, displayed evidence of an unprecedented 7/9 folding pattern in solution.

